# Dynamically-generated baryon resonances with heavy flavor

Romanets, Olena

# Dynamically-generated baryon resonances with heavy flavor



This work was supported by the Ubbo Emmius Programme and partially by the Rosalind Franklin Fellowship.

Printed by: *GrafiMedia*, Groningen, December 2013

rijksuniversiteit
groningen

# Dynamically-generated baryon resonances with heavy flavor

**Proefschrift**

ter verkrijging van de graad van doctor aan de
Rijksuniversiteit Groningen
op gezag van de
rector magnificus, prof. dr. E. Sterken
en volgens besluit van het College voor Promoties.

De openbare verdediging zal plaatsvinden op

vrijdag 10 januari 2014 om 11.00 uur

door

**Olena Romanets**

geboren op 18 november 1987
te Stryi, Oekraïne

**Promotor**:
Prof. dr. R.G.E. Timmermans

**Copromotor**:
Dr. L. Tolos

**Beoordelingscommissie**:
Prof. dr. D. Boer
Prof. dr. D. Jido
Prof. dr. A. Ramos

ISBN: 978-90-367-6751-4 Printed version
ISBN: 978-90-367-6752-1 Electronic version

# Contents

# Chapter 1

# Introduction

## 1.1 Quantum Chromodynamics at low energies and its symmetries

Quantum Cromodynamics (QCD) is the theory that describes the strong interactions between quarks and gluons. It is a Yang-Mills gauge theory, based on a color gauge group $SU_C(3)$. Quark fields are the fermion degrees of freedom of the theory, and the gluons are its gauge fields. Quarks and gluons are the building blocks of hadrons, which are color singlets, and are normally classified into two groups: mesons (quark-antiquark pair, $q\bar{q}$) and baryons (three-quark states, $qqq$).

The running of the coupling constant $\alpha_s$ of the theory with energy determines two prominent features of QCD: confinement and asymptotic freedom. As the energy increases, the coupling constant reduces its value, resulting in asymptotic freedom. In this regime quarks interact weakly, and one can make use of perturbative calculations, taking $\alpha_s$ as a small parameter. With decrease of the energy the coupling constant increases, and quarks and gluons are bound; this is called color confinement. In this case it is not possible to perform calculations perturbatively. These two regimes of QCD are usually separated by the momentum scale $\Lambda_{\rm QCD}$, for which experimental measurements yield a value of about 200 MeV. QCD perturbation theory is valid when the momentum scale $Q$ is somewhat larger than $\Lambda_{\rm QCD}$, above 1 GeV, and the strong interactions are treated non-perturbatively at distances larger than $1/\Lambda_{\rm QCD}$, which is roughly the size of the light hadrons. In the low-energy regime QCD can be solved using lattice calculations, but they are extremely consuming of time and computer resources.

In order to describe physics in the low-energy regime, effective field theories are widely used [1–3]. The idea is to build a Lagrangian, which contains all assumed QCD symmetries, and to take into account the degrees of freedom that are relevant for a specific energy scale. Since at low energies due to color confinement quarks are bound in hadrons, the latter are taken as the physical degrees of freedom of these theories. This naturally leads to the idea of molecular states, as these are produced by the attractive interaction of their hadron components.

Phenomenological models based on effective field theory are built considering (approximate) symmetries of QCD, for example an SU(2) isospin symmetry, or an SU(3) flavor

symmetry for the three light $u$, $d$, and $s$ quarks. The SU(3) symmetry is surprisingly well realized in the baryon spectrum, despite the fact that the $s$ quark is about 90 MeV heavier than $u$ and $d$. The masses of the six known quarks including these three lightest ones, together with their electric charges can be found in Table 1.1. Although the flavor symmetry is not an exact one, all hadrons can be classified into isospin, SU(3), and SU(4) multiplets, as well as the corresponding spin-flavor multiplets. If the corresponding symmetry was exact, the masses of hadrons belonging to the same multiplet would be the same, which is of course not the case. Nevertheless, their masses are often fairly close to each other, so one can make use of the flavor symmetry.

| flavor | $u$ (up) | $d$ (down) | $s$ (strange) |
|---|---|---|---|
| charge [e] | $2/3$ | $-1/3$ | $-1/3$ |
| mass | $2.3^{+0.7}_{-0.5}$ MeV | $4.8^{+0.7}_{-0.3}$ MeV | $95 \pm 5$ MeV |
| flavor | $c$ (charm) | $b$ (bottom) | $t$ (top) |
| charge [e] | $2/3$ | $-1/3$ | $2/3$ |
| mass | $1.275 \pm 0.025$ GeV | $4.18 \pm 0.03$ GeV | $160^{+5}_{-4}$ GeV |

Table 1.1: Quark flavors and their charges and masses, ordered by increasing quarks mass (we work with "God-given" units, $\hbar = c = 1$). The masses are taken from the Particle Data Group (PDG) [4]. The electric charge is given in units of the positron charge. The masses of the quarks are found in a $\overline{\text{MS}}$ (modified minimal subtraction, see e.g. [5]) renormalization scheme.

An example of effective field theory is chiral perturbation theory ($\chi$PT). It uses the approximate chiral $\text{SU}(3)_L \times \text{SU}(3)_R$ symmetry of QCD for vanishing $u$-, $d$-, and $s$-quark masses $m_q \to 0$ [6–10]. In $\chi$PT the octet of light mesons ($\pi$, $K$, and $\eta$ mesons) are Goldstone boson fields.

In recent years, the introduction of nonperturbative methods has led to the extension of the region of applicability of the chiral effective theory to much higher energies, and thus in the vicinity of resonances [11]. These methods implement unitarity taking into account all channels with the same quantum numbers, that is, the coupled-channels structure. The constraints imposed by unitarity allow one to extend the information contained in the chiral Lagrangian to higher energies, which is not accessible with the standard $\chi$PT expansion. In this framework chiral amplitudes are used as a kernel to solve the scattering equations. Chiral perturbation theory unitarized in coupled channels turned out to be very successful in describing some of the existing experimental data (see [11] for an overview of different nonperturbative methods and how their predictions agree with experimental data; more references regarding chiral perturbation theory models in coupled channels are mentioned in what follows).

The resonances that are predicted by the unitarized coupled-channels models are usually called dynamically-generated resonances, since they are created from the dynamical interaction of the ground-state hadrons included as building blocks of the model.

While for the three light $u$, $d$, $s$ quarks it is a good approximation to take the vanishing quarks masses $m_q \to 0$, leading to the chiral symmetry, for heavy quarks ($Q$) it is a

good approximation to take $m_Q \to \infty$. In this limit QCD shows other symmetries, the heavy-quark spin and flavor symmetries [12–14]. Let us consider a $Q\bar{q}$ meson that contains a heavy quark $Q$ (with the mass $m_Q \gg \Lambda_{\rm QCD}$) and a light antiquark $\bar{q}$ (with the mass $m_{\bar{q}} \ll \Lambda_{\rm QCD}$). The typical momentum transfer between $Q$ and $\bar{q}$ is of the order of $\Lambda_{\rm QCD}$ [14]. The velocity $v$ of the heavy quark in the hadron is almost unchanged by such an interaction, even though the momentum $p$ of the heavy quark changes by about $\Lambda_{\rm QCD}$, since $\Delta v = \Delta p/m_Q$. The heavy quark's velocity does not change with time, the heavy quark behaves like a static external color source, and the meson dynamics reduces to that of the light degrees of freedom interacting with this color source. The immediate consequence is that the mass of the heavy quark is irrelevant in the $m_Q \to \infty$ limit, and thus all heavy quarks interact in the same way within heavy mesons. This is the heavy-quark flavor symmetry, which states that the dynamics is unchanged under the exchange of heavy quark flavors in the limit of infinitively heavy quark masses. The finite mass effects can be taken into account by the $1/m_Q$ corrections, which are different for heavy quarks with different flavors. Consequently, heavy-quark flavor symmetry breaking effects are proportional to $(1/m_{Q_i} - 1/m_{Q_j})$, where $Q_i$ and $Q_j$ are two heavy quark flavors.

A heavy quark interacts strongly only with gluons. In the limit of infinitely massive quarks, $m_Q \to \infty$, the static heavy quark can interact with gluons only via its chromo-electric charge. This interaction is spin independent. The spin-dependent interactions are proportional to the chromomagnetic moment of the quark and are of the order $1/m_Q$ [14]. As a consequence, this leads to the heavy-quark spin symmetry (HQSS), which states that all types of spin interactions vanish for infinitely massive quarks, the dynamics is unchanged under arbitrary transformations in the spin of the heavy quark.

## 1.2 Hadrons

The discovery of the $\Omega(1672)$ in 1964 [15] was a triumph of the SU(3) flavor symmetry and its "eightfold way" version [16]. The $\Omega(1672)$ particle was predicted two years earlier by Gell-Mann [16], based on the mass splitting between $\Delta(1232)$, $\Sigma_{3/2^+}(1385)$, and $\Xi_{3/2^+}(1530)$. It was realized that there are three states that make the fundamental representation **3** of the flavor SU(3) group, named quarks [17]. The actual baryons are thus realized as the flavor representations found in the $\mathbf{3} \times \mathbf{3} \times \mathbf{3}$ product. That was the beginning of the quark model, which describes hadrons as bound states of quarks and antiquarks ($qqq$ for baryons and $q\bar{q}$ for mesons).

In that time there were many models built to describe hadrons as bound states of quarks. Some popular examples include potential models (see [18] for an overview of potential models), the one-gluon exchange model [19], the quark model with relativistic kinematics (e.g. [20]), the relativistic quark model [21, 22], the MIT bag model [23], skyrmions and other soliton models [24, 25], and QCD sum rules [26, 27]. These models are usually very successful in describing low-lying hadrons and resonances, but often fail in reproducing experimental data for hadrons with higher masses. Lattice QCD (LQCD) calculations [28] turn out to be very successful in describing light hadrons, but LQCD involving charm or bottom flavors is problematic because of significant discretization effects, caused by the mass of the heavy quark itself, and accessible lattice spacings. Therefore,

for heavy flavors, effective field theories are needed in addition to LQCD (see Ref. [29] for a review of the baryon spectroscopy in LQCD and models that deal with heavy flavors). Particles that cannot be described with quark models are sometimes called exotic. Examples of exotic mesons are $\pi_1(1400)$ and $\pi_1(1600)$ with $J^{PC} = 1^{-+}$ (quantum numbers that cannot come from $q\bar{q}$), or states like $f_0(980)$, $a_0(980)$, $f_0(1500)$, and $X(3872)$, which have attracted a lot of attention from the theoretical community. The possibilities for the interpretation of exotic mesons include glueballs (bound states of gluons, $gg$ or $ggg$), hybrids (states made of quarks and a gluon, $q\bar{q}g$), tetraquarks ($qq\bar{q}\bar{q}$), and the interpretation as molecular states (bound state of two mesons).

There are also a few examples of baryons that cannot be interpreted within the quark model. An example is the Roper resonance, $N_{1/2^+}(1440)$. This is the lowest-mass nucleon resonance with quantum numbers of the nucleon, which is found at much lower mass than expected by quark models. It turned out to be difficult to interpret it as a $qqq$ state. A coupled-channels meson-exchange model based on an effective chiral-symmetric Lagrangian [30] has successfully interpreted the Roper resonance as generated dynamically by the $N\pi$ components. Nevertheless, this interpretation suffers from some inconsistencies with the sign of the helicity amplitudes [31, 32]. Then, there was an idea that the Roper resonance consists of two resonances [33], but this interpretation was ruled out, since no two-poles structure[1] has been observed [34]. Another example of an exotic baryon is the $N_{1/2^-}(1535)$ resonance. Its observed mass is in agreement with predictions of quark models, but its unusually large decay branching ratio to $N\eta$ invited speculations that it could be created dynamically. This resonance is successfully reproduced by an effective chiral Lagrangian in Ref. [35]. Another example is $\Lambda_{1/2^-}(1405)$. Its mass is difficult to reproduce in quark models. It has been suggested to be a $N\bar{K}$ quasibound state by Dalitz and Tuan already in 1959-1960 [36, 37]. In models exploiting chiral symmetry and imposing unitarity $\Lambda_{1/2^-}(1405)$ is interpreted as being dynamically generated by the interaction of mesons and baryons in coupled channels. In Ref. [38] Jido *et al.* suggested the two-pole structure of $\Lambda_{1/2^-}(1405)$.

One of the possibilities for building other kinds of exotic baryons is in the form of a pentaquark, a particle made of five bound quarks and antiquarks ($qqqq\bar{q}$, $q\bar{q}\bar{q}\bar{q}\bar{q}$). There were several theoretical works predicting the existence of pentaquarks [39, 40], but no conclusive experimental results were obtained for these states [41, 42]. Some years ago, a $\Theta^+(1540)$ pentaquark was found experimentally [43], and later confirmed in a couple of low-statistics experiments. This caused a lot of excitement in theoretical and experimental research. Nevertheless, this state was not confirmed in later experiments with improved statistics, and therefore nowadays the existence of $\Theta^+(1540)$ and pentaquarks in general is questionable [44].

Many baryon resonances that cannot be described as three-quark states are thought to be molecular states, dynamically generated by baryon-meson interactions. As it is mentioned above, unitarized chiral theory in coupled channels appears to be very successful in describing hadron resonances. For example, in the particular case of baryons, several resonances can be identified with states generated dynamically from the scattering

[1] Two hadron resonances with same quantum numbers form a two-pole structure when the masses of these resonances are close to each other, as compared with their widths. The corresponding peaks, thus, overlap when analyzing scattering observables, such as cross sections.

of $0^-$ octet Goldstone bosons off baryons of the ground-state $1/2^+$ octet [35, 38, 45–64]. The two-pole nature of the $\Lambda(1405)$ resonance mentioned above is predicted in unitarized chiral theory in coupled channels [38, 52, 56, 59, 65–67], and was confirmed experimentally [68, 69]. A number of works have also been dedicated to the study of $J^P = 3/2^-$ baryon resonances [70–81]. Early works considered the interaction of pseudoscalar $0^-$ mesons with the $3/2^+$ decuplet baryons. Vector mesons were incorporated in the coupled-channels models for studies of the axial $1^+$ meson resonances in Refs. [82, 83], but until recently they have not been considered in the baryon-meson interaction. In Ref. [78] the nonet of lowest-lying vector mesons was incorporated into the contact interaction term of the lowest-order chiral Lagrangian (the Weinberg-Tomozawa interaction, WT), extended to the SU(6) spin-flavor symmetry. This latter model successfully reproduces the SU(3)-flavor WT results for the lowest-lying odd-parity baryon resonances ($N(1535)$, $N(1650)$, $\Lambda(1390)$, $\Lambda(1405)$, $\Lambda(1520)$, $\Lambda(1690)$, $\Lambda(1670)$, $\Xi(1620)$, $\Xi(1690)$). It also provides some information on the dynamics of the heavier baryon resonances, such as $\Lambda(1800)$ and $\Lambda(2325)$ [79–81].

It can happen that a resonance can be described both within a quark model and also as a dynamically-generated state. An example is $\Delta(1232)$ resonance, which can be considered as a $N\pi$ resonance, and at the same time as a state of three light quarks. Other examples are $\Lambda_b(5912)$ and $\Lambda_b(5920)$ beauty-flavored baryon resonances, that appear in a constituent quark model, but can also be interpreted as molecular states.

## 1.3 Baryon resonances with heavy flavor

Another important discovery in particle physics was the observation of what we now call the $J/\psi$ meson. It was observed independently and simultaneously at two experimental facilities: by the Ting group at Brookhaven National Laboratory (BNL), where it was called a $J$ particle ($J$ looks similar to the Chinese character of Ting's name) [84]; and at the SLAC facility in Stanford, where it was called $\psi$ (since $\psi$ contains "SP", after SPEAR accelerator at SLAC)[2] [85]. The observations of the two groups were published in the same issue of Physical Review Letters, back to back. This new particle has been interpreted as a bound state of a charm quark and its antiquark, $c\bar{c}$, thus the new flavor of quark was discovered. This finding was also another proof of the existence of quarks, and was called the "November revolution". Two years later a narrow state at 1865 MeV was observed in $e^+e^-$ annihilation, decaying to $K\pi$ and $K\pi\pi\pi$. The charmed $D$ meson was observed [86].

In connection with the discovery of charmed mesons, predictions for charmed baryons were done as well [19,87]. The experimental evidence for the existence of a charmed baryon was seen at BNL [88] in the $\nu_\mu p \to \mu^- \Lambda \pi^+ \pi^+ \pi^+ \pi^-$. The $\Sigma_c$ baryon was discovered.

Later, in 1977, the bottom quark was found, in the form of the upsilon meson $\Upsilon = b\bar{b}$. The heaviest known quark, the top quark, was only discovered in 1995. It was found at the Fermilab $p\bar{p}$ collider, with an unexpectedly large mass of about 175 GeV.

In the last decades the interest in the properties of hadrons with heavy flavor has

[2]By coincidence the image of the decay of $\psi(2S)$ to $J/\psi$ and $\pi^+\pi^-$ with consecutive decay of $J/\psi$ to $e^+e^-$ in the spark chamber reproduces the shape of $\psi$.

increased. There have been many experimental facilities built that study heavy-flavor physics. Examples include CLEO [a dedicated program of charm physics at the Cornell Electron Storage Ring (CESR)], Belle [an experiment at the KEK B-factory that is mainly dedicated to study the origin of the CP violation, and also the charm and beauty physics], BaBar [an experiment at SLAC, which involves studies of charm and beauty physics], LHCb [a collaboration dedicated to beauty physics at CERN] and others [89–130]. Also, planned experiments such as PANDA (anti-Proton ANnihilation at DArmstadt) and CBM (Compressed Baryonic Matter) at the FAIR (Facility for Antiproton and Ion Research) at GSI Helmholtzzentrum für Schwerionenforschung [131, 132], which involve studies of charm physics, open the possibility in the near future for the observation of more states with exotic quantum numbers of charm and strangeness. The discovery of new states and the plausible explanation of their nature is a very active topic of research. The ultimate goal is to understand whether those states can be described with the usual three-quark baryon or the quark-antiquark meson interpretation or, alternatively, qualify better as hadron molecules. The PANDA experiment is well-suited for a comprehensive baryon spectroscopy program, in particular with regards to the spectroscopy of (multi-) strange and charmed baryons. In $\bar{p}p$ collisions, a large fraction of the inelastic cross section is associated with channels resulting in a baryon-antibaryon pair in the final state. Thus, reactions of the type $\bar{p}p \to \bar{\Lambda}_c\Lambda_c, \bar{\Sigma}_c\Sigma_c, \bar{\Lambda}_c\Sigma_c/\Lambda_c\bar{\Sigma}_c$ will take place, for which there is no experimental data yet [132]. For charmed baryon resonances the range of excitation energies accessible is restricted due to the kinematic limit at the High-Energy Storage Ring (HESR) of $\sqrt{s} = 5.5$ GeV, which allows to populate excitation energies up to 0.93 GeV above the $\Lambda_c$ ground state. Searches for hidden-charm states are also a part of PANDA program [132]. With the available energy limit, hidden-charm states with masses up to approximately 4.5 GeV can be obtained in the reactions of the type $\bar{p}p \to N_{\bar{c}c}\bar{p}$.

The BESIII experiment is nowadays extensively studying heavy-flavor physics, paying special attention to hidden-charm mesons. Unfortunately, the energy available at this experiment ($\sqrt{s} = 4.6$ GeV) is not enough to study charm or hidden-charm baryon resonances [133]. The on-going LHCb experiment at CERN with $\sqrt{s}$ can also offer information on states with both charm and bottom degrees of freedom [134]. Searches for heavy-flavored baryons are not in the list of the main scientific goals of the 12 GeV upgrade at Jefferson Lab. The charm photoproduction is only used as a tool to study properties of the nuclear target, such as multi-quark, gluonic, and hidden-color correlations in nucleons and nuclei [135]. The energy available at the facility is, however, sufficient for finding charmed baryon resonances, as well as for the hidden-charm ones [136].

Recently the charm degree of freedom has been incorporated in the unitarized coupled-channels models, and several experimental states have been described as dynamically-generated baryon molecules [137–153]. This is the case, for example, of the $\Lambda_c(2595)$, which is the charm sector counterpart of the $\Lambda(1405)$. Some of these approaches are based on a bare baryon-meson interaction saturated with the $t$-channel exchange of vector mesons between pseudoscalar mesons and baryons [137–146], others make use of the Jülich meson-exchange model [147–149] or some rely on the hidden gauge formalism [150–153]. In these studies the $\Lambda_c(2595)$ shows a two-pole structure, like its counterpart in the strange sector, the $\Lambda(1405)$.

These models do not explicitly incorporate the heavy-quark spin symmetry, and there-

fore it is unclear whether this symmetry is respected. HQSS connects vector and pseudoscalar mesons containing heavy quarks. For example, if the symmetry is exact, $D$ and $D^*$ mesons are degenerate, and therefore in order to respect HQSS both of them have to be included. In contrast, the above-mentioned unitarized models in coupled channels within the charm sector study the interaction of baryons with the pseudoscalar, and with the vector mesons separately.

## 1.4 Outline of the thesis

In this thesis we study dynamically-generated baryon resonances[3] with heavy (charm and bottom) flavor. We use a unitarized model in coupled-channels, implementing the heavy-quark spin symmetry constraints. We study charmed $C = 1$ baryon resonances with strangeness $S = -2,\ -1,\ 0$, as well as $C = 2,\ 3$ states. Baryon resonances with hidden charm are also analyzed in this thesis. One chapter is dedicated to baryon resonances with bottom flavor.

This thesis is organized in the following way. In Chapter 2 we introduce the model. The lowest-order chiral Lagrangian is presented, followed by the extension of its Weinberg-Tomozawa term to the SU(6) symmetry, and then to the spin-flavor symmetry for four flavors with the heavy-quark spin symmetry constraints. Furthermore, we introduce the Bethe-Salpeter (BS) equation in coupled channels and its on-shell form, and the regularization method for the baryon-meson loop function that appears in the BS equation. Then, we study baryon resonances that appear as poles of the scattering amplitude and the interpretation of states as they appear in different Riemann sheets. Finally in this chapter we present the symmetry-breaking pattern. We break the symmetry adiabatically, which allows us to unambiguously identify the corresponding group multiplets among the resonances generated dynamically.

In Chapter 3 we study charmed baryon resonances. First, the analysis of the symmetry multiplets and their group reduction are introduced, and the expected number of charmed resonances with $C = 1,\ 2,\ 3$ is estimated in different sectors of strangeness, isospin and total angular momentum. The following sections are dedicated to charmed $C = 1$ and non-strange $\Lambda_c$ and $\Sigma_c$ resonances. For the $\Lambda_c$ states we test the changes that appear when one considers only the coupled channels to which each resonance couples the strongest. Besides, we study the effect of the inclusion of an additional suppression factor in the interaction for the case of the charmed meson exchange, in analogy with the $t$-channel vector-meson exchange models. Further, we show our results for the $C = 1$ baryon resonances with strangeness $S = -1$ ($\Xi_c$) and $S = -2$ ($\Omega_c$). After that, we discuss the double-charmed states: $\Xi_{cc}$, with zero strangeness, and $\Omega_{cc}$ with $S = -1$. Finally, results are introduced for $C = 3$ $\Omega_{ccc}$ ($S = 0$) resonances.

Chapter 4 is dedicated to the hidden-charm $N$ and $\Delta$ baryon resonances. Similarly to the previous chapter, we begin with the analysis of the group multiplets, showing the results afterwards. We compare the predictions of our model with the findings of other theoretical models (there is no experimental information yet available in this sector).

[3]Often we refer to all poles generically as resonances, regardless of their nature, since usually they can decay through other channels not included in the model space.

In Chapter 5 we study baryon resonances with beauty flavor. We check if the $\Lambda_b(5912)$ and $\Lambda_b(5920)$ resonances that were found by the LHCb collaboration last year can be interpreted as dynamically-generated resonances. Besides $\Lambda_b$ states we also study $\Xi_b$ resonances.

We finish this thesis with an overview and conclusions. Several appendices are devoted to technical issues.

# Chapter 2

# The phenomenological model

In this chapter we introduce the Lagrangian which we use to describe the interaction between mesons and baryons with charm. We start with the chiral Lagrangian, present the Weinberg-Tomozawa interaction, and then discuss its SU(6) spin-flavor (SF) extension. Then, we present its extension to a spin-flavor model for four flavors that includes charm, and the implementation of heavy-quark spin symmetry (HQSS) constraints. The discussed phenomenological model describes the interaction between states with the charm degree of freedom, and is consistent with known symmetries of QCD. In particular, the Lagrangian embodies chiral symmetry in the light-hadron sector, and HQSS when heavy hadrons are treated. This model takes into account both pseudoscalar and vector light and heavy mesons, as well as spin-$1/2^+$ and spin-$3/2^+$ light and heavy baryons. Implementation of HQSS constraints requires some modification of the Lagrangian. The obtained interaction is applied for studying open-charm and hidden-charm states in Chapters 3 and 4. The same interaction is applied for studying beauty-flavored baryon resonances in Chapter 5. The interest in developing such a model is corroborated by present and planned experiments (see Section 1.3), which involve studies of heavy-flavor physics, and in which the results of the model can be verified. Later in this chapter we discuss unitarization in coupled channels by means of the Bethe-Salpeter (BS) equation in coupled channels, taking, as bare interaction, the phenomenological interaction previously described. The loop function that appears in the BS equation is ultraviolet-divergent and needs to be regularized. Thus, the subtraction point regularization method is analyzed. Baryon resonances appear as poles of the scattering amplitude in the complex-energy plane, and as causality imposes the absence of poles in the physical Riemann sheet, one has to search for them by performing the analytical continuation of the scattering amplitudes. Therefore, we present the behavior of the scattering amplitudes in the second Riemann sheet. As the SF symmetry is strongly broken in nature, the breaking of the symmetry is introduced at the end of this chapter. The SF symmetry is broken adiabatically down to an SU(2) isospin symmetry, by incorporating the physical masses of hadrons and meson weak-decay constants. In this way the resonances are labeled with the corresponding group multiplets, and the HQSS partners are defined.

## 2.1 Interaction potential

### 2.1.1 SU(3) chiral baryon-meson Lagrangian

The QCD Lagrangian respects chiral symmetry in the limit of massless quarks. Chiral perturbation theory ($\chi$PT) is an effective field theory based on this limit. The $\chi$PT SU(3) lowest-order Lagrangian describes the interaction of the octet of pseudoscalar mesons with the octet of $1/2^+$ baryons, and reads (e.g. [9, 154])

$$\mathcal{L}_{\rm LO} =: {\rm Tr}(\bar{B}i\gamma^\mu\nabla_\mu B) - M{\rm Tr}(\bar{B}B) + \frac{1}{2}D{\rm Tr}(\bar{B}\gamma^\mu\gamma_5\{u_\mu, B\}) + \frac{1}{2}F{\rm Tr}(\bar{B}\gamma^\mu\gamma_5[u_\mu, B]) :, \quad (2.1)$$

where two colons indicate normal order,

$$\begin{aligned} \nabla_\mu B &= \partial_\mu B + [\Gamma_\mu, B], \\ \Gamma_\mu &= \frac{1}{2}(u^+\partial_\mu u + u\partial_\mu u^+), \\ U = u^2 &= \exp(i\sqrt{2}\Phi/f), \\ u_\mu &= iu^+\partial_\mu U u^+; \end{aligned} \quad (2.2)$$

and $\Phi$ and $B$ are the SU(3) matrices of pseudoscalar mesons and $1/2^+$ baryons octets, respectively[1]:

$$\Phi = \begin{pmatrix} \frac{1}{\sqrt{2}}\pi^0 + \frac{1}{\sqrt{6}}\eta & \pi^+ & K^+ \\ \pi^- & -\frac{1}{\sqrt{2}}\pi^0 + \frac{1}{\sqrt{6}}\eta & K^0 \\ K^- & \bar{K}^0 & -\frac{2}{\sqrt{6}}\eta \end{pmatrix},$$

$$B = \begin{pmatrix} \frac{1}{\sqrt{2}}\Sigma^0 + \frac{1}{\sqrt{6}}\Lambda & \Sigma^+ & p \\ \Sigma^- & -\frac{1}{\sqrt{2}}\Sigma^0 + \frac{1}{\sqrt{6}}\Lambda & n \\ \Xi^- & \Xi^0 & -\frac{2}{\sqrt{6}}\Lambda \end{pmatrix}.$$

Further, $M$ is the average octet baryon mass, and $D$ and $F$ are coupling constants. We use Bjorken and Drell [158] conventions for the metric tensor and the Dirac matrices. By expanding the covariant derivative in Eq. (2.1), we obtain the Weinberg-Tomozawa (WT) term [159, 160]

$$\mathcal{L}_{\rm WT} = \frac{i}{4f^2} : {\rm Tr}(\bar{B}i\gamma^\mu[\Phi(\partial_\mu\Phi) - (\partial_\mu\Phi)\Phi, B]) : . \quad (2.3)$$

From this SU(3) WT chiral Lagrangian one can find the interaction potential

$$V_{ij} = C_{ij}\frac{1}{4f^2}\bar{u}(p')\gamma^\mu u(p)(k_\mu + k'_\mu), \quad (2.4)$$

where we use the convention $V = -\mathcal{L}$, and where $i$ and $j$ are the indexes of the incoming and outgoing baryon-meson pair, $p$, $p'$ ($k$, $k'$) are the initial and final momentum of the

[1] Here the same phase convention is used as in J. J. de Swart, Rev. Mod. Phys. **35**, 916 (1963) [Erratum-ibid. **37**, 326 (1965)] (Ref. [155]). Later, when studying the baryon resonances with charm, a different phase convention is used, from G. E. Baird, L. C. Biedenharn, J. Math. Phys. **5**, 1723 (1964) (Ref. [156]), and the relative phases between flavor multiplets inside a spin-flavor multiplet are defined as in C. Garcia-Recio and L. L. Salcedo, J. Math. Phys. **52**, 043503 (2011) (Ref. [157]).

baryon (meson), respectively, and finally, $u$, $\bar{u}$ are the Dirac spinors. The pion weak-decay constant is taken $f \simeq 93$ MeV, while $C_{ij}$ are the WT SU(3) matrix coefficients that can be written as

$$C_{ij} = \sum_{\mu,\gamma,\gamma'} \lambda_{\mu_\gamma \to \mu_{\gamma'}} \left( \begin{array}{cc|c} \mathbf{8} & \mathbf{8} & \mu_\gamma \\ I_M Y_M & I_B Y_B & IY \end{array} \right) \left( \begin{array}{cc|c} \mathbf{8} & \mathbf{8} & \mu_{\gamma'} \\ I'_{M'} Y'_{M'} & I'_{B'} Y'_{B'} & IY \end{array} \right), \tag{2.5}$$

where $\mu$ runs over the SU(3) decomposition of the product of the **8** (meson) and **8** (baryon) representations,

$$\mathbf{8} \otimes \mathbf{8} = \mathbf{27} \oplus \mathbf{10} \oplus \mathbf{10}^* \oplus \mathbf{8_s} \oplus \mathbf{8_a} \oplus \mathbf{1}, \tag{2.6}$$

and $\gamma$, $\gamma'$ are used to account for two octets ($\mathbf{8}_s$ and $\mathbf{8}_a$) that appear in the decomposition. The SU(3) eigenvalues are $\lambda_{\mathbf{27}} = 2$, $\lambda_{\mathbf{8}_s} = \lambda_{\mathbf{8}_a} = -3$, $\lambda_{\mathbf{1}} = -6$, $\lambda_{\mathbf{10}} = \lambda_{\mathbf{10}^*} = \lambda_{\mathbf{8}_s \leftrightarrow \mathbf{8}_a} = 0$ [59]. The last two terms in Eq. (2.5) are the SU(3) isoscalar factors [155]. Thus, chiral symmetry puts constraints on the couplings, which otherwise would be arbitrary functions of $s$.

For low energies the interaction potential of Eq. (2.4) simplifies to

$$V_{ij} = C_{ij} \frac{1}{2f^2} (\sqrt{s} - M) \left( \frac{E+M}{2M} \right), \tag{2.7}$$

where $E$ is the baryon center-of-mass energy.

It is worth noticing that the same potential can be derived from $t$-channel vector-meson exchange (TVME) interaction by taking the zero-range ($t \to 0$) approximation. The interaction potential due to the exchange of the vector meson "$X$" reads (e.g. Ref. [144]):

$$V_{ij} = \sum_X g^2 C_{ij} \bar{u}(\vec{p}_i) \gamma^\mu \left[ -g_{\mu\nu} + \frac{k_\mu k_\nu}{m_X^2} \right] \frac{1}{t - m_X^2} (q_i + q_j)^\nu u(\vec{p}_j), \tag{2.8}$$

with $k$ being the momentum transfer ($t \equiv k^2 = k^\mu k_\mu$), $g$ is the vector-meson coupling constant, and $m_X$ stands for the mass of the exchanged meson. By expanding $1/(t - m_X^2)$ in powers of $t/m_X^2$, and simplifying, such as disregarding the terms of order $\mathcal{O}(1/m_X^2)$, and making the interaction to be zero ranged, one obtains the potential of Eq. (2.7).

### 2.1.2 SU(6) extension of the Weinberg-Tomozawa baryon-meson Lagrangian

Already about fifty years ago it was suggested that it might be a useful approximation to assume that apart from the SU(3) flavor symmetry the interactions between light quarks are spin-independent [161–163]. This assumption leads to the SU(6) symmetry group, which means that six light quark states ($u$, $d$ and $s$, each with spin up or down) are treated equally. Despite the Coleman-Mandula theorem [164], which forbids combining space-time and internal symmetries, there exist several predictions based on SU(6) (relative closeness of baryon octet and decuplet masses, the axial current coefficient ratio $F/D = 2/3$, the magnetic moment ratio $\mu_p/\mu_n = -3/2$), which are remarkably well satisfied in nature [165]; this suggests that SU(6) might be a useful approximate symmetry.

Remarkably, the spin-flavor (SF) symmetry is exact for ground-state baryons in the large $N_c$ (number of colors) limit [166]; in the real $N_c = 3$ world, the zeroth-order SF symmetry breaking appears to be similar in magnitude to $\mathcal{O}(N_c^{-1})$ breaking effects [167]. Further, in the meson sector, an underlying static (meaning non-relativistic; linear momenta of the participating particles are set equal zero [168,169]) U(6) × U(6) symmetry has been used by Caldi and Pagels [168,170], in which vector mesons would be "dormant"[2] Goldstone bosons acquiring mass through relativistic corrections. This model solves a number of theoretical problems in the classification of mesons, and makes predictions that are in remarkable agreement with the experiment.

A consistent SU(6) extension of the Weinberg-Tomozawa baryon-meson chiral Lagrangian has been developed by Garcia-Recio, Nieves, and Salcedo in Ref. [78], and further used in Ref. [81] for the study of the $\Lambda(1520)$ production, and in Ref. [171], where nonexotic baryon resonances with strangeness numbers $S = 0, -1, -2, -3$ were analyzed, many of them being identified with experimentally known odd-parity $N$, $\Delta$, $\Sigma$, $\Lambda$, $\Xi$, and $\Omega$ resonances. The generalization of the model to an arbitrary number of colors has been done in [172], and to the arbitrary number of colors and flavors in [173]. The authors of the SU(6) model aimed at developing a scheme, which includes interactions of baryons with both pseudoscalar and vector mesons. Inclusion of vector mesons definitely influences the properties of baryon resonances which can be created as result of such interactions. Below we review features of the SU(6) model of Refs. [78,81].

In the SU(6) scheme the mesons (36 quark-antiquark states) fall in the representations

$$\mathbf{6} \otimes \mathbf{6}^* = \mathbf{35} \oplus \mathbf{1} = (\mathbf{8_1} \oplus \mathbf{8_3} \oplus \mathbf{1_3}) \oplus \mathbf{1_1}, \tag{2.9}$$

where multiplets without lower index are the SU(6) representations denoting their dimension, and the ones with lower indices are the SU(3) multiplets, written as $\mu_{2J+1}$ with $\mu$ being the dimension of the representation, and $J$ the spin. The **35** multiplet includes the octet of pseudoscalar mesons ($K$, $\pi$, $\eta$, $\bar{K}$) and the nonet of the vector mesons ($K^*$, $\rho$, $\omega$, $\bar{K}^*$, $\phi$), and the singlet **1** of SU(6) represents the $\eta'$ meson. In the case of baryons, with the inclusion of the spin, one finds 216 three-quark states

$$\begin{aligned}\mathbf{6} \otimes \mathbf{6} \otimes \mathbf{6} = \mathbf{56} \oplus \mathbf{20} \oplus \mathbf{70} \oplus \mathbf{70} =& (\mathbf{8_2} \oplus \mathbf{10_4}) \oplus (\mathbf{1_4} \oplus \mathbf{8_2}) \\ &\oplus 2 \times (\mathbf{10_2} \oplus \mathbf{8_4} \oplus \mathbf{8_2} \oplus \mathbf{1_2}).\end{aligned} \tag{2.10}$$

The lowest-lying baryons, including the spin-1/2 baryon octet ($N$, $\Sigma$, $\Lambda$, $\Xi$), and the spin-3/2 baryon decuplet ($\Delta$, $\Sigma^*$, $\Xi^*$, $\Omega$), are assigned to the symmetric **56** SU(6) representation. Here we consider the $s$-wave interaction between the lowest-lying meson multiplet **35** and the lowest-lying baryons **56** multiplet. The SU(6) decomposition of the product of the **35** (meson) and **56** (baryon) representations yields

$$\mathbf{35} \otimes \mathbf{56} = \mathbf{56} \oplus \mathbf{70} \oplus \mathbf{700} \oplus \mathbf{1134}. \tag{2.11}$$

Thus, assuming that the $s$-wave effective baryon-meson Hamiltonian is SU(6) invariant, there are only four Wigner-Eckart reduced matrix elements, which are functions of the baryon-meson Mandelstam variable $s$.

[2] A dormant Goldstone boson is defined to be a boson that in the static, nonrelativistic limit becomes a true Goldstone boson associated with the spontaneous vacuum breaking of a static Hamiltonian symmetry [168].

Let us denote a meson state from $\mu_M$ representation with spin $J_M$, isospin $I_M$, and hypercharge $Y_M$ such as $\mathcal{M} = [(\mu_M)_{2J_M+1}, I_M, Y_M]$, and use a similar notation for baryons $\mathcal{B}$. The baryon-meson states expressed in terms of the SU(6) coupled basis $\left|\phi; \mu^{\alpha}_{2J+1} IY\right\rangle$ are

$$\begin{aligned} |\mathcal{MB}; JIY\rangle = \sum_{\mu,\alpha,\phi} & \left( \begin{array}{cc|c} \mu_M & \mu_B & \mu \\ I_M Y_M & I_B Y_B & IY \end{array} \right) \\ & \times \left( \begin{array}{cc|c} \mathbf{35} & \mathbf{56} & \phi \\ \mu_M J_M & \mu_B J_B & \mu J \alpha \end{array} \right) \left|\phi; \mu^{\alpha}_{2J+1} IY\right\rangle , \end{aligned} \tag{2.12}$$

with $Y = Y_M + Y_B$, $|I_M - I_B| \leq I \leq I_M + I_B$, and for $s$-wave scattering $|J_M - J_B| \leq J \leq J_M + J_B$. The first and second factors in Eq. (2.12) are the SU(3) isoscalar factors [155] and the SU(6)-multiplet coupling factors, respectively [174]. The multiplets $\phi$ stand for the resulting four SU(6) irreducible representations **56**, **70**, **700**, and **1134**, and $\mu^{\alpha}_{2J+1}$ for the SU(3) representations of spin $J$, with $\alpha$ being the corresponding multiplicity. The index $\mu$ runs over all SU(3) representations for the octet-octet, octet-decuplet, singlet-octet, and singlet-decuplet decompositions. Note that chiral symmetry defines the coupling constants for the octet-octet interaction in the WT potential (Eq. (2.5)).

The assumption that the $s$-wave baryon-meson potential is an SU(6)-invariant operator implies that $\left|\phi; \mu^{\alpha}_{2J+1} IY\right\rangle$ are eigenvectors of the potential, and the corresponding eigenvalues $V_\phi(s)$ depend only on the Mandelstam variable $s$ and on the SU(6) representation $\phi$. Therefore, the matrix element of the potential can be written as

$$V_{\mathcal{MB},\mathcal{M}'\mathcal{B}'} = \langle \mathcal{M}', \mathcal{B}'; JIY \,|V|\, \mathcal{M}, \mathcal{B}; JIY\rangle = \sum_{\phi} V_\phi(s) \mathcal{P}^{\phi,JIY}_{\mathcal{MB},\mathcal{M}'\mathcal{B}'}, \tag{2.13}$$

with the projection operators

$$\begin{aligned} \mathcal{P}^{\phi,JIY}_{\mathcal{MB},\mathcal{M}'\mathcal{B}'} = & \sum_{\mu,\alpha} \left( \begin{array}{cc|c} \mathbf{35} & \mathbf{56} & \phi \\ \mu_M J_M & \mu_B J_B & \mu J \alpha \end{array} \right) \left( \begin{array}{cc|c} \mu_M & \mu_B & \mu \\ I_M Y_M & I_B Y_B & IY \end{array} \right) \\ & \times \left( \begin{array}{cc|c} \mu'_{M'} & \mu'_{B'} & \mu \\ I'_{M'} Y'_{M'} & I'_{B'} Y'_{B'} & IY \end{array} \right) \left( \begin{array}{cc|c} \mathbf{35} & \mathbf{56} & \phi \\ \mu'_{M'} J'_{M'} & \mu'_{B'} J'_{B'} & \mu J \alpha \end{array} \right) . \end{aligned} \tag{2.14}$$

It turns out [78] that there is a unique extension of the chiral SU(3) WT potential to the SU(6) symmetric case. This is done by taking

$$V_\phi(s) = \bar{\lambda}_\phi \frac{1}{2f^2} (\sqrt{s} - M) \left( \frac{E+M}{2M} \right) , \tag{2.15}$$

with $\bar{\lambda}_{\mathbf{56}} = -12$, $\bar{\lambda}_{\mathbf{70}} = -18$, $\bar{\lambda}_{\mathbf{700}} = 6$, and $\bar{\lambda}_{\mathbf{1134}} = -2$, and $M$ the baryon mass averaged over the octet and the decuplet. In this way, when restricted to the $\mathbf{8}_1 \otimes \mathbf{8}_2$ sector, the seven SU(3) WT couplings are reproduced [78, 81].

The SU(6) symmetry is broken in nature, so that it is necessary to implement the symmetry breaking. The SU(6) symmetry breaking effects are taken into account by

using the physical hadron masses and meson weak-decay constants. For this purpose the following replacements in Eq. (2.15) were performed:

$$\begin{aligned} \left(\sqrt{s}-M\right)/2f^2 &\rightarrow \left(2\sqrt{s}-M_i-M_j\right)/4f_if_j, \\ \frac{E+M}{2M} &\rightarrow \sqrt{\frac{E_i+M_i}{2M_i}}\sqrt{\frac{E_j+M_j}{2M_j}}, \end{aligned} \tag{2.16}$$

where $M_i$ ($M_j$) and $E_i$ ($E_j$) stand for the incoming (outgoing) baryon masses and center-of-mass energies, and $f_i$ ($f_j$) for the weak-decay constants of the incoming (outgoing) mesons.

The extension of the WT interaction to SF symmetry for any number of flavors $N_F$ has been studied in Ref. [172]. The corresponding Hamiltonian can be written as

$$-\mathcal{L}_{\rm WT} = H^{\rm sf}_{\rm WT}(x) = -\frac{\rm i}{4f^2} : [\Phi, \partial_0\Phi]^A{}_B \mathcal{B}^\dagger_{ACD}\mathcal{B}^{BCD} :, \quad A,B,\ldots = 1,\ldots,2N_F. \tag{2.17}$$

The indices $A, B, \ldots$ denote spin and flavor, and so they take $2N_F$ values. $\Phi^A{}_B(x)$ is the meson field, a $2N_F \times 2N_F$ Hermitian matrix which contains the fields of $0^-$ (pseudoscalar) and $1^-$ (vector) mesons. This matrix is not traceless; for later convenience it includes the SU($2N_F$) singlet meson (the mathematical $\eta_1$). The contribution of $\eta_1$ to $\Phi$ is proportional to the identity matrix and so it does not couple in $H^{\rm sf}_{\rm WT}$. The normalization of $\Phi(x)$ is such that a mass term (with a common mass $m$ for all mesons) would read $\frac{1}{2}m^2{\rm tr}(\Phi^2)$.

The quantity $\mathcal{B}(x)$ is the baryon field. $\mathcal{B}^{ABC}$ is a completely symmetric tensor; it has 56 components for $N_F = 3$, and 120 components for $N_F = 4$, and contains the lowest-lying baryons with $J^P = \frac{1}{2}^+$ and $\frac{3}{2}^+$. The normalization of the field $\mathcal{B}$ is such that a mass term (with a common mass $M$ for all baryons) would take the form $M\frac{1}{3!}\mathcal{B}^\dagger_{ABC}\mathcal{B}^{ABC}$. E.g. the fields $\mathcal{B}^{123}(x)$, $\mathcal{B}^{112}(x)/\sqrt{2}$, and $\mathcal{B}^{111}(x)/\sqrt{6}$ have the standard normalization of a fermionic field. We refer to the Appendix A for the detailed construction of $\Phi^A{}_B(x)$ and $\mathcal{B}^{ABC}(x)$ in terms of the individual meson and baryon fields for $N_F = 4$, which is relevant for the states studied in this thesis.

### 2.1.3 Inclusion of charm – spin-flavor extension of the WT Lagrangian for four flavors including HQSS constraints

In this section we discuss an extension of the WT SU(3) chiral Lagrangian to implement SF symmetry in order to incorporate the charm degree of freedom [175–177], including heavy-quark spin symmetry (HQSS) constraints. HQSS is a proper QCD spin-flavor symmetry when the quark masses become much larger than the typical confinement scale ($\Lambda_{\rm QCD} \approx 200$ MeV). HQSS predicts that all types of spin interactions involving heavy quarks vanish for infinitely massive quarks, as the spin-dependent interactions are of the order of $1/m_Q$, with $m_Q$ being the heavy-quark mass. Consequently, the spin of the light degrees of freedom is also conserved in this limit. Thus, HQSS connects vector and pseudoscalar mesons containing charmed quarks, and heavy hadrons come in HQSS multiplets.

We start by considering an SU(8) SF model. In this scheme there are 64 quark-antiquark states ($q\bar{q}$), as it is shown below together with decomposition into SU(4) multiplets (those are denoted by $\mathbf{n}_{2J+1}$ with $\mathbf{n}$ being a dimension of the representation and $J$ a spin):

$$\mathbf{8}\otimes\mathbf{8}^*=\mathbf{63}\oplus\mathbf{1}=(\mathbf{15_1}\oplus\mathbf{15_3}\oplus\mathbf{1_3})\oplus\mathbf{1_1}. \tag{2.18}$$

The **63** multiplet includes the SU(4) **15**-plet of pseudoscalar mesons ($\pi$, $K$, $\bar{K}$, $\eta$, $\eta_c$, $D$, $\bar{D}$, $D_s$, $\bar{D}_s$) and the **16**-plet of vector mesons ($\rho$, $K^*$, $\bar{K}^*$, $\omega$, $\phi$, $J/\psi$, $D^*$, $\bar{D}^*$, $D_s^*$, $\bar{D}_s^*$), while $\eta'$ belongs to the singlet **1** of SU(8). Pure $c\bar{c}$ wave functions are used for $\eta_c$ and $J/\psi$ mesons, while $\eta=\frac{1}{\sqrt{6}}(u\bar{u}+d\bar{d}-2s\bar{s})$, $\eta'=\frac{1}{\sqrt{3}}(u\bar{u}+d\bar{d}+s\bar{s})$, $\omega=-\frac{1}{\sqrt{2}}(u\bar{u}+d\bar{d})$, and $\phi=s\bar{s}$ for the physical isoscalar mesons. This implies some mixing between the isoscalar SU(4) mathematical states to build the physical ones.

Moreover, there are 512 three-quark states ($qqq$),

$$\begin{aligned}\mathbf{8}\otimes\mathbf{8}\otimes\mathbf{8}=&\mathbf{120}\oplus\mathbf{56}\oplus\mathbf{168}\oplus\mathbf{168}=\\&(\mathbf{20_2}\oplus\mathbf{20'_4})\oplus(\mathbf{4_4}\oplus\mathbf{20_2})\oplus\mathbf{2}\times(\mathbf{20'_2}\oplus\mathbf{20_4}\oplus\mathbf{20_2}\oplus\mathbf{4_2}).\end{aligned} \tag{2.19}$$

The lowest-lying baryons are assigned to the **120** multiplet of SU(8), as it is the fully symmetric representation for the SF part of the wave function, to yield a fully antisymmetric total wave function. The other states that belong to the $\mathbf{20_2}$ and $\mathbf{20'_2}$ SU(4) multiplets are charmed, double-, and triple-charmed baryons ($\Lambda_c$, $\Sigma_c$, $\Xi_c$, $\Xi'_c$, $\Omega_c$, $\Xi_{cc}$, $\Omega_{cc}$, and $\Sigma_c^*$, $\Xi_c^*$, $\Omega_c^*$, $\Xi_{cc}^*$, $\Omega_{cc}^*$, $\Omega_{ccc}$ respectively).

One can now build the $s$-wave interaction between the lowest-lying mesons of the **63** SU(8) multiplet, and the lowest-lying baryons of **120** at low energies, close to the relevant thresholds. In the $s$-channel the baryon-meson space reduces into four SU(8) irreps,

$$\mathbf{63}\otimes\mathbf{120}=\mathbf{120}\oplus\mathbf{168}\oplus\mathbf{2520}\oplus\mathbf{4752}. \tag{2.20}$$

It is mandatory that the SU(8) amplitudes for the scattering of the octet of the pseudoscalar mesons off the octet of $J^P=1/2^+$ baryons reduce to the SU(3) chiral symmetry amplitudes. Then, similarly to the SU(6) case, there is a choice of the four couplings for the $\mathbf{63}\otimes\mathbf{120}$ that, when restricted to the $\mathbf{8}\otimes\mathbf{8}$ sector, produces the seven SU(3) WT couplings uniquely. The appropriate $s$-channel couplings turn out to be proportional to the following four eigenvalues [175]:

$$\lambda_{\mathbf{120}}=-16,\quad \lambda_{\mathbf{168}}=-22,\quad \lambda_{\mathbf{2520}}=6,\quad \lambda_{\mathbf{4752}}=-2. \tag{2.21}$$

In our convention for the potential, a negative sign in the eigenvalues implies an attractive interaction. Then, from the eigenvalues, we find that the multiplets **120** and **168** are the most attractive ones, while the **4752**-plet is weakly attractive and the **2520**-plet is repulsive. As it will be also discussed in Section 3.1, for studying charmed baryon resonances with $C=1,\ 2,\ 3$, we consider only states that belong to the two most attractive representations **120** and **168**.

It is also instructive to draw attention here to some of the findings of Ref. [78] when the number of colors $N_C$ departs from 3 [172]. There it is shown that, in the **168** SU(8) irreducible space, the SU(8) extension of the WT $s$-wave baryon-meson interaction scales as $\mathcal{O}(1)$. Note that the SU(3) WT counterpart in some channels also scales as $\mathcal{O}(1)$

because the coupling strength for some channels scales as $\mathcal{O}(N_C)$, which compensates $\mathcal{O}(1/N_C)$ coming from the square of the meson decay constant [178]. However, the WT interaction behaves as $\mathcal{O}(1/N_C)$ within the **120** and **4752** baryon-meson spaces. This presumably implies that the **4752** states do not appear in the large-$N_C$ QCD spectrum, since both excitation energies and widths grow with an approximate $\sqrt{N_C}$ rate.

HQSS is a fairly good approximate symmetry of QCD [12–14] and it is mandatory to implement it in any hadronic model involving charmed quarks. HQSS implies conservation of the number of charmed quarks, $N_c$, and of the number of charmed antiquarks, $N_{\bar{c}}$, with corresponding symmetry group $\mathrm{U}_c(1) \times \mathrm{U}_{\bar{c}}(1)$. Likewise, the terms in the QCD Hamiltonian which depend on the heavy quark or antiquark spin are suppressed, being of order $1/m_h$, where $m_h$ is the mass of the heavy quark. Therefore, in the heavy-quark limit, arbitrary rotations of the spin carried by the $c$ quarks and, independently, of the spin carried by the $\bar{c}$ antiquarks, would leave unchanged the energy of the hadronic state.[3] This implies a symmetry $\mathrm{SU}_c(2) \times \mathrm{SU}_{\bar{c}}(2)$ in the heavy-quark limit. These invariances are aspects of HQSS. In what follows we refer to $\mathrm{SU}_c(2) \times \mathrm{SU}_{\bar{c}}(2) \times \mathrm{U}_c(1) \times \mathrm{U}_{\bar{c}}(1)$ as the HQSS group.

First, it should be noted that SF symmetry by itself already guarantees HQSS in many sectors. Consider, for instance, the couplings involving the channels $ND$ and $ND^*$. These channels are related through HQSS since there should be invariance under rotations of the $c$ quark spin (leaving the light quarks unrotated), and this mixes $D$ and $D^*$. But the same invariance is already implied by SF, which requires symmetry under independent rotations of spin for each flavor separately. The only cases where SF does not by itself guarantee HQSS is when there are simultaneously $c$ quarks and $\bar{c}$ antiquarks: SF implies invariance under equal rotations for $c$ and $\bar{c}$, but HQSS requires also invariance when the two spin rotations are different.

To be more specific, let us consider baryon-meson channels, and let $N_c$ be the number of $c$ quarks and $N_{\bar{c}}$ the number of $\bar{c}$ antiquarks. $N_c$ ranges from 0 to 4, and $N_{\bar{c}}$ from 0 to 1. SF guarantees HQSS in the sectors $(N_c, N_{\bar{c}}) = (0,0), (0,1), (1,0), (2,0), (3,0), (4,0)$, thus whenever only heavy quarks are present (but not heavy antiquarks), or only heavy antiquarks are present (but not heavy quarks). In the sectors $(N_c, N_{\bar{c}}) = (1,1)$, $(2,1)$, $(3,1)$, $(4,1)$ SF does not guarantee HQSS; as compared to the former sectors, the latter ones contain extra $c\bar{c}$ pairs. This observation suggests a simple prescription to enforce HQSS in the interaction for the open-charm sectors considered in this work, namely, to drop baryon-meson channels containing $c\bar{c}$ pairs. Specifically, in Chapter 3 we study the sectors $(N_c, N_{\bar{c}}) = (1,0), (2,0), (3,0)$, for which the modified SU(8) WT interaction fulfills HQSS. It should be noted that SU(8) is no longer an exact symmetry in the truncated coupled-channel space. Nevertheless, for the low-lying resonances, the omitted channels are kinematically suppressed anyway, due to their large mass. For $s$-wave interactions (the ones of interest here), SU(6) SF is sufficient to guarantee HQSS in the sectors without hidden charm: a rotation of the single heavy quark (or antiquark) can be produced by a light-sector rotation followed by a global rotation, without changing the energy. In other words, in those sectors and for $s$-wave interactions, any SF-invariant interaction enjoys HQSS automatically. The hidden-charm sectors, in particular hidden-charm $N$ and $\Delta$

[3] However, all $c$ quarks present in the state, being identical particles, are rotated by a common rotation, and similarly for the $\bar{c}$.

resonances are studied in the Chapter 4[4].

It is perfectly possible to write down nontrivial models enjoying simultaneously SU(8) and HQSS invariances [namely, by requiring $\mathrm{SU}_q(8) \times \mathrm{SU}_{\bar{q}}(8)$], but they would not reduce to WT in the light sector. Concretely, SU(8)-WT conserves $C = N_c - N_{\bar{c}}$ but not $N_c$ and $N_{\bar{c}}$ separately. Of course, one could impose this by hand, but it is automatically taken care of by our modified interaction below [Eq. (2.30)]. Also, the restrictions of SU(8)-WT to the sectors $(N_c, N_{\bar{c}}) = (1,1), (2,1), (3,1), (4,1)$ turn out to violate HQSS.

In order to implement HQSS in the model let us analyze its content. We extract the trivial kinematic part and work directly in the space with only spin and flavor as degrees of freedom. The WT Hamiltonian with SF symmetry with four flavors takes the form of Eq. (2.17). This operator contains two distinct mechanisms which stem from expanding the meson commutator in Eq. (2.17),

$$\begin{aligned} H_{\mathrm{WT}} &= H_{\mathrm{ex}} + H_{\mathrm{ac}}, \\ H_{\mathrm{ex}} &= :M^A{}_C M^{\dagger C}{}_B B^{BDE} B^\dagger_{ADE}:, \\ H_{\mathrm{ac}} &= -:M^{\dagger A}{}_C M^C{}_B B^{BDE} B^\dagger_{ADE}:, \quad A,\ldots,E = 1,\ldots,2N_F. \end{aligned} \tag{2.22}$$

Here $M^A{}_B$ and $B^{ABC}$ are the annihilation operators of mesons and baryons, respectively, with $M^{\dagger A}{}_B = (M^B{}_A)^\dagger$, and $B^\dagger_{ABC} = (B^{ABC})^\dagger$, with $B^{ABC}$ being a completely symmetric tensor. The operators are normalized as

$$\begin{aligned} [M^A{}_B, M^{\dagger C}{}_D] &= \delta^A_D \delta^C_B, \\ \{B^{ABC}, B^\dagger_{A'B'C'}\} &= \delta^A_{A'}\delta^B_{B'}\delta^C_{C'} + \cdots \ \text{(six permutations)}. \end{aligned} \tag{2.23}$$

Note that in the SU(8)-WT model, the $\eta'$ [SU(8) singlet meson] does not couple and could be ignored; however, this meson has to be present in the corrected interaction since it mixes with the other mesons under HQSS.

Schematically, representing the quark and antiquark operators by $Q^A$ and $\bar{Q}_A$, one gets

$$M^A{}_B \sim Q^A \bar{Q}_B, \quad M^{\dagger A}{}_B \sim \bar{Q}^{\dagger A} Q^\dagger_B, \quad B^{ABC} \sim Q^A Q^B Q^C, \quad B^\dagger_{ABC} \sim Q^\dagger_A Q^\dagger_B Q^\dagger_C\ . \tag{2.24}$$

So, an upper index in $M$ or $B$ represents the SF of a quark to be annihilated, whereas in $M^\dagger$ it represents that of an antiquark to be created. Likewise, a lower index in $M^\dagger$ or $B^\dagger$ represents the SF of a quark to be created, while in $M$ it represents that of an antiquark to be annihilated. From this identification it is immediate to interpret the two mechanisms $H_{\mathrm{ex}}$ and $H_{\mathrm{ac}}$ in terms of quark and antiquark propagation.

The two mechanisms involved, $H_{\mathrm{ex}}$ and $H_{\mathrm{ac}}$ are displayed in Fig. 2.1. In $H_{\mathrm{ex}}$ (exchange) the quark with spin-flavor $A$ is transferred from the meson to the baryon, as is the quark with label $B$ from baryon to meson. On the other hand, in $H_{\mathrm{ac}}$ (annihilation-creation) an antiquark with spin-flavor $B$ in the meson annihilates with a similar quark in the baryon, with subsequent creation of a quark and an antiquark with spin-flavor $A$. In both mechanisms the quarks or antiquarks $C$, $D$ and $E$ are spectators from the point of their spin-flavor (the ubiquitous gluons are not explicit). Also in both mechanisms effectively a meson is exchanged. In passing, we note that the Okubo-Zweig-Iizuka (OZI) rule is automatically fulfilled with regards to the exchanged meson. OZI-rule-violating mechanisms would be of the type depicted in Fig. 2.2 and are not present in WT.

[4]In this thesis we refer collectively to the sectors with $(N_c, N_{\bar{c}}) = (1,1), (2,1), (3,1), (4,1)$ as sectors with "hidden charm", regardless of whether they have net charm or not.

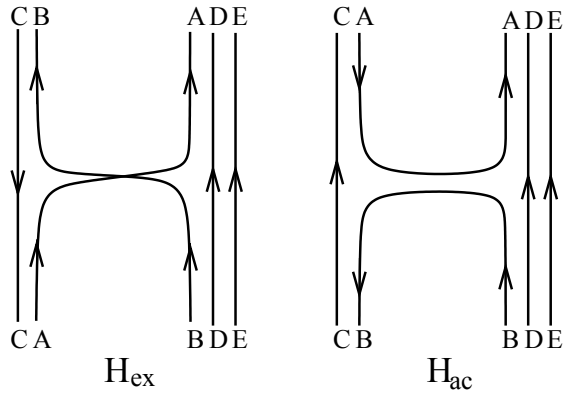


Figure 2.1: The two mechanisms acting in the SF extended WT interaction. $H_{\rm ex}$ (exchange of quarks) and $H_{\rm ac}$ (annihilation and creation of quark-antiquark pairs). In the HQSS corrected version of the interaction, Eq. (2.29), the labels $A$ and $B$ in $H_{\rm ac}$ only take light-flavor values.

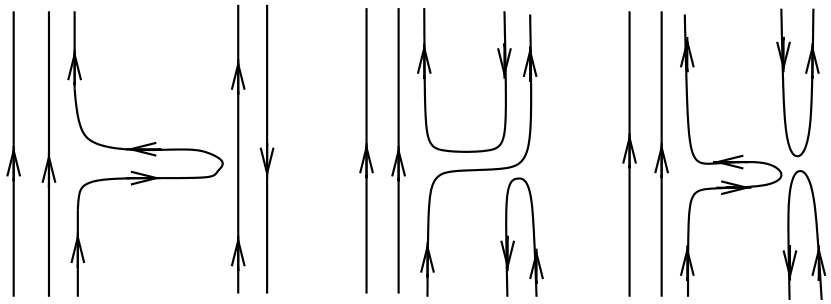

Figure 2.2: OZI-rule-violating mechanisms. Gluons are implicit.

It appears that $H_{\rm ac}$ can violate HQSS when the annihilation or creation of $q\bar{q}$ pairs involves heavy quarks, whereas $H_{\rm ex}$ would not be in conflict with HQSS. To expose this fact more clearly, let us consider the symmetries of these two interaction mechanisms. Let $N_F = 4$ and let $U$ be a matrix of SF SU(8). Upper indices transform with $U^\dagger$ and lower indices with $U$

$$\begin{aligned} &Q^A \to U^{\dagger A}{}_B Q^B, \quad \bar{Q}^{\dagger A} \to U^{\dagger A}{}_B \bar{Q}^{\dagger B}, \\ &\bar{Q}_A \to U^B{}_A \bar{Q}_B, \quad Q^\dagger_A \to U^B{}_A Q^\dagger_B. \end{aligned} \tag{2.25}$$

Therefore (with obvious matrix/tensor notation)

$$\begin{aligned} &M \to U^\dagger M U, \quad M^\dagger \to U^\dagger M^\dagger U, \\ &B \to (U^\dagger \otimes U^\dagger \otimes U^\dagger) B, \quad B^\dagger \to B^\dagger (U \otimes U \otimes U). \end{aligned} \tag{2.26}$$

The indices are so contracted that $H_{\rm ex}$ and $H_{\rm ac}$ are both invariant under these SU(8) transformations. However, HQSS requires also invariance when the charm quark and the charm antiquark receive different rotations. To examine this, let us consider the

transformation under $U \in \mathrm{SU}_q(8)$ and $\bar{U} \in \mathrm{SU}_{\bar{q}}(8)$, i.e., different transformations for quarks and antiquarks (previously $U = \bar{U}$). In this case

$$Q \to U^\dagger Q, \quad \bar{Q}^\dagger \to \bar{U}^\dagger \bar{Q}^\dagger, \quad \bar{Q} \to \bar{Q}\bar{U}, \quad Q^\dagger \to Q^\dagger U, \tag{2.27}$$

and therefore

$$\begin{aligned} &M \to U^\dagger M \bar{U}, \quad M^\dagger \to \bar{U}^\dagger M^\dagger U, \\ &B \to (U^\dagger \otimes U^\dagger \otimes U^\dagger) B, \quad B^\dagger \to B^\dagger (U \otimes U \otimes U). \end{aligned} \tag{2.28}$$

Clearly, the mechanism $H_{\mathrm{ex}}$, which depends on the combination $MM^\dagger$, is still invariant under this larger group, $\mathrm{SU}_q(8) \times \mathrm{SU}_{\bar{q}}(8)$.[5] It certainly preserves SF and HQSS. On the other hand, $H_{\mathrm{ac}}$ depends on the combination $M^\dagger M$, which transforms with $\bar{U}$, while $BB^\dagger$ transforms with $U$. $H_{\mathrm{ac}}$ is SF invariant ($U = \bar{U}$) but not HQSS invariant. A simple solution to enforce HQSS with minimal modifications is to remove just the offending contributions in $H_{\mathrm{ac}}$, which come from creation or annihilation of charm quark-antiquark pairs. This implies to remove the interaction when the labels $A$ or $B$ are of heavy type in $H_{\mathrm{ac}}$.[6] That is, we adopt the following modified version of the $H_{\mathrm{ac}}$ mechanism

$$H'_{\mathrm{ac}} = - : M^{\dagger \hat{A}}{}_C M^C{}_{\hat{B}} B^{\hat{B}DE} B^\dagger_{\hat{A}DE} :, \quad C, D, E = 1, \ldots, 8, \quad \hat{A}, \hat{B} = 1, \ldots, 6. \tag{2.29}$$

The indices with hats are restricted to SU(6). By construction $N_c$ and $N_{\bar{c}}$ are exactly conserved in $H'_{\mathrm{ac}}$. Also $\mathrm{SU}_c(2) \times \mathrm{SU}_{\bar{c}}(2)$ is conserved: when $U$ and $\bar{U}$ act only on the heavy sector, $M^{\dagger \hat{A}}{}_C M^C{}_{\hat{B}}$ and $B^{\hat{B}DE} B^\dagger_{\hat{A}DE}$ are unchanged, and therefore HQSS is preserved. On the other hand, when $U = \bar{U}$ and this matrix acts on the light sector, $H'_{\mathrm{ac}}$ is unchanged, so it enjoys SU(6) symmetry. Exact SF SU(8) and flavor SU(4) is no longer present. Presumably, this breaking of SU(4) is comparable to the breaking through the kinematics due to the substantially heavier mass of the charmed quark.

To summarize, our model (in all sectors) is defined by the modified interaction

$$H'_{\mathrm{WT}} = H_{\mathrm{ex}} + H'_{\mathrm{ac}}. \tag{2.30}$$

This model fulfills some desirable requirements: (i) it has symmetry SU(6) $\times$ HQSS, i.e., SF symmetry in the light sector and HQSS in the heavy sector, the two invariances being compatible, (ii) it reduces to SU(6)-WT in the light sector, so it is consistent with chiral symmetry in that sector, and (iii) is a minimal modification that preserves simplicity and does not introduce new adjustable parameters.

We can analyze the model in the different $(N_c, N_{\bar{c}})$ sectors, which, as already noted, do not mix due to HQSS. In all the sectors without hidden charm, namely, $(N_c, N_{\bar{c}}) = (0,1)$, $(0,0)$, $(1,0)$, $(2,0)$, $(3,0)$, $(4,0)$, $H'_{\mathrm{ac}}$ produces the same amplitudes as $H_{\mathrm{ac}}$ when the latter is restricted to the corresponding sector. Indeed, these interactions vanish unless the state contains a quark-antiquark pair with quark and antiquark of the same type. In the absence of hidden charm, the pair must be light and in this case the two operators produce

[5] Note that the commutation relations, Eq. (2.23), are also preserved by this symmetry.

[6] Keeping the contributions with $A = B$ of the heavy type would preserve $\mathrm{U}_c(1) \times \mathrm{U}_{\bar{c}}(1)$, i.e., conservation of $N_c$ and $N_{\bar{c}}$, but not $\mathrm{SU}_c(2) \times \mathrm{SU}_{\bar{c}}(2)$.

the same result. This is consistent with our previous observation that, when there are only heavy quarks or heavy antiquarks but not both, SF already implies HQSS. So in all these sectors, our model produces the same amplitudes as SU(8)-WT after removing channels involving hidden charm. This observation has been previously applied in [175, 176], and was used for studying charmed baryon resonances in Chapter 3 of this thesis.

It is noteworthy that in the sectors $(N_c, N_{\bar{c}}) = (0, 1)$ and $(4, 0)$, corresponding to $C = -1$ and $C = 4$, $H'_{\rm ac} = H_{\rm ac} = 0$, as they do not contain light quark-antiquark pairs. Also, these two sectors cannot couple to any other $(N_c, N_{\bar{c}})$ sector in the baryon-meson case. Therefore, for them our model coincides directly with SU(8)-WT.

Let us turn now to the sectors with hidden charm. These are $(N_c, N_{\bar{c}}) = (1, 1)$, $(2, 1)$, $(3, 1)$, $(4, 1)$. For all these sectors $H'_{\rm ac}$ vanishes. The reason is that in these sectors the relevant quark-antiquark pair (quark and antiquark with equal labels) is necessarily of heavy type, and such an amplitude has been removed from $H'_{\rm ac}$. (Note that $H_{\rm ac}$ does not vanish in these sectors.) So for the hidden-charm sectors $H'_{\rm WT}$ reduces to the exchange mechanism $H_{\rm ex}$.

After all the above considerations, the tree-level baryon-meson potential of the spin-flavor extended WT interaction with HQSS constraints reads [7]

$$V_{ab}^{IJSC}(\sqrt{s}) = D_{ab}^{IJSC}\frac{2\sqrt{s} - M_i - M_j}{4f_i f_j}\sqrt{\frac{E_i + M_i}{2M_i}}\sqrt{\frac{E_j + M_j}{2M_j}}, \tag{2.31}$$

similarly to Eq. (2.7) for SU(3) chiral scheme, or Eq. (2.15) and Eq. (2.16) for SU(6) model, where $IJSC$ are the baryon-meson isospin, total angular momentum, strangeness and charm quantum numbers respectively, $a$ and $b$ stand for the incoming and outgoing baryon-meson pairs, $M$ ($E$) is the mass (center-of-mass energy) of the baryon, and $f$ is the meson weak-decay constant (before implementing the SF symmetry breaking effects, the mass $M$ is averaged over the **120**, and $f$ over the **63** multiplets). Finally, $D_{ab}^{IJSC}$ are the matrix elements of $H'_{\rm WT}$ in Eq. (2.30) in a coupled-channel space. The $D$-matrices in the open-charm sectors are displayed in Appendix B, and those for the strangeless hidden charm $C = 0$ case, for which $H'_{\rm WT} = H_{\rm ex}$, are given in Appendix C.

## 2.2 Unitarization in coupled channels

### 2.2.1 The baryon-meson Bethe-Salpeter equation

The baryon-meson scattering amplitude is calculated using the Bethe-Salpeter (BS) equation [179]. The latter one was developed for describing bound states, in contrast to earlier techniques for scattering matrix calculations that were usually based on perturbation theory. As it will be discussed in Section 2.2.3, hadron resonances appear as poles of the scattering amplitude, and a finite sum of perturbative Feynman diagrams cannot create a pole, so one has to calculate an infinite number of such diagrams. The work of Bethe

[7] In Chapter 4, where we study the hidden-charm states, the potential was slightly modified to $V_{ij} = D_{ij}\,(k_i^0 + k_j'^0)/(4f_i f_j)$. The appropriate change of the factor $(E_i + M_i)/(2M_i)$ was done in the loop function, as discussed in Chapter 4.

and Salpeter provides an alternative technique to calculate scattering amplitudes, which considers an infinite number of rescattering diagrams [179].

The BS equation is an integral equation in momentum space, and omitting $C$, $S$, $I$, and $J$ labels, takes the form

$$\begin{aligned}\mathcal{T}_{ij}(k_i,k_j;P) =& V_{ij}(k_i,k_j;P)+ \\ & i\sum_l \int \frac{d^4k_l}{(2\pi)^4} V_{il}(k_i,k_l;P) D_B(k_l,P) D_m(k_l,P) \mathcal{T}_{lj}(k_l,k_j;P),\end{aligned} \tag{2.32}$$

where $k_i$ and $k_j$ are the relative initial and final four-momentum, $k_l$ is the four-momentum of the intermediate meson, and $P$ is the total four-momentum of the system. The sum over $l$ refers to the different coupled channels, while $V_{ij}$ is the kernel that describes the interaction between mesons and baryons. For this we use the WT SF extended potential described in the previous section [Eq. (2.31)]. Finally, the $D_B(k_l,P)$ and $D_m(k_l,P)$ functions are the baryon and the meson propagators, respectively.

The BS equation is tedious to solve due to its off-shell nature, and moreover, due to the poles along the integration contours contained in the meson and baryon propagators. Therefore, usually three-dimensional reductions are used, which are more practical for numerical solution. One of such approximations is the Lippmann-Schwinger equation [180]. The latter one can be obtained from the BS equation by integrating out the energy component of the intermediate meson $k_l^0$. In this thesis we make use of another method, which is the on-shell reduction of the BS equation. The on-shell formalism has been justified in Ref. [181] for the meson-meson interactions, and similarly used for the baryon-meson interaction in Ref. [47]. It turns out that when dealing only with the $s$-wave interaction, the on-shell information is sufficient. The potential can be split into an on-shell part and the rest. This second constituent gives rise to an amplitude with the same structure as the tree level one, and hence can be reabsorbed by a suitable renormalization of the masses and meson weak-decay constants. Therefore, the use of the physical values for the hadron masses and meson decay constants will incorporate these terms [47, 181].

The on-shell BS equation in coupled channels has the form

$$T_{ij} = (1 - V_{il}G^0_{ll})^{-1} V_{lj}, \tag{2.33}$$

where $G^0_{ll}$ is a diagonal matrix containing the baryon and meson propagators for each channel,

$$G^0_{ll} = i2M_l \int \frac{d^4k_l}{(2\pi)^4} \frac{1}{k_l^2 - m_l^2} \frac{1}{(P-k_l)^2 - M_l^2}. \tag{2.34}$$

The bare loop function $G^0_{ll}$ is logarithmically ultraviolet divergent and needs to be regularized. The following subsection is dedicated to the regularization procedure.

Note that the BS equation in coupled channels can be expressed in a compact form as

$$T = V + VGT, \tag{2.35}$$

where $T$ and $V$ are the scattering amplitude and potential, respectively, given by matrices, and $G$ is a diagonal matrix that accounts for the two-particle propagator of each channel. One can isolate the potential $V$ from Eq. (2.35) as $V = (1 - VG)T$, and multiplying by

the inverse matrix $1/V$, one obtains $T^{-1} = V^{-1} - G$. Given the previous expression, one can analyze the behavior of the $T$-matrix on the mass shell and whether the unitarity condition is fulfilled. The imaginary part of the inverse of the $T$-matrix is given by

$$-\mathrm{Im}T^{-1} = \mathrm{Im}G$$

due to the fact that the potential $V$ on the mass shell is real. From the last expression one can deduce

$$\mathrm{T} = T\mathrm{Im}GT^*,$$

which is the optical theorem. Thus, unitarity is fulfilled by the BS equation in coupled channels.

### 2.2.2 Loop regularization

In order to deal with the loop function, which is divergent, we use the one-subtraction regularization method at a subtraction point $\sqrt{s} = \mu$,

$$G_{ii}(s) = G^0_{ii}(s) - G^0_{ii}(\mu^2). \tag{2.36}$$

Here we adopt the prescription of [141], namely, $\mu$ depends only on $C$, $S$, and $I$, and equals $\sqrt{m^2_{\rm th} + M^2_{\rm th}}$, where $m_{\rm th}$ and $M_{\rm th}$ are, respectively, the masses of the meson and the baryon of the channel with the lowest threshold in the given $CSI$ sector. $G_{ii}$ is determined by the loop function $\bar{J}_0$ [53], that is

$$G_{ii}(s) = 2M_i(\bar{J}_0(s; M_i, m_i) - \bar{J}_0(\mu; M_i, m_i)), \tag{2.37}$$

with $\bar{J}_0$ given by

$$\bar{J}_0(s; M_i, m_i) = \frac{1}{(4\pi)^2}\left\{\left[\frac{M_i^2 - m_i^2}{s} - \frac{M_i - m_i}{M_i + m_i}\right]\ln\frac{M_i}{m_i} + L(s; M_i, m_i)\right\}, \tag{2.38}$$

$$L(s; M_i, m_i) \equiv L(s + i\epsilon; M_i, m_i) = \frac{\lambda^{1/2}(s, m_i^2, M_i^2)}{s}\left\{\ln\left[\frac{1 + \sqrt{\frac{s-s_+}{s-s_-}}}{1 - \sqrt{\frac{s-s_+}{s-s_-}}}\right] - i\pi\right\}, \tag{2.39}$$

where $\lambda(s, m_i^2, M_i^2)$ is the Källen triangle function,

$$\lambda(s, m_i^2, M_i^2) = s^2 + m_i^4 + M_i^4 - 2sm_i^2 - 2sM_i^2 - 2m_i^2M_i^2,$$

and the pseudothreshold $s_-$ and threshold $s_+$ variables are defined as

$$s_- = (m_i - M_i)^2, \quad s_+ = (m_i + M_i)^2, \tag{2.40}$$

while the logarithm is taken to be real. As we will discuss in the next subsection, for the study of bound states we need the analytical continuation of $L(z)$ in the complex energy plane. Thus, $L(z)$ reads

$$\begin{aligned} L(z, n) &= \frac{(\rho_+\rho_-)^{1/2}}{z}e^{i(\theta_+ + \theta_- + 2n\pi)/2}\{\ln|R(z)| + i\mathrm{Arg}[R(z)] - 2\pi i\}, \\ R(z) &= \frac{\rho_+^{1/2}e^{i\theta_+/2} + \rho_-^{1/2}e^{i\theta_-/2}e^{in\pi}}{\rho_+^{1/2}e^{i\theta_+/2} - \rho_-^{1/2}e^{i\theta_-/2}e^{in\pi}}, \end{aligned} \tag{2.41}$$

where $\rho_\pm = |z - s_\pm|$, $\theta_\pm$ of $|z - s_\pm|$ is defined to lie in the range $0 \leq \theta_+ < 2\pi$ and $-\pi \leq \theta_- < \pi$, whereas $\mathrm{Arg}[R(z)]$ is taken in the interval $]0, 2\pi]$ for $n = 0$ and in $[0, 2\pi[$ for $n = 1$. For $n = 0$ one gets the first Riemann sheet, which has a unitarity cut along the real axis $s_+ \leq s < \infty$. When crossing the unitary cut one jumps into the second Riemann sheet, $n = 1$. When looping twice around the threshold branch point $z = s_+$ the original Riemann sheet is reached again. Since we work in the coupled-channels frame, we have multiple Riemann sheets, as one crosses the mass thresholds of different coupled channels.

An enlightening discussion on the dependence of the loop function on the subtraction point has been presented in [64]. There, a natural value is introduced for the subtraction point, namely, the mass of the lightest baryon in the given coupled-channel sector (see [52] for an alternative definition of natural value). As argued in [64], the natural value does not need to coincide with the phenomenological one, and a comparison between both provides valuable information on the nature of the resonances generated dynamically, to wit, quark vs molecular structures. In the present work the phenomenological values, obtained from reproducing experimental data on the position of the resonances, are not available in general. With regard to the prescription of Ref. [141], this choice was justified by guaranteeing an approximate crossing symmetry although, as noted in [175], such a claim appears somewhat dubious because crossing symmetry involves isospin mixtures. Thus, choosing an alternative subtraction point might lead to yet another reasonable result. This prescription for the subtraction point was indeed used in the SU(6) model [171]. The SU(6) approach recovered previous results for the lowest-lying $1/2^-$ and $3/2^-$ baryon resonances appearing in the scattering of the octet of Goldstone bosons off the lowest baryon octet and decuplet given in Refs. [182, 183], and leads to new predictions for higher energy resonances, giving a phenomenological confirmation of its plausibility.

In Ref. [175] the value of the subtraction point was slightly modified to obtain the position of the $\Lambda_c(2595)$ resonance. In the present thesis the value has not been modified because, on the one hand, results for the resonances in $C = 1$, $S = 0$ sector did not change substantially by varying the value of the subtraction point and, on the other hand, there is scarce experimental information about resonances in the other strange and charm sectors beyond $C = 1$, $S = 0$. As we will see in Chapter 5, an exception is made for the bottom baryon resonances, also studied in this thesis, in particular for $J = 1/2$ and $J = 3/2$ resonances of $\Lambda_b$, in order to get better agreement between the masses predicted by our model and the ones found experimentally.

### 2.2.3 Resonances as poles of the scattering amplitude

The dynamically-generated baryon resonances[8] can be obtained as poles of the scattering amplitudes for given $CSIJ$ quantum numbers. One has to check both first and second Riemann sheets of the variable $\sqrt{s}$. The poles of the scattering amplitude on the first (physical) Riemann sheet (FRS) on the real axis that appear below threshold are interpreted as bound states. The poles that are found on the second (unphysical) Riemann sheet (SRS) below the real axis and above threshold are called resonances. The poles that appear elsewhere (later we will refer to these poles as the ones appearing in unphysical

[8]We remind the reader that we often refer to all poles generically as resonances.

regions of the Riemann surface) will be considered as artifacts. For any $CSIJ$ sector, there are as many branching points as channels involved, which implies a complicated geometry of the complex $s$-variable space [53].

The mass and the width of the resonances can be found from the position of the pole in the complex-energy plane. Close to the pole, the $T$-matrix behaves as

$$T_{ij}(s) \approx \frac{g_i g_j}{\sqrt{s} - \sqrt{s_R}} \,. \tag{2.42}$$

The mass and width of the resonance follow from $\sqrt{s_R} = m_R - \frac{i}{2}\Gamma_R$, while the constant $g_i$ is the coupling of the resonance to the $i$ channel, which is obtained from the behavior of $T_{ij}(s)$ around the pole [184] as

$$g_i = \left( \frac{\partial}{\partial \sqrt{s}} \frac{1}{T_{ii}(s)} \bigg|_{\sqrt{s}=\sqrt{s_R}} \right)^{-1/2} . \tag{2.43}$$

Since the dynamically-generated states may couple differently to their baryon-meson components, we will examine the $ij$-channel independent quantity

$$\tilde{T}^{IJSC}(s) \equiv \max \left\{ \sum_i |T^{IJSC}_{i1}(s)|, \;\; \sum_i |T^{IJSC}_{i2}(s)|, \;\; ... \;, \;\; \sum_i |T^{IJSC}_{in}(s)| \right\}, \tag{2.44}$$

where $n$ is a number of coupled channels, which allows us to identify all the resonances within a given sector at once.

## 2.3 Symmetry breaking

### 2.3.1 Open-charm sectors

In this section we introduce the symmetry breaking pattern in the open-charm sectors. As indicated in the previous section, we only keep channels without charmed antiquarks, so that the SU(8) WT interaction complies with HQSS. This means that we remove channels with extra $c\bar{c}$ pairs. Without removing coupled channels with $c\bar{c}$ in the open-charm sector, the matrix elements $D_{ij}$ [Eq. (2.31)] display exact SU(8) invariance. Such channels are heavier than the other ones, so they would be kinematically suppressed anyway. However, the suppression introduced by HQSS in the matrix elements is more severe and we simply take the infinite $c$-quark mass limit in those would-be couplings (but, of course, not in the charmed hadron masses).

In addition, several soft symmetry-breaking mechanisms are introduced. In the present work we use physical values for the masses of the hadrons and for the decay constants of the mesons, since we consider that baryon-meson states interact via a pointlike interaction given by the SU(8) model extension of the WT interaction modified according to the HQSS constraints. The values used in this work are quoted in Table 2.1. It was already checked in Ref. [171] that the SU(6) WT model leads to a reasonable description of the odd-parity light baryon resonances. Indeed, it is shown there that most of the low-lying three-

| Meson | mass | decay constant | SU(6) | SU(3) | HQSS | Baryon | mass | SU(6) | SU(3) | HQSS |
|---|---|---|---|---|---|---|---|---|---|---|
| $\pi$ | 138.03 | 92.4 | $\mathbf{35_{1,0}}$ | $\mathbf{8_1}$ | singlet | $N$ | 938.92 | $\mathbf{56_{1,0}}$ | $\mathbf{8_2}$ | singlet |
| $K$ | 495.68 | 113.0 | $\mathbf{35_{1,0}}$ | $\mathbf{8_1}$ | singlet | $\Lambda$ | 1115.68 | $\mathbf{56_{1,0}}$ | $\mathbf{8_2}$ | singlet |
| $\eta$ | 547.45 | 111.0 | $\mathbf{35_{1,0}}$ | $\mathbf{8_1}$ | singlet | $\Sigma$ | 1193.15 | $\mathbf{56_{1,0}}$ | $\mathbf{8_2}$ | singlet |
| $\rho$ | 775.49 | 153.0 | $\mathbf{35_{1,0}}$ | $\mathbf{8_3}$ | singlet | $\Xi$ | 1318.11 | $\mathbf{56_{1,0}}$ | $\mathbf{8_2}$ | singlet |
| $K^*$ | 893.88 | 153.0 | $\mathbf{35_{1,0}}$ | $\mathbf{8_3}$ | singlet | $\Delta$ | 1210.00 | $\mathbf{56_{1,0}}$ | $\mathbf{10_4}$ | singlet |
| $\omega$ | 782.57 | 138.0 | $\mathbf{35_{1,0}}$ | ideal | singlet | $\Sigma^*$ | 1384.57 | $\mathbf{56_{1,0}}$ | $\mathbf{10_4}$ | singlet |
| $\phi$ | 1019.46 | 163.0 | $\mathbf{35_{1,0}}$ | ideal | singlet | $\Xi^*$ | 1533.40 | $\mathbf{56_{1,0}}$ | $\mathbf{10_4}$ | singlet |
| $\eta'$ | 957.78 | 111.0 | $\mathbf{1_{1,0}}$ | $\mathbf{1_1}$ | singlet | $\Omega$ | 1672.45 | $\mathbf{56_{1,0}}$ | $\mathbf{10_4}$ | singlet |
| $D$ | 1867.23 | 157.4 | $\mathbf{6^*_{2,1}}$ | $\mathbf{3^*_1}$ | doublet | $\Lambda_c$ | 2286.46 | $\mathbf{21_{2,1}}$ | $\mathbf{3^*_2}$ | singlet |
| $D^*$ | 2008.35 | 157.4 | $\mathbf{6^*_{2,1}}$ | $\mathbf{3^*_3}$ | doublet | $\Xi_c$ | 2469.45 | $\mathbf{21_{2,1}}$ | $\mathbf{3^*_2}$ | singlet |
| $D_s$ | 1968.50 | 193.7 | $\mathbf{6^*_{2,1}}$ | $\mathbf{3^*_1}$ | doublet | $\Sigma_c$ | 2453.56 | $\mathbf{21_{2,1}}$ | $\mathbf{6_2}$ | doublet |
| $D_s^*$ | 2112.30 | 193.7 | $\mathbf{6^*_{2,1}}$ | $\mathbf{3^*_3}$ | doublet | $\Sigma_c^*$ | 2517.97 | $\mathbf{21_{2,1}}$ | $\mathbf{6_4}$ | doublet |
| $\eta_c$ | 2979.70 | 290.0 | $\mathbf{1_{1,0}}$ | $\mathbf{1_1}$ | doublet | $\Xi_c'$ | 2576.85 | $\mathbf{21_{2,1}}$ | $\mathbf{6_2}$ | doublet |
| $J/\psi$ | 3096.87 | 290.0 | $\mathbf{1_{3,0}}$ | $\mathbf{1_3}$ | doublet | $\Xi_c^*$ | 2646.35 | $\mathbf{21_{2,1}}$ | $\mathbf{6_4}$ | doublet |
| | | | | | | $\Omega_c$ | 2697.50 | $\mathbf{21_{2,1}}$ | $\mathbf{6_2}$ | doublet |
| | | | | | | $\Omega_c^*$ | 2768.30 | $\mathbf{21_{2,1}}$ | $\mathbf{6_4}$ | doublet |
| | | | | | | $\Xi_{cc}$ | 3519.00 | $\mathbf{6_{3,2}}$ | $\mathbf{3_2}$ | doublet |
| | | | | | | $\Xi_{cc}^*$ | 3600.00 | $\mathbf{6_{3,2}}$ | $\mathbf{3_4}$ | doublet |
| | | | | | | $\Omega_{cc}$ | 3712.00 | $\mathbf{6_{3,2}}$ | $\mathbf{3_2}$ | doublet |
| | | | | | | $\Omega_{cc}^*$ | 3795.00 | $\mathbf{6_{3,2}}$ | $\mathbf{3_4}$ | doublet |
| | | | | | | $\Omega_{ccc}$ | 4799.00 | $\mathbf{1_{4,3}}$ | $\mathbf{1_4}$ | singlet |

Table 2.1: Baryon masses, $M_i$, and meson masses, $m_i$, and decay constants $f_i$, (in MeV) used throughout this work. The masses are taken from the PDG [4], except the masses for $\Xi_{cc}^*$, $\Omega_{cc}$, $\Omega_{cc}^*$, and $\Omega_{ccc}$. While $\Xi_{cc}^*$ is obtained from $\Xi_{cc}$ by adding 80 MeV, similarly to the $\Xi_c' - \Xi_c^*$ mass splitting, the masses for $\Omega_{cc}$, $\Omega_{cc}^*$ are given in Ref. [185] and for $\Omega_{ccc}$ in Ref. [186]. The decay constants $f_i$ are taken from Ref. [175], except for $f_{\eta_c}$ and $f_{J/\Psi}$. We take $f_{J/\Psi}$ from the width of the $J/\Psi \to e^- e^+$ decay and we set $f_{\eta_c} = f_{J/\Psi}$, as predicted by HQSS and corroborated in the lattice evaluation of Ref. [187]. The SU(6) $\times$ SU$_C$(2) $\times$ U$_C$(1) and SU(3) $\times$ SU(2) labels are also displayed. The last column indicates the HQSS multiplets. Members of a doublet are placed in consecutive rows.

and four-star odd-parity baryon resonances with spin 1/2 and 3/2 can be dynamically-generated within this scheme.

The symmetry breaking pattern, with regards to flavor, follows the chain SU(8) $\supset$ SU(6) $\supset$ SU(3) $\supset$ SU(2), where the last group refers to isospin. To tag the resonances with these quantum numbers, we start from the SU(8)-symmetric scenario, where hadrons in the same SU(8) multiplet share common properties (mass and decay constants). As seen in Section 2.1.3, the **120** and **168** multiplets are attractive and, thus, a single resonance for the **120**-irrep and another for the **168**-irrep are produced. Subsequently, the SU(8) $\supset$ SU(6) breaking is introduced by means of a deformation of the mass and decay constant

parameters. Specifically, we use

$$\begin{aligned} m(x) &= (1-x)m_{\mathrm{SU}(8)} + x\, m_{\mathrm{SU}(6)}, \\ f(x) &= (1-x)f_{\mathrm{SU}(8)} + x\, f_{\mathrm{SU}(6)}. \end{aligned} \tag{2.45}$$

The parameter $x$ runs from 0 [SU(8)-symmetric scenario] to 1 [SU(6)-symmetric scenario]. The symmetric masses and decay constants are assigned by taking an average over the corresponding multiplet. The same procedure is applied to the symmetry breakings SU(6) $\supset$ SU(3) and SU(3) $\supset$ SU(2), with

$$\begin{aligned} m(x') &= (1-x')m_{\mathrm{SU}(6)} + x'\, m_{\mathrm{SU}(3)}, \\ f(x') &= (1-x')f_{\mathrm{SU}(6)} + x'\, f_{\mathrm{SU}(3)}, \end{aligned} \tag{2.46}$$

and

$$\begin{aligned} m(x'') &= (1-x'')m_{\mathrm{SU}(3)} + x''\, m_{\mathrm{SU}(2)}, \\ f(x'') &= (1-x'')f_{\mathrm{SU}(3)} + x''\, f_{\mathrm{SU}(2)}. \end{aligned} \tag{2.47}$$

It should be noted that SU(6) and SU(3), as well as HQSS, are broken only kinematically, through masses and meson decay constants. On the other hand, the breaking of SU(8) comes also from the interaction matrix elements, since we have truncated the SU(8) multiplets by removing channels with $c\bar{c}$ pairs, in order to enforce HQSS. Nevertheless, it is important in our scheme to have SU(8) assignments to be able to isolate the dominant **168** and **120** SU(8) irreps, and to get rid of the subdominant and exotic **4752**. Therefore, instead of starting from an SU(6) $\times$ HQSS symmetric scenario, we find it preferable to start from a SU(8) symmetric world, and let the charmed quarks mass get heavier. In this way the offending channels with $c\bar{c}$ pairs tend to decouple kinematically as we approach the physical point. At the end, we remove those channels and this introduces relatively small changes for the low-lying resonances that we are studying.

The procedure just described allows us to assign well-defined SU(8), SU(6), and SU(3) labels to the resonances. We show the reduction of the most attractive **120** and **168** multiplets of baryon resonances to the SU(6) representations, and the following reduction to the SU(3) multiplets in Section 3.1, while the corresponding number of the expected states is compiled in Table 3.1 of the same section. Conceivably the labels could depend on the precise choice of symmetric points, or change if different paths in the parameter manifold were followed, but this seems unlikely. At the same time, the HQSS multiplets form themselves at the physical point, since this symmetry is present in the interaction, and also, approximately, in the properties of the ground-state hadrons. In order to unambiguously identify those multiplets, one simply has to adiabatically move to the HQSS point, by imposing exact HQSS in the masses and decay constants of the basic hadrons. The members of a multiplet become exactly degenerate under this test.

Because light SF and HQSS are independent symmetries, the members of a HQSS multiplet always have equal SU(6), SU(3), and SU(2) labels. Quite often, the SU(8) label is also shared by the members of a HQSS multiplet, but not always, since this property is not ensured by construction.[9]

[9]Note that if HQSS were an exact symmetry of the basic hadrons, we could move from the physical

### 2.3.2 Hidden-charm sectors

In the sectors with hidden charm we also break the symmetry to SU(2), but in a different way.[10] We classify states under the symmetry group SU(6) × HQSS, as the SU(8) spin-flavor symmetry is not present in these sectors, and consider the breaking of the light SF SU(6) to SU(3) × $\mathrm{SU}_{J_l}(2)$ ($\mathrm{SU}_{J_l}(2)$ is a group of spin rotations of the light quarks). Subsequently we break the SU(3) light flavor group to SU(2) isospin symmetry group, preserving the HQSS, and finally we break the HQSS. The symmetry breaking is performed by an adiabatic change of hadron masses and meson weak-decay constants, in a similar way as in the previous subsection for open-charm sectors: at each symmetric point, the hadron masses and meson decay constants are averaged over the corresponding group multiplets. We again introduce three parameters, $x, x'$, and $x''$ that are changed from 0 to 1, to gradually break the symmetry from SU(6) × HQSS down to SU(3) × HQSS, then to SU(2) × HQSS, and finally down to SU(2) isospin, respectively:

$$\begin{aligned}
m(x) &= (1-x)\; m_{\mathrm{SU(6)\times HQSS}} + x\; m_{\mathrm{SU(3)\times HQSS}},\\
f(x) &= (1-x)\; f_{\mathrm{SU(6)\times HQSS}} + x\; f_{\mathrm{SU(3)\times HQSS}},\\
m(x') &= (1-x')\; m_{\mathrm{SU(3)\times HQSS}} + x'\; m_{\mathrm{SU(2)\times HQSS}},\\
f(x') &= (1-x')\; f_{\mathrm{SU(3)\times HQSS}} + x'\; f_{\mathrm{SU(2)\times HQSS}},\\
m(x'') &= (1-x'')\; m_{\mathrm{SU(2)\times HQSS}} + x''\; m_{\mathrm{SU(2)}},\\
f(x'') &= (1-x'')\; f_{\mathrm{SU(2)\times HQSS}} + x''\; f_{\mathrm{SU(2)}}.
\end{aligned} \tag{2.48}$$

In this way we can assign appropriate group representation labels to each found resonance, and also identify the HQSS multiplets. In Chapter 4 we show a diagram (Fig. 4.1) with the evolution of the hidden charm $N$ and $\Delta$ pole positions as the various symmetries are gradually broken.

## 2.4 Summary

In this chapter we have presented a phenomenological model within a coupled-channels unitary approach that implements the characteristic features of HQSS. This implies, for instance, that $D$ and $D^*$ mesons have to be treated on an equal footing and that channels containing a different number of $c$ or $\bar{c}$ quarks cannot be coupled. This is accomplished by extending the SU(3) WT chiral interaction to SF symmetric model for four flavors modified with HQSS constraints, and implementing a strong flavor symmetry breaking. Thus, our tree-level $s$-wave WT amplitudes are obtained not only by adopting the physical hadron masses, but also by introducing the physical weak-decay constants of the mesons involved in the transitions. With this interaction, we solve the BS equation in coupled channels to find the corresponding scattering amplitudes. For renormalization of the UV divergent baryon-meson loop function in the BS equation, we adopt the prescription of

point to the SU(6) symmetric point while preserving HQSS all the way. However, to reach the SU(8) symmetric point would require to restore channels with $c\bar{c}$ pairs, breaking HQSS, and in this way members of a common HQSS can end up in different SU(8) irreps.

[10] Chapter 4 is based on Ref. [188], so here we keep the same symmetry-breaking pattern as was used in this reference.

Ref. [141]. It amounts to force the renormalized loop function to vanish at certain scale that depends only on $CSI$. In this manner, we have no free parameters. We have then analyzed the symmetry breaking pattern for open-charm and hidden-charm sectors to SU(2) isospin symmetry.

# Chapter 3

# Charmed and strange baryon resonances[1]

In this chapter we study the dynamically-generated states obtained in the different charm and strange sectors. We have assigned to some of the found states a tentative identification with known states from the PDG [4]. This identification is made by comparing the data from the PDG on these states with the information we extract from the poles, namely the mass, width and, most important, the couplings. The couplings give us valuable information on the structure of the state and on the possible decay channels and their relative strength. Many of our dynamically-generated resonances do not have a straightforward identification and, thus, are predictions of our model, which require new experimental data. In this respect the scientific program of PANDA at the future facility FAIR is of particular relevance.

We start by showing the group reductions of the SU(8) multiplets to the SU(6) and SU(3) ones. From such analysis we find a number of expected states in each $CSIJ$ sector. In Sections 3.2 - 3.8 we discuss the obtained dynamically-generated baryon resonances. The masses, widths, and main couplings of the resonances found are displayed in Tables 3.2-3.9, which are organized according to the quantum numbers $CSI$. States with equal $CSI$ and spin $J = 1/2$ and $J = 3/2$ have been collected together in order to indicate which states belong to the same HQSS multiplets. As a rule, two states with $J = 1/2$ and $J = 3/2$ and equal SU(8), SU(6), and SU(3) labels form a HQSS doublet [with one exception in the case of the SU(8) label for $\Xi_{cc}$ resonances, as is shown below in Table 3.7]. The other states are HQSS singlets.

In what follows, we occasionally use an asterisk in the symbol of the states to indicate that a resonance has spin $J = 3/2$. For instance, $\Lambda_c^*$ denotes a state with $CSIJ = (1, 0, 1/2, 3/2)$. The symbol without asterisk may refer to the generic case or to the $J = 1/2$ case.

[1]This chapter is based on O. Romanets, L. Tolos, C. Garcia-Recio, J. Nieves, L. L. Salcedo, and R. G. E. Timmermans, Phys. Rev. D **85**, 114032 (2012) (Ref. [177]).

## 3.1 Analysis of the symmetry multiplets reduction in open-charm sectors with $C = 1,\ 2,\ 3$

As was mentioned in Section 2.1.3 of the previous chapter, the baryon-meson space reduces into four SU(8) group representations (Eq. 2.21): the two multiplets **120** and **168** are the most attractive ones, while the **4752**-plet is weakly attractive and the **2520**-plet is repulsive. Moreover, in the large-$N_C$ limit, the **4752** states are expected to disappear [172]. As a consequence, dynamically-generated baryon resonances are most likely to occur within the **120** and **168** sectors. Besides, as the interaction in the **4752** subspace is weak, small corrections (higher orders in the expansion, $d$-wave terms, etc) could strongly modify the properties of the states that belong to this representation. Therefore, we study baryon resonances that belong to these two most attractive **120** and **168** representations.

To take into account the breaking of flavor symmetry introduced by the heavy charmed quark, we consider the reduction

$$\mathrm{SU}(8) \supset \mathrm{SU}(6) \times \mathrm{SU}_C(2) \times \mathrm{U}_C(1), \tag{3.1}$$

where SU(6) is the spin-flavor group for three flavors, and $\mathrm{SU}_C(2)$ is the rotation group of quarks with charm. We consider only $s$-wave interactions, so $\boldsymbol{J}_C$ is just the spin carried by the charmed quarks or antiquarks. Finally, $U_C(1)$ is the group generated by the charm quantum number $C$.

The two most attractive SU(8) multiplets have the reductions

$$\begin{aligned} \mathbf{120} &= \mathbf{56_{1,0}} \oplus \mathbf{21_{2,1}} \oplus \mathbf{6_{3,2}} \oplus \mathbf{1_{4,3}}, \\ \mathbf{168} &= \mathbf{70_{1,0}} \oplus \mathbf{21_{2,1}} \oplus \mathbf{15_{2,1}} \oplus \mathbf{6_{1,2}} \oplus \mathbf{6_{3,2}} \oplus \mathbf{1_{2,3}}. \end{aligned} \tag{3.2}$$

For the right-hand side we use the notation $\boldsymbol{R}_{2J_C+1,C}$, where $\boldsymbol{R}$ is the SU(6) irrep label (for which we use the dimension), $J_C$ is the spin carried by the quarks with charm, and $C$ is the charm. Therefore, with $C = 1$ there are two $\mathbf{21_{2,1}}$: one from **120** and another one from **168**, and one $\mathbf{15_{2,1}}$ only from **168**. With $C = 2$ there are two $\mathbf{6_{3,2}}$: one from each SU(8) irrep, and one $\mathbf{6_{1,2}}$ from **168**. Finally, there are two representations with $C = 3$: $\mathbf{1_{4,3}}$ and $\mathbf{1_{2,3}}$.

The SU(6) multiplets can be reduced under $\mathrm{SU}(3) \times \mathrm{SU}_l(2)$. The factor $\mathrm{SU}_l(2)$ refers to the spin of the light quarks (i.e., with flavors $u$, $d$, and $s$). In order to connect with the labeling $(C, S, I, J)$ based on isospin multiplets, we further reduce $\mathrm{SU}_l(2) \times \mathrm{SU}_C(2) \supset \mathrm{SU}(2)$, where SU(2) refers to the total spin $J$, that is, we couple the spins of light and charmed quarks to form SU(3) multiplets with well-defined $J$. So, for instance, the multiplet $\mathbf{21_{2,1}}$ reduces as $\mathbf{6_2} \oplus \mathbf{3_2^*} \oplus \mathbf{6_4}$, where we use the notation $\boldsymbol{r}_{2J+1}$ and $\boldsymbol{r}$ stands for the SU(3) irrep. Indeed, the $\mathbf{21_{2,1}}$ irrep can be realized by a baryon with quark structure $llc$ with the two light quarks in a symmetric spin-flavor state. In the light sector, and from the point of view of SU(3), this is $(\mathbf{3_2} \otimes \mathbf{3_2})_s = \mathbf{6}_3 \oplus \mathbf{3_1^*}$, the subindex being $2J_l + 1$. The coupling of $J_l = 0, 1$ with $J_C = 1/2$ gives the decomposition quoted in the text. The $\mathbf{15_{2,1}}$ reduction follows similarly, but the pair $ll$ is antisymmetric. The charmed SU(6)

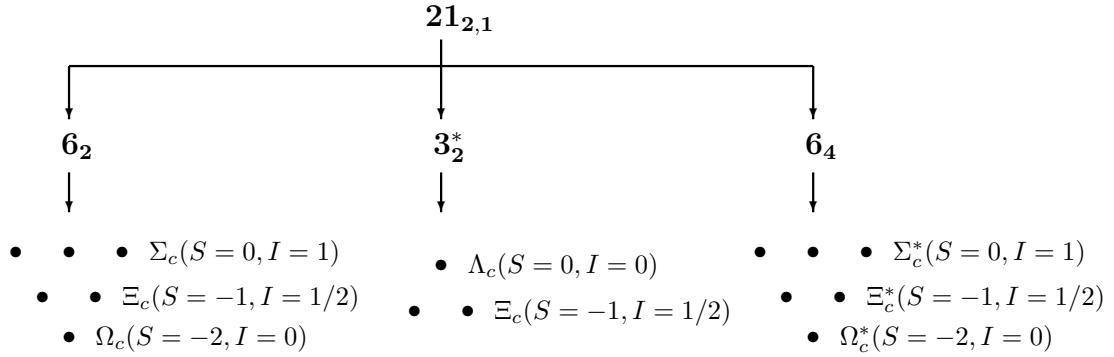


Figure 3.1: SU(3) × SU(2) reduction of the $\mathbf{21_{2,1}}$ multiplet of SU(6) × SU$_C$(2) × U$_C$(1).

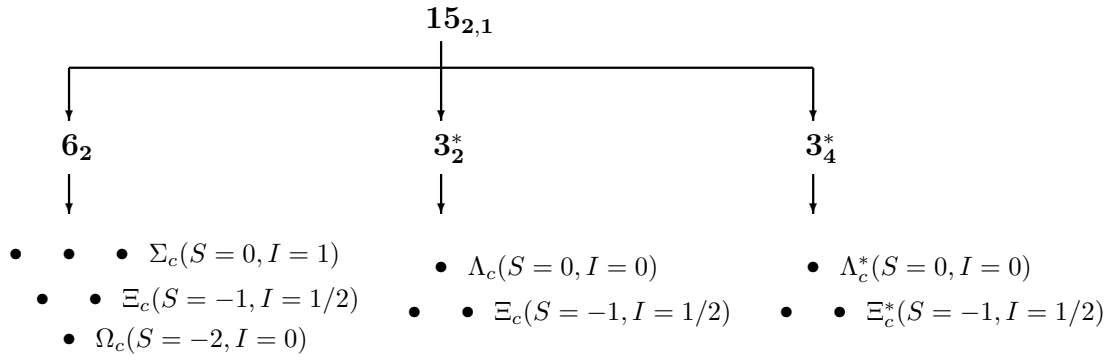


Figure 3.2: SU(3) × SU(2) reduction of the $\mathbf{15_{2,1}}$ multiplet of SU(6) × SU$_C$(2) × U$_C$(1).

multiplets reduce as

$$\begin{aligned}
\mathbf{21_{2,1}} &= \mathbf{6_2} \oplus \mathbf{3_2^*} \oplus \mathbf{6_4}, \\
\mathbf{15_{2,1}} &= \mathbf{6_2} \oplus \mathbf{3_2^*} \oplus \mathbf{3_4^*}, \\
\mathbf{6_{3,2}} &= \mathbf{3_2} \oplus \mathbf{3_4}, \\
\mathbf{6_{1,2}} &= \mathbf{3_2}, \\
\mathbf{1_{2,3}} &= \mathbf{1_2}, \\
\mathbf{1_{4,3}} &= \mathbf{1_4}.
\end{aligned} \tag{3.3}$$

The decomposition of the SU(6) × SU$_C$(2) × U$_C$(1) multiplets under SU(3) × SU(2) is shown in Figs. 3.1, 3.2, 3.3 for the multiplets in Eq. (3.2) with $C = 1, 2, 3$ (except the singlets). The further reduction into $(C, S, I, J)$ multiplets is also displayed.

Collecting the various $CSIJ$ multiplets in the strongly attractive representations **120** and **168**, we can estimate the expected number of dynamically-generated baryon-meson resonances [Eqs. (3.2), (3.3)]. These expected numbers of states are shown in Table 3.1. In this chapter we show the results of the model in the open-charm sectors, and we find that none of these states for the sectors with charm goes to an unphysical region of the Riemann surface in the complex $s$-plane, and so they can be identified with physical

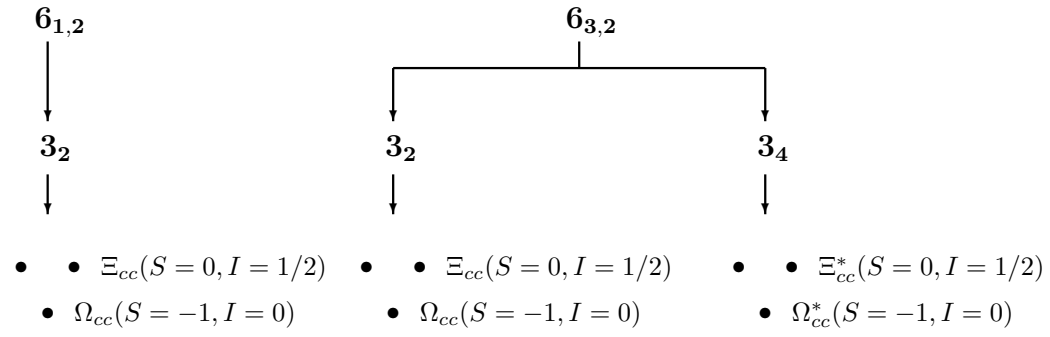


Figure 3.3: SU(3) × SU(2) reduction of the multiplets $\mathbf{6_{3,2}}$ and $\mathbf{6_{1,2}}$ of SU(6) × $\mathrm{SU}_C(2)$ × $\mathrm{U}_C(1)$.

states.[2]

| $C$ | $S$ | $I$ | state | $J^P$ $\frac{1}{2}^-$ | $J^P$ $\frac{3}{2}^-$ |
|---|---|---|---|---|---|
| 1 | 0 | 0 | $\Lambda_c$ | 3 | 1 |
| | | 1 | $\Sigma_c$ | 3 | 2 |
| | −1 | 1/2 | $\Xi_c$ | 6 | 3 |
| | −2 | 0 | $\Omega_c$ | 3 | 2 |
| 2 | 0 | 1/2 | $\Xi_{cc}$ | 3 | 2 |
| | −1 | 0 | $\Omega_{cc}$ | 3 | 2 |
| 3 | 0 | 0 | $\Omega_{ccc}$ | 1 | 1 |

Table 3.1: Expected number of baryonic resonances for the various $CSIJ$ sectors.

It should be stressed that there will be mixings between states with the same $CSIJ$ quantum numbers but belonging to different SU(8), SU(6), and/or SU(3) multiplets, since these symmetries are broken both within our approach and in nature. Additional breaking of SU(8) [and SU(6) and SU(3)] is expected to take place not only in the kinematics but also in the interaction amplitudes. This will occur when using more sophisticated models going beyond the lowest order retained here.

As a final comment, it should be mentioned that the SU(6) irrep $\mathbf{56_{1,0}}$ in Eq. (3.2) does not exactly coincide with the usual **56** irrep that one finds in spin-flavor with only $u$, $d$, and $s$ flavors. The latter is completely charmless, while the states in $\mathbf{56_{1,0}}$ contain hidden-charm components in general. Actually, in the SU(8) case, there are further $\mathbf{56_{1,0}}$ irreps (in **2520** or **4752**). Using a suitable angular mixing [similar to the ideal mixing in SU(3)] one can recover the purely charmless $\mathbf{56_{1,0}}$ and construct another $\mathbf{56_{1,0}}$ of the form $|lll\rangle\,|c\bar{c}\rangle$ ($l$ standing for light quarks). When the hidden charm components are dropped,

[2]This is not always the case, for instance in [59,171], some resonances move to unphysical regions of the Riemann surface after breaking the symmetry.

one $\mathbf{56_{1,0}}$ combination remains while the other one disappears. These considerations can be extended to the other irreps in Eq. (3.2). This explains why, when dropping the hidden-charm components, we still get the same number of expected states quoted in Table 3.1, even if the total dimension of the full baryon-meson space is reduced.

## 3.2 $\mathbf{\Lambda}_c$ states ($\boldsymbol{C=1}$, $\boldsymbol{S=0}$, $\boldsymbol{I=0}$)

In this section we present the poles obtained in the $C = 1$, $S = 0$, and $I = 0$ sector coming from the **120** and **168** SU(8) representations. Moreover, we determine the coupling constants to the various baryon-meson channels through the residues of the corresponding scattering amplitudes, as in Eq. (2.42), and we are able to assign SU(8), SU(6), and SU(3) labels to the resonances. Simultaneously, we also classify the resonances into HQSS multiplets, in practice doublets and singlets. This is of great interest as this symmetry is less broken than spin-flavor, being of a quality comparable to flavor SU(3).

### 3.2.1 Sector $J = 1/2$

In the sector $C = 1$, $S = 0$, $I = 0$, $J = 1/2$, there are 16 channels (the threshold energies, in MeV, are shown below each channel):

| | | | | | | | |
|---|---|---|---|---|---|---|---|
| $\Sigma_c\pi$ | $ND$ | $\Lambda_c\eta$ | $ND^*$ | $\Xi_cK$ | $\Lambda_c\omega$ | $\Xi_c'K$ | $\Lambda D_s$ |
| 2591.6, | 2806.1, | 2833.9, | 2947.3, | 2965.1, | 3069.0, | 3072.5, | 3084.2, |
| $\Lambda D_s^*$ | $\Sigma_c\rho$ | $\Lambda_c\eta'$ | $\Sigma_c^*\rho$ | $\Lambda_c\phi$ | $\Xi_cK^*$ | $\Xi_c'K^*$ | $\Xi_c^*K^*$ |
| 3228.0, | 3229.0, | 3244.2, | 3293.5, | 3305.9, | 3363.3, | 3470.7, | 3540.2. |

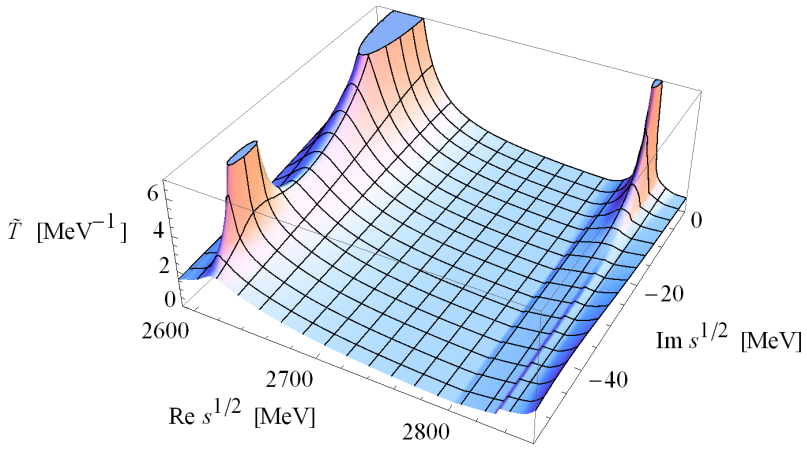


Figure 3.4: $\tilde{T}^{I=0,\ J=\frac{1}{2},\ S=0,\ C=1}(s)$ amplitude ($\Lambda_c$ resonances).

The dynamically-generated states are shown in Table 3.2. We obtain the three lowest-lying states as reported in Ref. [175] and later obtained in Ref [177]. In Ref. [175] an extension of the Weinberg-Tomozawa potential to the SU(8) spin-flavor symmetry was

| SU(8) irrep | SU(6) irrep | SU(3) irrep | $M_R$ | $\Gamma_R$ | Couplings to main channels | Status PDG | $J$ |
|---|---|---|---|---|---|---|---|
| **168** | $\mathbf{15_{2,1}}$ | $\mathbf{3^*_2}$ | 2617.3 | 89.8 | $\boldsymbol{g_{\Sigma_c\pi}=2.3}$, $g_{ND}=1.6$, $g_{ND^*}=1.4$, $g_{\Sigma_c\rho}=1.3$ | | 1/2 |
| **168** | $\mathbf{15_{2,1}}$ | $\mathbf{3^*_4}$ | 2666.6 | 53.7 | $\boldsymbol{g_{\Sigma_c^*\pi}=2.2}$, $g_{ND^*}=2.0$, $g_{\Sigma_c\rho}=0.8$, $g_{\Sigma_c^*\rho}=1.3$ | $\Lambda_c(2625)$ *** | 3/2 |
| **168** | $\mathbf{21_{2,1}}$ | $\mathbf{3^*_2}$ | 2618.8 | 1.2 | $\boldsymbol{g_{\Sigma_c\pi}=0.3}$, $g_{ND}=3.5$, $g_{ND^*}=5.6$, $g_{\Lambda D_s}=1.4$, $g_{\Lambda D_s^*}=2.9$, $g_{\Lambda_c\eta'}=0.9$ | $\Lambda_c(2595)$ *** | 1/2 |
| **120** | $\mathbf{21_{2,1}}$ | $\mathbf{3^*_2}$ | 2828.4 | 0.8 | $\boldsymbol{g_{ND}=0.3}$, $g_{\Lambda_c\eta}=1.1$, $g_{\Xi_cK}=1.6$, $g_{\Lambda D_s^*}=1.1$, $g_{\Sigma_c\rho}=1.1$, $g_{\Sigma_c^*\rho}=1.0$, $g_{\Xi_c^*K^*}=0.8$ | | 1/2 |

Table 3.2: $\Lambda_c$ ($J=1/2$) and $\Lambda_c^*$ ($J=3/2$) resonances predicted by our model in the **168** and **120** SU(8) irreps. The first three columns contain the SU(8), SU(6), and SU(3) representations of the corresponding state. $M_R$ and $\Gamma_R$ stand for the mass and width of the state, in MeV.[a] The next column displays the dominant couplings to the channels, ordered by their threshold energies. In boldface we indicate the channels which are open for decay. The last column shows the spin of the resonance. Pairs of states with $J=1/2$ and 3/2 and equal SU(8), SU(6), and SU(3) labels form HQSS doublets. They are displayed in consecutive rows. Tentative identifications with PDG resonances are shown when possible.

[a]We show the values for the masses and widths up to one significant digit in order to compare with predictions of other theoretical models. However, note that changes in the subtraction point within reasonable limits can account for changes in the mass and width of the predicted states by a few tens of MeV's.

used, as well as the Bethe-Salpeter equation in coupled channels, in the similar way as it is done in this thesis; it was applied to study the dynamically-generated baryon resonances with $C=1$ and $S=0$ in all possible isospin-spin sectors. However, the analysis of the dynamically-generated states in terms of the attractive SU(8) $\supset$ SU(6) $\supset$ SU(3) $\supset$ SU(2) multiplets was not done in Ref. [175]. We display in Fig. 3.4 the channel-independent scattering amplitude defined in Eq. (2.44) in the second Riemann sheet for this sector, where these three poles clearly show up. However, those states appear with slightly different masses as compared to Ref. [175]. The reason is that the subtraction point was slightly changed in this previous work in order to reproduce the position of the $\Lambda_c(2595)$ [4, 102, 103, 109, 189]. The same scaling factor for the subtraction point was introduced in all the sectors in [175]. Another difference with [175] is that there the value $f_{D_s^*}=f_{D^*}=157.4$ MeV was used, whereas here we use the more realistic value $f_{D_s^*}=f_{D_s}=193.7$ MeV. Indeed, the value of $f_{D_s}$ is known experimentally [110], and the $D_s$ and $D_s^*$ mesons are connected by the HQSS. These two modifications will affect the comparison with other sectors too. A permutation on the order of the two first resonances as compared to Ref. [175] is also observed.

The experimental $\Lambda_c(2595)$ resonance can be identified with the $\mathbf{21}_{2,1}$ pole that we found around 2618.8 MeV, as similarly done in Ref. [175]. The width in our case is,

however, bigger due to the increase of the phase space available for decay. As indicated in Ref. [175], we have not included the three-body decay channel $\Lambda_c\pi\pi$, which already represents almost one third of the decay events [4]. Therefore, the experimental value of $3.6^{+2.0}_{-1.3}$ MeV is still not reproduced. Our result for $\Lambda_c(2595)$ agrees with previous works on $t$-channel vector-meson exchange models [137, 141, 144, 146], but here as was first pointed out in Ref. [175], we claim a large (dominant) $ND^*$ component in its structure. This is in sharp contrast with the findings of the former references, where it was generated mostly as one $ND$ bound state.

In Fig. 3.4, we also observe a second broad resonance at 2617.3 MeV with a large coupling to the open channel $\Sigma_c\pi$, very close to $\Lambda_c(2595)$. This is precisely the same two-pole pattern found in the charmless $I=0, S=-1$ sector for the $\Lambda(1405)$ [38, 56, 59].

As discussed in Ref. [175], the pole found at around 2828 MeV, and stemming from the **120** SU(8) irreducible representation, mainly originates from a strong attraction in the $\Xi_c K$ channel but it cannot be assigned to the $\Lambda_c(2880)$ [4, 104–106] because of the spin-parity determined by the Belle collaboration.

Some of the states found have coupling to channels with hadrons which are themselves resonances, like $\Delta$ or $\rho$. Their widths can be taken into account in the calculation by doing a convolution of the loop function of the channel that contains these states with their spectral functions, as done for instance in [73] and [176]:

$$\tilde{G}_{ii}(s; M_i, m_i) = \frac{1}{N}\int_{(m_i-2\Gamma_i)^2}^{(m_i+2\Gamma_i)^2} d\tilde{M}^2 \mathcal{S}(\tilde{M}^2, m_i, \Gamma_i) G_{ii}(s; M_i, \tilde{m}_i), \tag{3.4}$$

with $m_i$ and $\Gamma_i$ being the mass and the width of the resonance, respectively, with the normalization factor and spectral function

$$\begin{aligned} N &= \int_{(m_i-2\Gamma_i)^2}^{(m_i+2\Gamma_i)^2} d\tilde{M}^2 \mathcal{S}(\tilde{M}^2, m_i, \Gamma_i), \\ \mathcal{S}(\tilde{M}^2, m_i, \Gamma_i) &= -\frac{1}{\pi}\mathrm{Im}\left(\frac{1}{\tilde{M}^2 - m_i^2 + i m_i \Gamma_i}\right). \end{aligned}$$

In practice the effect of introducing this improvement is found to be negligible on the position of the dynamically-generated states. The reason is that in all cases the decay thresholds for these channels are far above the pole, as compared to the widths involved. In fact, the widths of the basic hadrons can be safely neglected in all sectors for the low-lying states we obtain.

As can be seen from Table 3.2, every found $\Lambda_c$ baryon resonance couples strongly only to some of the 16 coupled channels. Therefore, we can study how the features (masses, widths and couplings) of the $\Lambda_c$ resonances change, when we consider only the dominant baryon-meson coupled channels. It turns out that the masses and widths, as well as couplings do not change drastically when we only consider the restricted coupled-channels space. For instance, the width of the $\Lambda_c(2617.3)$ resonance increases from 89.8 to 97.3 MeV, whereas the mass and the coupling to the $\Sigma_c\pi$ and other coupled channels stay almost unchanged. The $\Lambda_c(2618.8)$ resonance slightly increases its mass by 2.6 MeV, and the width decreases from 1.2 to 1.1 MeV, while the coupling to $ND^*$ channel remains

almost the same, as well as the other couplings. Finally, the mass of the $\Lambda_c(2828.4)$ state raises by 4.6 MeV, and its width is now 1.0 MeV; the couplings to the dominant $\Lambda_c\eta$ and $\Sigma_c^*\rho$ channels slightly vary: both of them decrease by about 0.3; couplings to the $\Xi_c K$ and $\Sigma_c\rho$ channels decrease by 0.2, and the one to the $\Xi_c^* K^*$ channel slightly increases by 0.1. The features (masses, widths, couplings) of the $\Lambda_c$ resonances with the coupled channels restricted to the main ones are collected in Table 3.3.

| $M_R$ | $\Gamma_R$ | Couplings to main channels |
|---|---|---|
| 2617.6 | 97.3 | $\boldsymbol{g_{\Sigma_c\pi} = 2.3}$, $g_{ND} = 1.9$, $g_{ND^*} = 1.3$, $g_{\Sigma_c\rho} = 1.3$ |
| 2667.8 | 61.9 | $\boldsymbol{g_{\Sigma_c^*\pi} = 2.2}$, $g_{ND^*} = 2.0$, $g_{\Sigma_c\rho} = 0.7$, $g_{\Sigma_c^*\rho} = 1.3$ |
| 2621.4 | 1.1 | $\boldsymbol{g_{\Sigma_c\pi} = 0.3}$, $g_{ND} = 3.5$, $g_{ND^*} = 5.7$, $g_{\Lambda D_s} = 1.4$, $g_{\Lambda D_s^*} = 3.0$, $g_{\Lambda_c\eta'} = 0.95$ |
| 2833.0 | 1.0 | $\boldsymbol{g_{ND} = 0.3}$, $g_{\Lambda_c\eta} = 0.8$, $g_{\Xi_c K} = 1.4$, $g_{\Lambda D_s^*} = 1.1$, $g_{\Sigma_c\rho} = 0.9$, $g_{\Sigma_c^*\rho} = 0.7$, $g_{\Xi_c^* K^*} = 0.7$ |

Table 3.3: The masses, widths, and couplings to main channels of the $\Lambda_c$ ($J = 1/2$) and $\Lambda_c^*$ ($J = 3/2$) resonances predicted by our model in the **168** and **120** SU(8) irreps. Here the number of coupling channels was restricted to the main ones (see text for details). The order of states remains the same as in Table 3.2.

### 3.2.2 Sector $J = 3/2$

For the $C = 1$, $S = 0$, $I = 0$, $J = 3/2$ sector, the 11 channels and thresholds (in MeV) are:

$$\begin{array}{ccccccccc} \Sigma_c^*\pi & ND^* & \Lambda_c\omega & \Xi_c^* K & \Lambda D_s^* & \Sigma_c\rho & \Sigma_c^*\rho & \Lambda_c\phi & \\ 2656.0, & 2947.3, & 3069.0, & 3142.0, & 3228.0, & 3229.1, & 3293.5, & 3305.9, & \\ & & \Xi_c K^* & \Xi_c' K^* & \Xi_c^* K^* & & & & \\ & & 3363.3, & 3470.7, & 3540.2. & & & & \end{array}$$

We find one pole in this sector (see Fig. 3.5 and Table 3.2) located at $\sqrt{s} = 2666.6 - i26.7$ MeV.

In Ref. [175], this structure had a Breit-Wigner shape with a width of 38 MeV and it coupled most strongly to $\Sigma_c^*\pi$. It was assigned to the experimental $\Lambda_c(2625)$ [4, 102, 107–109]. The $\Lambda_c(2625)$ has a very narrow width, $\Gamma < 1.9$ MeV, and decays mostly to $\Lambda_c\pi\pi$. The reason for the assignment lies in the fact that changes in the subtraction point could move the resonance closer to the position of the experimental one, reducing its width significantly as it will stay below its dominant $\Sigma_c^*\pi$ channel. In our present calculation, we expect then a similar behavior.

A similar resonance was found at 2660 MeV in the $t$-channel vector-exchange model of Ref. [142]. The novelty of our calculation is that we obtain a non-negligible contribution

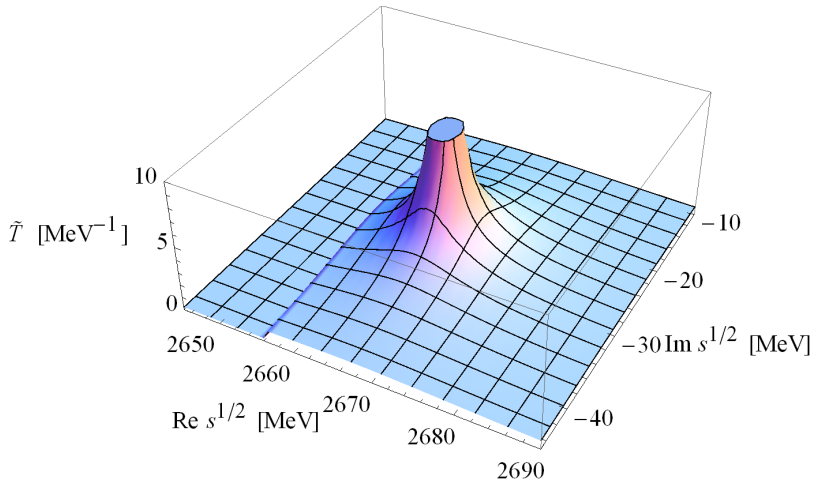


Figure 3.5: $\tilde{T}^{I=0,\ J=\frac{3}{2},\ S=0,\ C=1}(s)$ ($\Lambda_c^*$ resonance).

from the baryon-vector meson channels to the generation of this resonance, as already observed in Ref. [175].

When restricting the number of coupled channels to the four ones, to which $\Lambda_c(2666.6)$ couples the most, namely $\Sigma_c^*\pi$, $ND^*$, $\Sigma_c\rho$, $\Sigma_c^*\rho$, the resonance features are changed as follows. The mass somewhat increases by 1.2 MeV, while the width grows by 8.2 MeV, and the couplings remain almost unchanged, as can be seen in Table 3.3.

## 3.3 $\boldsymbol{\Sigma_c}$ states ($\boldsymbol{C=1}$, $\boldsymbol{S=0}$, $\boldsymbol{I=1}$)

### 3.3.1 Sector $J = 1/2$

The 22 channels and thresholds (in MeV) in this sector are:

| | | | | | | | |
|---|---|---|---|---|---|---|---|
| $\Lambda_c\pi$ | $\Sigma_c\pi$ | $ND$ | $ND^*$ | $\Xi_cK$ | $\Sigma_c\eta$ | $\Lambda_c\rho$ | $\Xi_c'K$ |
| 2424.5, | 2591.6, | 2806.1, | 2947.3, | 2965.1, | 3001.0, | 3062.0, | 3072.5, |
| $\Sigma D_s$ | $\Delta D^*$ | $\Sigma_c\rho$ | $\Sigma_c\omega$ | $\Sigma_c^*\rho$ | $\Sigma_c^*\omega$ | $\Sigma D_s^*$ | $\Xi_cK^*$ |
| 3161.7, | 3218.3, | 3229.1, | 3236.1, | 3293.5, | 3300.5, | 3305.5, | 3363.3, |
| | $\Sigma_c\eta'$ | $\Xi_c'K^*$ | $\Sigma_c\phi$ | $\Sigma^*D_s^*$ | $\Sigma_c^*\phi$ | $\Xi_c^*K^*$ | |
| | 3411.3, | 3470.7, | 3473.0, | 3496.9, | 3537.4, | 3540.2. | |

The three resonances obtained for $J = 1/2$ (Table 3.4 and Fig. 3.6) are predictions of our model, since no experimental data have been observed in this energy region. Our predictions here nicely agree with the three lowest lying resonances found in Ref. [175].

The model of Ref. [146], based on the full $t$-channel vector exchange using the interaction between $1/2^+$ baryons and pseudoscalar mesons in coupled channels and the Lippmann-Schwinger equation for obtaining scattering amplitudes, predicts the existence of two resonances with $I = 1,\ J = \frac{1}{2},\ S = 0,\ C = 1$. In this reference, the first one has a

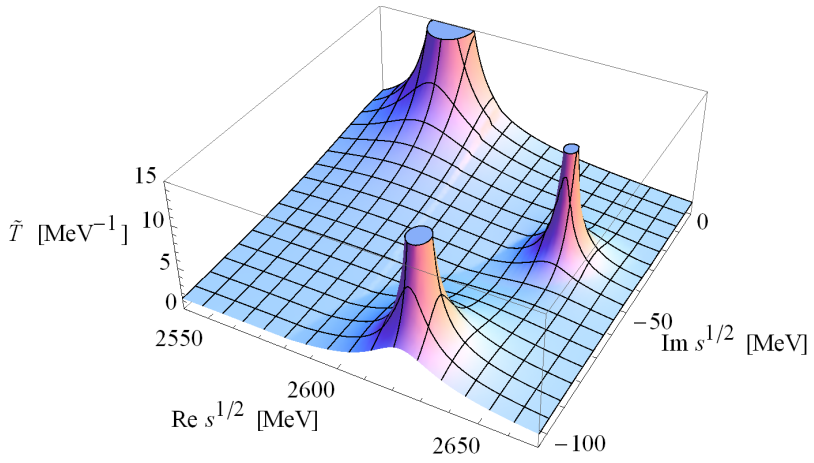


Figure 3.6: $\tilde{T}^{I=1,\ J=\frac{1}{2},\ S=0,\ C=1}(s)$ amplitude ($\Sigma_c$ resonances)

mass of 2551 MeV with a width 0.15 MeV. It couples strongly to the $\Sigma D_s$ and $ND$ channels and, therefore, might be associated with the resonance $\Sigma_c(2572)$ with $\Gamma = 0.8$ MeV of our model. Nevertheless, in our model this resonance couples most strongly to the other channels which incorporate vector mesons, such as $\Sigma^* D_s^*$ and $\Delta D^*$, as it is shown in Table 3.4 and seen in Ref. [175].

The second resonance predicted in Ref. [146] has a mass of 2804 MeV and a width of 5 MeV, and it cannot be compared to any of our results because it is far from the energy region of our present calculations. This resonance, though, was identified with the state found in Ref. [141] at a substantially lower energy, 2680 MeV. In this last reference a zero-range $t$-channel exchange of vector mesons was used for the $s$-wave scattering of pseudoscalar mesons off the baryons ground states in coupled channels. The interaction in this model is determined by chiral symmetry, large-$N_c$ consideration, and SU(4) symmetry. The 2804 MeV resonance of Ref. [146] was also identified with one of the found resonances in Ref. [144], around 2750 MeV. In Ref. [144] a model of Ref. [141] is adopted, but with modifications in several important aspects, such as the method of regularization and the zero-range $t$-channel meson-exchange interaction.

### 3.3.2 Sector $J = 3/2$

For the $\Sigma_c^*$ case, the 20 channels and thresholds (in MeV) are:

| | | | | | | | |
|---|---|---|---|---|---|---|---|
| $\Sigma_c^*\pi$ | $ND^*$ | $\Lambda_c\rho$ | $\Sigma_c^*\eta$ | $\Delta D$ | $\Xi_c^* K$ | $\Delta D^*$ | $\Sigma_c\rho$ |
| 2656.0, | 2947.3, | 3062.0, | 3065.4, | 3077.2, | 3142.0, | 3218.3, | 3229.1, |
| $\Sigma_c\omega$ | $\Sigma_c^*\rho$ | $\Sigma_c^*\omega$ | $\Sigma D_s^*$ | $\Sigma^* D_s$ | $\Xi_c K^*$ | $\Sigma_c^*\phi$ | $\Xi_c^* K^*$ |
| 3236.1, | 3293.5, | 3300.5, | 3305.5, | 3353.1, | 3363.3, | 3470.7, | 3473.0, |
| | | $\Xi_c' K^*$ | $\Sigma_c\phi$ | $\Sigma_c^*\eta'$ | $\Sigma^* D_s^*$ | | |
| | | 3475.8, | 3496.9, | 3537.4, | 3540.2. | | |

| SU(8) irrep | SU(6) irrep | SU(3) irrep | $M_R$ | $\Gamma_R$ | Couplings to main channels | $J$ |
|---|---|---|---|---|---|---|
| **168** | $\mathbf{21_{2,1}}$ | $\mathbf{6_2}$ | 2571.5 | 0.8 | $\boldsymbol{g_{\Lambda_c\pi}=0.1}$, $g_{ND}=2.2$, $g_{ND^*}=1.2$, $g_{\Sigma D_s}=1.5$, $g_{\Delta D^*}=6.6$, $g_{\Sigma D_s^*}=1.1$, $g_{\Sigma^* D_s^*}=2.8$ | 1/2 |
| **168** | $\mathbf{21_{2,1}}$ | $\mathbf{6_4}$ | 2568.4 | 0.0 | $g_{ND^*}=2.5$, $g_{\Delta D}=4.2$, $g_{\Delta D^*}=5.3$, $g_{\Sigma D_s^*}=2.2$, $g_{\Sigma^* D_s}=1.5$, $g_{\Sigma^* D_s^*}=2.3$ | 3/2 |
| **168** | $\mathbf{15_{2,1}}$ | $\mathbf{6_2}$ | 2622.7 | 188.0 | $\boldsymbol{g_{\Lambda_c\pi}=1.9}$, $\boldsymbol{g_{\Sigma_c\pi}=0.2}$, $g_{ND}=2.2$, $g_{ND^*}=3.8$, $g_{\Xi_c K}=0.8$, $g_{\Sigma_c\rho}=1.3$, $g_{\Sigma_c^*\rho}=1.5$ | 1/2 |
| **120** | $\mathbf{21_{2,1}}$ | $\mathbf{6_2}$ | 2643.4 | 87.0 | $\boldsymbol{g_{\Lambda_c\pi}=0.2}$, $\boldsymbol{g_{\Sigma_c\pi}=2.0}$, $g_{ND}=2.4$, $g_{ND^*}=1.7$, $g_{\Lambda_c\rho}=0.9$ $g_{\Delta D^*}=1.1$, $g_{\Sigma_c\rho}=0.9$, $g_{\Sigma^* D_s^*}=1.3$ | 1/2 |
| **120** | $\mathbf{21_{2,1}}$ | $\mathbf{6_4}$ | 2692.9 | 67.0 | $\boldsymbol{g_{\Sigma_c^*\pi}=1.9}$, $g_{ND^*}=2.7$, $g_{\Lambda_c\rho}=1.0$, $g_{\Sigma D_s^*}=1.0$, $g_{\Sigma^* D_s^*}=1.0$ | 3/2 |

Table 3.4: As in Table 3.2, for $\Sigma_c$ and $\Sigma_c^*$ resonances.

The two predicted states are shown in Fig. 3.7 and their properties are collected in Table 3.4. A bound state at 2568.4 MeV (2550 MeV in Ref. [175]), whose main baryon-meson components contain a charmed meson, lies below the threshold of any possible decay channel. This state is thought to be the charmed counterpart of the hyperonic $\Sigma(1670)$ resonance. While the $\Sigma(1670)$ strongly couples to $\Delta\bar{K}$ channel, this resonance is mainly generated by the analogous $\Delta D$ and $\Delta D^*$ channels.

The second state at 2692.9 MeV has not a direct comparison with the available experimental data, as discussed in Ref. [175]. In fact, the experimental $\Sigma_c(2520)$ [4, 111–113] cannot be assigned to any of these two states due to parity and because of the dominant decay channel, $\Lambda_c\pi$ ($d$-wave), which we do not consider in our approach.

With regards to the experimental $\Sigma(2800)$ [4,114,115], there is also no correspondence with any of our states due to its high mass and also the empirically dominant $\Lambda_c\pi$ component. Heavier resonances were produced in [175], but they come from the SU(8) irrep **4752** which we have disregarded here.

## 3.4 $\boldsymbol{\Xi_c}$ states ($\boldsymbol{C=1}$, $\boldsymbol{S=-1}$, $\boldsymbol{I=1/2}$)

We now study the $C=1$, $S=-1$, $I=1/2$ sector for different spin, $J=1/2$ and $J=3/2$. Those states are labeled by $\Xi_c$ and our model predicts the existence of nine states stemming from the strongly attractive **120** and **168** SU(8) irreducible representations.

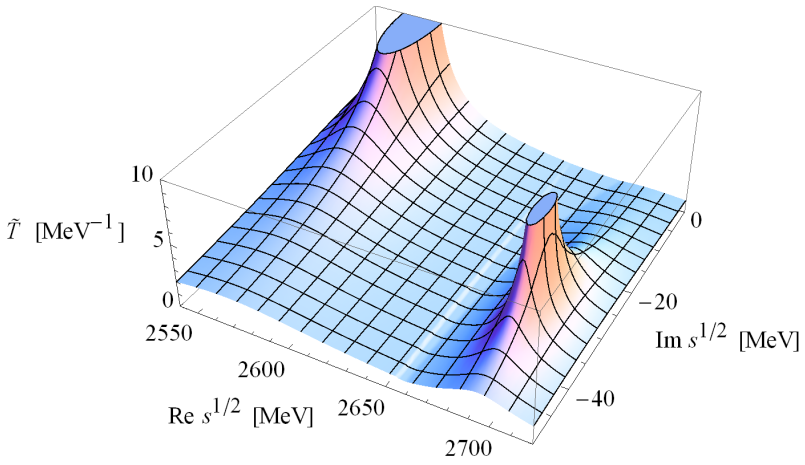


Figure 3.7: $\tilde{T}^{I=1,\ J=\frac{3}{2},\ S=0,\ C=1}(s)$ amplitude ($\Sigma_c^*$ resonances).

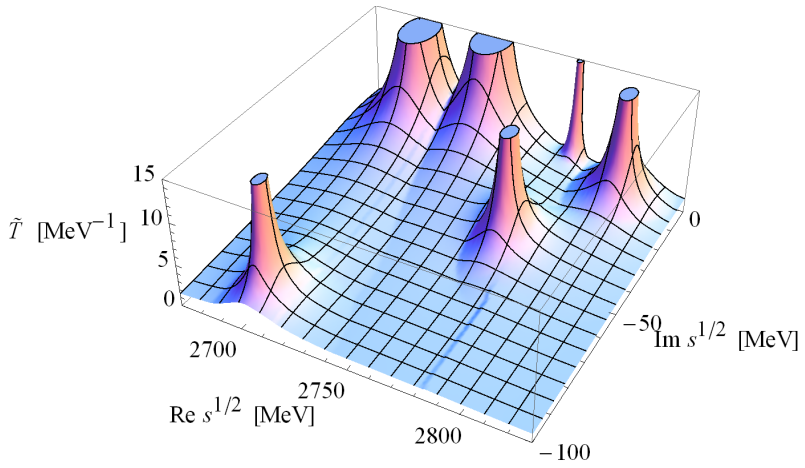


Figure 3.8: $\tilde{T}^{I=\frac{1}{2},\ J=\frac{1}{2},\ S=-1,\ C=1}(s)$ amplitude ($\Xi_c$ resonances)

### 3.4.1 Sector $J = 1/2$

The 31 channels and thresholds (in MeV) for this sector are:

| | | | | | | | |
|---|---|---|---|---|---|---|---|
| $\Xi_c\pi$ | $\Xi_c'\pi$ | $\Lambda_c\bar{K}$ | $\Sigma_c, \bar{K}$ | $\Lambda D$ | $\Xi_c\eta$ | $\Sigma D$ | $\Lambda D^*$ |
| 2607.5, | 2714.9, | 2782.1, | 2949.2, | 2982.9, | 3016.9, | 3060.4, | 3124.0, |
| $\Xi_c'\eta$ | $\Lambda_c\bar{K}^*$ | $\Omega_c K$ | $\Sigma D^*$ | $\Xi_c\rho$ | $\Xi_c\omega$ | $\Xi D_s$ | $\Sigma_c\bar{K}^*$ |
| 3124.3, | 3180.3, | 3193.2, | 3201.5, | 3244.9, | 3252.0, | 3286.6, | 3347.4, |
| $\Xi_c'\rho$ | $\Xi_c'\omega$ | $\Sigma^* D^*$ | $\Sigma_c^*\bar{K}^*$ | $\Xi_c^*\rho$ | $\Xi_c\eta'$ | $\Xi_c^*\omega$ | $\Xi D_s^*$ |
| 3352.3, | 3359.4, | 3392.9, | 3411.9, | 3421.8, | 3427.2, | 3428.9, | 3430.4, |

| | | | | | | |
|---|---|---|---|---|---|---|
| $\Xi_c\phi$ | $\Xi_c'\eta'$ | $\Omega_c K^*$ | $\Xi_c'\phi$ | $\Xi^* D_s^*$ | $\Omega_c^* K^*$ | $\Xi_c^*\phi$ |
| 3488.9, | 3534.6, | 3591.4, | 3596.3, | 3645.7, | 3662.2, | 3665.8. |

| SU(8) irrep | SU(6) irrep | SU(3) irrep | $M_R$ | $\Gamma_R$ | Couplings to main channels | Status PDG | $J$ |
|---|---|---|---|---|---|---|---|
| **168** | $\mathbf{15_{2,1}}$ | $\mathbf{6_2}$ | 2702.8 | 177.8 | $\boldsymbol{g_{\Xi_c\pi}=2.4}$, $g_{\Lambda D}=1.2$, $g_{\Sigma D}=1.1$, $g_{\Lambda D^*}=2.1$, $g_{\Sigma D^*}=1.7$, $g_{\Xi D_s^*}=1.1$ | | 1/2 |
| **168** | $\mathbf{21_{2,1}}$ | $\mathbf{3_2^*}$ | 2699.4 | 12.6 | $\boldsymbol{g_{\Xi_c\pi}=0.8}$, $g_{\Lambda D}=1.2$, $g_{\Sigma D}=3.4$, $g_{\Lambda D^*}=2.2$, $g_{\Sigma D^*}=5.4$, $g_{\Xi D_s}=1.9$, $g_{\Xi_c\eta'}=1.0$, $g_{\Xi D_s^*}=3.3$ | | 1/2 |
| **168** | $\mathbf{21_{2,1}}$ | $\mathbf{6_2}$ | 2733.0 | 2.2 | $\boldsymbol{g_{\Xi_c'\pi}=0.5}$, $g_{\Lambda D}=1.9$, $g_{\Sigma D}=1.8$, $g_{\Lambda D^*}=0.9$, $g_{\Sigma D^*}=1.2$, $g_{\Xi D_s}=1.2$, $g_{\Sigma^* D^*}=5.8$, $g_{\Xi_c'\eta'}=0.9$, $g_{\Xi^* D_s^*}=3.3$ | | 1/2 |
| **168** | $\mathbf{21_{2,1}}$ | $\mathbf{6_4}$ | 2734.3 | 0.0 | $g_{\Lambda D^*}=2.2$, $g_{\Sigma D^*}=2.1$, $g_{\Sigma^* D}=3.6$, $g_{\Sigma^* D^*}=4.6$, $g_{\Xi D_s^*}=1.3$, $g_{\Xi^* D_s}=2.1$, $g_{\Xi^* D_s^*}=2.6$ | | 3/2 |
| **120** | $\mathbf{21_{2,1}}$ | $\mathbf{3_2^*}$ | 2775.4 | 0.6 | $\boldsymbol{g_{\Xi_c\pi}=0.1}$, $\boldsymbol{g_{\Xi_c'\pi}=0.1}$, $g_{\Lambda_c\bar{K}}=1.4$, $g_{\Xi_c\eta}=0.9$, $g_{\Lambda D^*}=1.0$, $g_{\Sigma D^*}=1.4$, $g_{\Sigma_c\bar{K}^*}=1.0$, $g_{\Sigma_c^*\bar{K}^*}=1.3$ | | 1/2 |
| **168** | $\mathbf{15_{2,1}}$ | $\mathbf{3_2^*}$ | 2772.9 | 83.7 | $\boldsymbol{g_{\Xi_c\pi}=0.1}$, $\boldsymbol{g_{\Xi_c'\pi}=2.3}$, $g_{\Sigma_c\bar{K}}=1.2$, $g_{\Lambda D}=2.1$, $g_{\Lambda D^*}=1.5$, $g_{\Omega_c K}=0.9$, $g_{\Sigma D^*}=0.9$, $g_{\Xi_c\rho}=1.0$, $g_{\Sigma_c\bar{K}^*}=0.9$, $g_{\Xi_c'\rho}=1.0$, $g_{\Sigma^* D^*}=1.4$, $g_{\Xi^* D_s^*}=1.1$ | | 1/2 |
| **168** | $\mathbf{15_{2,1}}$ | $\mathbf{3_4^*}$ | 2819.7 | 32.4 | $\boldsymbol{g_{\Xi_c^*\pi}=1.9}$, $g_{\Sigma_c^*\bar{K}}=2.3$, $g_{\Lambda D^*}=2.0$, $g_{\Lambda_c\bar{K}^*}=1.0$, $g_{\Xi_c^*\eta}=1.1$, $g_{\Sigma D^*}=1.2$, $g_{\Xi_c\rho}=1.1$, $g_{\Sigma_c\bar{K}^*}=1.0$, $g_{\Sigma_c^*\bar{K}^*}=2.0$ | | 3/2 |
| **120** | $\mathbf{21_{2,1}}$ | $\mathbf{6_2}$ | 2804.8 | 20.7 | $\boldsymbol{g_{\Xi_c'\pi}=1.1}$, $g_{\Sigma_c\bar{K}}=2.4$, $g_{\Lambda D}=1.5$, $g_{\Sigma D}=1.2$, $g_{\Xi_c'\eta}=1.3$, $g_{\Lambda_c\bar{K}^*}=1.2$, $g_{\Sigma D^*}=0.9$, $g_{\Sigma_c\bar{K}^*}=1.8$, $g_{\Sigma^* D^*}=1.1$, $g_{\Sigma_c^*\bar{K}^*}=1.0$, $g_{\Xi^* D_s^*}=1.2$ | $\Xi_c(2790)$ *** | 1/2 |
| **120** | $\mathbf{21_{2,1}}$ | $\mathbf{6_4}$ | 2845.2 | 44.0 | $\boldsymbol{g_{\Xi_c^*\pi}=1.9}$, $g_{\Sigma_c^*\bar{K}}=2.1$, $g_{\Lambda D^*}=2.6$, $g_{\Lambda_c\bar{K}^*}=1.4$, $g_{\Xi_c^*\eta}=1.2$, $g_{\Sigma D^*}=1.2$, $g_{\Xi_c\rho}=0.9$, $g_{\Sigma_c\bar{K}^*}=0.9$, $g_{\Sigma_c^*\bar{K}^*}=1.7$, $g_{\Xi^* D_s}=0.9$, $g_{\Xi^* D_s^*}=1.1$ | $\Xi_c(2815)$ *** | 3/2 |

Table 3.5: As in Table 3.2, for the $\Xi_c$ and $\Xi_c^*$ resonances.

Six baryon resonances were expected (Table 3.1) and found in this sector. The mass, width and couplings to the main channels are given in Table 3.5 and Fig. 3.8. In the energy range where these six states predicted by our model lie, three experimental resonances have been seen by the Belle, E687, and CLEO Collaborations: $\Xi_c(2645)$ $J^P=3/2^+$ [4, 116–119], $\Xi_c(2790)$ $J^P=1/2^-$ [4, 120] and $\Xi_c(2815)$ $J^P=3/2^-$ [4, 116, 121]. While $\Xi_c(2645)$ cannot be identified with any of our states for $J=1/2$ and $J=3/2$ due to parity, the $\Xi_c(2790)$ might be assigned with one of the six resonances in the $J=1/2$ sector. The experimental $J^P=3/2^-$ $\Xi_c(2815)$ resonance will be analyzed in the $J=3/2$ sector.

The state $\Xi_c(2790)$ has a width of $\Gamma < 12 - 15$ MeV and it decays to $\Xi_c'\pi$, with $\Xi_c' \to \Xi_c\gamma$. We might associate it with our 2733, 2775.4, or 2804.8 states. Because of the small coupling of 2775.4 to the $\Xi_c'\pi$ channel, it seems unlikely that it might correspond to the observed $\Xi_c(2790)$ state. In fact, the assignment to the 2804.8 state might be better, because of its larger $\Xi_c'\pi$ coupling and the fact that a slight modification of the subtraction point can lower its position to 2790 MeV and most probably reduce its width as it will get closer to the $\Xi_c'\pi$ channel, the only channel open at those energies that couples to this resonance. Moreover, this seems to be a reasonable assumption in view of the fact that, in this manner, this $\Xi_c$ state is the HQSS partner of the 2845 $\Xi_c^*$ state, which we will identify with the $\Xi_c(2815)$ resonance of the PDG. Nevertheless, it is also possible to identify our pole at 2733 MeV from the **168** irreducible representation with the experimental $\Xi_c(2790)$ state. In that case, one might expect that if the resonance position gets closer to the physical mass of 2790 MeV, its width will increase and it will easily reach values of the order of 10 MeV.

In Ref. [146] five baryon resonances were found in this sector for a wide range of energies up to 2977 MeV. As discussed in this reference, none of these five states seemed to fit the experimental $\Xi_c(2790)$ because of the small width observed. Higher-mass experimental states, such as the $\Xi_c(2980)$ [4, 116, 122, 123], might correspond to one of the two higher-mass states in Ref. [146]. In our calculation, none of the states can be identified with such a heavy resonant state. In Ref. [141] three resonances appear below 3 GeV: 2691 MeV, 2793 MeV, and 2806 MeV, which mostly couple to $D\Sigma$, $\bar{K}\Sigma_c$, and $D\Lambda$, respectively. Those states are very similar in mass to some of those obtained in our calculations and we might identify the first two states, $\Xi_c(2691)$ and $\Xi_c(2793)$, to our $\Xi_c(2699.4)$ and $\Xi_c(2804.8)$ states because of the dominant decay channel.

### 3.4.2 Sector $J = 3/2$

The 26 channels (thresholds in MeV are also given) in the $\Xi_c^*$ sector are:

| | | | | | | |
|---|---|---|---|---|---|---|
| $\Xi_c^*\pi$ | $\Sigma_c^*\bar{K}$ | $\Lambda D^*$ | $\Lambda_c\bar{K}^*$ | $\Xi_c^*\eta$ | $\Sigma D^*$ | $\Xi_c\rho$ |
| 2784.4, | 3013.6, | 3124.0, | 3180.3, | 3193.8, | 3201.5, | 3244.9, |
| $\Sigma^* D$ | $\Xi_c\omega$ | $\Omega_c^* K$ | $\Sigma_c\bar{K}^*$ | $\Xi_c'\rho$ | $\Xi_c'\omega$ | $\Sigma^* D^*$ |
| 3251.8, | 3252.0, | 3264.0, | 3347.4, | 3352.3, | 3359.4, | 3392.9, |
| $\Sigma_c^*\bar{K}^*$ | $\Xi_c^*\rho$ | $\Xi_c^*\omega$ | $\Xi D_s^*$ | $\Xi_c\phi$ | $\Xi^* D_s$ | $\Omega_c K^*$ |
| 3411.8, | 3421.8, | 3428.9, | 3430.4, | 3488.9, | 3501.9, | 3591.4, |
| | $\Xi_c'\phi$ | $\Xi_c^*\eta'$ | $\Xi^* D_s^*$ | $\Omega_c^* K^*$ | $\Xi_c^*\phi$ | |
| | 3596.3, | 3604.1, | 3645.7, | 3662.2, | 3665.8. | |

The resonances predicted by the model and generated from the **120** and **168** irreducible representations are compiled in Table 3.5 and Fig. 3.9.

The only experimental $J^P = 3/2^-$ baryon resonance with a mass in the energy region of interest is $\Xi_c(2815)$ [4, 116, 121]. The full width is expected to be less than 3.5 MeV for $\Xi_c^+(2815)$ and less than 6.5 MeV for $\Xi_c^0(2815)$, and the decay modes are $\Xi_{c+}\pi^+\pi^-$, $\Xi_{c0}\pi^+\pi^-$. We obtain two resonances at 2819.7 MeV and 2845.2 MeV, respectively, that

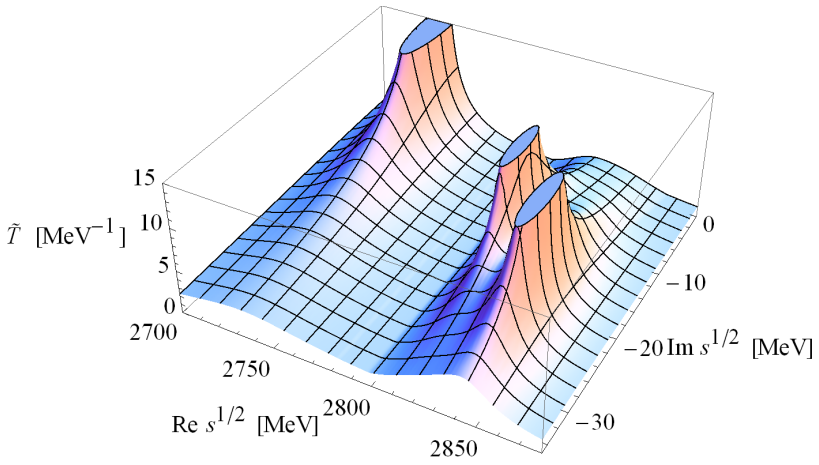


Figure 3.9: $\tilde{T}^{I=\frac{1}{2},\ J=\frac{3}{2},\ S=-1,\ C=1}(s)$ amplitude ($\Xi_c^*$ resonances).

couple strongly to $\Xi_c^*\pi$, with $\Xi_c^* \to \Xi_c\pi$. Allowing for this possible indirect three-body decay channel, we might identify one of them to the experimental result. This assignment is, indeed, possible for the state at 2845.2 MeV if we slightly change the subtraction point. In this way, we will lower its position and reduce its width as it gets closer to the open $\Xi_c^*\pi$ channel.

In Ref. [142] a resonance with a similar energy of 2838 MeV and width of 16 MeV was identified with the $\Xi_c(2815)$. In this reference the $J^P = 3/2^+$ baryon molecules were studied, using the zero-range exchange of vector mesons as a driving force for the $s$-wave scattering of the pseudoscalar mesons off the ground state $3/2^+$ baryons. It was suggested that its small width of the resonance was a consequence of its small coupling strength to the $\Xi_c\pi$ channel.

## 3.5 $\boldsymbol{\Omega_c}$ states ($\boldsymbol{C=1}$, $\boldsymbol{S=-2}$, $\boldsymbol{I=0}$)

In this section we will discuss the $C = 1$, $S = -2$, and $I = 0$ resonant states with $J = 1/2$ and $J = 3/2$ coming from the **120** and **168** SU(8) representations. States with the $I = 1$ and the $J = 5/2$ belong to the **4752**-plet and are not discussed in this work.

### 3.5.1 Sector $J = 1/2$

The 15 physical baryon-meson pairs that are incorporated in the $I = 0$, $J = 1/2$ sector are as follows:

| $\Xi_c\bar{K}$ | $\Xi_c'\bar{K}$ | $\Xi D$ | $\Omega_c\eta$ | $\Xi D^*$ | $\Xi_c\bar{K}^*$ | $\Xi_c'\bar{K}^*$ | $\Omega_c\omega$ |
|---|---|---|---|---|---|---|---|
| 2965.1, | 3072.5, | 3185.3, | 3245.0, | 3326.5, | 3363.3, | 3470.7, | 3480.1, |
| $\Xi_c^*\bar{K}^*$ | $\Xi^* D^*$ | $\Omega_c^*\omega$ | $\Omega_c\eta'$ | $\Omega_c\phi$ | $\Omega D_s^*$ | $\Omega_c^*\phi$ | |
| 3540.2, | 3541.8, | 3550.9, | 3655.3, | 3717.0, | 3784.8, | 3787.8. | |

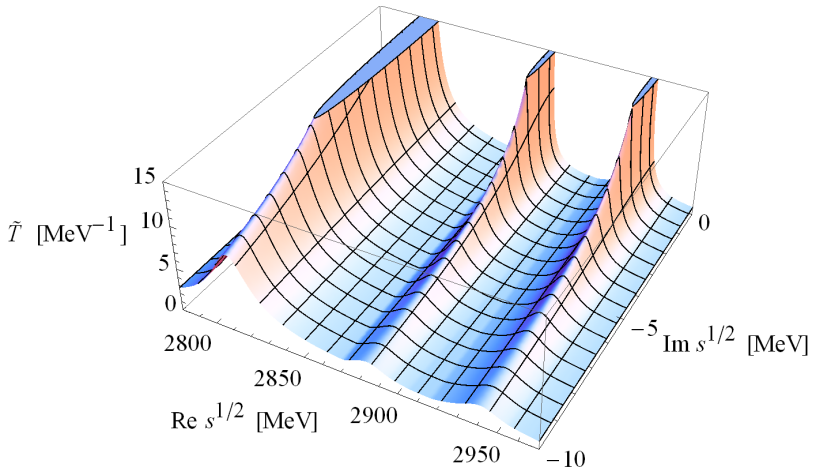


Figure 3.10: $\tilde{T}^{I=0,\ J=\frac{1}{2},\ S=-2,\ C=1}(s)$ amplitude ($\Omega_c$ resonances).

According to our analysis, there are three bound states which can be generated dynamically as baryon-meson molecular entities resulting from the strongly attractive representations of the SU(8) group. In Table 3.6 and Fig. 3.10 we show the masses, widths, and the largest couplings of those poles to the scattering channels.

| SU(8) irrep | SU(6) irrep | SU(3) irrep | $M_R$ | $\Gamma_R$ | Couplings to main channels | $J$ |
|---|---|---|---|---|---|---|
| **168** | $\mathbf{21_{2,1}}$ | $\mathbf{6_2}$ | 2810.9 | 0.0 | $g_{\Xi D} = 3.3$, $g_{\Xi D^*} = 1.7$, $g_{\Xi_c \bar{K}^*} = 0.9$, $g_{\Xi^* D^*} = 4.8$, $g_{\Omega_c \eta'} = 0.9$, $g_{\Omega D_s^*} = 4.2$ | 1/2 |
| **168** | $\mathbf{21_{2,1}}$ | $\mathbf{6_4}$ | 2814.3 | 0.0 | $g_{\Xi D^*} = 3.7$, $g_{\Xi^* D} = 3.1$, $g_{\Xi^* D^*} = 3.8$, $g_{\Omega D_s} = 2.7$, $g_{\Omega_c^* \eta'} = 0.9$, $g_{\Omega D_s^*} = 3.4$ | 3/2 |
| **168** | $\mathbf{15_{2,1}}$ | $\mathbf{6_2}$ | 2884.5 | 0.0 | $g_{\Xi_c \bar{K}} = 2.1$, $g_{\Xi D^*} = 1.7$, $g_{\Xi_c' \bar{K}^*} = 1.5$, $g_{\Xi_c^* \bar{K}^*} = 1.8$, $g_{\Omega_c \phi} = 0.9$, $g_{\Omega_c^* \phi} = 1.1$ | 1/2 |
| **120** | $\mathbf{21_{2,1}}$ | $\mathbf{6_2}$ | 2941.6 | 0.0 | $g_{\Xi_c' \bar{K}} = 1.9$, $g_{\Xi D} = 1.5$, $g_{\Omega_c \eta} = 1.7$, $g_{\Xi_c \bar{K}^*} = 1.4$, $g_{\Xi_c' \bar{K}^*} = 1.1$, $g_{\Omega_c \phi} = 1.0$, $g_{\Omega D_s^*} = 0.9$ | 1/2 |
| **120** | $\mathbf{21_{2,1}}$ | $\mathbf{6_4}$ | 2980.0 | 0.0 | $g_{\Xi_c^* \bar{K}} = 1.9$, $g_{\Omega_c^* \eta} = 1.6$, $g_{\Xi D^*} = 1.4$, $g_{\Xi_c \bar{K}^*} = 1.6$, $g_{\Xi_c^* \bar{K}^*} = 1.3$, $g_{\Omega_c^* \phi} = 1.2$ | 3/2 |

Table 3.6: $\Omega_c$ and $\Omega_c^*$ resonances.

There is no experimental information on those excited states. However, our predictions can be compared to recent calculations of Refs. [141, 146]. In Ref. [146] three resonances were found, one with mass $M_1 = 2959$ MeV and width $\Gamma_1 = 0$ MeV, a second one with $M_2 = 2966$ MeV and $\Gamma_2 = 1.1$ MeV, and the third one with $M_3 = 3117$ MeV and $\Gamma_3 = 16$ MeV. The dominant baryon-meson channels are $\bar{K}\Xi_c'$, $\bar{K}\Xi_c'$, and $D\Xi$, respectively.

Three resonant states with lower masses were also observed in Ref. [141], but with slightly different dominant coupled channels.

In both previous references, vector baryon-meson channels were not considered, breaking in this manner HQSS. In fact, it is worth noticing that the coupling to vector baryon-meson states plays an important role in the generation of the baryon resonances in this sector. Furthermore, we have checked that other states stemming from the **4752**-plet with the same quantum numbers might be seen in this energy region and, therefore, a straightforward identification of our states with the results of Refs. [141, 146] might not be possible.

### 3.5.2 Sector $J = 3/2$

In the $C = 1$, $S = -2$, $I = 0$, $J = 3/2$ sector, there are 15 coupled channels:

| $\Xi_c^*\bar{K}$ | $\Omega_c^*\eta$ | $\Xi D^*$ | $\Xi_c\bar{K}^*$ | $\Xi^* D$ | $\Xi_c'\bar{K}^*$ | $\Omega_c\omega$ | $\Xi_c^*\bar{K}^*$ |
|---|---|---|---|---|---|---|---|
| 3142.0, | 3315.8, | 3326.5, | 3363.3, | 3400.6, | 3470.7, | 3480.1, | 3540.2, |
| $\Xi^* D^*$ | $\Omega_c^*\omega$ | $\Omega D_s$ | $\Omega_c\phi$ | $\Omega_c^*\eta'$ | $\Omega D_s^*$ | $\Omega_c^*\phi$ | |
| 3541.8, | 3550.9, | 3641.0, | 3717.0, | 3726.1, | 3784.8, | 3787.8. | |

We obtain two bound $\Omega_c^*$ states (Table 3.6 and Fig. 3.11), with masses 2814.3, and 2980.0, which mainly couple to $\Xi D^*$ and $\Xi^* D^*$, and to $\Xi_c^*\bar{K}$, respectively. As seen in the $J = 1/2$ sector, no experimental information is available. In Ref. [142], two states at 2843 MeV and 3008 MeV with zero width were found. Those states couple most strongly to $D\Xi$ and $\bar{K}\Xi_c$, respectively, so an identification between the resonances in both models is not possible.

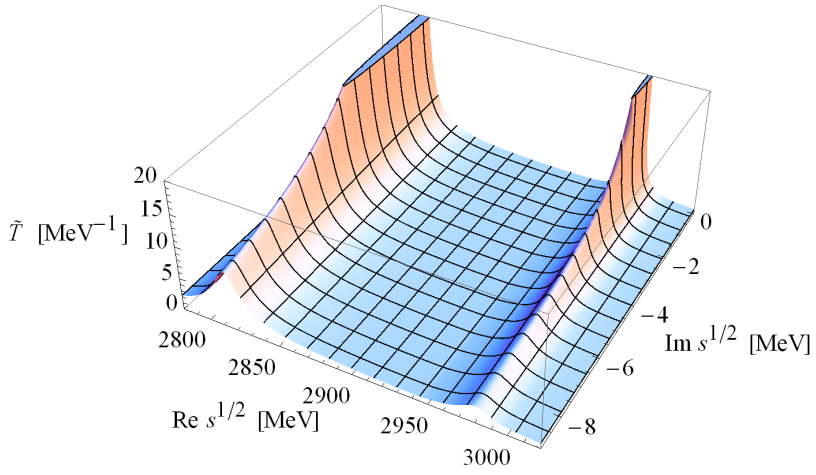


Figure 3.11: $\tilde{T}^{I=0,\ J=\frac{3}{2},\ S=-2,\ C=1}(s)$ amplitude ($\Omega_c^*$ resonances).

## 3.6 $\Xi_{cc}$ states ($C = 2$, $S = 0$, $I = 1/2$)

In the $C = 2$ sector no experimental information is available yet. Therefore, all our results are predictions of our spin-flavor extended WT model for four flavors.

### 3.6.1 Sector $J = 1/2$

The 22 channels for $C = 2$, $S = 0$, $I = 1/2$, and $J = 1/2$ are as follows:

| | | | | | | | |
|---|---|---|---|---|---|---|---|
| $\Xi_{cc}\pi$ | $\Xi_{cc}\eta$ | $\Lambda_c D$ | $\Omega_{cc}K$ | $\Xi_{cc}\rho$ | $\Lambda_c D^*$ | $\Xi_{cc}\omega$ | $\Sigma_c D$ |
| 3657.0, | 4066.5, | 4153.7, | 4207.7, | 4294.5, | 4294.8, | 4301.6, | 4320.8, |
| $\Xi^*_{cc}\rho$ | $\Xi^*_{cc}\omega$ | $\Xi_c D_s$ | $\Sigma_c D^*$ | $\Xi_{cc}\eta'$ | $\Sigma^*_c D^*$ | $\Xi_{cc}\phi$ | $\Xi'_c D_s$ |
| 4375.5, | 4382.6, | 4438.0, | 4461.9, | 4476.8, | 4526.3, | 4538.5, | 4545.4, |
| | $\Xi_c D^*_s$ | $\Omega_{cc}K^*$ | $\Xi^*_{cc}\phi$ | $\Omega^*_{cc}K^*$ | $\Xi'_c D^*_s$ | $\Xi^*_c D^*_s$ | |
| | 4581.8, | 4605.9, | 4619.5, | 4688.9, | 4689.2, | 4758.7. | |

| SU(8) irrep | SU(6) irrep | SU(3) irrep | $M_R$ | $\Gamma_R$ | Couplings to main channels | $J$ |
|---|---|---|---|---|---|---|
| **168** | $\mathbf{6_{1,2}}$ | $\mathbf{3_2}$ | 3698.1 | 1.3 | $\boldsymbol{g_{\Xi_{cc}\pi} = 0.3}$, $g_{\Lambda_c D^*} = 2.1$, $g_{\Sigma_c D} = 3.2$, $g_{\Sigma_c D^*} = 2.6$, $g_{\Sigma^*_c D^*} = 4.1$, $g_{\Xi'_c D_s} = 1.3$, $g_{\Xi_c D^*_s} = 1.4$, $g_{\Xi'_c D^*_s} = 1.1$, $g_{\Xi^*_c D^*_s} = 1.7$ | 1/2 |
| **120** | $\mathbf{6_{3,2}}$ | $\mathbf{3_2}$ | 3727.8 | 17.8 | $\boldsymbol{g_{\Xi_{cc}\pi} = 1.0}$, $g_{\Lambda_c D} = 2.0$, $g_{\Sigma_c D} = 1.1$, $g_{\Xi_c D_s} = 1.5$, $g_{\Sigma_c D^*} = 4.6$, $g_{\Xi_{cc}\eta'} = 1.4$, $g_{\Xi^*_{cc}\rho} = 0.9$, $g_{\Sigma^*_c D^*} = 3.6$, $g_{\Xi'_c D^*_s} = 2.0$, $g_{\Xi^*_c D^*_s} = 1.6$ | 1/2 |
| **168** | $\mathbf{6_{3,2}}$ | $\mathbf{3_4}$ | 3729.5 | 0.0 | $g_{\Lambda_c D^*} = 1.2$, $g_{\Sigma^*_c D} = 2.9$, $g_{\Sigma_c D^*} = 1.8$, $g_{\Sigma^*_c D^*} = 3.7$ $g_{\Xi_c D^*_s} = 1.3$, $g_{\Xi^*_c D_s} = 1.2$, $g_{\Xi^*_{cc}\eta'} = 1.1$, $g_{\Xi^*_c D^*_s} = 1.5$ | 3/2 |
| **168** | $\mathbf{6_{3,2}}$ | $\mathbf{3_2}$ | 3727.4 | 120.2 | $\boldsymbol{g_{\Xi_{cc}\pi} = 2.4}$, $g_{\Lambda_c D} = 2.4$, $g_{\Lambda_c D^*} = 1.5$, $g_{\Sigma_c D^*} = 2.3$, $g_{\Sigma^*_c D^*} = 1.4$, $g_{\Xi'_c D^*_s} = 1.0$ | 1/2 |
| **120** | $\mathbf{6_{3,2}}$ | $\mathbf{3_4}$ | 3790.8 | 83.9 | $\boldsymbol{g_{\Xi^*_{cc}\pi} = 2.0}$, $g_{\Lambda_c D^*} = 2.9$, $g_{\Sigma^*_c D} = 0.8$, $g_{\Sigma^*_c D^*} = 1.1$, $g_{\Xi_c D^*_s} = 0.8$, $g_{\Xi^*_c D_s} = 0.8$, $g_{\Xi^*_{cc}\eta'} = 0.8$, $g_{\Xi^*_c D^*_s} = 1.$ | 3/2 |

Table 3.7: $\Xi_{cc}$ and $\Xi^*_{cc}$ resonances. In this case, the HQSS classification differs from the SU(8) classification for the two HQSS doublets: the resonances in two pairs that form HQSS doublets stem from different SU(8) multiplets.

The three predicted poles in the $\Xi_{cc}$ sector can be seen in the Table 3.7 and Fig. 3.12 together with the width and couplings to the main channels. Their masses are 3698.1, 3727.4, and 3727.8 MeV, with widths 1.3, 120.2, and 17.8 MeV, respectively. The dominant channels for the generation of those states are, in order, $\Sigma^*_c D^*$, $\Xi_{cc}\pi$ and $\Lambda_c D$, and $\Sigma_c D^*$. In Ref. [141] six states were found, two of them coming from the weak interaction of the open-charm mesons and open-charm baryons in the SU(4) anti-sextet and 15-plet. In this chapter, we only consider those states coming from the strongly attractive SU(8)

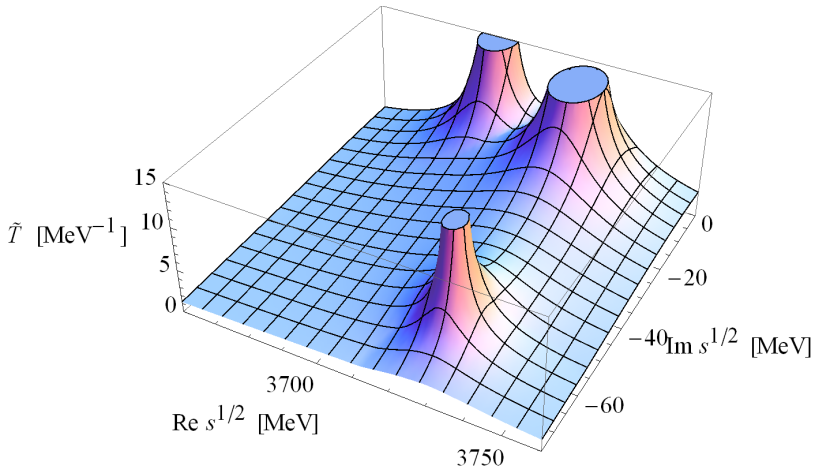


Figure 3.12: $\tilde{T}^{I=\frac{1}{2},\ J=\frac{1}{2},\ S=0,\ C=2}(s)$ amplitude ($\Xi_{cc}$ resonances).

**120**- and **168**-plets. Therefore, only three states are expected in this sector. Moreover, an identification among resonances in both models is complicated because the strong coupling of our states to channels with vector mesons, not considered in this previous reference.

### 3.6.2 Sector $J = 3/2$

In the $\Xi^*_{cc}$ sector, the following 20 channels are coupled:

| | | | | | | |
|---|---|---|---|---|---|---|
| $\Xi^*_{cc}\pi$ | $\Xi^*_{cc}\eta$ | $\Omega^*_{cc}K$ | $\Xi_{cc}\rho$ | $\Lambda_c D^*$ | $\Xi_{cc}\omega$ | $\Xi^*_{cc}\rho$ |
| 3738.0, | 4147.5, | 4290.7, | 4294.5, | 4294.8, | 4301.6, | 4375.5, |
| $\Xi^*_{cc}\omega$ | $\Sigma^*_c D$ | $\Sigma_c D^*$ | $\Sigma^*_c D^*$ | $\Xi_{cc}\phi$ | $\Xi^*_{cc}\eta'$ | $\Xi_c D^*_s$ |
| 4382.6, | 4385.2, | 4461.9, | 4526.3, | 4538.5, | 4557.8, | 4581.8, |
| $\Omega_{cc}K^*$ | $\Xi^*_c D_s$ | $\Xi^*_{cc}\phi$ | $\Omega^*_{cc}K^*$ | $\Xi'_c D^*_s$ | $\Xi^*_c D^*_s$ | |
| 4605.9, | 4614.9, | 4619.5, | 4688.9, | 4689.2, | 4758.7. | |

Two states, with masses 3729.5 and 3790.8 MeV have been obtained, which couple mainly to $\Sigma^*_c D$ and $\Sigma^*_c D^*$, and to $\Xi^*_{cc}\pi$ and $\Lambda_c D^*$, respectively (see Table 3.7 and Fig. 3.13).

In Ref. [142], two states were obtained at 3671 MeV and 3723 MeV, with dominant coupling to the channels $\Sigma_c D$ and $\Xi_{cc}\pi$, respectively. However, the analysis there was done on the basis that the $\Xi_{cc}(3519)$ resonance is, in fact, a $J^P = 3/2^+$ state, whereas in our calculation this resonance is the ground state, $J^P = 1/2^+$. It is argued in [142] that the second resonance should be more reliable in view of the dominant coupling to a baryon-Goldstone boson. Moreover, the necessity of implementing HQSS was mentioned, by incorporating $0^-$ and $1^-$ charmed mesons as well as $1/2^+$ and $3/2^+$ baryon in the coupled-channel basis.

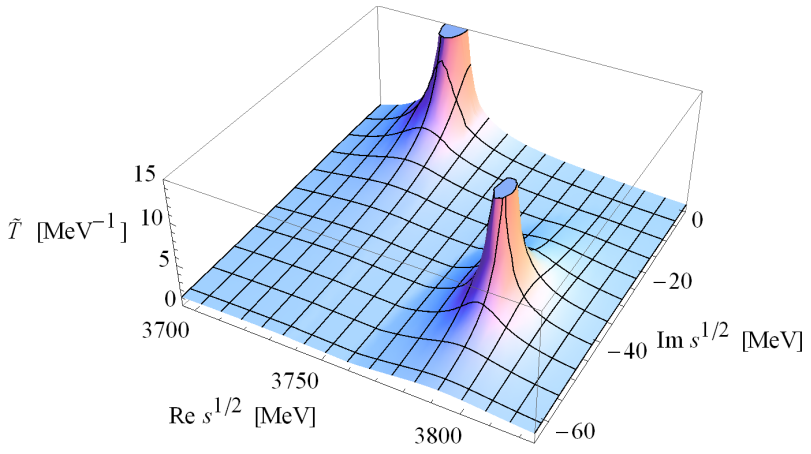


Figure 3.13: $\tilde{T}^{I=\frac{1}{2},\ J=\frac{3}{2},\ S=0,\ C=2}(s)$ amplitude ($\Xi_{cc}^*$ resonances).

## 3.7 $\Omega_{cc}$ states ($C = 2$, $S = -1$, $I = 0$)

### 3.7.1 Sector $J = 1/2$

The 17 channels in this $\Omega_{cc}$ sector are as follows:

| | | | | | | |
|---|---|---|---|---|---|---|
| $\Xi_{cc}\bar{K}$ | $\Omega_{cc}\eta$ | $\Xi_c D$ | $\Xi_{cc}\bar{K}^*$ | $\Xi_c' D$ | $\Xi_c D^*$ | $\Xi_{cc}^*\bar{K}^*$ |
| 4014.7, | 4259.5, | 4336.7, | 4412.9, | 4444.1, | 4477.8, | 4493.9, |
| $\Omega_{cc}\omega$ | $\Omega_{cc}^*\omega$ | $\Xi_c' D^*$ | $\Xi_c^* D^*$ | $\Omega_c D_s$ | $\Omega_{cc}\eta'$ | $\Omega_{cc}\phi$ |
| 4494.6, | 4577.6, | 4585.2, | 4654.7, | 4666.0, | 4669.8, | 4731.5, |
| | | $\Omega_c D_s^*$ | $\Omega_{cc}^*\phi$ | $\Omega_c^* D_s^*$ | | |
| | | 4809.8, | 4814.5, | 4880.6. | | |

There are three predicted bound states at 3761.8 MeV, 3792.8 MeV, and 3900.2 MeV, coupling strongly to $\Xi_c^* D^*$, $\Xi_c' D^*$ and $\Xi_{cc}\bar{K}$, respectively. They are shown in Table 3.8 and Fig. 3.14. In Ref. [141] four states were generated from the SU(4) 3-plet at 3.71 GeV, 3.74 GeV, and 3.81 GeV, and one coming from the SU(4) 15-plet at 4.57 GeV. We might be tempted to identify our three states with those coming from SU(4) 3-plet in Ref. [141] because the dominant channels are similar, if we do not consider those including vector mesons and $3/2^+$ baryons. However, the only clear identification that can be done is between our state at 3900.2 MeV and the one in Ref. [141] at 3.81 GeV because in this case the dominant channels coincide. For this state, channels with vector mesons and/or $3/2^+$ baryons do not play a significant role.

### 3.7.2 Sector $J = 3/2$

The 16 channels in the $\Omega_{cc}^*$ sector are:

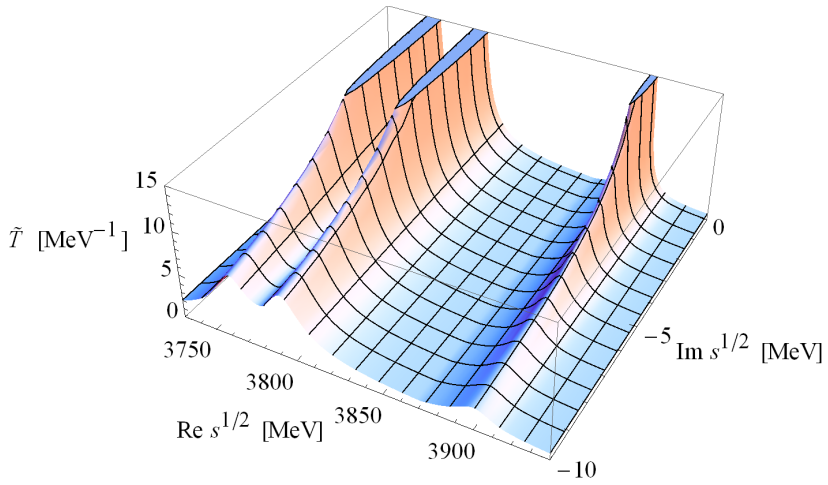


Figure 3.14: $\tilde{T}^{I=0,\ J=\frac{1}{2},\ S=-1,\ C=2}(s)$ amplitude ($\Omega_{cc}$ resonances).

| SU(8) irrep | SU(6) irrep | SU(3) irrep | $M_R$ | $\Gamma_R$ | Couplings to main channels | $J$ |
|---|---|---|---|---|---|---|
| **168** | $\mathbf{6_{1,2}}$ | $\mathbf{3_2}$ | 3761.8 | 0.0 | $g_{\Xi_c D}=1.2$, $g_{\Xi_c' D}=2.7$, $g_{\Xi_c D^*}=2.9$, $g_{\Xi_c' D^*}=2.0$, $g_{\Xi_c^* D^*}=3.6$, $g_{\Omega_c D_s}=1.9$, $g_{\Omega_c D_s^*}=1.4$, $g_{\Omega_c^* D_s^*}=2.5$ | 1/2 |
| **168** | $\mathbf{6_{3,2}}$ | $\mathbf{3_2}$ | 3792.8 | 0.0 | $g_{\Xi_{cc}\bar{K}}=0.9$, $g_{\Xi_c D}=2.3$, $g_{\Xi_c' D}=0.9$, $g_{\Omega_{cc}\eta'}=1.2$, $g_{\Xi_c' D^*}=3.5$, $g_{\Xi_{cc}^*\bar{K}^*}=1.1$, $g_{\Xi_c^* D^*}=2.7$, $g_{\Omega_c D_s^*}=2.6$, $g_{\Omega_c^* D_s^*}=2.0$ | 1/2 |
| **168** | $\mathbf{6_{3,2}}$ | $\mathbf{3_4}$ | 3802.9 | 0.0 | $g_{\Xi_c D^*}=2.5$, $g_{\Xi_c^* D}=2.6$, $g_{\Xi_c' D^*}=1.6$, $g_{\Xi_{cc}^*\bar{K}^*}=0.9$, $g_{\Xi_c^* D^*}=3.3$, $g_{\Omega_c^* D_s}=2.0$, $g_{\Omega_c D_s^*}=1.2$, $g_{\Omega_{cc}^*\eta'}=1.1$, $g_{\Omega_c^* D_s^*}=2.5$ | 3/2 |
| **120** | $\mathbf{6_{3,2}}$ | $\mathbf{3_2}$ | 3900.2 | 0.0 | $g_{\Xi_{cc}\bar{K}}=2.1$, $g_{\Omega_{cc}\eta}=1.1$, $g_{\Xi_c D}=1.6$, $g_{\Xi_c D^*}=0.9$, $g_{\Xi_{cc}^*\bar{K}^*}=1.3$, $g_{\Omega_c D_s^*}=1.$ | 1/2 |
| **120** | $\mathbf{6_{3,2}}$ | $\mathbf{3_4}$ | 3936.3 | 0.0 | $g_{\Xi_{cc}^*\bar{K}}=2.1$, $g_{\Xi_{cc}\bar{K}^*}=1.4$, $g_{\Omega_{cc}^*\eta}=1.$, $g_{\Xi_c D^*}=1.6$, $g_{\Xi_{cc}^*\bar{K}^*}=1.3$, $g_{\Omega_c^* D_s^*}=0.9$ | 3/2 |

Table 3.8: $\Omega_{cc}$ and $\Omega_{cc}^*$ resonances.

| | | | | | | |
|---|---|---|---|---|---|---|
| $\Xi_{cc}^*\bar{K}$ | $\Omega_{cc}^*\eta$ | $\Xi_{cc}\bar{K}^*$ | $\Xi_c D^*$ | $\Xi_{cc}^*\bar{K}^*$ | $\Omega_{cc}\omega$ | $\Xi_c^* D$ |
| 4095.7, | 4342.5, | 4412.9, | 4477.8, | 4493.9, | 4494.6, | 4513.6, |
| $\Omega_{cc}^*\omega$ | $\Xi_c' D^*$ | $\Xi_c^* D^*$ | $\Omega_{cc}\phi$ | $\Omega_c^* D_s$ | $\Omega_{cc}^*\eta'$ | $\Omega_c D_s^*$ |
| 4577.6, | 4585.2, | 4654.7, | 4731.5, | 4736.8, | 4752.8, | 4809.8, |
| $\Omega_{cc}^*\phi$ | $\Omega_c^* D_s^*$ | | | | | |
| 4814.5, | 4880.6. | | | | | |

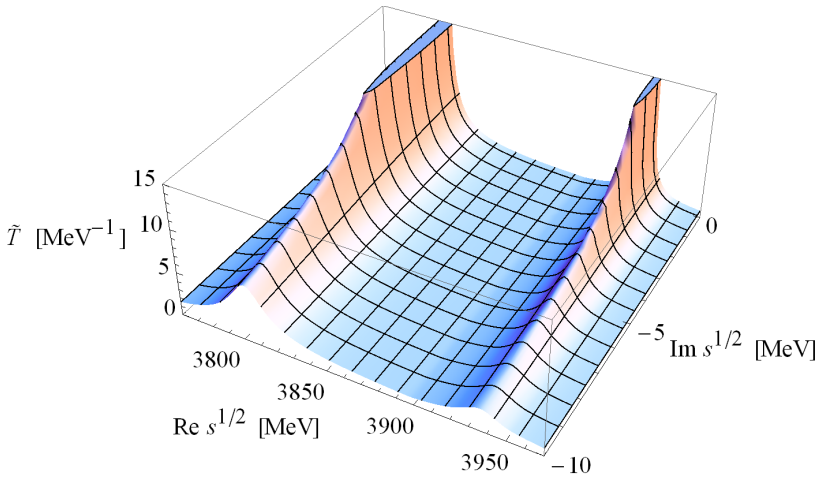


Figure 3.15: $\tilde{T}^{I=0,\ J=\frac{3}{2},\ S=-1,\ C=2}(s)$ amplitude ($\Omega^*_{cc}$ resonances).

Two bound states at 3802.9 MeV and 3936.3 MeV have been observed, which couple mostly to $\Xi^*_c D^*$ and $\Xi^*_{cc}\bar{K}$, respectively (see Table 3.8 and Fig. 3.15). Compared to Ref. [142], we observe a similar pattern as observed in the $C = 2$, $S = 0$, $I = 1/2$, $J = 3/2$ sector. The two expected states are obtained with larger masses and the dominant molecular composition incorporates a vector meson, or a vector meson and $3/2^+$ baryon state when heavy-quark symmetry is implemented. As indicated also in Ref. [142], the second resonance should be more reliable, as its main molecular contribution comes from the interaction of a baryon with a Goldstone boson.

## 3.8 $\Omega_{ccc}$ states ($C = 3$, $S = 0$, $I = 0$)

We finally study baryon resonances with charm $C = 3$ and strangeness $S = 0$.

### 3.8.1 Sector $J = 1/2$

The 8 coupled channels in the sector with $J = 1/2$ are as follows:

| $\Xi_{cc}D$ | $\Xi_{cc}D^*$ | $\Omega_{ccc}\omega$ | $\Xi^*_{cc}D^*$ | $\Omega_{cc}D_s$ | $\Omega_{ccc}\phi$ | $\Omega_{cc}D^*_s$ | $\Omega^*_{cc}D^*_s$ |
|---|---|---|---|---|---|---|---|
| 5386.2, | 5527.3, | 5581.6, | 5608.4, | 5680.5, | 5818.5, | 5824.3, | 5907.3. |

There is only one baryon state generated by the model in this sector. The mass (4358.2 MeV), width (0 MeV), and the couplings are shown in the Table 3.9 and Fig. 3.16. In Ref. [141], a resonance at 4.31 - 4.33 GeV was also obtained. In both schemes, the $\Omega_{ccc}$ resonance couples strongly to $\Xi_{cc}D$ and $\Omega_{cc}D_s$, but in our model the dominant contribution comes from channels with vector mesons and/or $3/2^+$ baryons. Therefore, this result points to the necessity of extending the coupled-channels basis to incorporate channels with charmed vector mesons and $3/2^+$ baryons as required by heavy-quark symmetry.

| SU(8) irrep | SU(6) irrep | SU(3) irrep | $M_R$ | $\Gamma_R$ | Couplings to main channels | $J$ |
|---|---|---|---|---|---|---|
| **168** | $\mathbf{1_{2,3}}$ | $\mathbf{1_2}$ | 4358.2 | 0.0 | $g_{\Xi_{cc}D}=2.9$, $g_{\Omega_{cc}D_s}=1.3$, $g_{\Xi_{cc}D^*}=1.9$, $g_{\Xi^*_{cc}D^*}=4.6$, $g_{\Omega^*_{cc}D^*_s}=2.1$ | 1/2 |
| **120** | $\mathbf{1_{4,3}}$ | $\mathbf{1_4}$ | 4501.4 | 0.0 | $g_{\Xi_{cc}D^*}=2.9$, $g_{\Xi^*_{cc}D}=2.4$, $g_{\Omega_{cc}D^*_s}=1.8$, $g_{\Xi^*_{cc}D^*}=2.9$, $g_{\Omega^*_{cc}D_s}=1.5$, $g_{\Omega_{ccc}\eta'}=1.2$, $g_{\Omega^*_{cc}D^*_s}=1.9$ | 3/2 |

Table 3.9: $\Omega_{ccc}$ and $\Omega^*_{ccc}$ resonances. These two states are HQSS singlets.

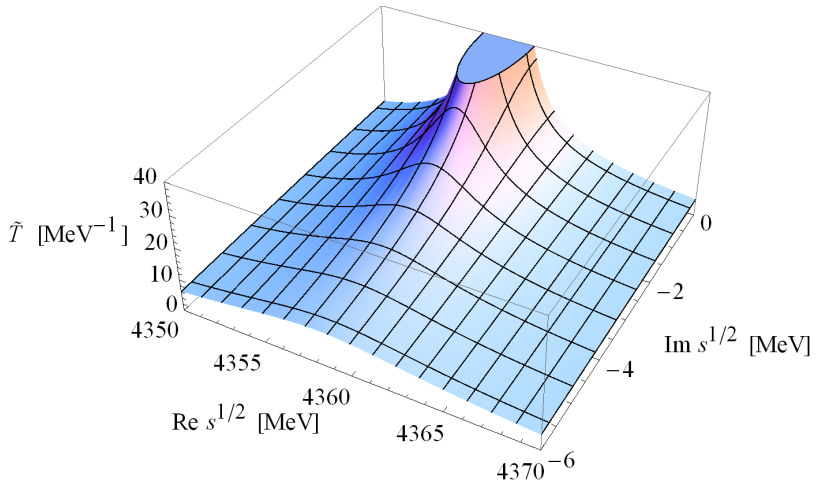


Figure 3.16: $\tilde{T}^{I=0,\ J=\frac{1}{2},\ S=0,\ C=3}(s)$ amplitude ($\Omega_{ccc}$ resonance).

### 3.8.2 Sector $J = 3/2$

The 10 channels and thresholds (in MeV) in the sector $\Omega^*_{ccc}$ are as follows:

| | | | | | | | |
|---|---|---|---|---|---|---|---|
| $\Omega_{ccc}\eta$ | $\Xi^*_{cc}D$ | $\Xi_{cc}D^*$ | $\Omega_{ccc}\omega$ | $\Xi^*_{cc}D^*$ | $\Omega_{ccc}\eta'$ | $\Omega^*_{cc}D_s$ | $\Omega_{ccc}\phi$ |
| 5346.5, | 5467.2, | 5527.3, | 5581.6, | 5608.4, | 5756.8, | 5763.5, | 5818.5, |
| | | | $\Omega_{cc}D^*_s$ | $\Omega^*_{cc}D^*_s$ | | | |
| | | | 5824.3, | 5907.3. | | | |

The $\Omega^*_{ccc}$ resonance with $J = 3/2$ has a mass approximately 1 GeV below the lowest baryon-meson threshold. This resonance stems from the **120** irrep of SU(8) and it is shown in Table 3.9 and Fig. 3.17. One resonance was also seen in Ref. [142], much below the first open threshold, coupling dominantly to $\Xi_{cc}D$. Our results show that this bound state mainly couples to $\Xi_{cc}D^*$, $\Xi^*_{cc}D^*$ and $\Xi^*_{cc}D$ states as we incorporate charmed vector mesons and $3/2^+$ baryons according to heavy-quark symmetry. The large separation from the closest threshold suggests that interaction mechanisms involving $d$-waves could

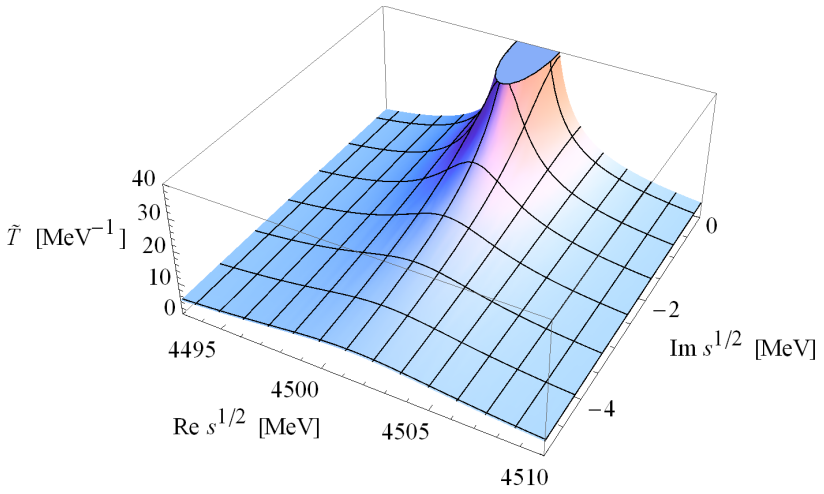


Figure 3.17: $\tilde{T}^{I=0,\ J=\frac{3}{2},\ S=0,\ C=3}(s)$ amplitude ($\Omega^*_{ccc}$ resonance).

be relevant for this resonance. This remark applies also to the $\Omega_{ccc}$ dynamically-generated resonance with $J = 1/2$.

## 3.9 HQSS in the results

The factor $\mathrm{SU}_C(2) \times \mathrm{U}_C(1)$ in Eq. (3.1) implements HQSS for the sectors studied in this work. The HQSS group acts by changing the coupling of spin of the charmed quarks, relative to the spin of the block formed by light quarks. At the level of basic hadrons, it reflects in the nearly degeneracy of $D$ and $D^*$ mesons, which form a HQSS doublet.[3] Other doublets are $(\bar{D}_s, \bar{D}^*_s)$, and $(\eta_c, J/\psi)$ in mesons, and $(\Sigma_c, \Sigma^*_c)$, $(\Xi'_c, \Xi^*_c)$, $(\Omega_c, \Omega^*_c)$, $(\Xi_{cc}, \Xi^*_{cc})$, $(\Omega_{cc}, \Omega^*_{cc})$, in baryons. On the other hand, $\Lambda_c$, $\Xi_c$ and $\Omega_{ccc}$ are singlets, as are all the other basic hadrons not containing charmed quarks. This information is collected in Table 2.1. The classification of basic hadrons into HQSS multiplets can be obtained from the hadron wavefunctions that are included in Appendix A. For instance, for $\Sigma_c$ and $\Sigma^*_c$ the two light quarks are coupled to spin triplet (since they form an isospin triplet and color is antisymmetric) and this can give $J = 1/2$ or $J = 3/2$ when coupled to the spin of the charmed quark. A systematic classification can be found in [190].

HQSS multiplets form also in the baryon-meson states. Specifically, in the reduction in Eq. (3.3) and Figs. 3.1, 3.2, and 3.3, the pair $(\mathbf{6_2}, \mathbf{6_4})$ forms a HQSS doublet in the reduction of $\mathbf{21_{2,1}}$, while $\mathbf{3^*_2}$ is a singlet. Similarly, $(\mathbf{3^*_2}, \mathbf{3^*_4})$ in $\mathbf{15_{2,1}}$, and $(\mathbf{3_2}, \mathbf{3_4})$ in $\mathbf{6_{3,2}}$, are doublets, whereas all other SU(3) × SU(2) representations are HQSS singlets.

HQSS is much less broken than spin-flavor of light quarks, implemented by SU(6), so HQSS is more visible in the results. If we imposed strict HQSS, by setting equal masses and decay constants as required by the symmetry, exactly degenerated HQSS multiplet

[3] We use "doublet" to indicate that only two multiplets with well-defined $CSIJ$ get mixed by the HQSS group. The space spanned by the eight $D$ or $D^*$ states reduces into two dimension-four irreducible subspaces under HQSS, corresponding to the four spin states of $D$ and $D^*$ with given charge.

would form, regardless of the amount of breaking of SU(6). We break HQSS only through the use of physical masses and decay constants[4], but not in the interaction. Therefore we estimate that our breaking is no larger than that present in QCD. This suggests that the amount of breaking we find is not an overestimation due to the model, on the contrary, we expect to find more degeneracy than actually exists.

The approximate HQSS doublets can be observed in the results by comparing states with equal SU(8) and SU(6) $\times$ SU$_C$(2) $\times$ U$_C$(1) labels with $J = 1/2$ and $J = 3/2$. The only exception is for the $\Xi_{cc}$ states in Table 3.7 where the SU(8) labels are mixed in the two doublets. As noted in Section 2.3 this reflects the fact that exact SU(8) symmetry is broken in the interaction after dropping the channels with extra $c\bar{c}$ pairs.

For convenience we have arranged the tables so that HQSS partners are in consecutive rows. So, in Table 3.2, the $\Lambda_c$ state 2617.3 MeV with labels $(\mathbf{168}, \mathbf{15_{2,1}}, \mathbf{3^*_2})$, matches the $\Lambda_c^*$ state 2666.6 MeV with labels $(\mathbf{168}, \mathbf{15_{2,1}}, \mathbf{3^*_4})$. The matching refers not only to the mass but also the width and the couplings, taking into account that, e.g., $\Sigma_c$ in one state corresponds to $\Sigma_c^*$ in the other. (Note that HQSS also implies relations between couplings in the same resonance.) If the identifications in Table 3.2 are correct, it would imply that $\Lambda_c(2595)$ is a HQSS singlet whereas $\Lambda_c(2625)$ belongs to a doublet. Similarly, in Table 3.4, the $\Sigma_c$ state 2571.5 MeV is the HQSS partner of the $\Sigma_c^*$ state 2568.4 MeV [both in $(\mathbf{168}, \mathbf{21_{2,1}})$], whereas the states 2643.4 MeV and 2692.9 MeV are partners in $(\mathbf{120}, \mathbf{21_{2,1}})$. Of special interest is the case of $\Xi_c$ states. Here we find that the two three-star resonances $\Xi_c(2790)$ and $\Xi_c(2815)$ are candidates to form a HQSS doublet. Further doublets are predicted for $\Omega_c$ and for the $C = 2$ resonances, $\Xi_{cc}$ and $\Omega_{cc}$. On the other hand, no doublet is present in the $\Omega_{ccc}$ sector. All these considerations follow unambiguously from the SU(8) structure if the **168** and **120** irreps are dominant, as predicted by the extended WT scheme.

## 3.10 Inclusion of an additional charm-exchange suppression factor

In this section we discuss the effect of the inclusion of a suppression factor in the interaction when charm-exchange is present, in order to compare to previous works [144, 145].

In our approach, the interactions are implemented by a contact term, and each matrix element is affected by the decay constants of the mesons in the external legs of the interaction vertex. In particular, the charm-exchange terms always involve a $D \leftrightarrow \pi$-like transition, and thus they carry a factor $1/(f_\pi f_D)$. This source of flavor symmetry breaking turns out to enhance (suppress) these transitions with respect to some others like $ND \to ND$ ($\Sigma_c\pi \to \Sigma_c\pi$), where there is no charm exchange, and that scale instead like $1/f_D^2$ ($1/f_\pi^2$).

On the other hand, only decay constants of light mesons are involved in the $t$-channel vector-meson exchange models, as the one used in [141, 142, 144]. Nevertheless, there is another source of quenching for charm-exchange interactions, coming from the larger mass

[4]Most of the values in Table 2.1 are obtained from experiment, while some of them are guesses from models or from lattice calculations.

of the charmed meson exchanged, as compared to those of the vector mesons belonging to the $\rho$ nonet. Qualitatively, a factor $\kappa_c = 1/4 \simeq m_\rho^2/m_{D^*}^2$ is applied in the matrix elements involving charm exchange, whereas $\kappa_c = 1$ is kept in the remaining matrix elements [144]. The introduction of these quenching factors does not spoil HQSS (note, however, that neither the scheme of Ref. [141,142] nor that of Ref. [144] are consistent with HQSS) but it is a new source of flavor breaking. Here, in this section, we study the effects of including this suppression factor $\kappa_c$ within our scheme. In this case, the potential looks as follows:

$$V_{ij}(s) = \kappa_c D_{ij} \frac{2\sqrt{s} - M_i - M_j}{4\, f_i f_j} \sqrt{\frac{E_i + M_i}{2M_i}} \sqrt{\frac{E_j + M_j}{2M_j}}. \tag{3.5}$$

| SU(8) irrep | SU(6) irrep | SU(3) irrep | $M_R$ | $\Gamma_R$ | Couplings to main channels | Status PDG | $J$ |
|---|---|---|---|---|---|---|---|
| **168** | $\mathbf{15_{2,1}}$ | $\mathbf{3_2}$ | 2624.6 | 103.9 | $\boldsymbol{g_{\Sigma_c\pi} = 2.3}$, $g_{ND} = 0.4$, $g_{ND^*} = 0.4$, $g_{\Sigma_c\rho} = 1.6$ | | 1/2 |
| **168** | $\mathbf{15_{2,1}}$ | $\mathbf{3_4}$ | 2675.1 | 65.7 | $\boldsymbol{g_{\Sigma_c^*\pi} = 2.1}$, $g_{ND^*} = 0.5$, $g_{\Sigma_c\rho} = 0.9$, $g_{\Sigma_c^*\rho} = 1.6$ | $\Lambda_c(2625)$ *** | 3/2 |
| **168** | $\mathbf{21_{2,1}}$ | $\mathbf{3_2}$ | 2624.1 | 0.1 | $\boldsymbol{g_{\Sigma_c\pi} = 0.1}$, $g_{ND} = 3.4$, $g_{ND^*} = 5.7$, $g_{\Lambda D_s} = 1.4$, $g_{\Lambda D_s^*} = 3.0$, $g_{\Lambda_c\eta'} = 0.2$ | $\Lambda_c(2595)$ *** | 1/2 |
| **120** | $\mathbf{21_{2,1}}$ | $\mathbf{3_2}$ | 2824.9 | 0.4 | $\boldsymbol{g_{ND} = 0.1}$, $g_{\Lambda_c\eta} = 1.1$, $g_{\Xi_c K} = 1.9$, $g_{\Lambda D_s^*} = 1.1$, $g_{\Sigma_c\rho} = 1.1$, $g_{\Sigma_c^*\rho} = 1.4$, $g_{\Xi_c^* K^*} = 1.0$ | | 1/2 |

Table 3.10: $\Lambda_c$ and $\Lambda_c^*$ resonances with inclusion of the suppression factor $\kappa_c$.

In Tables 3.10 and 3.11 we show the results including the $\kappa_c$ factor for the sectors with $C = 1$, $S = 0$. As can be seen, there are some small changes in the masses and the widths of the resonances in comparison with the values shown in Tables 3.2 and 3.4, while the values of the couplings also change in some cases. However, in general, the changes induced by the inclusion of this new source of flavor breaking are not dramatic, and they do not modify the main conclusions of this work.

## 3.11 Summary

In this chapter we discuss the predictions of the model for all $C = 1$ strange sectors and analyzed the $C = 2$ and 3 predicted states. The extended to SF symmetry WT model modified with HQSS constraints generates a great number of states, most of them stemming from the **4752** representation. The interaction in this subspace, though attractive, is much weaker than in the **168** and **120** ones. Indeed, in the large $N_C$ limit, we expect that the **4752** states will disappear and only those related to the **168** representation will remain [172]. Besides, being so weak the interaction in the **4752** subspace, small corrections (higher orders in the expansion, $d$-wave terms, etc) could strongly modify the properties

| SU(8) irrep | SU(6) irrep | SU(3) irrep | $M_R$ | $\Gamma_R$ | Couplings to main channels | Status PDG | $J$ |
|---|---|---|---|---|---|---|---|
| **168** | $\mathbf{21_{2,1}}$ | $\mathbf{6_2}$ | 2583.4 | 0.0 | $\boldsymbol{g_{\Lambda_c\pi}=0.03}$, $g_{ND}=2.4$, $g_{ND^*}=1.3$, $g_{\Sigma D_s}=1.7$, $g_{\Delta D^*}=6.8$, $g_{\Sigma D_s^*}=1.2$, $g_{\Sigma^* D_s^*}=3.1$ | | 1/2 |
| **168** | $\mathbf{21_{2,1}}$ | $\mathbf{6_4}$ | 2577.8 | 0.0 | $g_{ND^*}=2.7$, $g_{\Delta D}=4.3$, $g_{\Delta D^*}=5.4$, $g_{\Sigma D_s^*}=2.4$, $g_{\Sigma^* D_s}=1.6$, $g_{\Sigma^* D_s^*}=2.4$ | | 3/2 |
| **168** | $\mathbf{15_{2,1}}$ | $\mathbf{6_2}$ | 2691.3 | 137.6 | $\boldsymbol{g_{\Lambda_c\pi}=1.6}$, $\boldsymbol{g_{\Sigma_c\pi}=0.3}$, $g_{ND}=0.5$, $g_{ND^*}=0.7$, $g_{\Xi_c K}=1.1$, $g_{\Sigma_c\rho}=1.8$, $g_{\Sigma_c^*\rho}=2.5$, $g_{\Xi_c^* K^*}=0.9$ | | 1/2 |
| **120** | $\mathbf{21_{2,1}}$ | $\mathbf{6_2}$ | 2653.9 | 95.0 | $\boldsymbol{g_{\Lambda_c\pi}=0.2}$, $\boldsymbol{g_{\Sigma_c\pi}=2.0}$, $g_{ND}=0.6$, $g_{ND^*}=0.4$, $g_{\Lambda_c\rho}=1.7$ $g_{\Delta D^*}=0.4$, $g_{\Sigma_c\rho}=1.3$, $g_{\Sigma^* D_s^*}=0.4$ | | 1/2 |
| **120** | $\mathbf{21_{2,1}}$ | $\mathbf{6_4}$ | 2697.2 | 65.8 | $\boldsymbol{g_{\Sigma_c^*\pi}=1.9}$, $g_{ND^*}=0.6$, $g_{\Lambda_c\rho}=1.7$, $g_{\Sigma_c^*\rho}=1.1$, $g_{\Sigma D_s^*}=0.3$, $g_{\Sigma^* D_s^*}=0.3$ | | 3/2 |

Table 3.11: $\Sigma_c$ and $\Sigma_c^*$ resonances with inclusion of the suppression factor $\kappa_c$.

of the states that arise from this representation. For these reasons, we have restricted our study in this work to the 288 states (counting multiplicities in spin and isospin) that stem from the **168** and **120** representations, for which we believe the predictions of the model are more robust.

To identify these states, we have adiabatically followed the trajectories of the **168** and **120** poles, generated in a symmetric SU(8) world, when the symmetry is broken down to SU(6) $\times$ SU$_C$(2) and later SU(6) is broken down to SU(3) $\times$ SU(2). In this way, we have been able to assign well-defined SU(8), SU(6) and SU(3) labels to the resonances. A first result of this work is that we have been able to identify the **168** and **120** resonances among the plethora of resonances predicted in Ref. [175] for the different strangeless $C=1$ sectors. As expected, they turn out to be the lowest-lying ones, and we expect them to find experimental confirmation in the near future. This appreciation is being reinforced by the previous study of Ref. [171] in the light SU(6) sector. Thus, we interpret the $\Lambda_c(2595)$ and $\Lambda_c(2625)$ as the members of the SU(8) **168**-plet, and in both cases with a dynamics strongly influenced by the $ND^*$ channel, in sharp contrast with previous studies inconsistent with HQSS. Moreover, the changes induced by a suppression factor in the interaction when charm is exchanged do not modify the conclusions. Second, we have identified the HQSS multiplets in which the resonances are arranged. Specifically, the $\Lambda_c$, $\Lambda_c^*$ sector arranges into two singlets, the $\Lambda_c(2595)$ being one of them, a doublet, which contains the $\Lambda_c(2625)$. Similarly, the $\Sigma_c$, $\Sigma_c^*$ sector contains one singlet and two doublets. For the $\Xi_c$, $\Xi_c^*$ sector, there are three doublets and three singlets. According to our tentative identification, $\Xi_c(2790)$ and $\Xi_c(2815)$ form a HQSS doublet. Finally, $\Omega_c$, $\Omega_c^*$ states form two doublets and one singlet. Third, we have worked out the predictions of the model of Ref. [175] for strange charmed and $C=2$ and $C=3$ resonances linked to the strongly attractive **168** and **120** subspaces. To our knowledge, these are the first

predictions in these sectors deduced from a model fulfilling HQSS. The organization into HQSS multiplets is also given in this case. There is scarce experimental information in these sectors, and we have only identified the three-star $\Xi_c(2790)$ and $\Xi_c(2815)$ resonances, but we believe that the rest of our predictions will find experimental confirmation in the future. Of particular relevance in this respect will be the program of PANDA at the future facility FAIR.

# Chapter 4

# Hidden-charm baryon resonances[1]

In this chapter we study dynamically-generated baryon resonances with hidden charm, in particular charmless ($C = 0$) and strangeless ($S = 0$) states $N$ ($I = 1/2$; $J = 1/2,\ 3/2,\ 5/2$) and $\Delta$ ($I = 3/2$; $J = 1/2,\ 3/2$).

We start this chapter with the analysis of the structure of the group multiplets. We classify the possible states under the symmetry group SU(6) $\times$ HQSS. Subsequently, we study the breaking of the light SF SU(6) down to the SU(3) $\times$ SU(2) (flavor symmetry and spin symmetry for light flavors, respectively), keeping HQSS. Further, the SU(3) flavor symmetry is broken to SU(2) isospin symmetry, and finally the HQSS symmetry is broken. Furthermore, in this chapter we present our dynamically-generated hidden-charm states. We predict the existence of seven $N$-like and five $\Delta$-like resonances, with masses around 4 GeV, most of them as bound states. We also identify the different HQSS multiplets, which are nearly degenerate in mass.

There are some recent works [150–153] that predict the existence of a few $N$-like states with masses around 4 GeV, which result from the baryon-meson scattering in this hidden-charm sector. We compare our results with the results of these other theoretical models. No experimental data is yet available for the states we study, but the predicted new resonances might be subject to experimental detection in the forthcoming PANDA experiment at FAIR. If confirmed, they definitely cannot be accommodated by quark models with three constituent quarks.

[1] This chapter is based on C. Garcia-Recio, J. Nieves, O. Romanets, L. L. Salcedo, and L. Tolos, Phys. Rev. D **87**, 074034 (2013) (Ref. [188]).

## 4.1 Analysis of the hidden-charm sector with $C = 0$

We want to classify the possible states in the hidden-charm sectors under the symmetry group SU(6) × HQSS, with HQSS = $\mathrm{SU}_c(2) \times \mathrm{SU}_{\bar{c}}(2) \times \mathrm{U}_c(1) \times \mathrm{U}_{\bar{c}}(1)$. Since in the hidden-charm sectors there is exactly one heavy antiquark, it is not necessary to specify the irrep of the factor $\mathrm{SU}_{\bar{c}}(2) \times \mathrm{U}_{\bar{c}}(1)$ and we can use the notation $\boldsymbol{R}_{2J_c+1,C}$ for the irreps of SU(6) × HQSS, $\boldsymbol{R}$ being the SU(6) irrep of the light sector, $C$ the charm quantum number and $J_c$ the total spin carried by one or more $c$ quarks (not including the spin of the $\bar{c}$ antiquarks). The corresponding dimension is $\dim \boldsymbol{R} \times (2J_c + 1) \times 2$ (the last factor coming from the two possible spin states of the $\bar{c}$).

Subsequently, we study the breaking of light SF SU(6) down to $\mathrm{SU}(3) \times \mathrm{SU}(2)$ keeping HQSS, and enumerate the number of attractive channels in each $(C, \boldsymbol{r}, J)$ sector, where $\boldsymbol{r}$ is the SU(3) irrep and $J$ is the total spin.

In practice we will assume exact isospin and spin $\mathrm{SU}(2)_I \times \mathrm{SU}(2)_J$, as well as conservation of each flavor, but not exact SU(3) and HQSS, for the baryons and mesons forming the coupled-channels space. Therefore the sectors are labeled by $(C, S, I, J)$, $S = 0$ being the strangeness quantum number and $I$ the isospin. This implies a further breaking of each $(C, \boldsymbol{r}, J)$ sector into $(C, S, I, J)$ subsectors. Here we consider the hidden-charm sector with $C = 0$, i.e. $N_{\bar{c}} = 1$ and $N_c = 1$.

For $C = 0$, the quark content is $\ell\ell\ell c\bar{c}$, with two possibilities of grouping into baryon-meson: $(\ell\ell\ell)(c\bar{c})$ and $(\ell\ell c)(\ell\bar{c})$. (Here $\ell$ denotes any light flavor quark, $u, d, s$.) The total dimension of the space is $56 \times 2 \times 2 + 21 \times 2 \times 6 \times 2 = 728$, and contains the following SU(6) × HQSS multiplets:[2]

$$\mathcal{H}_{C=0} = \mathbf{56}_{2,0} \oplus \mathbf{56}_{2,0} \oplus \mathbf{70}_{2,0} \qquad [\mathrm{SU}(6) \times \mathrm{HQSS}]. \tag{4.1}$$

The eigenvalues turn out to be

$$\lambda_{\mathbf{56}_{2,0}} = \lambda_{\mathbf{70}_{2,0}} = -2, \qquad \lambda'_{\mathbf{56}_{2,0}} = 6. \tag{4.2}$$

An accidental degeneracy between $\mathbf{70}_{2,0}$ and one $\mathbf{56}_{2,0}$ that occurs in our model is not a necessary consequence of SU(6) × HQSS. This symmetry does not fix the three eigenvalues and the precise splitting between the two copies of $\mathbf{56}_{2,0}$. The accidental symmetry is lifted in $V$ and the $T$-matrix even when an exact SU(6) × HQSS invariance is assumed in the hadron masses and meson decay constants.

Next, we consider the breaking of light SF SU(6) down to $\mathrm{SU}(3) \times \mathrm{SU}_{J_\ell}(2)$, e.g., $\mathbf{56} = \mathbf{8}_2 \oplus \mathbf{10}_4$, while HQSS is unbroken. After recoupling the spin carried by light and heavy quarks and antiquarks to yield the total spin $J$, we obtain the representations of $\mathrm{SU}(3) \times \mathrm{SU}(2)_J$ labeled as $\boldsymbol{r}_{2J+1}$, where $\boldsymbol{r}$ is the SU(3) irrep. This yields the following reductions (the two $\mathbf{56}_{2,0}$ have the same reduction):

$$\begin{aligned}
\mathbf{56}_{2,0} =& (\mathbf{8}_2 \oplus \mathbf{10}_4)_{2,0} = (\mathbf{8}_2 \oplus \mathbf{8}_2 \oplus \mathbf{8}_4) \oplus (\mathbf{10}_2 \oplus \mathbf{10}_4 \oplus \mathbf{10}_4 \oplus \mathbf{10}_6), \\
\mathbf{70}_{2,0} =& (\mathbf{1}_2 \oplus \mathbf{8}_2 \oplus \mathbf{8}_4 \oplus \mathbf{10}_2)_{2,0} = (\mathbf{1}_2 \oplus \mathbf{1}_2 \oplus \mathbf{1}_4) \oplus (\mathbf{8}_2 \oplus \mathbf{8}_2 \oplus \mathbf{8}_4) \\
& \oplus (\mathbf{8}_2 \oplus \mathbf{8}_4 \oplus \mathbf{8}_4 \oplus \mathbf{8}_6) \oplus (\mathbf{10}_2 \oplus \mathbf{10}_2 \oplus \mathbf{10}_4).
\end{aligned} \tag{4.3}$$

[2] $(\ell\ell\ell)(c\bar{c})$ is purely $\mathbf{56}_{2,0}$ from the symmetry of the three light quarks. The two light quarks in $(\ell\ell c)$ are symmetric giving a $\mathbf{21}$ of SU(6), that couples to the light quark in $(\ell\bar{c})$ giving $\mathbf{21} \otimes \mathbf{6} = \mathbf{56} \oplus \mathbf{70}$. These two $\mathbf{56}_{2,0}$ are not directly those in Eqs. (4.1) and (4.2).

In the reduction $(\mathbf{8}_2)_{2,0} = (\mathbf{8}_2 \oplus \mathbf{8}_2 \oplus \mathbf{8}_4)$ in $\mathbf{56}_{2,0}$, the three octets only differ in how the light-sector spin is coupled to the heavy-sector spin; therefore these three irreps are degenerated if exact HQSS is assumed. The $(\mathbf{8}_2 \oplus \mathbf{8}_2 \oplus \mathbf{8}_4)$ is a multiplet of $\mathrm{SU}(3) \times \mathrm{HQSS}$. Similar statements hold in the other cases: each $\mathbf{56}_{2,0}$ produces two such multiplets and $\mathbf{70}_{2,0}$ produces four. Consequently, in the hidden-charm sector with $C = 0$ we expect to find eight different eigenvalues after $\mathrm{SU}(6) \times \mathrm{HQSS}$ is broken down to $\mathrm{SU}(3) \times \mathrm{HQSS}$. Let $\lambda_1$, $\lambda_2$ be the eigenvalues of the two multiplets in the repulsive $\mathbf{56}_{2,0}$, $\lambda_3$, $\lambda_4$ in the attractive $\mathbf{56}_{2,0}$, and $\lambda_5$, $\lambda_6$, $\lambda_7$, $\lambda_8$ those in $\mathbf{70}_{2,0}$. In this case, the spectra in each $(C, \boldsymbol{r}, J)$ sector are as follows:

$$\begin{aligned}
\mathbf{1}_2 &: (\lambda_5, \lambda_5), \\
\mathbf{1}_4 &: (\lambda_5), \\
\mathbf{8}_2 &: (\lambda_1, \lambda_1, \lambda_3, \lambda_3, \lambda_6, \lambda_6, \lambda_7), \\
\mathbf{8}_4 &: (\lambda_1, \lambda_3, \lambda_6, \lambda_7, \lambda_7), \\
\mathbf{8}_6 &: (\lambda_7), \\
\mathbf{10}_2 &: (\lambda_2, \lambda_4, \lambda_8, \lambda_8), \\
\mathbf{10}_4 &: (\lambda_2, \lambda_2, \lambda_4, \lambda_4, \lambda_8), \\
\mathbf{10}_6 &: (\lambda_2, \lambda_4).
\end{aligned} \tag{4.4}$$

In the SU(6) limit, $\lambda_1 = \lambda_2$, $\lambda_3 = \lambda_4$, $\lambda_5 = \lambda_6 = \lambda_7 = \lambda_8$. Breaking down the symmetry to SU(3), one expects

$$\lambda_{3,4,5,6,7,8} < 0 < \lambda_{1,2}. \tag{4.5}$$

Each negative eigenvalue can give rise to a resonance or bound state. Each such state is a full multiplet of $\mathrm{SU}(3) \times \mathrm{SU}(2)_J$. This implies the following expected number of states in each $(C, \boldsymbol{r}, J)$ sector: up to two states in $\mathbf{1}_2$, one in $\mathbf{1}_4$, five in $\mathbf{8}_2$, four in $\mathbf{8}_4$, one in $\mathbf{8}_6$, three in $\mathbf{10}_2$, three in $\mathbf{10}_4$, and one in $\mathbf{10}_6$, all of them with $C = 0$. These results are also summarized in Table 4.1.

| | C | | 0 | |
|---|---|---|---|---|
| J | SU(3) | **1** | **8** | **10** |
| 1/2 | | 2 | 7 | 4 |
| | | (2) | (5) | (3) |
| 3/2 | | 1 | 5 | 5 |
| | | (1) | (4) | (3) |
| 5/2 | | 0 | 1 | 2 |
| | | (0) | (1) | (1) |

Table 4.1: Total number of channels for each $J$ and each SU(3) irrep, for the hidden-charm $C = 0$ sector. Here each channel represents a full SU(3) and spin multiplet $(C, \boldsymbol{r}, J)$ [rather than a isospin-spin multiplet, $(C, S, I, J)$]. The expected number of resonances in each case is shown between parentheses.

## 4.2 Dynamically-generated hidden-charm $N$ and $\Delta$ states

As was mentioned in Section 2.1.3, we use a slightly different expression for the potential, as compared to Eq. (2.31). This was done to be consistent with Ref. [188]. The potential reads

$$V_{ij}(\sqrt{s}) = D_{ij}\frac{1}{4f_i f_j}(k_i^0 + k_j'^0), \tag{4.6}$$

where $k_i^0$ and $k_j'^0$ are the center-of-mass energies of the incoming and outgoing mesons, respectively, and $f_i$ and $f_j$ are the decay constants of the meson in the $i$-channel and $j$-channel. The $D_{ij}$ matrices for this sector are collected in Appendix C. With this prescription for the potential, the loop function that appears in the Bethe-Salpeter equation (2.33) reads

$$G_{ii}(s) = \frac{(\sqrt{s}+M_i)^2 - m_i^2}{2\sqrt{s}}(\bar{J}_0(s; M_i, m_i) - \bar{J}_0(\mu; M_i, m_i)). \tag{4.7}$$

As compared to Eq. (2.37), there is a factor $(E_i + M_i)/(2M_i)$ difference.

We find several $I = 1/2$ and $I = 3/2$ hidden-charm states, which correspond to $N$-like and $\Delta$-like states, respectively (here we use the same notation as in Refs. [150, 151]). All these states have odd parity and different values ($J = 1/2,\ 3/2$ and $5/2$) of total angular momentum.

In this hidden-charm sector and in the SU(6) $\times$ HQSS limit, we saw [Eqs. (4.1) and (4.2)] that the group structure of the HQSS-constrained extension of the WT interaction developed in this work consists of two $\mathbf{56_{2,0}}$ and one $\mathbf{70_{2,0}}$ representations. One of the $\mathbf{56_{2,0}}$ multiplets and the $\mathbf{70_{2,0}}$ one are attractive. Thus, from the decomposition in Eq. (4.3) (see also Table 4.1), we could expect up to a total of ten $N$-like and seven $\Delta$-like resonances.[3] Because of the breaking of the SU(6) $\times$ HQSS symmetry due to the use of physical hadron masses and meson decay constants, we only find seven heavy $N$ and five heavy $\Delta$ states in the second Riemann sheets. They have masses around 4 GeV and most of them turn out to be bound. The remaining missing states show up in an unphysical region of the Riemann surface. The evolution of all states as we gradually break the symmetry from SU(6) $\times$ HQSS down to SU(3) $\times$ HQSS, then to SU(2) $\times$ HQSS, and finally down to SU(2) isospin, is depicted in Fig. 4.1. Thanks to this latter study, we could assign SU(6) $\times$ HQSS and SU(3) $\times$ HQSS labels to each of the predicted resonances, which are all of them collected in Tables 4.2 and 4.4, and could also identify two HQSS multiplets in each isospin sector.

### 4.2.1 $N$ states ($C = 0$, $S = 0$, $I = 1/2$)

As mentioned above, we find seven heavy nucleon resonances: three states with the spin-parity $J^P = \frac{1}{2}^-$, also three states with $\frac{3}{2}^-$ sectors, and one state with $J^P = \frac{5}{2}^-$. Their masses, widths and couplings to the different channels are compiled in Table 4.2.

[3] Those lie in the SU(3) octets and decuplets irreps, respectively, contained in the attractive $\mathbf{56_{2,0}}$ and $\mathbf{70_{2,0}}$ multiplets.

- $\mathbf{J = 1/2}$ : In this sector, there are seven coupled channels, with the following threshold energies (in MeV):

$$\begin{array}{ccccccc} N\eta_c & NJ/\psi & \Lambda_c\bar{D} & \Lambda_c\bar{D}^* & \Sigma_c\bar{D} & \Sigma_c\bar{D}^* & \Sigma_c^*\bar{D}^* \\ 3918.6, & 4035.8, & 4153.7, & 4294.8, & 4320.8, & 4461.9, & 4526.3. \end{array}$$

- $\mathbf{J = 3/2}$ : In this sector, there are five coupled channels, with the following threshold energies:

$$\begin{array}{ccccc} NJ/\psi & \Lambda_c\bar{D}^* & \Sigma_c^*\bar{D} & \Sigma_c\bar{D}^* & \Sigma_c^*\bar{D}^* \\ 4035.8, & 4294.8, & 4385.2, & 4461.9, & 4526.3. \end{array}$$

- $\mathbf{J = 5/2}$ : In this sector there is only one channel, $\Sigma_c^*\bar{D}^*$, with threshold equal to 4526.3 MeV.

From the group decomposition of the SU(6) $\times$ HQSS representations, we could expect up to a maximum of five states with spin $J = 1/2$ (see Table 4.1): one state from each of the two $J = 1/2$ octets encoded in the attractive $\mathbf{56_{2,0}}$ representation, and three states corresponding to the each of the $\mathbf{8_2}$ octets that appear in the reduction of the $\mathbf{70_{2,0}}$ representation [Eq. (4.3)]. However, the two poles related to the $\mathbf{56_{2,0}}$ representation appear in an unphysical region of the Riemann surface at the physical point (i.e., at the point of the evolution when the hadron masses and meson decay constants attain their physical values). As it can be seen from Fig. 4.1, these poles disappear from the physical sheet when we pass from the SU(3) $\times$ HQSS limit to the SU(2) $\times$ HQSS one. Indeed, we could observe how the $(\mathbf{8_2})_{\mathbf{2,0}} \subset (\mathbf{56_2})_{\mathbf{2,0}}$ pole almost coincides with the threshold value of the degenerated $N\eta_c$ and $NJ/\psi$ channels in the first steps of this evolution until it finally disappears. On the other hand, the $(\mathbf{8_2})_{\mathbf{2,0}} \subset (\mathbf{56_2})_{\mathbf{2,0}}$ pole also gives rise to an octet of $J = 3/2$ states [see Eq. (4.3)], which is also lost at the physical point. Thus, for $J = 3/2$ we are also left only with the three baryon resonances stemming from the $\mathbf{70_{2,0}}$ representation, one from $(\mathbf{8_2})_{\mathbf{2,0}}$, and two from $(\mathbf{8_4})_{\mathbf{2,0}}$. The $J = 5/2$ state is originated also from this latter multiplet.

From the above discussion, it is clear that the $N$-like resonances found in this work, and collected in Table 4.2, form two HQSS multiplets. In the first one the light degrees of freedom have quantum numbers $(\mathbf{8_2})_{\mathbf{2,0}} \subset \mathbf{70_{2,0}}$. This multiplet is formed by the three first resonances of the table (two with spin 1/2 and third one with spin 3/2) that correspond to the blue lines with labels $\mathbf{70_{2,0}}$ and $(\mathbf{8_2})_{\mathbf{2,0}}$ in Fig. 4.1. They only differ in how the light-sector spin is coupled to the spin of the $c\bar{c}$ pair. The second HQSS multiplet corresponds to $(\mathbf{8_4})_{\mathbf{2,0}} \subset \mathbf{70_{2,0}}$ quantum numbers for the light sector, and it consists of the four remaining states in Table 4.2 (displayed with green lines with labels $\mathbf{70_{2,0}}$ and $(\mathbf{8_4})_{\mathbf{2,0}}$ in Fig. 4.1): one with spin 1/2, two with spin 3/2 and a third one with spin 5/2. The members of each HQSS multiplet are nearly degenerate, but not totally because we also break the HQSS by the use of physical hadron masses.

A word of caution is needed here. The mass of the $J = 5/2$ resonance is around 4027.2 MeV. In this sector there is only one channel ($\Sigma_c^*\bar{D}^*$, with threshold equal to

4526.3 MeV), thus this state is around five hundred MeV bound. We expect our model to work well close to threshold, and therefore, in this case, interaction mechanisms neglected here and involving higher partial waves could be relevant for determining the actual properties of this resonance.

| SU(6)× HQSS irrep | SU(3)× HQSS irrep | $M_R$[ MeV] | $\Gamma_R$[ MeV] | Couplings to main channels | $J$ |
|---|---|---|---|---|---|
| $\mathbf{70_{2,0}}$ | $(\mathbf{8_2})_{\mathbf{2,0}}$ | 3918.3 | 0.0 | $g_{N\eta_c} = 0.5$, $g_{NJ/\psi} = 0.6$, $g_{\Lambda_c\bar{D}} = 3.1$, $g_{\Lambda_c\bar{D}^*} = 0.5$, $g_{\Sigma_c\bar{D}} = 0.2$ , $g_{\Sigma_c\ \bar{D}^*} = 2.6$, $g_{\Sigma_c^*\ \bar{D}^*} = 2.6$ | 1/2 |
| $\mathbf{70_{2,0}}$ | $(\mathbf{8_2})_{\mathbf{2,0}}$ | 3926.0 | 0.1 | $\boldsymbol{g_{N\eta_c} = 0.2}$, $g_{NJ/\psi} = 0.04$, $g_{\Lambda_c\bar{D}} = 0.4$, $g_{\Lambda_c\bar{D}^*} = 3.0$, $g_{\Sigma_c\bar{D}} = 4.2$, $g_{\Sigma_c\bar{D}^*} = 0.2$, $g_{\Sigma_c^*\bar{D}^*} = 0.7$ | 1/2 |
| $\mathbf{70_{2,0}}$ | $(\mathbf{8_2})_{\mathbf{2,0}}$ | 3946.1 | 0. | $g_{NJ/\psi} = 0.2$, $g_{\Lambda_c\bar{D}^*} = 3.4$, $g_{\Sigma_c^*\bar{D}} = 3.6$, $g_{\Sigma_c\bar{D}^*} = 1.1$, $g_{\Sigma_c^*\bar{D}^*} = 1.5$ | 3/2 |
| $\mathbf{70_{2,0}}$ | $(\mathbf{8_4})_{\mathbf{2,0}}$ | 3974.3 | 2.8 | $\boldsymbol{g_{N\eta_c} = 0.5}$, $g_{NJ/\psi} \sim 0.05$, $g_{\Lambda_c\bar{D}} = 0.4$, $g_{\Lambda_c\bar{D}^*} = 2.2$, $g_{\Sigma_c\bar{D}} = 2.1$, $g_{\Sigma_c\bar{D}^*} = 3.4$, $g_{\Sigma_c^*\bar{D}^*} = 3.1$ | 1/2 |
| $\mathbf{70_{2,0}}$ | $(\mathbf{8_4})_{\mathbf{2,0}}$ | 3986.5 | 0. | $g_{NJ/\psi} = 0.2$, $g_{\Lambda_c\bar{D}^*} = 1.0$, $g_{\Sigma_c^*\bar{D}} = 2.7$, $g_{\Sigma_c\bar{D}^*} = 4.3$, $g_{\Sigma_c^*\bar{D}^*} = 1.8$ | 3/2 |
| $\mathbf{70_{2,0}}$ | $(\mathbf{8_4})_{\mathbf{2,0}}$ | 4005.8 | 0. | $g_{NJ/\psi} = 0.3$, $g_{\Lambda_c\bar{D}^*} = 1.$, $g_{\Sigma_c^*\bar{D}} = 1.6$, $g_{\Sigma_c\bar{D}^*} = 3.2$, $g_{\Sigma_c^*\bar{D}^*} = 4.2$ | 3/2 |
| $\mathbf{70_{2,0}}$ | $(\mathbf{8_4})_{\mathbf{2,0}}$ | 4027.1 | 0. | $g_{\Sigma_c^*\ \bar{D}^*} = 5.6$ | 5/2 |

Table 4.2: Odd-parity hidden-charm $N$ ($J = 1/2$, $J = 3/2$, and $J = 5/2$) resonances found in this work. The first two columns contain the SU(6) × HQSS and SU(3) × HQSS quantum numbers of each state, while $M_R$ and $\Gamma_R$ stand for its mass and width (in MeV). The largest couplings of each pole, ordered by their threshold energies, are collected in the next column. In boldface, we highlight the channels which are open for decay. Finally, the spin of the state is given in the last column. Resonances with equal SU(6) × HQSS and SU(3) × HQSS labels form HQSS multiplets, and they are collected in consecutive rows.

There exist previous works on hidden-charm odd-parity nucleon states, also named crypto-exotic hadronic states. These studies can be divided in two types. Namely, those based on a constituent-quark description of the resonances, and those where they are described as baryon-meson bound molecules or resonating states. Some of the predictions of these other models are compiled in Table 4.3.

The baryon-meson coupled-channel zero-range vector exchange model by Hofmann and Lutz [141,142] makes predictions for the hidden-charm $N$ resonances. Baryon resonances with $J^P = 1/2^-$ are predicted from the interaction of pseudoscalar mesons with $J^P = 1/2^+$

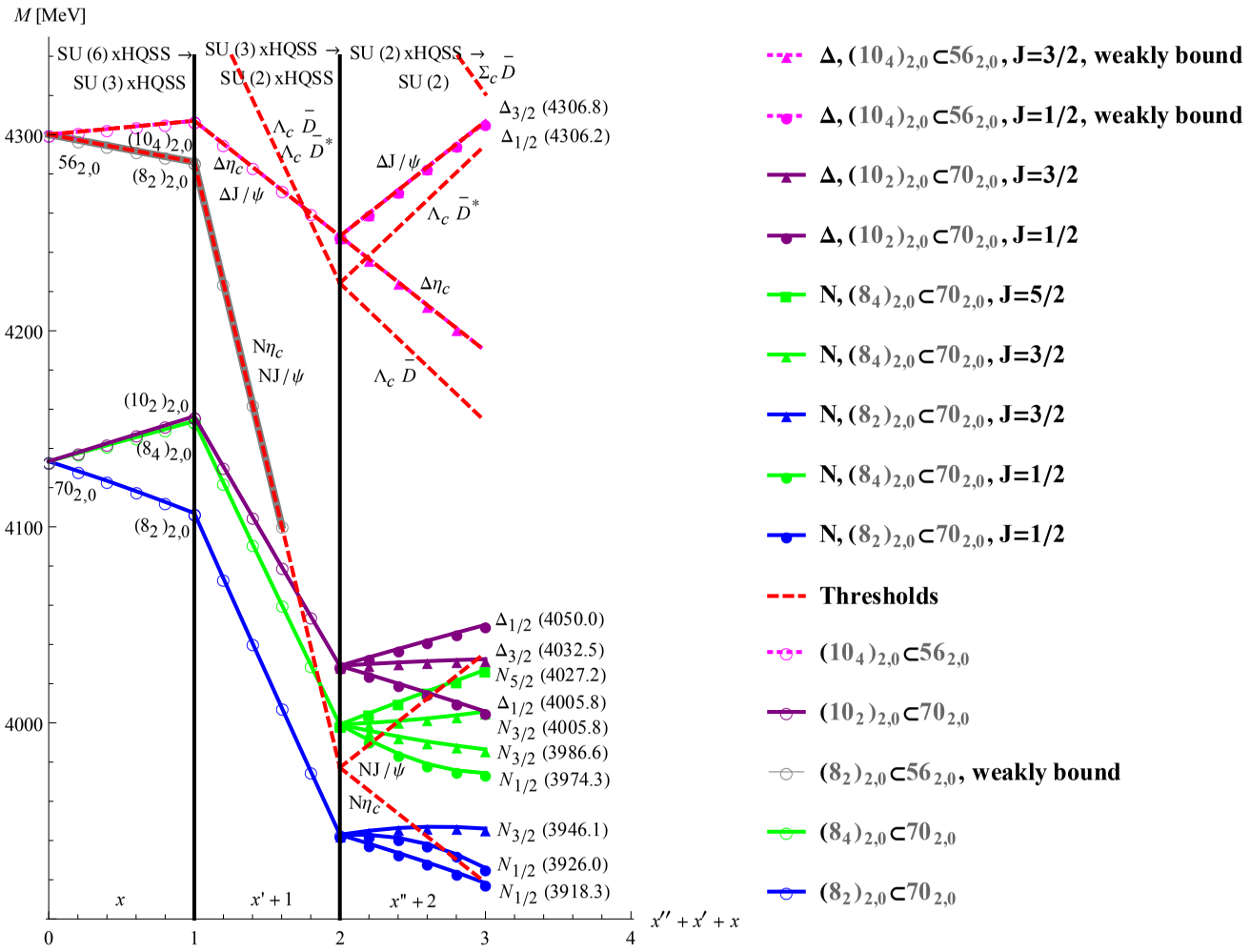


Figure 4.1: Evolution of the poles as symmetries, starting from SU(6) × HQSS, are sequentially broken to reach the isospin symmetric final crypto-exotic $N$ and $\Delta$ odd-parity resonances. The meanings of $x$, $x'$, and $x''$ can be found in Eq. (2.48). The lower index of the final states stands for the spin $J$ of the corresponding resonance. The thresholds (red dashed lines) are marked together with the respective baryon-meson channel. The SU(6) × HQSS labels $\mathbf{70_{2,0}}$ and $\mathbf{56_{2,0}}$, and the SU(3) × HQSS labels $(\mathbf{8_2})_{\mathbf{2,0}}$, $(\mathbf{8_4})_{\mathbf{2,0}}$, $(\mathbf{10_2})_{\mathbf{2,0}}$, $(\mathbf{10_4})_{\mathbf{2,0}}$ are also shown at the corresponding symmetric points.

| | | $N(1/2^-)$ | | | | | | $N(3/2^-)$ | | | | | $N(5/2^-)$ | |
|---|---|---|---|---|---|---|---|---|---|---|---|---|---|---|
| | | $M_R$ | $g$ to main-channels | | | | | $M_R$ | $g$ to main-channels | | | | $M_R$ | $g$ |
| Ref. | Model | [MeV] | $\Lambda_c\bar{D}$ | $\Lambda_c\bar{D}^*$ | $\Sigma_c\bar{D}$ | $\Sigma_c\bar{D}^*$ | $\Sigma_c^*\bar{D}^*$ | [MeV] | $\Lambda_c\bar{D}^*$ | $\Sigma_c^*\bar{D}$ | $\Sigma_c\bar{D}^*$ | $\Sigma_c^*\bar{D}^*$ | [MeV] | $\Sigma_c^*\bar{D}^*$ |
| This work | $(\mathbf{8_2})_{\mathbf{2,0}} \subset (\mathbf{70_2})_{\mathbf{2,0}}$ | 3918 | 3.0 | 0.6 | 0.2 | 2.6 | 2.6 | | | | | | | |
| | | 3926 | 0.4 | 2.9 | 4.2 | 0.4 | 0.7 | 3946 | 3.3 | 3.6 | 1.0 | 1.5 | | |
| | $(\mathbf{8_4})_{\mathbf{2,0}} \subset (\mathbf{70_2})_{\mathbf{2,0}}$ | 3974 | 0.4 | 2.2 | 2.0 | 3.3 | 3.0 | 3987 | 1.0 | 2.7 | 4.2 | 1.8 | | |
| | | | | | | | | 4006 | 0.9 | 1.5 | 3.1 | 4.1 | 4027 | 5.5 |
| [141, 142] | zero-range vector exchange | 3520 | | | 5.3 | | | 3430 | | 5.6 | | | | |
| [151] | hidden-gauge | 4265 | 0.1 | | 3.0 | | | | | | | | | |
| | | 4415 | | 0.1 | | 2.8 | | 4415 | 0.1 | | 2.8 | | | |
| [152] | hidden-gauge | 4315 | × | | × | | | | | | | | | |
| | | 4454 | | × | | × | | 4454 | × | | × | | | |
| [191] | quark model | FS-CM | | | | | | FS-CM | | | | | FS-CM | |
| | $uudc\bar{c}$ | 3933−4267 | | | | | | | | | | | | |
| | | 4013−4363 | | | | | | 4013−4389 | | | | | | |
| | | 4119−4377 | | | | | | 4119−4445 | | | | | | |
| | | 4136−4471 | | | | | | 4136−4476 | | | | | | |
| | | 4156−4541 | | | | | | 4236−4526 | | | | | 4236−4616 | |

Table 4.3: Comparison of the whole spectrum of hidden-charm nucleons (or crypto-exotic nucleons) with odd-parity and angular momentum $L = 0$ predicted by our model, with some results from previous models. In all cases, masses and couplings ($g$) to the dominant channels (when available) are shown in sequential rows. In the hidden-gauge model of Ref. [152], the numerical values of the couplings are not given. In this case, we indicate with a symbol × the elements of the coupled-channels space used to generate each resonance. On the other hand, in the case of the predictions of this work, in the column "Model" we give the HQSS multiplet. Besides, we have also omitted the small couplings to the $N\eta_c$ and $NJ/\psi$ channels that can be seen in Table 4.2.

ground-state baryons [141], and the $J^P = 3/2^-$ baryon resonances are predicted from the interaction of pseudoscalar mesons with $J^P = 3/2^+$ ground-state baryons [142]. Vector mesons in the coupled-channel space were omitted in those early studies, thus channels like $\Sigma_c \bar{D}^*$ or $\Lambda_c \bar{D}^*$ were not considered.

More recently baryon-meson calculations using a hidden-gauge model have been carried out in Refs. [150–152]. These works consider $1/2^+$ baryons interacting with pseudoscalar mesons that generate dynamically $J^P = 1/2^-$ hidden-charm nucleon resonances as poles in the $T$-matrix. Yet, the interaction of vector mesons with $1/2^+$ baryons is also taken into account in [150–152], which leads to additional and degenerate $J^P = 1/2^-$ and $3/2^-$ hidden-charm nucleons. However, the $J = 3/2^+$ baryons are not included, and thus some channels like $\Sigma_c^* \bar{D}^*$ are excluded.

The main difference between our scheme and the hidden-gauge models is the definition of the coupled-channels space. We consider simultaneously pseudoscalar meson–baryon ($PB$) and vector meson–baryon ($VB$) channels, with $J^P = 1/2^+$ and $3/2^+$ baryons. However, in the approaches of Refs. [150–152] all interaction terms of the type $PB \to VB$ are neglected. Furthermore, channels with $J^P = 3/2^+$ baryons are not considered either. The potential used in [150–152] for the $PB \to PB$ transitions, with $J^P = 1/2^+$ baryons, is similar to that derived here. However, there exist important differences in all transitions involving vector mesons. When restricting our model to the $PB \to PB$ sector, we still do not obtain the same results as in Refs. [150–152]. This is mainly due to i) the use of a different renormalization scheme and, ii) the presence in these latter works of a suppression factor in those transitions that involve a $t$-channel exchange of a heavy charm vector meson, as discussed in Sect. 3.10.

However, when we use our full space, the inclusion of a similar suppression factor in our HQSS kernel is not quantitatively relevant for the dynamical generation of the resonances. Note that HQSS does not require the presence of such suppression factor. In summary, when we compare our approach with the other molecular-type ones, we observe in our model a rich structure of resonances due to the many channels cooperating to create them. Our states are much lighter than those predicted in Refs. [150–152], though significantly less bound that the crypto-exotic baryons reported in Refs. [141, 142].

Finally, we will pay attention to the recent work of Ref. [191]. There a constituent-quark model is used to describe isospin $I = 1/2$ baryons with $uudc\bar{c}$ quark content. The mass spectra is evaluated with three types of hyperfine interactions: the color-magnetic interaction (CM) based on one-gluon exchange, a chiral interaction (FS) based on meson exchange, and an instanton-induced interaction (INST) based on the non-perturbative QCD vacuum structure. The FS (CM) model predicts the lowest (highest) mass for each state. Results for the FS and CM models are displayed in Table 4.3. In all cases, the mass predicted by the INST model (not displayed in the table) lies between the values predicted by the other two models. Our results are closer to those predicted by the FS model, specially for the lowest lying states.

### 4.2.2 $\Delta$ states ($C = 0$, $S = 0$, $I = 3/2$)

In this sector we find five heavy resonances (bound states; all of them appear below threshold): three with spin-parity $J^P = \frac{1}{2}^-$ and another two with $J^P = \frac{3}{2}^-$. Their

masses, widths and couplings to the different channels are compiled in Table 4.4.

- $\mathbf{J = 1/2}$ : In this sector, there are four coupled channels, with the following threshold energies (in MeV):

$$\begin{array}{cccc} \Delta J/\psi & \Sigma_c\bar{D} & \Sigma_c\bar{D}^* & \Sigma_c^*\bar{D}^* \\ 4306.9, & 4320.8, & 4461.9, & 4526.3. \end{array}$$

- $\mathbf{J = 3/2}$ : In this sector, there are five coupled channels, with the following threshold energies:

$$\begin{array}{ccccc} \Delta\eta_c & \Delta J/\psi & \Sigma_c^*\bar{D} & \Sigma_c\bar{D}^* & \Sigma_c^*\bar{D}^* \\ 4189.7, & 4306.9, & 4385.2, & 4461.9, & 4526.3. \end{array}$$

- $\mathbf{J = 5/2}$ : In this sector there are only two channels, with the following threshold energies:

$$\begin{array}{cc} \Delta J/\psi & \Sigma_c^*\bar{D}^* \\ 4306.9, & 4526.3. \end{array}$$

We obtain three $\Delta$ ($J = 1/2$) states as expected from the group decomposition of the SU(6) $\times$ HQSS representations (see Table 4.1): one state from each of the two $J = 1/2$ decuplets encoded in the attractive $\mathbf{70_{2,0}}$ representation, and a further state corresponding to the $J = 1/2$ decuplet that appears in the reduction of the $\mathbf{56_{2,0}}$ representation [Eq. (4.3)]. The evolution of the corresponding poles is shown in Fig. 4.1.

The pole that corresponds to $(\mathbf{10_4})_{\mathbf{2,0}} \subset \mathbf{56_{2,0}}$ (light magenta circles with labels $\mathbf{56_{2,0}}$ and $(\mathbf{10_4})_{\mathbf{2,0}}$ in Fig. 4.1) has a mass quite close to the $\Delta\eta_c$ and $\Delta J/\psi$ degenerated thresholds, between the SU(6) $\times$ HQSS and the SU(2) $\times$ HQSS symmetric points. Later, while moving to the SU(2) isospin symmetric point, the spin-1/2 $\Delta$ resonance keeps having a mass close to the $\Delta J/\psi$ threshold, and ends up with a final mass of 4306.2 MeV (the $\Delta J/\psi$ threshold is at 4306.9 MeV). However, the spin-5/2 and the two spin-3/2 states, that are also originated from this $(\mathbf{10_4})_{\mathbf{2,0}} \subset \mathbf{56_{2,0}}$ pole, essentially disappear. One of the $J = 3/2$ states still shows up as a cusp very close to the $\Delta J/\psi$ threshold, and it has been included in the table. The second state with spin-3/2 (light magenta triangles disappearing between SU(2) $\times$ HQSS and SU(2) symmetric points in Fig. 4.1) and the spin-5/2 one appear as small unnoticeable peaks right at the $\Delta\eta_c$ and $\Delta J/\Psi$ thresholds, respectively.

From the discussion above, the $(\mathbf{10_4})_{\mathbf{2,0}} \subset \mathbf{56_{2,0}}$ HQSS multiplet could be incomplete. However, the three $\Delta$ states (dark magenta circles for the two $J^P = 1/2^-$ states and dark magenta triangles for the $J^P = 3/2^-$ resonance in Fig. 4.1) that stem from the $(\mathbf{10_2})_{\mathbf{2,0}} \subset \mathbf{70_{2,0}}$ configuration of the light degrees of freedom turn out to be quite bound. Indeed, we find binding energies of at least 250 (150) MeV in the spin-1/2 (3/2) sector. These three states, nearly degenerate, form a clear HQSS multiplet.

| SU(6)× HQSS irrep | SU(3)× HQSS irrep | $M_R$ | $\Gamma_R$ | Couplings to main channels | $J$ |
|---|---|---|---|---|---|
| $\mathbf{70_{2,0}}$ | $(\mathbf{10_2})_{\mathbf{2,0}}$ | 4005.8 | 0. | $g_{\Delta J/\psi} = 0.3$, $g_{\Sigma_c\bar{D}} = 2.7$, $g_{\Sigma_c\bar{D}^*} = 4.4$, $g_{\Sigma_c^*\bar{D}^*} = 1.2$ | 1/2 |
| $\mathbf{70_{2,0}}$ | $(\mathbf{10_2})_{\mathbf{2,0}}$ | 4032.5 | 0. | $g_{\Delta\eta_c} = 0.2$, $g_{\Delta J/\psi} = 0.1$, $g_{\Sigma_c^*\bar{D}} = 2.9$, $g_{\Sigma_c\bar{D}^*} = 1.8$, $g_{\Sigma_c^*\bar{D}^*} = 4.1$ | 3/2 |
| $\mathbf{70_{2,0}}$ | $(\mathbf{10_2})_{\mathbf{2,0}}$ | 4050.0 | 0. | $g_{\Delta J/\psi} = 0.2$, $g_{\Sigma_c\bar{D}} = 0.8$, $g_{\Sigma_c\bar{D}^*} = 1.9$, $g_{\Sigma_c^*\bar{D}^*} = 5.1$ | 1/2 |
| $\mathbf{56_{2,0}}$ | $(\mathbf{10_4})_{\mathbf{2,0}}$ | 4306.2 | 0. (cusp) | $g_{\Delta J/\psi} = 1.3$, $g_{\Sigma_c\bar{D}} = 0.3$, $g_{\Sigma_c\bar{D}^*} = 0.3$, $g_{\Sigma_c^*\bar{D}^*} = 0.3$ | 1/2 |
| $\mathbf{56_{2,0}}$ | $(\mathbf{10_4})_{\mathbf{2,0}}$ | 4306.8 | 0. (cusp) | $g_{\Delta\eta_c} \sim 0.1$, $g_{\Delta J/\psi} = 0.8$, $g_{\Sigma_c^*\bar{D}} = 0.2$, $g_{\Sigma_c\bar{D}^*} = 0.2$, $g_{\Sigma_c^*\bar{D}^*} = 0.1$ | 3/2 |

Table 4.4: As in Table 4.2, for the $\Delta$ ($J = 1/2$, $J = 3/2$) resonances with hidden-charm content.

The models based on vector-meson exchange naturally use a suppression factor in the baryon-meson amplitudes involving exchange of charm, from the propagator of the exchanged heavy vector meson. In the heavy-quark limit, the suppression factor is of the order of $1/m_H$.[4] Therefore, in that limit, one expects a quenching of order $m_V/m_{D^*}$ for the charm exchanging amplitudes of those models. (Of course, the true factor for large but finite physical heavy hadron masses does not need to coincide exactly with this heavy-quark limit estimate). Our model is not directly based on exchange of vector mesons. Nevertheless, we have verified that adding such suppression by hand in the charm-exchanging amplitudes does not have an impact on our results. Even a factor $(m_V/m_{D^*})^2$, proposed in the literature [144] has a very small effect in the position of the resonances we find. Presumably, this is due to the fact that the relevant channels have a small coupling. An exception comes from the two very weakly-bound $\Delta$ resonances from the $\mathbf{56}_{2,0}$ irrep, which disappear due to the suppression of their dominant decay channel $\Delta J/\psi$.

## 4.3 Summary

In this chapter we studied hidden-charm $N$ and $\Delta$ resonances. We have carried out a detailed analysis of the hidden-charm sector (i.e., with $c\bar{c}$ pairs) with $C = 0$ and its breaking as the symmetry is lifted from SU(6) × HQSS to SU(3) × HQSS (and then to SU(2) × HQSS and SU(2) of isospin). This allows to count the expected number of bound states or resonances, and to classify them into multiplets corresponding to the various

[4]The boson propagator is approximately $1/(2m_H(E_H - m_H))$, with $m_H$ the mass of the heavy vector meson and $E_H$ its energy, and $E_H - m_H$ is $O(1)$ in the heavy-quark limit.

symmetries.

After analyzing the charmless and strangeless sector, we have dynamically generated several $N$ and $\Delta$ states. Actually, we predict the existence of seven $N$-like and five $\Delta$-like states with masses around 4 GeV, most of them as bound states. These states form heavy-quark spin multiplets, which are almost degenerate in mass. The $N$ states form two HQSS multiplets. The lowest one has the light quark flavor-spin content coupled to $\mathbf{8_2}$. Since the $\bar{c}c$ pair can couple to spin $S_{c\bar{c}} = 0, 1$, this HQSS multiplet consists of three nucleon states with $J = 1/2,\ 1/2$, and $3/2$, and masses around 3930 MeV. On the other hand, the highest HQSS nucleon-like multiplet contains four resonances with $J = 1/2,\ 3/2,\ 3/2$, and $5/2$, and masses around 4000 MeV. In this case, these states are originated from the $\mathbf{8_4}$ SF light configuration. These two SU(3) $\times$ HQSS multiplets arise from the **70**-plet of SU(6) $\times$ HQSS. There are no $N$ physical states coming from the **56**-plet. With regards to $\Delta$ states, we find two multiples with very different average masses, because in this case they are originated from different SU(6) $\times$ HQSS representations. The $\Delta$ multiplet coming from the $(\mathbf{10_2})_{\mathbf{2,0}} \subset \mathbf{70_{2,0}}$ irrep is formed by 3 states ($J = 1/2,\ 1/2,\ 3/2$) with an average mass of 4035 MeV. Besides, we find only two ($J = 1/2,\ 3/2$) $\Delta$ resonances at the physical point out of the four states originated from the $(\mathbf{10_4})_{\mathbf{2,0}} \subset \mathbf{56_{2,0}}$ in the SU(6) limit. These two states are nearly degenerate, with a mass of 4306 MeV.

When we compare our approach with the other molecular-type ones, we observe in our model a rich structure of resonances due to the many channels cooperating to create them. Our states are much lighter than those predicted in the hidden-gauge scheme [150–152], though significantly less bound than the crypto-exotic baryons reported in the zero-range vector meson exchange model of Refs. [141, 142]. Moreover, we have presented the first prediction for exotic hidden-charm $\Delta$-like resonances within a molecular baryon-meson scheme.

In comparison with the quark model of Ref. [191], we find that our results are closer to those predicted by the FS hyperfine interaction discussed in Ref. [191], especially for the lowest-lying states.

The predicted new resonances definitely cannot be accommodated by quark models with three constituent quarks and they might be looked for in the forthcoming PANDA experiment at the future FAIR facility.

# Chapter 5

# Baryon resonances with beauty[1]

In this chapter we study dynamically-generated baryon resonances with beauty (or bottom) flavor, in particular $\Lambda_b$ and $\Xi_b$ particles. Such a study was motivated by the discovery of two narrow baryon resonances with beauty by the LHCb Collaboration in 2012 [126], with masses $5911.97 \pm 0.12\,(stat) \pm 0.02\,(syst) \pm 0.66\,(\Lambda_b^0\,\text{mass})\,\text{MeV}$, and $5919.77 \pm 0.08\,(stat) \pm 0.02\,(syst) \pm 0.66\,(\Lambda_b^0\,\text{mass})\,\text{MeV}$. These states are interpreted as the orbitally-excited $\Lambda_b^0(5912)$ and $\Lambda_b^0(5920)$ bottom baryon resonances, with spin–parity $J^P = 1/2^-$ and $J^P = 3/2^-$, respectively. The limits on the natural widths of these states are $\Gamma_{\Lambda_b^0(5912)} \leq 0.82\,\text{MeV}$ and $\Gamma_{\Lambda_b^0(5920)} \leq 0.72\,\text{MeV}$ at 95% confidence level [126].

We use our phenomenological model for predicting these states. In Chapter 2 we normally referred to a charm quark as the heavy one in the system. The prescription here is to replace the $c$ quark by a bottom $b$ quark. We obtain the masses, the quantum numbers, and the couplings of the $\Lambda_b$ resonances to the different baryon-meson channels. We find that the resonances $\Lambda_b^0(5912)$ and $\Lambda_b^0(5920)$ are HQSS partners, which naturally explains their approximate mass degeneracy. We also predict $\Xi_b$ resonances that belong to the same SU(3) $\times$ HQSS representations as generated $\Lambda_b$ and $\Lambda_b^*$ states. The two $\Lambda_b$ resonances found by the LHCb Collaboration, and $\Xi_b(6035.4)$ ($J^P = \frac{1}{2}^-$) and $\Xi_b(6043.3)$ ($J^P = \frac{3}{2}^-$) states complete a multiplet of SU(3) $\times$ HQSS.

There exists an old prediction for the masses of the two $\Lambda_b$ resonances by Capstick and Isgur [20], which is in very good agreement with the results reported by the LHCb Collaboration. Their relativistic quark model predicts 5912 MeV and 5920 MeV for the masses of the lightest orbitally-excited states, with quantum numbers $J^P = 1/2^+$ and $J^P = 3/2^+$ [20]. In this work we describe these odd-parity excited states as dynamically-generated resonances obtained within our unitarized baryon-meson coupled-channels scheme.

[1] This chapter is based on C. Garcia-Recio, J. Nieves, O. Romanets, L. L. Salcedo, and L. Tolos, Phys. Rev. D **87**, 034032 (2013) (Ref. [192]).

## 5.1 Beautiful dynamically-generated $\Lambda_b$ and $\Xi_b$ resonances

In this section we study dynamically-generated bottom-flavored $\Lambda_b$ ($J^P = 1/2^-$) and $\Lambda_b^*$ ($J^P = 3/2^-$) resonances. Similarly to Chapter 3, we consider baryon resonances that stem from the most attractive **120** and **168** SU(8) representations. We also study the $\Xi_b$ $J^P = 1/2^-$ and $J^P = 3/2^-$ resonances that belong to the same SU(3) $\times$ HQSS representations as the $\Lambda_b$ states. We use the phenomenological model described in Chapter 2. By replacing the $c$-quark by the $b$-quark we move to the baryon-meson sector with bottom $B = -1$. The $D$-matrices in the $B = -1$ sector, which are needed for calculating the potential [Eq. (2.31)], are the same as in Appendix B for $C = 1$ sectors with obvious renaming of the heavy hadrons. We consider a system with baryon number one, one bottom quark ($B = -1$) and strangeness, isospin, and spin-parity given by: $(S, I, J^P) = (0, 0, 1/2^-)$ denoted as $\Lambda_b$, $(0, 0, 3/2^-)$ as $\Lambda_b^*$, $(-1, 1/2, 1/2^-)$ as $\Xi_b$ and $(-1, 1/2, 3/2^-)$ as $\Xi_b^*$.

The bottomed baryon masses are given in Table 5.1, while the masses and the weak-decay constants of the bottom-flavored mesons are collected in Table 5.2.

| Baryon | $M$ [MeV] | $\Gamma$ [MeV] | SU(6) | SU(3)$_{2J+1}$ | HQSS |
|---|---|---|---|---|---|
| $\Lambda_b$ | 5619.37 [193] | | **21** | $\mathbf{3_2^*}$ | singlet |
| $\Xi_b$ | 5789.55 [4] | | **21** | $\mathbf{3_2^*}$ | singlet |
| $\Sigma_b$ | 5813.4 [4] | 7.3 | **21** | $\mathbf{6_2}$ | doublet |
| $\Sigma_b^*$ | 5833.55 [4] | 9.5 | **21** | $\mathbf{6_4}$ | doublet |
| $\Xi_b'$ | 5926 [194] | | **21** | $\mathbf{6_2}$ | doublet |
| $\Xi_b^*$ | 5945 [195] | | **21** | $\mathbf{6_4}$ | doublet |
| $\Omega_b$ | 6050.3 [196] | | **21** | $\mathbf{6_2}$ | doublet |
| $\Omega_b^*$ | 6069 [197] | | **21** | $\mathbf{6_4}$ | doublet |

Table 5.1: Masses and widths of the ground-state baryons with beauty used throughout this work. The SU(6) and SU(3)$_{2J+1}$ labels are also displayed. The last column indicates the HQSS multiplets. Members of a HQSS doublet are placed in consecutive rows.

### 5.1.1 $\Lambda_b$ and $\Lambda_b^*$ states

In the $\Lambda_b$ sector ($B = -1,\ C = 0,\ S = 0,\ I = 0,\ J^P = 1/2^-$), the following sixteen channels are involved:

$$\begin{array}{cccccccc} \Sigma_b\pi & \Lambda_b\eta & N\bar{B} & N\bar{B}^* & \Xi_b K & \Lambda_b\omega & \Xi_b' K & \Lambda\bar{B}_s^0 \\ \Lambda\bar{B}_s^* & \Lambda_b\eta' & \Sigma_b\rho & \Sigma_b^*\rho & \Lambda_b\phi & \Xi_b K^* & \Xi_b' K^* & \Xi_b^* K^* \end{array} .$$

Likewise for the $\Lambda_b^*$ sector ($B = -1,\ C = 0,\ S = 0,\ I = 0,\ J^P = 3/2^-$), there are eleven channels:

| Meson | $m$ [MeV] | $f$ [MeV] | SU(6) | $SU(3)_{2J+1}$ | HQSS |
|---|---|---|---|---|---|
| $\bar{B}$ | 5279.335 [4] | 133.6 [198] | $\mathbf{6^*}$ | $\mathbf{3^*_1}$ | doublet |
| $\bar{B}^*$ | 5325.2 [4] | $f_{\bar{B}}$ | $\mathbf{6^*}$ | $\mathbf{3^*_3}$ | doublet |
| $\bar{B}_s$ | 5366.3 [4] | 159.1 [199] | $\mathbf{6^*}$ | $\mathbf{3^*_1}$ | doublet |
| $\bar{B}^*_s$ | 5415.4 [4] | $f_{\bar{B}_s}$ | $\mathbf{6^*}$ | $\mathbf{3^*_3}$ | doublet |

Table 5.2: Masses, $m$, and decay constants, $f$, of the mesons with bottom flavor used throughout this work. The SU(6) and $SU(3)_{2J+1}$ labels are also displayed. The last column indicates the HQSS multiplets. Members of a HQSS doublet are placed in consecutive rows.

$$\begin{array}{lllll} \Sigma_b^*\pi & N\bar{B}^* & \Lambda_b\omega & \Xi_b^*K & \Lambda\bar{B}_s^* \quad \Sigma_b\rho \\ \Sigma_b^*\rho & \Lambda_b\phi & \Xi_bK^* & \Xi_b'K^* & \Xi_b^*K^* \end{array} .$$

In both cases the channels are ordered by increasing mass thresholds.

Several states are generated in each of the two sectors. The three lowest-lying $\Lambda_b$ resonances have masses of 5880 and 5949 MeV ($J^P = 1/2^-$) and 5963 MeV ($J^P = 3/2^-$). As one can expect, the situation in the $J = 1/2^-$ channel is analogous to that of the $\Lambda_c(2595)$ resonance in the charm sector [175, 177]. For both heavy flavors the structure obtained mimics the well-known two-pole pattern of the $\Lambda(1405)$ [38, 59]. Thus, we find that the state at 5880 strongly couples to the $N\bar{B}$ and $N\bar{B}^*$ channels, with a negligible $\Sigma_b\pi$ coupling, while the 5949 MeV state has a sizable coupling to this latter channel. On the other hand, the $J^P = 3/2^-$ state at 5963 is generated mainly by the ($N\bar{B}^*$, $\Sigma_b^*\pi$) coupled-channel dynamics. This state is the bottom counterpart of the $\Lambda(1520)$ and $\Lambda_c^*(2625)$ resonances.

These results are encouraging, but to achieve a better description of the $\Lambda_b(5912)$ and $\Lambda_b(5920)$ states reported by the LHCb Collaboration, we have slightly changed the value of the subtraction point used in the RS defined by Eqs. (2.36) and (2.37) [175]. Thus, in this sector, we have set the baryon-meson loop to be zero at the center-of-mass energy $\sqrt{s} = \mu$ given by

$$\mu^2 = \alpha \ (M_{\Sigma_b}^2 + m_\pi^2) \ . \tag{5.1}$$

For $\alpha = 0.967$, we find two poles above the $\Lambda_b^0\pi\pi$ threshold, with masses 5910.1 MeV ($J^P = 1/2^-$) and 5921.5 MeV ($J^P = 3/2^-$), which admit a natural identification with the two experimental $\Lambda_b$ resonances observed in [126]. The results for the masses, the widths, and the couplings are presented in Table 5.3. We have assigned well-defined group labels to the resonances. The multiplets of SU(6) $\times$ HQSS and of SU(3) $\times$ HQSS to which the resonances belong are identified by means of the procedure discussed in Section 2.3, namely, by adiabatically following the trajectories of the poles generated as the various symmetries are restored or broken. The mass differences $\Delta M_R$ of the resonances with respect of ground state $\Lambda_b$ are also shown in Table 5.3. They are defined by

$$\Delta M_R = M_R - M_{\Lambda_b(g.s.)}. \tag{5.2}$$

| SU(6) irrep | SU(3)$_{2J+1}$ irrep | $\Delta M_R$ MeV | $M_R$ MeV | $\Gamma_R$ | Couplings to main channels | $J$ | Experimental LHCb | Decay mode |
|---|---|---|---|---|---|---|---|---|
| **21** | $\mathbf{3^*_2}$ | 178 | 5797.6 | 0 | $g_{N\bar{B}} = 4.9$, $g_{N\bar{B}^*} = 8.3$, $g_{\Lambda\bar{B}^0_s} = 2.1$, $g_{\Lambda\bar{B}^*_s} = 3.6$, $g_{\Lambda_b\eta'} = 1.0$, $g_{\Sigma^*_b\rho} = 0.6$ | 1/2 | | $\Lambda_b\gamma$ |
| **15** | $\mathbf{3^*_2}$ | 291 | 5910.1 | 0 | $g_{\Sigma_b\pi} = 1.8$, $g_{N\bar{B}} = 4.6$, $g_{N\bar{B}^*} = 3.0$, $g_{\Lambda_b\omega} = 1.4$ | 1/2 | $\Lambda_b(5912)$ | $\Lambda_b\pi\pi$ |
| **15** | $\mathbf{3^*_4}$ | 301 | 5921.5 | 0 | $g_{\Sigma^*_b\pi} = 1.8$, $g_{N\bar{B}^*} = 5.7$, $g_{\Lambda_b\omega} = 1.5$ | 3/2 | $\Lambda^*_b(5920)$ | $\Lambda_b\pi\pi$ |
| **21** | $\mathbf{3^*_2}$ | 390 | 6009.3 | 0 | $\boldsymbol{g_{\Sigma_b\pi} \sim 0.05}$, $g_{\Lambda_b\eta} = 2.0$, $g_{N\bar{B}} = 1.1$, $g_{N\bar{B}^*} = 1.7$, $g_{\Xi_bK} = 0.8$, $g_{\Lambda\bar{B}^0_s} = 3.9$, $g_{\Lambda\bar{B}^*_s} = 6.0$, $g_{\Sigma^*_b\rho} = 0.7$, $g_{\Xi^*_bK^*} = 0.9$ | 1/2 | | $\Sigma_b\pi$ |

Table 5.3: $\Lambda_b$ ($J^P = 1/2^-$) and $\Lambda^*_b$ ($J^P = 3/2^-$) resonances predicted in this work. The parameter $\alpha$ in Eq. (5.1) has been set to 0.967. The SU(6) and SU(3) $\times$ SU(2) representations of the corresponding states are shown in the first two columns. $M_R$, $\Gamma_R$, and $\Delta M_R$ stand for the mass, the width, and the mass difference with respect to the ground state ($J^P = 1/2^+$) $\Lambda_b$. The next column displays the (absolute value of the) dominant couplings to the different baryon-meson channels, ordered by their threshold energies. The couplings to channels open for decay are highlighted in bold font. The seventh column shows the spin of the resonance. Tentative identifications with experimental resonances of LHCb are also given in the following column. Finally, in the last column we show the decay channel with largest phase space allowed by strong interactions (or electromagnetic ones when the strong decay is forbidden). The two states in the **15** of SU(6) form a HQSS doublet, the other two states are HQSS singlets. The three lightest states belong to the **168** of SU(8), the heaviest one belongs to the **120** (note that it is precisely in these two SU(8) irreps where the WT interaction is more attractive, and thus the lowest-lying states stem from them).

For each resonance, the decay mode with largest phase-space allowed by strong interactions (or electromagnetic ones when the strong decay is forbidden) is shown in the last column.

We find that the states $\Lambda_b(5912)$ and $\Lambda_b^*(5920)$ are HQSS partners. Indeed, these two states would be part of a $\mathbf{3}^*$ irreducible representation (irrep) of SU(3), embedded in a **15** irrep of SU(6) (which in turn belongs to the irrep **168** of SU(8) [Section 3.1]). Thus, the light-quark structure of these two states is the same, and in particular their total spin, $j_l = 1$. Hence, the coupling of the $b$-quark spin ($j_b = 1/2$) with the spin of the light degrees of freedom yields $J = 1/2$ and $J = 3/2$. Then the two states, $\Lambda_b(5912)$ and $\Lambda_b^*(5920)$, form an approximate degenerate doublet; they are connected by a spin rotation of the $b$-quark.

Comparison of Table 5.3 with Table 3.2 in the charm sector shows that states with the same group labels in both tables are the heavy-flavor counterpart of each other. In particular, the $\Lambda_b(5920)$ resonance is the bottom version of $\Lambda_c(2625)$ one, while the $\Lambda_b(5912)$ would not be the counterpart of the $\Lambda_c(2595)$ resonance, but it would be of the second charmed state that appears around 2595 MeV, and that gives rise to the two-pole structure mentioned above. The same conclusion follows from inspection of their couplings: the $\Lambda_c(2595)$ couples weakly to $\Sigma_c\pi$, while the coupling to $\Sigma_b\pi$ is sizable for the $\Lambda_b(5912)$ state.

The two states observed by the LHCb Collaboration are detected through their decay to $\Lambda_b(\text{g.s.})\pi\pi$. The fit to the data of the experiment of Ref. [126] yields

$$N(pp \to \Lambda_b(5912) \to \Lambda_b\pi\pi) = 17.6 \pm 4.8 \text{ events}, \tag{5.3}$$

with mass $M_{\Lambda_b(5912)} = 5911.97 \pm 0.12\,\text{MeV}$ and

$$N(pp \to \Lambda_b^*(5920) \to \Lambda_b\pi\pi) = 52.5 \pm 8.1 \text{ events}, \tag{5.4}$$

with mass $M_{\Lambda_b^*(5920)} = 5919.77 \pm 0.08\,\text{MeV}$. The experimental setup of LHCb and the strong decay mechanism of the resonances observed guarantees that the decay to $\Lambda_b\pi\pi$ always takes place within the space and time intervals set for detection [200]. Therefore, no bias is expected from the possible different decay rates of the two resonances, and

$$\frac{N(pp \to \Lambda_b^*(5920))}{N(pp \to \Lambda_b(5912))} = \frac{N(pp \to \Lambda_b^*(5920) \to \Lambda_b\pi\pi)}{N(pp \to \Lambda_b(5912) \to \Lambda_b\pi\pi)}. \tag{5.5}$$

This translates into an experimental ratio of cross sections

$$\left.\frac{\sigma(pp \to \Lambda_b^*(5920))}{\sigma(pp \to \Lambda_b(5912))}\right|_{\text{exp}} = \frac{N(pp \to \Lambda_b^*(5920))}{N(pp \to \Lambda_b(5912))} = 3.0 \pm 1.0. \tag{5.6}$$

From the theoretical side, due to the dominant strong interactions taking place during creation and hadronization of the quark $b$, a natural assumption is that the $b$-quark spin ends up in a random state. In that case, and assuming that $\Lambda_b(5912)$ and $\Lambda_b^*(5920)$ form a HQSS doublet, the ratio of production of these states should be the quotient of multiplicities, that is,

$$\frac{\sigma(pp \to \Lambda_b^*(5920))}{\sigma(pp \to \Lambda_b(5912))} \approx \frac{2J_{\Lambda_b^*} + 1}{2J_{\Lambda_b} + 1} = 2. \tag{5.7}$$

Although not fully satisfactory, this ratio is not inconsistent with the observed ratio in Eq. (5.6), and it gives support to our conclusion that the two observed states form a HQSS doublet.

From the couplings shown in Table 5.3, the dominant decay mechanisms of $\Lambda_b(5912)$ is expected to be of the form $\Lambda_b(5912) \to \Sigma_b\pi$ with subsequent decay of the off-shell heavy baryon $\Sigma_b \to \Lambda_b\pi$. Its heavy-quark partner, $\Lambda_b^*(5920)$, follows a similar pattern with $\Sigma_b^*$. The approximate HQSS requires the two resonances to have a similar width. In order to estimate this width, we consider the effective Lagrangian

$$\mathcal{L}(x) = \frac{g_{\Sigma_b\pi}}{\sqrt{3}}\vec{\Sigma}_b^\dagger\vec{\pi}\Lambda_b^{\rm res} + g\,\vec{\Sigma}_b^\dagger\sigma_i\partial_i\vec{\pi}\,\Lambda_b + \text{H.c.} \tag{5.8}$$

The averaged experimental decay width of the $\Sigma_b$, 7.3 MeV, allows to extract the value $g \approx 51$. The value of $g_{\Sigma_b\pi} = 1.8$ taken from our calculation, Table 5.3, gives a small width for $\Lambda_b(5912)$ around 8 keV. A similar calculation for $\Lambda_b^*(5920)$ yields a width around 12 keV.[2] The smallness of the widths are due to the reduced phase space available since the resonances are fairly close to the threshold. This is consistent with the experimental bounds quoted in [126].

Different quark models [20, 201–204] have also conjectured the existence of one or more excited $\Lambda_b(1/2^-)$ and $\Lambda_b(3/2^-)$ states. While the predicted masses for [201–204] differ few tenths of MeV from the LHCb experimental ones (see Table VIII of Ref. [204] for a summary of some of the results), the early work of Capstick and Isgur [20] generated the first two excited $\Lambda_b(1/2^-)$ and $\Lambda_b(3/2^-)$ states with masses that are in very good agreement with the ones observed by the LHCb collaboration. Indeed, their relativistic quark model predicts 5912 MeV and 5920 MeV for the masses of the lightest orbitally-excited states [20]. However, the same model yields a mass of the ground state $\Lambda_b^0$ ($J^P = 1/2^+$) which is about 35 MeV smaller than the measured value [4]. More recently, Garcilazo, Vijande, and Valcarce [201] have also presented results from a constituent-quark model scheme. They adjusted the mass of the $\Lambda_b^0$ ground state and predicted the masses of the $J^P = 1/2^-$ and $3/2^-$ orbitally excited $\Lambda_b$ states, which turned out to be around 30 MeV lower than the LHCb experimental values. Note, however, that the masses predicted in [201] are in turn 20-30 MeV higher than those obtained in other schemes based also on the relativistic quark model [202], or on the color hyperfine interaction [203] or on the heavy-quark effective theory [204]. More recently, in [205] heavy baryonic resonances $\Lambda_b$ ($\Lambda_c$) with $J^P = 3/2^-$ were studied in a constituent-quark model as a molecular state composed by nucleons and $\bar{B}^*$ ($D^*$) mesons.

Our model reproduces the experimental $\Lambda_b(5912)$ and $\Lambda_b(5920)$, but with an alternative explanation of their nature as molecular states, which moreover are HQSS partners. It is known that some baryon states can be constructed as a $qqq$ state in a quark model, and simultaneously as a dynamically generated resonance in a baryon-meson coupled-channel description (that is a $qqq$ - $q\bar{q}$ molecular state) [206]. Some of their properties might however differ, and it is thus interesting to consider both points of view in order to get in the future a joint or integral description of hadronic resonances in terms of quarks and hadrons degrees of freedom.

[2] These numbers are just estimates. Being close to threshold any refinement in the treatment will induce relatively large changes in the values quoted.

### 5.1.2 $\Xi_b$ and $\Xi_b^*$ states

Next, we analyze the ($B = -1,\ C = 0,\ S = -1\ , I = 1/2$) sector, for both $J = 1/2$ and $J = 3/2$ spins ($\Xi_b$ and $\Xi_b^*$ states, respectively). Our model predicts the existence of nine states (6 $\Xi_b$ and 3 $\Xi_b^*$) stemming from the strongly attractive **120** and **168** SU(8) irreducible representations (analogously to the charm sector, see Section 3.1). However, only three $\Xi_b$ and one $\Xi_b^*$ belong to the same SU(3)×HQSS multiplets as the $\Lambda_b$ and $\Lambda_b^*$ states reported in Table 5.3. In this exploratory study, we restrict our discussion to these states.

In the $\Xi_b$ sector, the following 31 channels are involved:

$$\begin{array}{llllllll} \Xi_b\pi & \Xi_b'\pi & \Lambda_b\bar{K} & \Sigma_b\bar{K} & \Xi_b\eta & \Lambda\bar{B} & \Lambda\bar{B}^* & \Sigma\bar{B} \\ \Xi_b'\eta & \Lambda_b\bar{K}^* & \Sigma\bar{B}^* & \Omega_bK & \Xi_b\rho & \Xi_b\omega & \Xi\bar{B}_s & \Xi_b'\rho \\ \Sigma_b\bar{K}^* & \Xi_b'\omega & \Sigma^*\bar{B}^* & \Xi_b^*\rho & \Sigma_b^*\bar{K}^* & \Xi_b^*\omega & \Xi\bar{B}_s^* & \Xi_b\eta' \\ \Xi_b\phi & \Xi_b'\eta' & \Omega_bK^* & \Xi_b'\phi & \Xi^*\bar{B}_s^* & \Omega_b^*K^* & \Xi_b^*\phi & , \end{array}$$

while in the $\Xi_b^*$ sector, the 26 channels, ordered by increasing thresholds, are:

$$\begin{array}{llllllll} \Xi_b^*\pi & \Sigma_b^*\bar{K} & \Lambda\bar{B}^* & \Xi_b^*\eta & \Lambda_b\bar{K}^* & \Sigma\bar{B}^* & \Omega_b^*K & \Xi_b\rho \\ \Xi_b\omega & \Sigma^*\bar{B} & \Xi_b'\rho & \Sigma_b\bar{K}^* & \Xi_b'\omega & \Sigma^*\bar{B}^* & \Xi_b^*\rho & \Sigma_b^*\bar{K}^* \\ \Xi_b^*\omega & \Xi\bar{B}_s^* & \Xi_b\phi & \Xi^*\bar{B}_s & \Xi_b^*\eta' & \Omega_bK^* & \Xi_b'\phi & \Xi^*\bar{B}_s^* \\ \Omega_b^*K^* & \Xi_b^*\phi & . \end{array}$$

For the subtraction point we use $\mu^2 = M_{\Xi_b}^2 + m_\pi^2$, and thus we assume our default value $\alpha = 1$ in Eq. (5.1). There is no particularly good reason to use the same value as in the $\Lambda_b$ case. Even SU(3) does not relate the two $\mu^{SI}$ points, $M_{\Sigma_b}^2 + m_\pi^2$ and $M_{\Xi_b}^2 + m_\pi^2$, required to fix the RS in each sector. If instead we take $\alpha = 0.967$ as in the $\Lambda_b$ sector, $\Xi_b$ and $\Xi_b^*$ binding energies (masses) will be larger (smaller) by about 60-80 MeV. These 60-80 MeV should be admitted as an intrinsic systematic uncertainty in our predictions in this sector.

In this way, we find the $\Xi_b$ and $\Xi_b^*$ states that complete the $\Lambda_b$ and $\Lambda_b^*$ SU(3)×HQSS multiplets. The properties of the dynamically-generated $\Xi_b$ and $\Xi_b^*$ states are compiled in Table 5.4. By studying the evolution of the poles from the SU(6)×HQSS symmetric point, we find that $\Lambda_b(5797.6)$ and $\Xi_b(5874)$ belong to the same irreducible representation, and similarly the $\Lambda_b(6009.3)$ and $\Xi_b(6072.8)$ states. Also, the pair $\Xi_b(6035.4)$ and $\Xi_b^*(6043.3)$, in the **15** irrep of SU(6), form the HQSS doublet related by SU(3) to the doublet formed by the $\Lambda_b(5910.1)$ and $\Lambda_b^*(5921.5)$ states.

The three $\Xi_b$ and one $\Xi_b^*$ states have also partners in the charm sector. We find that states with the same group labels are the heavy flavor counterpart of each other, as already noted for the $\Lambda_b$ and $\Lambda_b^*$ sectors. By comparing Table 5.4 with Table 3.5 of the Chapter 3, we see that the HQSS partners in the charm sector coming from the **15** representation, $\Xi_c(2772.9)$ and $\Xi_c^*(2819.7)$, are the bottom counterparts of the $\Xi_b(6035.4)$ and $\Xi_b^*(6043.3)$ states. Moreover, the charmed $\Xi_c(2699.4)$ and $\Xi_c(2775.4)$ resonances are analogous to the $\Xi_b(5874)$ and $\Xi_b(6072.8)$ ones in the bottom sector, respectively. None of these bottomed states have been seen experimentally yet. Schemes based on quark models [20, 201–204] predict $\Xi_b(1/2^-)$ and $\Xi_b(3/2^-)$ states with similar masses to our estimates, although there

| SU(6) irrep | $SU(3)_{2J+1}$ irrep | $\Delta M_R$ MeV | $M_R$ MeV | $\Gamma_R$ MeV | Couplings to main channels | $J$ | Main decay mode |
|---|---|---|---|---|---|---|---|
| **21** | $\mathbf{3^*_2}$ | 255 | 5874. | 0. | $g_{\Lambda\bar{B}} = 1.3$, $g_{\Sigma\bar{B}} = 4.4$, $g_{\Lambda\bar{B}^*} = 2.3$, $g_{\Sigma\bar{B}^*} = 7.3$, $g_{\Xi\bar{B}_s} = 2.6$, $g_{\Xi_b\eta'} = 1.0$, $g_{\Xi\bar{B}^*_s} = 4.5$ | 1/2 | $\Xi_b\gamma$ |
| **15** | $\mathbf{3^*_2}$ | 416 | 6035.4 | 0. | $\boldsymbol{g_{\Xi_b\pi} \sim 0.05}$, $g_{\Sigma_b\bar{K}} = 2.3$, $g_{\Lambda\bar{B}} = 1.$, $g_{\Sigma\bar{B}} = 4.5$, $g_{\Sigma\bar{B}^*} = 2.8$, $g_{\Xi_b\omega} = 1.2$, $g_{\Sigma^*\bar{B}^*} = 2.3$ | 1/2 | $\Xi_b\pi$ |
| **15** | $\mathbf{3^*_4}$ | 424 | 6043.3 | 0. | $g_{\Sigma^*_b\bar{K}} = 2.3$, $g_{\Lambda\bar{B}^*} = 1.1$, $g_{\Sigma\bar{B}^*} = 5.5$, $g_{\Sigma^*\bar{B}} = 1.4$, $g_{\Xi_b\omega} = 1.2$, $g_{\Sigma^*\bar{B}^*} = 1.7$ | 3/2 | $\Xi_b\pi$ |
| **21** | $\mathbf{3^*_2}$ | 453 | 6072.8 | 0.3 | $\boldsymbol{g_{\Xi_b\pi} = 0.1}$, $\boldsymbol{g_{\Xi'_b\pi} = 0.1}$, $g_{\Xi_b\eta} = 2.4$, $g_{\Lambda\bar{B}} = 1.4$, $g_{\Lambda\bar{B}^*} = 2.3$, $g_{\Sigma\bar{B}} = 1.1$, $g_{\Sigma\bar{B}^*} = 1.6$, $g_{\Xi\bar{B}_s} = 2.9$, $g_{\Xi\bar{B}^*_s} = 4.5$ | 1/2 | $\Xi_b\pi$, $\Xi'_b\pi$ |

Table 5.4: SU(3) partners of the states in Table 5.3. Predictions for $\Xi_b$ ($J^P = 1/2^-$) and $\Xi^*_b$ ($J^P = 3/2^-$) resonances (with $\alpha = 1$ in Eq. (5.1)). No experimental excited $\Xi_b$ or $\Xi^*_b$ resonances have been detected yet. The two states in the **15** of SU(6) form a HQSS doublet.

exist some differences between the various predictions. The experimental observation of the $\Xi_b$ and $\Xi_b^*$ excited states and their decays might, on the other hand, provide some valuable information concerning the nature of these states, whether they can be described as pure quark states or they have an important molecular component.

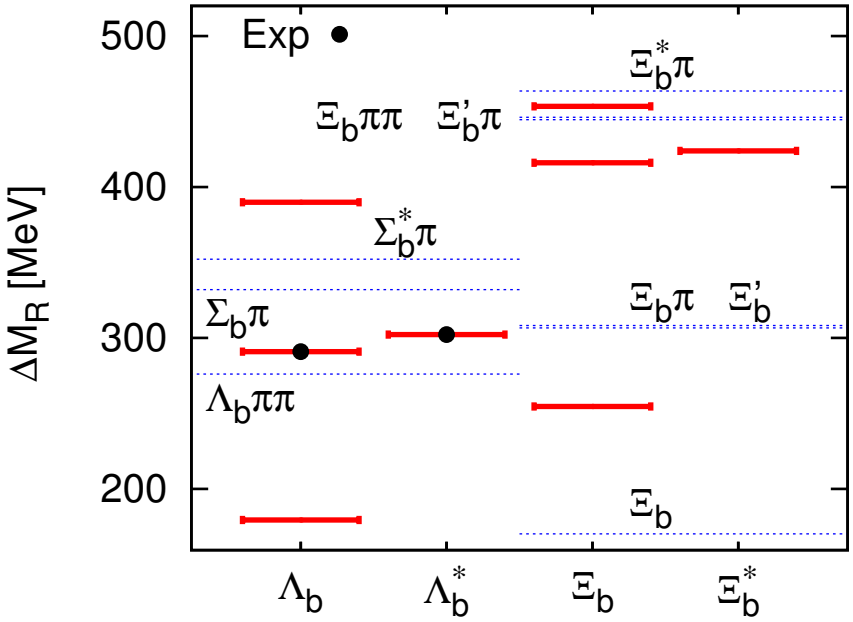


Figure 5.1: Summary of the new predicted states, which are represented by red lines. We also show the experimentally observed $\Lambda_b^0(5912)$ and $\Lambda_b^0(5920)$ states as black dots, and some relevant hadronic thresholds with blue dashed lines. The experimental errors are small ($\pm 0.8$ MeV for $\Lambda_b(5912)$ and $\pm 0.76$ for $\Lambda_b(5920)$) and are, thus, covered by the size of the dots.

Fig. 5.1 shows a summary of the masses of the predicted $\Lambda_b(1/2^-)$, $\Lambda_b(3/2^-)$, $\Xi_b(1/2^-)$ and $\Xi_b(3/2^-)$ states with respect to the mass of the ground state $\Lambda_b$, together with several thresholds for possible two- and three-body decay channels. The experimental $\Lambda_b^0(5912)$ and $\Lambda_b^0(5920)$ of LHCb are given for reference. Tables 5.3 and 5.4 show that, except for $\Xi_b(6072.8)$, our predicted states have a negligible width. This implies that they do not strongly couple to two-body channels with lower mass, such as $\Sigma_b\pi$ or $\Xi_b\pi$. Three-body channels are not included in our calculation. These channels allow the possibility of strong decay for some of the states. This is the case of the $\Lambda_b(3/2^-)$ and the two $\Lambda_b(1/2^-)$ which lie above the threshold of $\Lambda_b\pi\pi$, but it is not the case for the lightest $\Lambda_b$ and $\Xi_b$ states. They are below all hadronic channels, and hence they are stable under strong interactions. These states could be detected through electric dipole decay to $\Lambda_b\gamma$ and $\Xi_b\gamma$. Note that the strong decay of $\Xi_b(3/2^-)$ to $\Xi_b\pi$ is forbidden in $s$-wave but allowed through $d$-wave mechanisms not included in our model.

In Fig. 5.2, we depict the $(\pm|T|)$-matrix for the four $(SIJ)$ sectors studied in this work. Sectors related through SU(3) or by HQSS are plotted with opposite sign to better

appreciate the degree of fulfillment or breaking of these symmetries. The extra poles stand for other states which stem from other SU(8)/SU(6) irreps to those considered in this exploratory study.

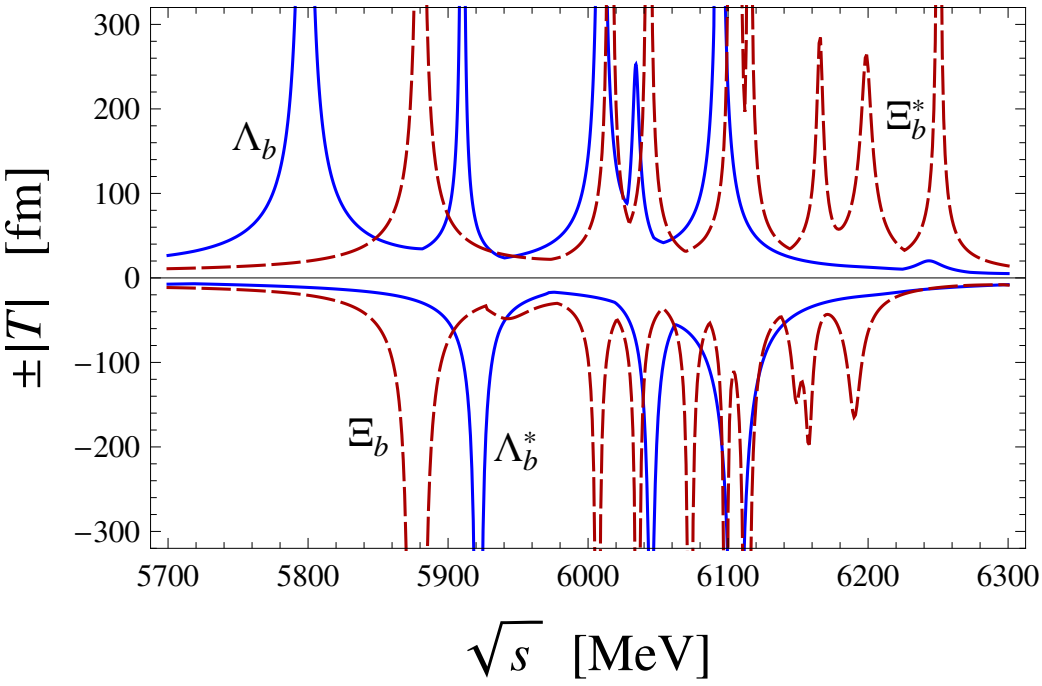


Figure 5.2: $\pm \max_j \sum_i |T_{ij}(\sqrt{s})|$ for the four $(I, J)$ sectors studied. We use the "plus" sign for the sectors $\Lambda_b$ (blue, solid line) and $\Xi_b^*$ (red, dashed line) and the "minus" sign for $\Lambda_b^*$ (blue, solid line) and $\Xi_b$ (red, dashed line). Exact SU(3) or HQSS symmetries would translate into exact mirror symmetries in the plot.

As we now deal with even heavier quarks, we would like to address one present technical aspect at this point. It follows from QCD that, as one flavor of quarks becomes heavy, the spectrum of hadrons with one such quark tends to a universal pattern, shifted by the heavy-quark mass. However, it is well known [53] that the renormalized loop function, $G$, grows logarithmically as any one of the hadrons in the loop gets heavy. This implies that, in the infinitely-heavy-quark limit, the interaction (and so the binding energy in attractive sectors) would effectively increase at a logarithmic rate, rather than stabilizing. By artificially increasing the bottomed-hadron masses we have verified that such spurious binding would indeed arise for sufficiently large masses,[3] however, it is not clear how sizable the effect is in a realistic scenario. As we have seen above, the generic subtraction point [Eq. (2.36)] actually produces too little binding and we have to move to a phenomenological subtraction point to pinpoint the experimentally observed states. This would suggest that the problem is not yet a pressing one at the bottom scale, at least for the sector we are considering and those related to it by softly broken symmetries. It can be expected that whenever the subtraction point is shifted to finetune the

[3]Simultaneously, we find that the gaps between resonances decrease as $1/m_Q$.

overall position of a multiplet of resonances, any spurious binding will produce at most a residual distortion in the individual positions, without compromising the existence and main couplings of the resonances under study.

## 5.2 Summary

We have analyzed odd-parity baryon resonances with one bottom quark. A summary of our predictions is graphically shown in Fig. 5.1. The experimental states $\Lambda_b^0(5912)$ and $\Lambda_b^0(5920)$ reported by the LHCb collaboration are obtained as dynamically-generated baryon-meson molecular states. Within our scheme, these states are identified as HQSS partners, which naturally explains their approximate mass degeneracy. Other $\Lambda(1/2^-)$ states coming from the same attractive SU(6) $\times$ HQSS representations are also analyzed, and we find a close analogy to the charm and strange sectors. In particular, the $\Lambda_b^0(5920)$ is the bottomed counterpart of the $\Lambda^*(1520)$ and $\Lambda_c^*(2625)$ resonances. Moreover, the $\Lambda_b^0(5912)$ is part of a two-pole structure similar to the one observed in the case of the $\Lambda(1405)$ and $\Lambda_c(2595)$ resonances.

Mass and decay mode predictions are also obtained for some $\Xi_b(1/2^-)$ and $\Xi_b(3/2^-)$ resonances, which belong to the same SU(3) multiplets as the $\Lambda_b(1/2^-)$ and $\Lambda_b(3/2^-)$ states. We find three $\Xi_b(1/2^-)$ and one $\Xi_b(3/2^-)$ states coming from the most attractive SU(6) $\times$ HQSS representations. Two of these predicted states, $\Xi_b(6035.4)$ and $\Xi_b^*(6043.3)$, form a HQSS doublet similar to that formed by the experimental $\Lambda_b(5912)$ and $\Lambda_b^*(5920)$ resonances. None of these states have been detected yet, and their existence is also predicted by constituent-quark models. It constitutes a clear case for discovery.

# Chapter 6

# Conclusions and overview

In the last few decades, in connection with many on-going experiments, such as Belle, CLEO, BaBar, and future ones, like CBM and PANDA at FAIR facility, the attention of the theoretical community has turned towards predicting features of possible states with heavy flavor. The goal is the explanation of the nature of the newly discovered states. Effective field theory is a commonly used tool for exploring the low-energy regime of Quantum Chromodynamics (QCD). The development of nonperturbative techniques has led to the extension of the applicability of effective field theories to higher energies, and thus made it suitable for studies of resonances or bound states. Heavy flavor has been studied using unitarized coupled-channels models, and the latter has proved to be successful in describing existing experimental data in the light sector. When dealing with heavy quarks, a new symmetry of QCD plays an important role, the heavy-quark spin symmetry (HQSS). This is a proper symmetry of QCD in the limit of infinitely massive quarks. Thus, implementation of the HQSS constraints in the unitarized coupled-channels models seems to be a natural step.

In this thesis we study baryon resonances with heavy flavor, which are dynamically generated by the interaction of mesons and baryons. For this purpose we use an extension of the chiral Weinberg-Tomozawa potential to the spin-flavor (SF) symmetry for four flavors (three light ones, and one heavy) with HQSS constraints. The resulting potential takes into account two mechanisms: the one that involves an exchange of quarks between the scattered meson and baryon, and the mechanism of an annihilation of a light antiquark in the meson with a similar quark in the baryon and the subsequent creation of an antiquark-quark pair to form a new meson and baryon. The potential is then implemented in the on-shell Bethe-Salpeter (BS) equation, in order to obtain the scattering amplitudes. The baryon-meson loop function that appears in the BS equation is logarithmically divergent, and needs to be regularized; this is done using the subtraction point method. Baryon resonances appear as poles of the scattering amplitude. The poles on the first Riemann sheet on the real axis, that appear below threshold, are interpreted as bound states. The poles that are found on the second Riemann sheet below the real axis and above threshold are interpreted as resonances. Poles on the second Riemann sheet on, or below the real axis, but below threshold, are virtual states. From the analysis of the pole in the complex energy plane we find the mass and the width of the corresponding baryon resonances, while the couplings to the baryon-meson channels are obtained from the residues of the

scattering amplitudes. The couplings indicate the possible decay channels of the found resonances.

In addition, several soft symmetry-breaking mechanisms are introduced. This is done by the implementation of the physical values of hadron masses and meson decay constants. The symmetry is broken adiabatically to the isospin SU(2) symmetry. In this way the baryon resonances can be labeled with the original group representations, and in particular the HQSS multiplets can be determined.

With such phenomenological model we have studied baryon resonances with heavy flavor in several sectors, e.g. $C = 1$ sectors and also the $C = 2$ and 3 states. The model generates a large number of states, stemming from three SU(8) representations: **4752**, **168**, and **120**. The interaction in the first one, although attractive, is much weaker than in the last two representations. Therefore, we have restricted our study to the 288 states (counting multiplicities in spin and isospin) that result from the **168** and **120** representations. We have determined the masses, the widths, and the coupling constants of the found resonances, and analyzed the underlying group multiplet structure. Some of our states could be identified with the experimentally known particles, whereas many others are predictions of the model. For example, we reproduce the $\Lambda_c(2595)$ and $\Lambda_c(2625)$ resonances, and interpret them as a members of the SU(8) **168**-plet, and in both cases with a dynamics strongly influenced by the $ND^*$ channel, in sharp contrast with previous studies, where this coupled channel was not considered. We have also studied the changes induced by a suppression factor in the interaction when charm is exchanged in the $\Lambda_c$ sector, and found that such changes do not modify the conclusions. Moreover, we have identified the HQSS multiplets to which the resonances belong. Specifically, in the ($\Lambda_c$, $\Lambda_c^*$) sector two singlets are found, the $\Lambda_c(2595)$ being one of them, and one doublet, which contains the $\Lambda_c(2625)$. Similarly, the ($\Sigma_c$, $\Sigma_c^*$) sector contains one singlet and two doublets. For the ($\Xi_c$, $\Xi_c^*$) sector, there are three doublets and three singlets. We reproduce the $\Xi_c(2790)$ and $\Xi_c(2815)$ resonances, and according to our tentative identification, these states form a HQSS doublet. Finally, $\Omega_c$ and $\Omega_c^*$ states form two doublets and one singlet. Furthermore, we have also analyzed the strange and charmed resonances with $C = 2$ and $C = 3$ linked to the strongly attractive **168** and **120** subspaces. To our knowledge, these are the first predictions in these sectors obtained from a model fulfilling HQSS. The organization into HQSS multiplets is also given in this case. There is scarce experimental information in these sectors, but we believe that our predictions are robust, and will find experimental confirmation in the future.

We have also studied hidden-charm $N$ and $\Delta$ resonances. We have carried out a detailed analysis of the hidden-charm sector (i.e., with $c\bar{c}$ pairs) with $C = 0$ and its breaking as the symmetry is lifted from SU(6) $\times$ HQSS to SU(3) $\times$ HQSS (and then to SU(2) $\times$ HQSS and SU(2) of isospin). We predict seven $N$-like and five $\Delta$-like states with masses around 4 GeV, most of them as bound states. These states form HQSS multiplets, which are almost degenerate in mass. The $N$ states form two HQSS multiplets. The lowest one has the light-quark flavor-spin content coupled to $\mathbf{8_2}$, the light-flavor octet of states with spin 1/2. Since the $\bar{c}c$ pair can couple to spin $S_{c\bar{c}} = 0, 1$, this HQSS multiplet consists of three nucleon states with $J = 1/2,\ 1/2$, and $3/2$, and masses around 3930 MeV. On the other hand, the highest HQSS nucleon-like multiplet contains four resonances with $J = 1/2,\ 3/2,\ 3/2$, and $5/2$, and masses around 4000 MeV. In this

case, these states originate from the $\mathbf{8_4}$ SF light configuration. These two SU(3) $\times$ HQSS $(\mathbf{8_2})_{\mathbf{2,0}}$ and $(\mathbf{8_4})_{\mathbf{2,0}}$ multiplets arise from the **70**-plet of SU(6) $\times$ HQSS. According to our analysis, there are no $N$ physical states coming from the **56**-plet. With regards to $\Delta$ states, we find two multiples with very different average masses, because in this case they originate from different SU(6) $\times$ HQSS representations. There is the $\Delta$ multiplet coming from the light-flavor decuplet with spin 1/2, which comes from the $\mathbf{70_{2,0}}$ SU(6) $\times$ HQSS representation, $(\mathbf{10_2})_{\mathbf{2,0}} \subset \mathbf{70_{2,0}}$, and it is formed by 3 states ($J = 1/2,\ 1/2,\ 3/2$) with an average mass of 4035 MeV. Besides this multiplet, another one is formed by only two $\Delta$ ($J = 1/2,\ 3/2$) resonances at the physical point out of the four states originating from the $(\mathbf{10_4})_{\mathbf{2,0}} \subset \mathbf{56_{2,0}}$ in the SU(6) limit. These two states are nearly degenerate, with a mass of 4306 MeV. When we compare our approach with other molecular-type ones, we observe in our model a richer structure of resonances due to the many channels cooperating to create them. We have compared the $N$-like states found in our model with findings of other approaches. Our states are much lighter than those predicted in the hidden-gauge scheme [150–152], although significantly less bound than the crypto-exotic baryons reported in the zero-range $t$-channel vector meson exchange model [141, 142]. We also compared our results with findings of a constituent-quark model, and obtain that our predictions are close to those seen by the chiral interaction, based on meson exchange [191], especially for the lowest-lying states. To our knowledge, our results for exotic hidden-charm $\Delta$-like resonances within a molecular baryon-meson scheme are the first predictions in this sector.

We have finally analyzed even heavier baryon resonances, with one bottom quark. This study was inspired by the finding of the LHCb collaboration, where two narrow resonances with beauty flavor were seen, $\Lambda_b^0(5912)$ and $\Lambda_b^0(5920)$. Using our phenomenological model, these states are interpreted as dynamically-generated baryon-meson molecular states, and identified as HQSS partners, which naturally explains their approximate mass degeneracy. We also find a close analogy with the charm and strange sectors. In particular, the $\Lambda_b^*(5920)$ is the bottomed counterpart of the $\Lambda^*(1520)$ and $\Lambda_c^*(2625)$ resonances. Moreover, the $\Lambda_b(5912)$ is part of a two-pole structure similar to the one observed in the case of the $\Lambda(1405)$ and $\Lambda_c(2595)$ resonances. Mass and decay mode predictions are also obtained for the $\Xi_b(1/2^-)$ and $\Xi_b(3/2^-)$ resonances, which belong to the same SU(3) multiplets as the $\Lambda_b(1/2^-)$ and $\Lambda_b(3/2^-)$ states. We find three $\Xi_b(1/2^-)$ and one $\Xi_b(3/2^-)$ states coming from the most attractive SU(6) $\times$ HQSS representations. Two of these predicted states, $\Xi_b(6035.4)$ and $\Xi_b^*(6043.3)$, form a HQSS doublet similar to that of the experimental $\Lambda_b(5912)$ and $\Lambda_b^*(5920)$ resonances. None of these states have been detected yet, and their existence is also predicted by constituent-quark models [201]. It constitutes a clear case for discovery.

Thus, exploiting the phenomenological model that uses the SF extension of the WT interaction for four flavors with HQSS constraints, we have studied a rich number of baryon resonances with charm and beauty flavors. The prominent features of our model are the inclusion of the vector mesons and $J = 3/2^+$ baryons in order to fulfill HQSS, and the subsequent richer spectrum of the generated states as compared with previous models. Some of the states generated in the model can be readily identified with the experimentally known states, whereas others need more data for verification. For the open-charm and hidden-charm states studied in this thesis, desirable data might be provided by the future

PANDA experiment at FAIR facility.

# Appendix A

# Spin-flavor states

In this appendix we give details regarding the construction of the tensors $M^A{}_B$ and $B^{ABC}$, and the computation of the matrix elements of the interaction.

The wave functions in spin-flavor space of the basic meson and baryons are constructed in terms of bosonic quark and antiquark operators with spin and flavor labels, namely, $Q^\dagger_{f\uparrow}$,$Q^\dagger_{f\downarrow}$, $Q^\dagger_{\bar{f}\uparrow}$ $Q^\dagger_{\bar{f}\downarrow}$, $f = u, d, s, c$. The wave functions are shown below for the ground-state hadrons, for states with the highest isospin projection ($I_3$) in each isospin multiplet.

**Wave functions for the ground-state hadrons:**

Pseudoscalar mesons

$|\pi\rangle = \frac{1}{\sqrt{2}}(Q^\dagger_{u\uparrow}Q^\dagger_{\bar{d}\downarrow} - Q^\dagger_{u\downarrow}Q^\dagger_{\bar{d}\uparrow})|0\rangle,$

$|K\rangle = -\frac{1}{\sqrt{2}}(Q^\dagger_{u\uparrow}Q^\dagger_{\bar{s}\downarrow} - Q^\dagger_{u\downarrow}Q^\dagger_{\bar{s}\uparrow})|0\rangle, \quad |\bar{K}\rangle = \frac{1}{\sqrt{2}}(Q^\dagger_{s\uparrow}Q^\dagger_{\bar{d}\downarrow} - Q^\dagger_{s\downarrow}Q^\dagger_{\bar{d}\uparrow})|0\rangle,$

$|D\rangle = \frac{1}{\sqrt{2}}(Q^\dagger_{c\uparrow}Q^\dagger_{\bar{d}\downarrow} - Q^\dagger_{c\downarrow}Q^\dagger_{\bar{d}\uparrow})|0\rangle, \quad |D_s\rangle = -\frac{1}{\sqrt{2}}(Q^\dagger_{c\uparrow}Q^\dagger_{\bar{s}\downarrow} - Q^\dagger_{c\downarrow}Q^\dagger_{\bar{s}\uparrow})|0\rangle,$

$|\bar{D}\rangle = \frac{1}{\sqrt{2}}(Q^\dagger_{u\uparrow}Q^\dagger_{\bar{c}\downarrow} - Q^\dagger_{u\downarrow}Q^\dagger_{\bar{c}\uparrow})|0\rangle, \quad |\bar{D}_s\rangle = \frac{1}{\sqrt{2}}(Q^\dagger_{s\uparrow}Q^\dagger_{\bar{c}\downarrow} - Q^\dagger_{s\downarrow}Q^\dagger_{\bar{c}\uparrow})|0\rangle,$

$|\eta\rangle = \frac{1}{\sqrt{12}}(Q^\dagger_{u\uparrow}Q^\dagger_{\bar{u}\downarrow} - Q^\dagger_{u\downarrow}Q^\dagger_{\bar{u}\uparrow} + Q^\dagger_{d\uparrow}Q^\dagger_{\bar{d}\downarrow} - Q^\dagger_{d\downarrow}Q^\dagger_{\bar{d}\uparrow} - 2Q^\dagger_{s\uparrow}Q^\dagger_{\bar{s}\downarrow} + 2Q^\dagger_{s\downarrow}Q^\dagger_{\bar{s}\uparrow})|0\rangle,$

$|\eta'\rangle = \frac{1}{\sqrt{6}}(Q^\dagger_{u\uparrow}Q^\dagger_{\bar{u}\downarrow} - Q^\dagger_{u\downarrow}Q^\dagger_{\bar{u}\uparrow} + Q^\dagger_{d\uparrow}Q^\dagger_{\bar{d}\downarrow} - Q^\dagger_{d\downarrow}Q^\dagger_{\bar{d}\uparrow} + Q^\dagger_{s\uparrow}Q^\dagger_{\bar{s}\downarrow} - Q^\dagger_{s\downarrow}Q^\dagger_{\bar{s}\uparrow})|0\rangle,$

$|\eta_c\rangle = \frac{1}{\sqrt{2}}(Q^\dagger_{c\uparrow}Q^\dagger_{\bar{c}\downarrow} - Q^\dagger_{c\downarrow}Q^\dagger_{\bar{c}\uparrow})|0\rangle.$

Vector mesons

$|\rho\rangle = -Q^\dagger_{u\uparrow}Q^\dagger_{\bar{d}\uparrow}|0\rangle,$

$|K^*\rangle = Q^\dagger_{u\uparrow}Q^\dagger_{\bar{s}\uparrow}|0\rangle, \quad |\bar{K}^*\rangle = -Q^\dagger_{s\uparrow}Q^\dagger_{\bar{d}\uparrow}|0\rangle,$

$|D^*\rangle = -Q^\dagger_{c\uparrow}Q^\dagger_{\bar{d}\uparrow}|0\rangle, \quad |D^*_s\rangle = Q^\dagger_{c\uparrow}Q^\dagger_{\bar{s}\uparrow}|0\rangle, \quad |\bar{D}^*\rangle = -Q^\dagger_{u\uparrow}Q^\dagger_{\bar{c}\uparrow}|0\rangle, \quad |\bar{D}^*_s\rangle = -Q^\dagger_{s\uparrow}Q^\dagger_{\bar{c}\uparrow}|0\rangle,$

$|\omega\rangle = -\frac{1}{\sqrt{2}}(Q^\dagger_{u\uparrow}Q^\dagger_{\bar{u}\uparrow} + Q^\dagger_{d\uparrow}Q^\dagger_{\bar{d}\uparrow})|0\rangle, \quad |\phi\rangle = Q^\dagger_{s\uparrow}Q^\dagger_{\bar{s}\uparrow}|0\rangle,$

$|J/\psi\rangle = -Q^\dagger_{c\uparrow}Q^\dagger_{\bar{c}\uparrow}|0\rangle.$

Spin-1/2 baryons

$|\Lambda\rangle = -\frac{1}{\sqrt{2}}(Q^\dagger_{u\uparrow}Q^\dagger_{d\downarrow}Q^\dagger_{s\uparrow} - Q^\dagger_{u\downarrow}Q^\dagger_{d\uparrow}Q^\dagger_{s\uparrow})|0\rangle$, $|N\rangle = -\frac{1}{\sqrt{3}}(Q^\dagger_{u\uparrow}Q^\dagger_{u\uparrow}Q^\dagger_{d\downarrow} - Q^\dagger_{u\uparrow}Q^\dagger_{u\downarrow}Q^\dagger_{d\uparrow})|0\rangle$,

$|\Sigma\rangle = -\frac{1}{\sqrt{3}}(Q^\dagger_{u\uparrow}Q^\dagger_{u\uparrow}Q^\dagger_{s\downarrow} - Q^\dagger_{u\uparrow}Q^\dagger_{u\downarrow}Q^\dagger_{s\uparrow})|0\rangle$, $|\Xi\rangle = -\frac{1}{\sqrt{3}}(Q^\dagger_{u\uparrow}Q^\dagger_{s\downarrow}Q^\dagger_{s\uparrow} - Q^\dagger_{u\downarrow}Q^\dagger_{s\uparrow}Q^\dagger_{s\uparrow})|0\rangle$,

$|\Sigma_c\rangle = -\frac{1}{\sqrt{3}}(Q^\dagger_{u\uparrow}Q^\dagger_{u\uparrow}Q^\dagger_{c\downarrow} - Q^\dagger_{u\uparrow}Q^\dagger_{u\downarrow}Q^\dagger_{c\uparrow})|0\rangle$,

$|\Xi'_c\rangle = -\frac{1}{\sqrt{6}}(2Q^\dagger_{u\uparrow}Q^\dagger_{s\uparrow}Q^\dagger_{c\downarrow} - Q^\dagger_{u\uparrow}Q^\dagger_{s\downarrow}Q^\dagger_{c\uparrow} - Q^\dagger_{u\downarrow}Q^\dagger_{s\uparrow}Q^\dagger_{c\uparrow})|0\rangle$,

$|\Omega_c\rangle = -\frac{1}{\sqrt{3}}(Q^\dagger_{s\uparrow}Q^\dagger_{s\uparrow}Q^\dagger_{c\downarrow} - Q^\dagger_{s\uparrow}Q^\dagger_{s\downarrow}Q^\dagger_{c\uparrow})|0\rangle$, $|\Xi_c\rangle = -\frac{1}{\sqrt{2}}(Q^\dagger_{u\uparrow}Q^\dagger_{s\downarrow}Q^\dagger_{c\uparrow} - Q^\dagger_{u\downarrow}Q^\dagger_{s\uparrow}Q^\dagger_{c\uparrow})|0\rangle$,

$|\Lambda_c\rangle = -\frac{1}{\sqrt{2}}(Q^\dagger_{u\uparrow}Q^\dagger_{d\downarrow}Q^\dagger_{c\uparrow} - Q^\dagger_{u\downarrow}Q^\dagger_{d\uparrow}Q^\dagger_{c\uparrow})|0\rangle$, $|\Xi_{cc}\rangle = -\frac{1}{\sqrt{3}}(Q^\dagger_{u\uparrow}Q^\dagger_{c\downarrow}Q^\dagger_{c\uparrow} - Q^\dagger_{u\downarrow}Q^\dagger_{c\uparrow}Q^\dagger_{c\uparrow})|0\rangle$,

$|\Omega_{cc}\rangle = -\frac{1}{\sqrt{3}}(Q^\dagger_{s\uparrow}Q^\dagger_{c\downarrow}Q^\dagger_{c\uparrow} - Q^\dagger_{s\downarrow}Q^\dagger_{c\uparrow}Q^\dagger_{c\uparrow})|0\rangle$.

Spin-3/2 baryons

$|\Delta\rangle = \frac{1}{\sqrt{6}}(Q^\dagger_{u\uparrow}Q^\dagger_{u\uparrow}Q^\dagger_{u\uparrow})|0\rangle$, $|\Sigma^*\rangle = \frac{1}{\sqrt{2}}(Q^\dagger_{u\uparrow}Q^\dagger_{u\uparrow}Q^\dagger_{s\uparrow})|0\rangle$, $|\Xi^*\rangle = \frac{1}{\sqrt{2}}(Q^\dagger_{u\uparrow}Q^\dagger_{s\uparrow}Q^\dagger_{s\uparrow})|0\rangle$,

$|\Omega\rangle = \frac{1}{\sqrt{6}}(Q^\dagger_{s\uparrow}Q^\dagger_{s\uparrow}Q^\dagger_{s\uparrow})|0\rangle$, $|\Sigma^*_c\rangle = \frac{1}{\sqrt{2}}(Q^\dagger_{u\uparrow}Q^\dagger_{u\uparrow}Q^\dagger_{c\uparrow})|0\rangle$, $|\Xi^*_c\rangle = \frac{1}{\sqrt{2}}(Q^\dagger_{u\uparrow}Q^\dagger_{s\uparrow}Q^\dagger_{c\uparrow})|0\rangle$,

$|\Omega^*_c\rangle = \frac{1}{\sqrt{2}}(Q^\dagger_{s\uparrow}Q^\dagger_{s\uparrow}Q^\dagger_{c\uparrow})|0\rangle$, $|\Xi^*_{cc}\rangle = \frac{1}{\sqrt{2}}(Q^\dagger_{u\uparrow}Q^\dagger_{c\uparrow}Q^\dagger_{c\uparrow})|0\rangle$, $|\Omega^*_{cc}\rangle = \frac{1}{\sqrt{2}}(Q^\dagger_{s\uparrow}Q^\dagger_{c\uparrow}Q^\dagger_{c\uparrow})|0\rangle$,

$|\Omega_{ccc}\rangle = \frac{1}{\sqrt{6}}(Q^\dagger_{c\uparrow}Q^\dagger_{c\uparrow}Q^\dagger_{c\uparrow})|0\rangle$.

As compared to the wave functions that are given in the Appendix A of [175], there is a minus sign difference in all $1/2^+$ baryons, in all $0^-$ mesons except $\eta$, $\eta'$, and $\eta_c$, and in $\phi$, $\omega$, and $J/\psi$ (denoted $\psi$ in [175]). No difference of sign appears in the wave functions of $3/2^+$ baryons, neither in $\eta$, $\eta'$, and $\eta_c$, nor in $1^-$ mesons (except $\phi$, $\omega$ and $J/\psi$).

The states just defined are standard with respect to the flavor and spin-flavor groups conventions of [157]. In particular they are $SU(2)_J$, $SU(2)_I$ standard and follow the convention of [156] for flavor SU(3) and SU(4). The only exceptions come from the neutral mesons for which we use ideal mixing. In terms of these, the states of [157] are given by:

$$|\eta'\rangle_{\rm stan} = |\eta'\rangle \qquad [\mathrm{SU}(3)], \tag{A.1}$$

$$|\eta'\rangle_{\rm stan} = \sqrt{\frac{3}{4}}|\eta'\rangle + \frac{1}{2}|\eta_c\rangle \qquad [\mathrm{SU}(4)], \tag{A.2}$$

$$|\eta_c\rangle_{\rm stan} = -\frac{1}{2}|\eta'\rangle + \sqrt{\frac{3}{4}}|\eta_c\rangle \qquad [\mathrm{SU}(4)], \tag{A.3}$$

$$|\omega_8\rangle = \sqrt{\frac{1}{3}}|\omega\rangle + \sqrt{\frac{2}{3}}|\phi\rangle \qquad [\mathrm{SU}(3) \text{ and } \mathrm{SU}(4)], \tag{A.4}$$

$$|\omega_1\rangle = \sqrt{\frac{2}{3}}|\omega\rangle - \sqrt{\frac{1}{3}}|\phi\rangle \qquad [\mathrm{SU}(3)], \tag{A.5}$$

$$|\omega_1\rangle = \sqrt{\frac{1}{2}}|\omega\rangle - \frac{1}{2}|\phi\rangle + \frac{1}{2}|J/\psi\rangle \qquad [\mathrm{SU}(4)], \tag{A.6}$$

$$|\psi\rangle = -\sqrt{\frac{1}{6}}|\omega\rangle + \sqrt{\frac{1}{12}}|\phi\rangle + \sqrt{\frac{3}{4}}|J/\psi\rangle \qquad [\mathrm{SU}(4)]. \tag{A.7}$$

In these formulas, the right-hand sides contain the physical (or rather ideally-mixed) neutral mesons that we use in this work; their wave functions are shown above. The left-hand sides contain the standard or mathematical states used in [157]. They have proper quantum numbers with respect to SU(6) or SU(8) (and their corresponding chain of subgroups).[1]

In order to construct the tensors $M^A{}_B$ and $B^{ABC}$, $M^{\dagger A}{}_B$ and $B^\dagger_{ABC}$, the following procedure is used: For all flavors $f = u, d, s, c$, and for the various creation operators $Q^\dagger_{f\uparrow}$, $Q^\dagger_{f\downarrow}$, $Q^\dagger_{\bar{f}\uparrow}$, and $Q^\dagger_{\bar{f}\downarrow}$, appearing in the wave-functions of the hadrons, the following replacements are to be applied:

$$Q^\dagger_{f\uparrow} \to +Q^\dagger_{f1}, \quad Q^\dagger_{f\downarrow} \to +Q^\dagger_{f2}, \quad Q^\dagger_{\bar{f}\uparrow} \to -\bar{Q}^{\dagger f2}, \quad Q^\dagger_{\bar{f}\downarrow} \to +Q^\dagger_{f1}. \tag{A.8}$$

Note i) the minus sign in $Q^\dagger_{\bar{f}\uparrow}$, and ii) for quarks, the labels 1 and 2 correspond to spin up and down, respectively, but for antiquarks they correspond to spin down and up, respectively.

After the replacement, there are only operators $Q^\dagger_A$, and $\bar{Q}^{\dagger A}$ for creation (and $Q^A$, and $\bar{Q}_A$ for annihilation), carrying any of the eight labels $A = u1, d1, s1, c1, u2, d2, s2, c2$. These operators transform under SU(8) in the way indicated in Eq. (2.25).

The meson matrix is then obtained by replacing $\bar{Q}^{\dagger A} Q^\dagger_B$ with $M^{\dagger A}{}_B$ and expressing it in terms of meson operators by inverting the wave function equations. Similarly, for the baryons, $Q^\dagger_A Q^\dagger_B Q^\dagger_C$ is replaced with $B^\dagger_{ABC}$ and then expressed in terms of baryon operators. The wave functions of baryons and mesons are constructed from these annihilation and creation operators, for instance,

$|\pi\rangle = \frac{1}{\sqrt{2}}(M^{\dagger 2}{}_1 + M^{\dagger 6}{}_5)|0\rangle, \quad |N\rangle = -\frac{1}{\sqrt{3}}(B^\dagger{}_{116} - B^\dagger{}_{152})|0\rangle.$

[1] Note that $|\psi\rangle$ of [175] corresponds to $-|J/\psi\rangle$ here, not to $|\psi\rangle$ of [157] and of Eq. (A.7).

# Appendix B

# $D$-matrices for open-charm sectors

In this appendix the coefficients $D_{ij}^{IJSC}$ appearing in Eq. (2.31) are shown for the various $C$ (charm), $S$ (strangeness), $I$ (isospin), and $J$ (spin) sectors studied in this work (Tables B.1 - B.18). The $D$-matrices for the sectors with charm $C = 1$ and strangeness $S = 0$ can be found in the Appendix B of Ref. [175]. The tables for the $\Xi_c$ ($C = 1$, $S = -1$, $I = 1/2$, $J = 1/2$) and for the $\Xi_c^*$ ($C = 1$, $S = -1$, $I = 1/2$, $J = 3/2$) have been divided into three blocks each.

| | $\Sigma_c\pi$ | $ND$ | $\Lambda_c\eta$ | $ND^*$ | $\Xi_cK$ | $\Lambda_c\omega$ | $\Xi_c'K$ | $\Lambda D_s$ | $\Lambda D_s^*$ | $\Sigma_c\rho$ | $\Lambda_c\eta'$ | $\Sigma_c^*\rho$ | $\Lambda_c\phi$ | $\Xi_cK^*$ | $\Xi_c'K^*$ | $\Xi_c^*K^*$ |
|---|---|---|---|---|---|---|---|---|---|---|---|---|---|---|---|---|
| $\Sigma_c\pi$ | $-4$ | $\sqrt{\frac{3}{2}}$ | $0$ | $\frac{1}{\sqrt{2}}$ | $0$ | $0$ | $-\sqrt{3}$ | $0$ | $0$ | $\frac{8}{\sqrt{3}}$ | $0$ | $4\sqrt{\frac{2}{3}}$ | $0$ | $\sqrt{3}$ | $2$ | $\sqrt{2}$ |
| $ND$ | $\sqrt{\frac{3}{2}}$ | $-3$ | $-\frac{1}{\sqrt{2}}$ | $3\sqrt{3}$ | $0$ | $\frac{3}{\sqrt{2}}$ | $0$ | $-\sqrt{3}$ | $3$ | $\frac{1}{\sqrt{2}}$ | $-1$ | $2$ | $0$ | $0$ | $0$ | $0$ |
| $\Lambda_c\eta$ | $0$ | $-\frac{1}{\sqrt{2}}$ | $0$ | $\sqrt{\frac{3}{2}}$ | $\sqrt{3}$ | $0$ | $0$ | $\sqrt{\frac{2}{3}}$ | $-\sqrt{2}$ | $0$ | $0$ | $0$ | $0$ | $0$ | $-\sqrt{3}$ | $\sqrt{6}$ |
| $ND^*$ | $\frac{1}{\sqrt{2}}$ | $3\sqrt{3}$ | $\sqrt{\frac{3}{2}}$ | $-9$ | $0$ | $\sqrt{\frac{3}{2}}$ | $0$ | $3$ | $-3\sqrt{3}$ | $\frac{5}{\sqrt{6}}$ | $\sqrt{3}$ | $-\frac{2}{\sqrt{3}}$ | $0$ | $0$ | $0$ | $0$ |
| $\Xi_cK$ | $0$ | $0$ | $\sqrt{3}$ | $0$ | $-2$ | $0$ | $0$ | $\frac{1}{\sqrt{2}}$ | $-\sqrt{\frac{3}{2}}$ | $\sqrt{3}$ | $0$ | $-\sqrt{6}$ | $0$ | $0$ | $0$ | $0$ |
| $\Lambda_c\omega$ | $0$ | $\frac{3}{\sqrt{2}}$ | $0$ | $\sqrt{\frac{3}{2}}$ | $0$ | $0$ | $-1$ | $0$ | $0$ | $4$ | $0$ | $2\sqrt{2}$ | $0$ | $1$ | $\frac{2}{\sqrt{3}}$ | $\sqrt{\frac{2}{3}}$ |
| $\Xi_c'K$ | $-\sqrt{3}$ | $0$ | $0$ | $0$ | $0$ | $-1$ | $-2$ | $\sqrt{\frac{3}{2}}$ | $\frac{1}{\sqrt{2}}$ | $2$ | $0$ | $\sqrt{2}$ | $-\sqrt{2}$ | $0$ | $\frac{4}{\sqrt{3}}$ | $2\sqrt{\frac{2}{3}}$ |
| $\Lambda D_s$ | $0$ | $-\sqrt{3}$ | $\sqrt{\frac{2}{3}}$ | $3$ | $\frac{1}{\sqrt{2}}$ | $0$ | $\sqrt{\frac{3}{2}}$ | $-1$ | $\sqrt{3}$ | $0$ | $-\frac{1}{\sqrt{3}}$ | $0$ | $-\sqrt{3}$ | $-\sqrt{\frac{3}{2}}$ | $\frac{1}{\sqrt{2}}$ | $2$ |
| $\Lambda D_s^*$ | $0$ | $3$ | $-\sqrt{2}$ | $-3\sqrt{3}$ | $-\sqrt{\frac{3}{2}}$ | $0$ | $\frac{1}{\sqrt{2}}$ | $\sqrt{3}$ | $-3$ | $0$ | $1$ | $0$ | $-1$ | $-\frac{1}{\sqrt{2}}$ | $\frac{5}{\sqrt{6}}$ | $-\frac{2}{\sqrt{3}}$ |
| $\Sigma_c\rho$ | $\frac{8}{\sqrt{3}}$ | $\frac{1}{\sqrt{2}}$ | $0$ | $\frac{5}{\sqrt{6}}$ | $\sqrt{3}$ | $4$ | $2$ | $0$ | $0$ | $-\frac{20}{3}$ | $0$ | $\frac{2\sqrt{2}}{3}$ | $0$ | $-2$ | $-\frac{7}{\sqrt{3}}$ | $\sqrt{\frac{2}{3}}$ |
| $\Lambda_c\eta'$ | $0$ | $-1$ | $0$ | $\sqrt{3}$ | $0$ | $0$ | $0$ | $-\frac{1}{\sqrt{3}}$ | $1$ | $0$ | $0$ | $0$ | $0$ | $0$ | $0$ | $0$ |
| $\Sigma_c^*\rho$ | $4\sqrt{\frac{2}{3}}$ | $2$ | $0$ | $-\frac{2}{\sqrt{3}}$ | $-\sqrt{6}$ | $2\sqrt{2}$ | $\sqrt{2}$ | $0$ | $0$ | $\frac{2\sqrt{2}}{3}$ | $0$ | $-\frac{22}{3}$ | $0$ | $-\sqrt{2}$ | $\sqrt{\frac{2}{3}}$ | $-\frac{8}{\sqrt{3}}$ |
| $\Lambda_c\phi$ | $0$ | $0$ | $0$ | $0$ | $0$ | $0$ | $-\sqrt{2}$ | $-\sqrt{3}$ | $-1$ | $0$ | $0$ | $0$ | $0$ | $\sqrt{2}$ | $-2\sqrt{\frac{2}{3}}$ | $-\frac{2}{\sqrt{3}}$ |
| $\Xi_cK^*$ | $\sqrt{3}$ | $0$ | $0$ | $0$ | $0$ | $1$ | $0$ | $-\sqrt{\frac{3}{2}}$ | $-\frac{1}{\sqrt{2}}$ | $-2$ | $0$ | $-\sqrt{2}$ | $\sqrt{2}$ | $-2$ | $-\frac{4}{\sqrt{3}}$ | $-2\sqrt{\frac{2}{3}}$ |
| $\Xi_c'K^*$ | $2$ | $0$ | $-\sqrt{3}$ | $0$ | $0$ | $\frac{2}{\sqrt{3}}$ | $\frac{4}{\sqrt{3}}$ | $\frac{1}{\sqrt{2}}$ | $\frac{5}{\sqrt{6}}$ | $-\frac{7}{\sqrt{3}}$ | $0$ | $\sqrt{\frac{2}{3}}$ | $-2\sqrt{\frac{2}{3}}$ | $-\frac{4}{\sqrt{3}}$ | $-2$ | $0$ |
| $\Xi_c^*K^*$ | $\sqrt{2}$ | $0$ | $\sqrt{6}$ | $0$ | $0$ | $\sqrt{\frac{2}{3}}$ | $2\sqrt{\frac{2}{3}}$ | $2$ | $-\frac{2}{\sqrt{3}}$ | $\sqrt{\frac{2}{3}}$ | $0$ | $-\frac{8}{\sqrt{3}}$ | $-\frac{2}{\sqrt{3}}$ | $-2\sqrt{\frac{2}{3}}$ | $0$ | $-2$ |

Table B.1: $C = 1$, $S = 0$, $I = 0$, $J = 1/2$.

| | $\Sigma_c^*\pi$ | $ND^*$ | $\Lambda_c\omega$ | $\Xi_c^*K$ | $\Lambda D_s^*$ | $\Sigma_c\rho$ | $\Sigma_c^*\rho$ | $\Lambda_c\phi$ | $\Xi_cK^*$ | $\Xi_c'K^*$ | $\Xi_c^*K^*$ |
|---|---|---|---|---|---|---|---|---|---|---|---|
| $\Sigma_c^*\pi$ | $-4$ | $-\sqrt{2}$ | $0$ | $-\sqrt{3}$ | $0$ | $-\frac{4}{\sqrt{3}}$ | $4\sqrt{\frac{5}{3}}$ | $0$ | $\sqrt{3}$ | $-1$ | $\sqrt{5}$ |
| $ND^*$ | $-\sqrt{2}$ | $0$ | $-\sqrt{6}$ | $0$ | $0$ | $\sqrt{\frac{2}{3}}$ | $-\sqrt{\frac{10}{3}}$ | $0$ | $0$ | $0$ | $0$ |
| $\Lambda_c\omega$ | $0$ | $-\sqrt{6}$ | $0$ | $-1$ | $0$ | $-2$ | $2\sqrt{5}$ | $0$ | $1$ | $-\frac{1}{\sqrt{3}}$ | $\sqrt{\frac{5}{3}}$ |
| $\Xi_c^*K$ | $-\sqrt{3}$ | $0$ | $-1$ | $-2$ | $-\sqrt{2}$ | $-1$ | $\sqrt{5}$ | $-\sqrt{2}$ | $0$ | $-\frac{2}{\sqrt{3}}$ | $2\sqrt{\frac{5}{3}}$ |
| $\Lambda D_s^*$ | $0$ | $0$ | $0$ | $-\sqrt{2}$ | $0$ | $0$ | $0$ | $2$ | $\sqrt{2}$ | $\sqrt{\frac{2}{3}}$ | $-\sqrt{\frac{10}{3}}$ |
| $\Sigma_c\rho$ | $-\frac{4}{\sqrt{3}}$ | $\sqrt{\frac{2}{3}}$ | $-2$ | $-1$ | $0$ | $-\frac{8}{3}$ | $\frac{2\sqrt{5}}{3}$ | $0$ | $1$ | $-\frac{1}{\sqrt{3}}$ | $\sqrt{\frac{5}{3}}$ |
| $\Sigma_c^*\rho$ | $4\sqrt{\frac{5}{3}}$ | $-\sqrt{\frac{10}{3}}$ | $2\sqrt{5}$ | $\sqrt{5}$ | $0$ | $\frac{2\sqrt{5}}{3}$ | $-\frac{16}{3}$ | $0$ | $-\sqrt{5}$ | $\sqrt{\frac{5}{3}}$ | $-\frac{5}{\sqrt{3}}$ |
| $\Lambda_c\phi$ | $0$ | $0$ | $0$ | $-\sqrt{2}$ | $2$ | $0$ | $0$ | $0$ | $\sqrt{2}$ | $\sqrt{\frac{2}{3}}$ | $-\sqrt{\frac{10}{3}}$ |
| $\Xi_cK^*$ | $\sqrt{3}$ | $0$ | $1$ | $0$ | $\sqrt{2}$ | $1$ | $-\sqrt{5}$ | $\sqrt{2}$ | $-2$ | $\frac{2}{\sqrt{3}}$ | $-2\sqrt{\frac{5}{3}}$ |
| $\Xi_c'K^*$ | $-1$ | $0$ | $-\frac{1}{\sqrt{3}}$ | $-\frac{2}{\sqrt{3}}$ | $\sqrt{\frac{2}{3}}$ | $-\frac{1}{\sqrt{3}}$ | $\sqrt{\frac{5}{3}}$ | $\sqrt{\frac{2}{3}}$ | $\frac{2}{\sqrt{3}}$ | $-2$ | $0$ |
| $\Xi_c^*K^*$ | $\sqrt{5}$ | $0$ | $\sqrt{\frac{5}{3}}$ | $2\sqrt{\frac{5}{3}}$ | $-\sqrt{\frac{10}{3}}$ | $\sqrt{\frac{5}{3}}$ | $-\frac{5}{\sqrt{3}}$ | $-\sqrt{\frac{10}{3}}$ | $-2\sqrt{\frac{5}{3}}$ | $0$ | $-2$ |

Table B.2: $C = 1$, $S = 0$, $I = 0$, $J = 3/2$.

| | $\Lambda_c\pi$ | $\Sigma_c\pi$ | $ND$ | $ND^*$ | $\Xi_cK$ | $\Sigma_c\eta$ | $\Lambda_c\rho$ | $\Xi_c'K$ | $\Sigma D_s$ | $\Delta D^*$ | $\Sigma_c\rho$ | $\Sigma_c\omega$ | $\Sigma_c^*\rho$ | $\Sigma_c^*\omega$ | $\Sigma D_s^*$ | $\Xi_cK^*$ | $\Sigma_c\eta'$ | $\Xi_c'K^*$ | $\Sigma_c\phi$ | $\Sigma^*D_s^*$ | $\Sigma_c^*\phi$ | $\Xi_c^*K^*$ |
|---|---|---|---|---|---|---|---|---|---|---|---|---|---|---|---|---|---|---|---|---|---|---|
| $\Lambda_c\pi$ | 0 | 0 | $\sqrt{\frac{3}{2}}$ | $-\frac{3}{\sqrt{2}}$ | 1 | 0 | 0 | 0 | 0 | 0 | $-2\sqrt{2}$ | 0 | 4 | 0 | 0 | 0 | 0 | $-1$ | 0 | 0 | 0 | $\sqrt{2}$ |
| $\Sigma_c\pi$ | 0 | $-2$ | 1 | $\frac{1}{\sqrt{3}}$ | 0 | 0 | $-2\sqrt{2}$ | $-\sqrt{2}$ | 0 | $2\sqrt{\frac{2}{3}}$ | $\frac{4}{\sqrt{3}}$ | 0 | $2\sqrt{\frac{2}{3}}$ | 0 | 0 | $\sqrt{2}$ | 0 | $2\sqrt{\frac{2}{3}}$ | 0 | 0 | 0 | $\frac{2}{\sqrt{3}}$ |
| $ND$ | $\sqrt{\frac{3}{2}}$ | 1 | $-1$ | $-\frac{1}{\sqrt{3}}$ | 0 | $\frac{1}{\sqrt{6}}$ | $-\frac{3}{\sqrt{2}}$ | 0 | 1 | $4\sqrt{\frac{2}{3}}$ | $\frac{1}{\sqrt{3}}$ | $\frac{1}{\sqrt{6}}$ | $2\sqrt{\frac{2}{3}}$ | $\frac{2}{\sqrt{3}}$ | $\frac{1}{\sqrt{3}}$ | 0 | $\frac{1}{\sqrt{3}}$ | 0 | 0 | $2\sqrt{\frac{2}{3}}$ | 0 | 0 |
| $ND^*$ | $-\frac{3}{\sqrt{2}}$ | $\frac{1}{\sqrt{3}}$ | $-\frac{1}{\sqrt{3}}$ | $-\frac{1}{3}$ | 0 | $\frac{1}{3\sqrt{2}}$ | $-\sqrt{\frac{3}{2}}$ | 0 | $\frac{1}{\sqrt{3}}$ | $\frac{4\sqrt{2}}{3}$ | $\frac{5}{3}$ | $\frac{5}{3\sqrt{2}}$ | $-\frac{2\sqrt{2}}{3}$ | $-\frac{2}{3}$ | $\frac{1}{3}$ | 0 | $\frac{1}{3}$ | 0 | 0 | $\frac{2\sqrt{2}}{3}$ | 0 | 0 |
| $\Xi_cK$ | 1 | 0 | 0 | 0 | 0 | 0 | 0 | 0 | $\sqrt{\frac{3}{2}}$ | 0 | $\sqrt{2}$ | $-1$ | $-2$ | $\sqrt{2}$ | $-\frac{3}{\sqrt{2}}$ | 0 | 0 | 2 | $-\sqrt{2}$ | 0 | 2 | $-2\sqrt{2}$ |
| $\Sigma_c\eta$ | 0 | 0 | $\frac{1}{\sqrt{6}}$ | $\frac{1}{3\sqrt{2}}$ | 0 | 0 | 0 | $\sqrt{3}$ | $\sqrt{\frac{2}{3}}$ | $-\frac{4}{3}$ | 0 | 0 | 0 | 0 | $\frac{\sqrt{2}}{3}$ | $-\sqrt{3}$ | 0 | $-2$ | 0 | $\frac{4}{3}$ | 0 | $-\sqrt{2}$ |
| $\Lambda_c\rho$ | 0 | $-2\sqrt{2}$ | $-\frac{3}{\sqrt{2}}$ | $-\sqrt{\frac{3}{2}}$ | 0 | 0 | 0 | $-1$ | 0 | 0 | 0 | $-\frac{4}{\sqrt{3}}$ | 0 | $-2\sqrt{\frac{2}{3}}$ | 0 | 1 | 0 | $\frac{2}{\sqrt{3}}$ | 0 | 0 | 0 | $\sqrt{\frac{2}{3}}$ |
| $\Xi_c'K$ | 0 | $-\sqrt{2}$ | 0 | 0 | 0 | $\sqrt{3}$ | $-1$ | 0 | $-\frac{1}{\sqrt{2}}$ | 0 | $2\sqrt{\frac{2}{3}}$ | $-\frac{2}{\sqrt{3}}$ | $\frac{2}{\sqrt{3}}$ | $-\sqrt{\frac{2}{3}}$ | $-\frac{1}{\sqrt{6}}$ | 2 | 0 | 0 | $-2\sqrt{\frac{2}{3}}$ | $\frac{4}{\sqrt{3}}$ | $-\frac{2}{\sqrt{3}}$ | 0 |
| $\Sigma D_s$ | 0 | 0 | 1 | $\frac{1}{\sqrt{3}}$ | $\sqrt{\frac{3}{2}}$ | $\sqrt{\frac{2}{3}}$ | 0 | $-\frac{1}{\sqrt{2}}$ | $-1$ | $-4\sqrt{\frac{2}{3}}$ | 0 | 0 | 0 | 0 | $-\frac{1}{\sqrt{3}}$ | $-\frac{3}{\sqrt{2}}$ | $-\frac{1}{\sqrt{3}}$ | $-\frac{1}{\sqrt{6}}$ | $\frac{1}{\sqrt{3}}$ | $-2\sqrt{\frac{2}{3}}$ | $2\sqrt{\frac{2}{3}}$ | $-\frac{2}{\sqrt{3}}$ |
| $\Delta D^*$ | 0 | $2\sqrt{\frac{2}{3}}$ | $4\sqrt{\frac{2}{3}}$ | $\frac{4\sqrt{2}}{3}$ | 0 | $-\frac{4}{3}$ | 0 | 0 | $-4\sqrt{\frac{2}{3}}$ | $-\frac{32}{3}$ | $-\frac{2\sqrt{2}}{3}$ | $\frac{4}{3}$ | $-\frac{2}{3}$ | $\frac{2\sqrt{2}}{3}$ | $-\frac{4\sqrt{2}}{3}$ | 0 | $-\frac{4\sqrt{2}}{3}$ | 0 | 0 | $-\frac{16}{3}$ | 0 | 0 |
| $\Sigma_c\rho$ | $-2\sqrt{2}$ | $\frac{4}{\sqrt{3}}$ | $\frac{1}{\sqrt{3}}$ | $\frac{5}{3}$ | $\sqrt{2}$ | 0 | 0 | $2\sqrt{\frac{2}{3}}$ | 0 | $-\frac{2\sqrt{2}}{3}$ | $-\frac{14}{3}$ | $\frac{8\sqrt{2}}{3}$ | $\frac{2\sqrt{2}}{3}$ | $-\frac{4}{3}$ | 0 | $-2\sqrt{\frac{2}{3}}$ | 0 | $-\frac{7\sqrt{2}}{3}$ | 0 | 0 | 0 | $\frac{2}{3}$ |
| $\Sigma_c\omega$ | 0 | 0 | $\frac{1}{\sqrt{6}}$ | $\frac{5}{3\sqrt{2}}$ | $-1$ | 0 | $-\frac{4}{\sqrt{3}}$ | $-\frac{2}{\sqrt{3}}$ | 0 | $\frac{4}{3}$ | $\frac{8\sqrt{2}}{3}$ | $-\frac{8}{3}$ | $-\frac{4}{3}$ | $\frac{2\sqrt{2}}{3}$ | 0 | $\frac{2}{\sqrt{3}}$ | 0 | $\frac{7}{3}$ | 0 | 0 | 0 | $-\frac{\sqrt{2}}{3}$ |
| $\Sigma_c^*\rho$ | 4 | $2\sqrt{\frac{2}{3}}$ | $2\sqrt{\frac{2}{3}}$ | $-\frac{2\sqrt{2}}{3}$ | $-2$ | 0 | 0 | $\frac{2}{\sqrt{3}}$ | 0 | $-\frac{2}{3}$ | $\frac{2\sqrt{2}}{3}$ | $-\frac{4}{3}$ | $-\frac{16}{3}$ | $\frac{10\sqrt{2}}{3}$ | 0 | $-\frac{2}{\sqrt{3}}$ | 0 | $\frac{2}{3}$ | 0 | 0 | 0 | $-\frac{8\sqrt{2}}{3}$ |
| $\Sigma_c^*\omega$ | 0 | 0 | $\frac{2}{\sqrt{3}}$ | $-\frac{2}{3}$ | $\sqrt{2}$ | 0 | $-2\sqrt{\frac{2}{3}}$ | $-\sqrt{\frac{2}{3}}$ | 0 | $\frac{2\sqrt{2}}{3}$ | $-\frac{4}{3}$ | $\frac{2\sqrt{2}}{3}$ | $\frac{10\sqrt{2}}{3}$ | $-\frac{10}{3}$ | 0 | $\sqrt{\frac{2}{3}}$ | 0 | $-\frac{\sqrt{2}}{3}$ | 0 | 0 | 0 | $\frac{8}{3}$ |
| $\Sigma D_s^*$ | 0 | 0 | $\frac{1}{\sqrt{3}}$ | $\frac{1}{3}$ | $-\frac{3}{\sqrt{2}}$ | $\frac{\sqrt{2}}{3}$ | 0 | $-\frac{1}{\sqrt{6}}$ | $-\frac{1}{\sqrt{3}}$ | $-\frac{4\sqrt{2}}{3}$ | 0 | 0 | 0 | 0 | $-\frac{1}{3}$ | $-\sqrt{\frac{3}{2}}$ | $-\frac{1}{3}$ | $-\frac{5}{3\sqrt{2}}$ | $\frac{5}{3}$ | $-\frac{2\sqrt{2}}{3}$ | $-\frac{2\sqrt{2}}{3}$ | $\frac{2}{3}$ |
| $\Xi_cK^*$ | 0 | $\sqrt{2}$ | 0 | 0 | 0 | $-\sqrt{3}$ | 1 | 2 | $-\frac{3}{\sqrt{2}}$ | 0 | $-2\sqrt{\frac{2}{3}}$ | $\frac{2}{\sqrt{3}}$ | $-\frac{2}{\sqrt{3}}$ | $\sqrt{\frac{2}{3}}$ | $-\sqrt{\frac{3}{2}}$ | 0 | 0 | 0 | $-2\sqrt{\frac{2}{3}}$ | 0 | $-\frac{2}{\sqrt{3}}$ | 0 |
| $\Sigma_c\eta'$ | 0 | 0 | $\frac{1}{\sqrt{3}}$ | $\frac{1}{3}$ | 0 | 0 | 0 | 0 | $-\frac{1}{\sqrt{3}}$ | $-\frac{4\sqrt{2}}{3}$ | 0 | 0 | 0 | 0 | $-\frac{1}{3}$ | 0 | 0 | 0 | 0 | $-\frac{2\sqrt{2}}{3}$ | 0 | 0 |
| $\Xi_c'K^*$ | $-1$ | $2\sqrt{\frac{2}{3}}$ | 0 | 0 | 2 | $-2$ | $\frac{2}{\sqrt{3}}$ | 0 | $-\frac{1}{\sqrt{6}}$ | 0 | $-\frac{7\sqrt{2}}{3}$ | $\frac{7}{3}$ | $\frac{2}{3}$ | $-\frac{\sqrt{2}}{3}$ | $-\frac{5}{3\sqrt{2}}$ | 0 | 0 | $-\frac{8}{3}$ | $-\frac{\sqrt{2}}{3}$ | $-\frac{4}{3}$ | $\frac{2}{3}$ | $\frac{2\sqrt{2}}{3}$ |
| $\Sigma_c\phi$ | 0 | 0 | 0 | 0 | $-\sqrt{2}$ | 0 | 0 | $-2\sqrt{\frac{2}{3}}$ | $\frac{1}{\sqrt{3}}$ | 0 | 0 | 0 | 0 | 0 | $\frac{5}{3}$ | $-2\sqrt{\frac{2}{3}}$ | 0 | $-\frac{\sqrt{2}}{3}$ | 0 | $-\frac{2\sqrt{2}}{3}$ | 0 | $\frac{2}{3}$ |
| $\Sigma^*D_s^*$ | 0 | 0 | $2\sqrt{\frac{2}{3}}$ | $\frac{2\sqrt{2}}{3}$ | 0 | $\frac{4}{3}$ | 0 | $\frac{4}{\sqrt{3}}$ | $-2\sqrt{\frac{2}{3}}$ | $-\frac{16}{3}$ | 0 | 0 | 0 | 0 | $-\frac{2\sqrt{2}}{3}$ | 0 | $-\frac{2\sqrt{2}}{3}$ | $-\frac{4}{3}$ | $-\frac{2\sqrt{2}}{3}$ | $-\frac{8}{3}$ | $-\frac{2}{3}$ | $-\frac{2\sqrt{2}}{3}$ |
| $\Sigma_c^*\phi$ | 0 | 0 | 0 | 0 | 2 | 0 | 0 | $-\frac{2}{\sqrt{3}}$ | $2\sqrt{\frac{2}{3}}$ | 0 | 0 | 0 | 0 | 0 | $-\frac{2\sqrt{2}}{3}$ | $-\frac{2}{\sqrt{3}}$ | 0 | $\frac{2}{3}$ | 0 | $-\frac{2}{3}$ | 0 | $-\frac{2\sqrt{2}}{3}$ |
| $\Xi_c^*K^*$ | $\sqrt{2}$ | $\frac{2}{\sqrt{3}}$ | 0 | 0 | $-2\sqrt{2}$ | $-\sqrt{2}$ | $\sqrt{\frac{2}{3}}$ | 0 | $-\frac{2}{\sqrt{3}}$ | 0 | $\frac{2}{3}$ | $-\frac{\sqrt{2}}{3}$ | $-\frac{8\sqrt{2}}{3}$ | $\frac{8}{3}$ | $\frac{2}{3}$ | 0 | 0 | $\frac{2\sqrt{2}}{3}$ | $\frac{2}{3}$ | $-\frac{2\sqrt{2}}{3}$ | $-\frac{2\sqrt{2}}{3}$ | $-\frac{10}{3}$ |

Table B.3: $C = 1$, $S = 0$, $I = 1$, $J = 1/2$.

| | $\Sigma_c^*\pi$ | $ND^*$ | $\Lambda_c\rho$ | $\Sigma_c^*\eta$ | $\Delta D$ | $\Xi_c^*K$ | $\Delta D^*$ | $\Sigma_c\rho$ | $\Sigma_c\omega$ | $\Sigma_c^*\rho$ | $\Sigma_c^*\omega$ | $\Sigma D_s^*$ | $\Sigma^*D_s$ | $\Xi_cK^*$ | $\Sigma_c^*\phi$ | $\Xi_c^*K^*$ | $\Xi_c'K^*$ | $\Sigma_c\phi$ | $\Sigma_c^*\eta'$ | $\Sigma^*D_s^*$ |
|---|---|---|---|---|---|---|---|---|---|---|---|---|---|---|---|---|---|---|---|---|
| $\Sigma_c^*\pi$ | $-2$ | $-\frac{2}{\sqrt{3}}$ | $-2\sqrt{2}$ | $0$ | $1$ | $-\sqrt{2}$ | $-\sqrt{\frac{5}{3}}$ | $-\frac{2}{\sqrt{3}}$ | $0$ | $2\sqrt{\frac{5}{3}}$ | $0$ | $0$ | $0$ | $\sqrt{2}$ | $0$ | $\sqrt{\frac{10}{3}}$ | $-\sqrt{\frac{2}{3}}$ | $0$ | $0$ | $0$ |
| $ND^*$ | $-\frac{2}{\sqrt{3}}$ | $-\frac{4}{3}$ | $\sqrt{6}$ | $-\frac{\sqrt{2}}{3}$ | $-\frac{4}{\sqrt{3}}$ | $0$ | $\frac{4\sqrt{5}}{3}$ | $\frac{2}{3}$ | $\frac{\sqrt{2}}{3}$ | $-\frac{2\sqrt{5}}{3}$ | $-\frac{\sqrt{10}}{3}$ | $\frac{4}{3}$ | $-\frac{2}{\sqrt{3}}$ | $0$ | $0$ | $0$ | $0$ | $0$ | $-\frac{2}{3}$ | $\frac{2\sqrt{5}}{3}$ |
| $\Lambda_c\rho$ | $-2\sqrt{2}$ | $\sqrt{6}$ | $0$ | $0$ | $0$ | $-1$ | $0$ | $0$ | $\frac{2}{\sqrt{3}}$ | $0$ | $-2\sqrt{\frac{5}{3}}$ | $0$ | $0$ | $1$ | $0$ | $\sqrt{\frac{5}{3}}$ | $-\frac{1}{\sqrt{3}}$ | $0$ | $0$ | $0$ |
| $\Sigma_c^*\eta$ | $0$ | $-\frac{\sqrt{2}}{3}$ | $0$ | $0$ | $-\sqrt{\frac{2}{3}}$ | $\sqrt{3}$ | $\frac{\sqrt{10}}{3}$ | $0$ | $0$ | $0$ | $0$ | $-\frac{2\sqrt{2}}{3}$ | $\sqrt{\frac{2}{3}}$ | $-\sqrt{3}$ | $0$ | $-\sqrt{5}$ | $1$ | $0$ | $0$ | $-\frac{\sqrt{10}}{3}$ |
| $\Delta D$ | $1$ | $-\frac{4}{\sqrt{3}}$ | $0$ | $-\sqrt{\frac{2}{3}}$ | $-4$ | $0$ | $4\sqrt{\frac{5}{3}}$ | $-\frac{2}{\sqrt{3}}$ | $2\sqrt{\frac{2}{3}}$ | $-\sqrt{\frac{5}{3}}$ | $\sqrt{\frac{10}{3}}$ | $\frac{4}{\sqrt{3}}$ | $-2$ | $0$ | $0$ | $0$ | $0$ | $0$ | $-\frac{2}{\sqrt{3}}$ | $2\sqrt{\frac{5}{3}}$ |
| $\Xi_c^*K$ | $-\sqrt{2}$ | $0$ | $-1$ | $\sqrt{3}$ | $0$ | $0$ | $0$ | $-\sqrt{\frac{2}{3}}$ | $\frac{1}{\sqrt{3}}$ | $\sqrt{\frac{10}{3}}$ | $-\sqrt{\frac{5}{3}}$ | $\sqrt{\frac{2}{3}}$ | $\sqrt{2}$ | $2$ | $-\sqrt{\frac{10}{3}}$ | $0$ | $0$ | $\sqrt{\frac{2}{3}}$ | $0$ | $-\sqrt{\frac{10}{3}}$ |
| $\Delta D^*$ | $-\sqrt{\frac{5}{3}}$ | $\frac{4\sqrt{5}}{3}$ | $0$ | $\frac{\sqrt{10}}{3}$ | $4\sqrt{\frac{5}{3}}$ | $0$ | $-\frac{20}{3}$ | $-\frac{2\sqrt{5}}{3}$ | $\frac{2\sqrt{10}}{3}$ | $\frac{1}{3}$ | $-\frac{\sqrt{2}}{3}$ | $-\frac{4\sqrt{5}}{3}$ | $2\sqrt{\frac{5}{3}}$ | $0$ | $0$ | $0$ | $0$ | $0$ | $\frac{2\sqrt{5}}{3}$ | $-\frac{10}{3}$ |
| $\Sigma_c\rho$ | $-\frac{2}{\sqrt{3}}$ | $\frac{2}{3}$ | $0$ | $0$ | $-\frac{2}{\sqrt{3}}$ | $-\sqrt{\frac{2}{3}}$ | $-\frac{2\sqrt{5}}{3}$ | $-\frac{2}{3}$ | $-\frac{4\sqrt{2}}{3}$ | $\frac{2\sqrt{5}}{3}$ | $-\frac{2\sqrt{10}}{3}$ | $0$ | $0$ | $\sqrt{\frac{2}{3}}$ | $0$ | $\frac{\sqrt{10}}{3}$ | $-\frac{\sqrt{2}}{3}$ | $0$ | $0$ | $0$ |
| $\Sigma_c\omega$ | $0$ | $\frac{\sqrt{2}}{3}$ | $\frac{2}{\sqrt{3}}$ | $0$ | $2\sqrt{\frac{2}{3}}$ | $\frac{1}{\sqrt{3}}$ | $\frac{2\sqrt{10}}{3}$ | $-\frac{4\sqrt{2}}{3}$ | $\frac{4}{3}$ | $-\frac{2\sqrt{10}}{3}$ | $\frac{2\sqrt{5}}{3}$ | $0$ | $0$ | $-\frac{1}{\sqrt{3}}$ | $0$ | $-\frac{\sqrt{5}}{3}$ | $\frac{1}{3}$ | $0$ | $0$ | $0$ |
| $\Sigma_c^*\rho$ | $2\sqrt{\frac{5}{3}}$ | $-\frac{2\sqrt{5}}{3}$ | $0$ | $0$ | $-\sqrt{\frac{5}{3}}$ | $\sqrt{\frac{10}{3}}$ | $\frac{1}{3}$ | $\frac{2\sqrt{5}}{3}$ | $-\frac{2\sqrt{10}}{3}$ | $-\frac{10}{3}$ | $\frac{4\sqrt{2}}{3}$ | $0$ | $0$ | $-\sqrt{\frac{10}{3}}$ | $0$ | $-\frac{5\sqrt{2}}{3}$ | $\frac{\sqrt{10}}{3}$ | $0$ | $0$ | $0$ |
| $\Sigma_c^*\omega$ | $0$ | $-\frac{\sqrt{10}}{3}$ | $-2\sqrt{\frac{5}{3}}$ | $0$ | $\sqrt{\frac{10}{3}}$ | $-\sqrt{\frac{5}{3}}$ | $-\frac{\sqrt{2}}{3}$ | $-\frac{2\sqrt{10}}{3}$ | $\frac{2\sqrt{5}}{3}$ | $\frac{4\sqrt{2}}{3}$ | $-\frac{4}{3}$ | $0$ | $0$ | $\sqrt{\frac{5}{3}}$ | $0$ | $\frac{5}{3}$ | $-\frac{\sqrt{5}}{3}$ | $0$ | $0$ | $0$ |
| $\Sigma D_s^*$ | $0$ | $\frac{4}{3}$ | $0$ | $-\frac{2\sqrt{2}}{3}$ | $\frac{4}{\sqrt{3}}$ | $\sqrt{\frac{2}{3}}$ | $-\frac{4\sqrt{5}}{3}$ | $0$ | $0$ | $0$ | $0$ | $-\frac{4}{3}$ | $\frac{2}{\sqrt{3}}$ | $\sqrt{6}$ | $-\frac{2\sqrt{5}}{3}$ | $\frac{\sqrt{10}}{3}$ | $-\frac{\sqrt{2}}{3}$ | $\frac{2}{3}$ | $\frac{2}{3}$ | $-\frac{2\sqrt{5}}{3}$ |
| $\Sigma^*D_s$ | $0$ | $-\frac{2}{\sqrt{3}}$ | $0$ | $\sqrt{\frac{2}{3}}$ | $-2$ | $\sqrt{2}$ | $2\sqrt{\frac{5}{3}}$ | $0$ | $0$ | $0$ | $0$ | $\frac{2}{\sqrt{3}}$ | $-1$ | $0$ | $-\sqrt{\frac{5}{3}}$ | $-\sqrt{\frac{10}{3}}$ | $-2\sqrt{\frac{2}{3}}$ | $-\frac{2}{\sqrt{3}}$ | $-\frac{1}{\sqrt{3}}$ | $\sqrt{\frac{5}{3}}$ |
| $\Xi_cK^*$ | $\sqrt{2}$ | $0$ | $1$ | $-\sqrt{3}$ | $0$ | $2$ | $0$ | $\sqrt{\frac{2}{3}}$ | $-\frac{1}{\sqrt{3}}$ | $-\sqrt{\frac{10}{3}}$ | $\sqrt{\frac{5}{3}}$ | $\sqrt{6}$ | $0$ | $0$ | $-\sqrt{\frac{10}{3}}$ | $0$ | $0$ | $\sqrt{\frac{2}{3}}$ | $0$ | $0$ |
| $\Sigma_c^*\phi$ | $0$ | $0$ | $0$ | $0$ | $0$ | $-\sqrt{\frac{10}{3}}$ | $0$ | $0$ | $0$ | $0$ | $0$ | $-\frac{2\sqrt{5}}{3}$ | $-\sqrt{\frac{5}{3}}$ | $-\sqrt{\frac{10}{3}}$ | $0$ | $\frac{\sqrt{2}}{3}$ | $\frac{\sqrt{10}}{3}$ | $0$ | $0$ | $\frac{1}{3}$ |
| $\Xi_c^*K^*$ | $\sqrt{\frac{10}{3}}$ | $0$ | $\sqrt{\frac{5}{3}}$ | $-\sqrt{5}$ | $0$ | $0$ | $0$ | $\frac{\sqrt{10}}{3}$ | $-\frac{\sqrt{5}}{3}$ | $-\frac{5\sqrt{2}}{3}$ | $\frac{5}{3}$ | $\frac{\sqrt{10}}{3}$ | $-\sqrt{\frac{10}{3}}$ | $0$ | $\frac{\sqrt{2}}{3}$ | $-\frac{4}{3}$ | $\frac{2\sqrt{5}}{3}$ | $\frac{\sqrt{10}}{3}$ | $0$ | $\frac{\sqrt{2}}{3}$ |
| $\Xi_c'K^*$ | $-\sqrt{\frac{2}{3}}$ | $0$ | $-\frac{1}{\sqrt{3}}$ | $1$ | $0$ | $0$ | $0$ | $-\frac{\sqrt{2}}{3}$ | $\frac{1}{3}$ | $\frac{\sqrt{10}}{3}$ | $-\frac{\sqrt{5}}{3}$ | $-\frac{\sqrt{2}}{3}$ | $-2\sqrt{\frac{2}{3}}$ | $0$ | $\frac{\sqrt{10}}{3}$ | $\frac{2\sqrt{5}}{3}$ | $\frac{4}{3}$ | $\frac{5\sqrt{2}}{3}$ | $0$ | $-\frac{2\sqrt{10}}{3}$ |
| $\Sigma_c\phi$ | $0$ | $0$ | $0$ | $0$ | $0$ | $\sqrt{\frac{2}{3}}$ | $0$ | $0$ | $0$ | $0$ | $0$ | $\frac{2}{3}$ | $-\frac{2}{\sqrt{3}}$ | $\sqrt{\frac{2}{3}}$ | $0$ | $\frac{\sqrt{10}}{3}$ | $\frac{5\sqrt{2}}{3}$ | $0$ | $0$ | $-\frac{2\sqrt{5}}{3}$ |
| $\Sigma_c^*\eta'$ | $0$ | $-\frac{2}{3}$ | $0$ | $0$ | $-\frac{2}{\sqrt{3}}$ | $0$ | $\frac{2\sqrt{5}}{3}$ | $0$ | $0$ | $0$ | $0$ | $\frac{2}{3}$ | $-\frac{1}{\sqrt{3}}$ | $0$ | $0$ | $0$ | $0$ | $0$ | $0$ | $\frac{\sqrt{5}}{3}$ |
| $\Sigma^*D_s^*$ | $0$ | $\frac{2\sqrt{5}}{3}$ | $0$ | $-\frac{\sqrt{10}}{3}$ | $2\sqrt{\frac{5}{3}}$ | $-\sqrt{\frac{10}{3}}$ | $-\frac{10}{3}$ | $0$ | $0$ | $0$ | $0$ | $-\frac{2\sqrt{5}}{3}$ | $\sqrt{\frac{5}{3}}$ | $0$ | $\frac{1}{3}$ | $\frac{\sqrt{2}}{3}$ | $-\frac{2\sqrt{10}}{3}$ | $-\frac{2\sqrt{5}}{3}$ | $\frac{\sqrt{5}}{3}$ | $-\frac{5}{3}$ |

Table B.4: $C = 1$, $S = 0$, $I = 1$, $J = 3/2$.

| | $\Xi_c\pi$ | $\Xi_c'\pi$ | $\Lambda_c\bar{K}$ | $\Sigma_c\bar{K}$ | $\Lambda D$ | $\Xi_c\eta$ | $\Sigma D$ | $\Lambda D^*$ | $\Xi_c'\eta$ | $\Lambda_c\bar{K}^*$ | $\Omega_c K$ | $\Sigma D^*$ | $\Xi_c\rho$ | $\Xi_c\omega$ | $\Xi D_s$ | $\Sigma_c\bar{K}^*$ |
|---|---|---|---|---|---|---|---|---|---|---|---|---|---|---|---|---|
| $\Xi_c\pi$ | $-2$ | $0$ | $\sqrt{\frac{3}{2}}$ | $0$ | $\frac{\sqrt{\frac{3}{2}}}{2}$ | $0$ | $\frac{\sqrt{\frac{3}{2}}}{2}$ | $-\frac{3}{2\sqrt{2}}$ | $0$ | $0$ | $0$ | $-\frac{3}{2\sqrt{2}}$ | $0$ | $0$ | $0$ | $-\frac{1}{\sqrt{2}}$ |
| $\Xi_c'\pi$ | $0$ | $-2$ | $0$ | $\frac{1}{\sqrt{2}}$ | $\frac{3}{2\sqrt{2}}$ | $0$ | $-\frac{1}{2\sqrt{2}}$ | $\frac{\sqrt{\frac{3}{2}}}{2}$ | $0$ | $-\sqrt{\frac{3}{2}}$ | $-\sqrt{3}$ | $-\frac{1}{2\sqrt{6}}$ | $-2$ | $0$ | $0$ | $-\sqrt{\frac{2}{3}}$ |
| $\Lambda_c\bar{K}$ | $\sqrt{\frac{3}{2}}$ | $0$ | $-1$ | $0$ | $1$ | $\sqrt{\frac{3}{2}}$ | $0$ | $-\sqrt{3}$ | $0$ | $0$ | $0$ | $0$ | $0$ | $0$ | $0$ | $-\sqrt{3}$ |
| $\Sigma_c\bar{K}$ | $0$ | $\frac{1}{\sqrt{2}}$ | $0$ | $-3$ | $0$ | $0$ | $1$ | $0$ | $-\frac{3}{\sqrt{2}}$ | $-\sqrt{3}$ | $0$ | $\frac{1}{\sqrt{3}}$ | $-\frac{1}{\sqrt{2}}$ | $\sqrt{\frac{3}{2}}$ | $0$ | $2\sqrt{3}$ |
| $\Lambda D$ | $\frac{\sqrt{\frac{3}{2}}}{2}$ | $\frac{3}{2\sqrt{2}}$ | $1$ | $0$ | $-1$ | $\frac{1}{2\sqrt{6}}$ | $0$ | $0$ | $\frac{1}{2\sqrt{2}}$ | $-\sqrt{3}$ | $0$ | $-\sqrt{3}$ | $-\frac{3}{2\sqrt{2}}$ | $-\frac{\sqrt{\frac{3}{2}}}{2}$ | $\sqrt{\frac{3}{2}}$ | $0$ |
| $\Xi_c\eta$ | $0$ | $0$ | $\sqrt{\frac{3}{2}}$ | $0$ | $\frac{1}{2\sqrt{6}}$ | $0$ | $-\frac{\sqrt{\frac{3}{2}}}{2}$ | $-\frac{1}{2\sqrt{2}}$ | $0$ | $0$ | $0$ | $\frac{3}{2\sqrt{2}}$ | $0$ | $0$ | $1$ | $\frac{3}{\sqrt{2}}$ |
| $\Sigma D$ | $\frac{\sqrt{\frac{3}{2}}}{2}$ | $-\frac{1}{2\sqrt{2}}$ | $0$ | $1$ | $0$ | $-\frac{\sqrt{\frac{3}{2}}}{2}$ | $-3$ | $-\sqrt{3}$ | $\frac{1}{2\sqrt{2}}$ | $0$ | $0$ | $2\sqrt{3}$ | $-\frac{3}{2\sqrt{2}}$ | $\frac{3\sqrt{\frac{3}{2}}}{2}$ | $-\sqrt{\frac{3}{2}}$ | $\frac{1}{\sqrt{3}}$ |
| $\Lambda D^*$ | $-\frac{3}{2\sqrt{2}}$ | $\frac{\sqrt{\frac{3}{2}}}{2}$ | $-\sqrt{3}$ | $0$ | $0$ | $-\frac{1}{2\sqrt{2}}$ | $-\sqrt{3}$ | $-1$ | $\frac{1}{2\sqrt{6}}$ | $-1$ | $0$ | $2$ | $-\frac{\sqrt{\frac{3}{2}}}{2}$ | $-\frac{1}{2\sqrt{2}}$ | $-\frac{1}{\sqrt{2}}$ | $0$ |
| $\Xi_c'\eta$ | $0$ | $0$ | $0$ | $-\frac{3}{\sqrt{2}}$ | $\frac{1}{2\sqrt{2}}$ | $0$ | $\frac{1}{2\sqrt{2}}$ | $\frac{1}{2\sqrt{6}}$ | $0$ | $-\sqrt{\frac{3}{2}}$ | $\sqrt{3}$ | $\frac{1}{2\sqrt{6}}$ | $0$ | $0$ | $\frac{1}{\sqrt{3}}$ | $\sqrt{6}$ |
| $\Lambda_c\bar{K}^*$ | $0$ | $-\sqrt{\frac{3}{2}}$ | $0$ | $-\sqrt{3}$ | $-\sqrt{3}$ | $0$ | $0$ | $-1$ | $-\sqrt{\frac{3}{2}}$ | $-1$ | $0$ | $0$ | $\sqrt{\frac{3}{2}}$ | $\frac{1}{\sqrt{2}}$ | $0$ | $2$ |
| $\Omega_c K$ | $0$ | $-\sqrt{3}$ | $0$ | $0$ | $0$ | $0$ | $0$ | $0$ | $\sqrt{3}$ | $0$ | $-2$ | $0$ | $-\sqrt{3}$ | $1$ | $-1$ | $0$ |
| $\Sigma D^*$ | $-\frac{3}{2\sqrt{2}}$ | $-\frac{1}{2\sqrt{6}}$ | $0$ | $\frac{1}{\sqrt{3}}$ | $-\sqrt{3}$ | $\frac{3}{2\sqrt{2}}$ | $2\sqrt{3}$ | $2$ | $\frac{1}{2\sqrt{6}}$ | $0$ | $0$ | $-7$ | $-\frac{\sqrt{\frac{3}{2}}}{2}$ | $\frac{3}{2\sqrt{2}}$ | $\frac{5}{\sqrt{2}}$ | $\frac{5}{3}$ |
| $\Xi_c\rho$ | $0$ | $-2$ | $0$ | $-\frac{1}{\sqrt{2}}$ | $-\frac{3}{2\sqrt{2}}$ | $0$ | $-\frac{3}{2\sqrt{2}}$ | $-\frac{\sqrt{\frac{3}{2}}}{2}$ | $0$ | $\sqrt{\frac{3}{2}}$ | $-\sqrt{3}$ | $-\frac{\sqrt{\frac{3}{2}}}{2}$ | $-2$ | $0$ | $0$ | $-\sqrt{\frac{2}{3}}$ |
| $\Xi_c\omega$ | $0$ | $0$ | $0$ | $\sqrt{\frac{3}{2}}$ | $-\frac{\sqrt{\frac{3}{2}}}{2}$ | $0$ | $\frac{3\sqrt{\frac{3}{2}}}{2}$ | $-\frac{1}{2\sqrt{2}}$ | $0$ | $\frac{1}{\sqrt{2}}$ | $1$ | $\frac{3}{2\sqrt{2}}$ | $0$ | $0$ | $0$ | $\sqrt{2}$ |
| $\Xi D_s$ | $0$ | $0$ | $0$ | $0$ | $\sqrt{\frac{3}{2}}$ | $1$ | $-\sqrt{\frac{3}{2}}$ | $-\frac{1}{\sqrt{2}}$ | $\frac{1}{\sqrt{3}}$ | $0$ | $-1$ | $\frac{5}{\sqrt{2}}$ | $0$ | $0$ | $-2$ | $0$ |
| $\Sigma_c\bar{K}^*$ | $-\frac{1}{\sqrt{2}}$ | $-\sqrt{\frac{2}{3}}$ | $-\sqrt{3}$ | $2\sqrt{3}$ | $0$ | $\frac{3}{\sqrt{2}}$ | $\frac{1}{\sqrt{3}}$ | $0$ | $\sqrt{6}$ | $2$ | $0$ | $\frac{5}{3}$ | $-\sqrt{\frac{2}{3}}$ | $\sqrt{2}$ | $0$ | $-7$ |

Table B.5: $C = 1$, $S = -1$, $I = 1/2$, $J = 1/2$.

| | $\Xi_c'\rho$ | $\Xi_c'\omega$ | $\Sigma^* D^*$ | $\Sigma_c^*\bar{K}^*$ | $\Xi_c^*\rho$ | $\Xi_c\eta'$ | $\Xi_c^*\omega$ | $\Xi D_s^*$ | $\Xi_c\phi$ | $\Xi_c'\eta'$ | $\Omega_c K^*$ | $\Xi_c'\phi$ | $\Xi^* D_s^*$ | $\Omega_c^* K^*$ | $\Xi_c^*\phi$ |
|---|---|---|---|---|---|---|---|---|---|---|---|---|---|---|---|
| $\Xi_c\pi$ | $-2$ | $0$ | $0$ | $1$ | $2\sqrt{2}$ | $0$ | $0$ | $0$ | $0$ | $0$ | $-\sqrt{3}$ | $0$ | $0$ | $\sqrt{6}$ | $0$ |
| $\Xi_c'\pi$ | $\frac{4}{\sqrt{3}}$ | $0$ | $\frac{2}{\sqrt{3}}$ | $-\frac{1}{\sqrt{3}}$ | $2\sqrt{\frac{2}{3}}$ | $0$ | $0$ | $0$ | $0$ | $0$ | $2$ | $0$ | $0$ | $\sqrt{2}$ | $0$ |
| $\Lambda_c\bar{K}$ | $-\sqrt{\frac{3}{2}}$ | $-\frac{1}{\sqrt{2}}$ | $0$ | $\sqrt{6}$ | $\sqrt{3}$ | $0$ | $1$ | $0$ | $0$ | $0$ | $0$ | $-1$ | $0$ | $0$ | $\sqrt{2}$ |
| $\Sigma_c\bar{K}$ | $-\sqrt{\frac{2}{3}}$ | $\sqrt{2}$ | $2\sqrt{\frac{2}{3}}$ | $\sqrt{6}$ | $-\frac{1}{\sqrt{3}}$ | $0$ | $1$ | $0$ | $\sqrt{3}$ | $0$ | $0$ | $2$ | $0$ | $0$ | $\sqrt{2}$ |
| $\Lambda D$ | $\frac{\sqrt{\frac{3}{2}}}{2}$ | $\frac{1}{2\sqrt{2}}$ | $\sqrt{6}$ | $0$ | $\sqrt{3}$ | $\frac{1}{2\sqrt{3}}$ | $1$ | $-\frac{1}{\sqrt{2}}$ | $0$ | $\frac{1}{2}$ | $0$ | $0$ | $2$ | $0$ | $0$ |
| $\Xi_c\eta$ | $0$ | $0$ | $0$ | $-3$ | $0$ | $0$ | $0$ | $-\sqrt{3}$ | $0$ | $0$ | $\sqrt{3}$ | $0$ | $0$ | $-\sqrt{6}$ | $0$ |
| $\Sigma D$ | $-\frac{1}{2\sqrt{6}}$ | $\frac{1}{2\sqrt{2}}$ | $\sqrt{6}$ | $2\sqrt{\frac{2}{3}}$ | $-\frac{1}{\sqrt{3}}$ | $-\frac{\sqrt{3}}{2}$ | $1$ | $\frac{5}{\sqrt{2}}$ | $0$ | $\frac{1}{2}$ | $0$ | $0$ | $2$ | $0$ | $0$ |
| $\Lambda D^*$ | $\frac{5}{2\sqrt{2}}$ | $\frac{5}{2\sqrt{6}}$ | $\sqrt{2}$ | $0$ | $-1$ | $-\frac{1}{2}$ | $-\frac{1}{\sqrt{3}}$ | $\frac{5}{\sqrt{6}}$ | $0$ | $\frac{1}{2\sqrt{3}}$ | $0$ | $0$ | $\frac{2}{\sqrt{3}}$ | $0$ | $0$ |
| $\Xi_c'\eta$ | $0$ | $0$ | $-\frac{2}{\sqrt{3}}$ | $\sqrt{3}$ | $0$ | $0$ | $0$ | $\frac{1}{3}$ | $0$ | $0$ | $-2$ | $0$ | $\frac{4\sqrt{2}}{3}$ | $-\sqrt{2}$ | $0$ |
| $\Lambda_c\bar{K}^*$ | $-\sqrt{2}$ | $-\sqrt{\frac{2}{3}}$ | $0$ | $\sqrt{2}$ | $-1$ | $0$ | $-\frac{1}{\sqrt{3}}$ | $0$ | $1$ | $0$ | $0$ | $\frac{2}{\sqrt{3}}$ | $0$ | $0$ | $\sqrt{\frac{2}{3}}$ |
| $\Omega_c K$ | $2$ | $-\frac{2}{\sqrt{3}}$ | $0$ | $0$ | $\sqrt{2}$ | $0$ | $-\sqrt{\frac{2}{3}}$ | $-\frac{1}{\sqrt{3}}$ | $\sqrt{2}$ | $0$ | $\frac{4}{\sqrt{3}}$ | $-2\sqrt{\frac{2}{3}}$ | $2\sqrt{\frac{2}{3}}$ | $2\sqrt{\frac{2}{3}}$ | $-\frac{2}{\sqrt{3}}$ |
| $\Sigma D^*$ | $-\frac{5}{6\sqrt{2}}$ | $\frac{5}{2\sqrt{6}}$ | $\sqrt{2}$ | $-\frac{2\sqrt{2}}{3}$ | $\frac{1}{3}$ | $\frac{3}{2}$ | $-\frac{1}{\sqrt{3}}$ | $-\frac{13}{\sqrt{6}}$ | $0$ | $\frac{1}{2\sqrt{3}}$ | $0$ | $0$ | $\frac{2}{\sqrt{3}}$ | $0$ | $0$ |
| $\Xi_c\rho$ | $\frac{2}{\sqrt{3}}$ | $-2$ | $0$ | $-\frac{1}{\sqrt{3}}$ | $\sqrt{\frac{2}{3}}$ | $0$ | $-\sqrt{2}$ | $0$ | $0$ | $0$ | $2$ | $0$ | $0$ | $\sqrt{2}$ | $0$ |
| $\Xi_c\omega$ | $-2$ | $\frac{2}{\sqrt{3}}$ | $0$ | $1$ | $-\sqrt{2}$ | $0$ | $\sqrt{\frac{2}{3}}$ | $0$ | $0$ | $0$ | $-\frac{2}{\sqrt{3}}$ | $0$ | $0$ | $-\sqrt{\frac{2}{3}}$ | $0$ |
| $\Xi D_s$ | $0$ | $0$ | $-2$ | $0$ | $0$ | $-\frac{1}{\sqrt{2}}$ | $0$ | $\frac{4}{\sqrt{3}}$ | $-\frac{3}{\sqrt{2}}$ | $-\frac{1}{\sqrt{6}}$ | $-\frac{1}{\sqrt{3}}$ | $\frac{1}{\sqrt{6}}$ | $-2\sqrt{\frac{2}{3}}$ | $-2\sqrt{\frac{2}{3}}$ | $\frac{2}{\sqrt{3}}$ |
| $\Sigma_c\bar{K}^*$ | $-\frac{1}{3\sqrt{2}}$ | $\frac{1}{\sqrt{6}}$ | $-\frac{2\sqrt{2}}{3}$ | $\sqrt{2}$ | $\frac{1}{3}$ | $0$ | $-\frac{1}{\sqrt{3}}$ | $0$ | $-2$ | $0$ | $0$ | $-\frac{7}{\sqrt{3}}$ | $0$ | $0$ | $\sqrt{\frac{2}{3}}$ |

Table B.6: $C = 1$, $S = -1$, $I = 1/2$, $J = 1/2$ (continued).

| | $\Xi_c'\rho$ | $\Xi_c'\omega$ | $\Sigma^* D^*$ | $\Sigma_c^*\bar{K}^*$ | $\Xi_c^*\rho$ | $\Xi_c\eta'$ | $\Xi_c^*\omega$ | $\Xi D_s^*$ | $\Xi_c\phi$ | $\Xi_c'\eta'$ | $\Omega_c K^*$ | $\Xi_c'\phi$ | $\Xi^* D_s^*$ | $\Omega_c^* K^*$ | $\Xi_c^*\phi$ |
|---|---|---|---|---|---|---|---|---|---|---|---|---|---|---|---|
| $\Xi_c'\rho$ | $-\frac{10}{3}$ | $\frac{4}{\sqrt{3}}$ | $-\frac{2}{3}$ | $\frac{1}{3}$ | $\frac{\sqrt{2}}{3}$ | 0 | $-\sqrt{\frac{2}{3}}$ | 0 | 0 | 0 | $-\frac{7}{\sqrt{3}}$ | 0 | 0 | $\sqrt{\frac{2}{3}}$ | 0 |
| $\Xi_c'\omega$ | $\frac{4}{\sqrt{3}}$ | $-\frac{4}{3}$ | $\frac{2}{\sqrt{3}}$ | $-\frac{1}{\sqrt{3}}$ | $-\sqrt{\frac{2}{3}}$ | 0 | $\frac{\sqrt{2}}{3}$ | 0 | 0 | 0 | $\frac{7}{3}$ | 0 | 0 | $-\frac{\sqrt{2}}{3}$ | 0 |
| $\Sigma^* D^*$ | $-\frac{2}{3}$ | $\frac{2}{\sqrt{3}}$ | $-8$ | $-\frac{2}{3}$ | $-\frac{\sqrt{2}}{3}$ | 0 | $\sqrt{\frac{2}{3}}$ | $-\frac{2}{\sqrt{3}}$ | 0 | $-2\sqrt{\frac{2}{3}}$ | 0 | 0 | $-8\sqrt{\frac{2}{3}}$ | 0 | 0 |
| $\Sigma_c^*\bar{K}^*$ | $\frac{1}{3}$ | $-\frac{1}{\sqrt{3}}$ | $-\frac{2}{3}$ | $-8$ | $-\frac{\sqrt{2}}{3}$ | 0 | $\sqrt{\frac{2}{3}}$ | 0 | $-\sqrt{2}$ | 0 | 0 | $\sqrt{\frac{2}{3}}$ | 0 | 0 | $-\frac{8}{\sqrt{3}}$ |
| $\Xi_c^*\rho$ | $\frac{\sqrt{2}}{3}$ | $-\sqrt{\frac{2}{3}}$ | $-\frac{\sqrt{2}}{3}$ | $-\frac{\sqrt{2}}{3}$ | $-\frac{11}{3}$ | 0 | $\frac{5}{\sqrt{3}}$ | 0 | 0 | 0 | $\sqrt{\frac{2}{3}}$ | 0 | 0 | $-\frac{8}{\sqrt{3}}$ | 0 |
| $\Xi_c\eta'$ | 0 | 0 | 0 | 0 | 0 | 0 | 0 | $\sqrt{\frac{3}{2}}$ | 0 | 0 | 0 | 0 | 0 | 0 | 0 |
| $\Xi_c^*\omega$ | $-\sqrt{\frac{2}{3}}$ | $\frac{\sqrt{2}}{3}$ | $\sqrt{\frac{2}{3}}$ | $\sqrt{\frac{2}{3}}$ | $\frac{5}{\sqrt{3}}$ | 0 | $-\frac{5}{3}$ | 0 | 0 | 0 | $-\frac{\sqrt{2}}{3}$ | 0 | 0 | $\frac{8}{3}$ | 0 |
| $\Xi D_s^*$ | 0 | 0 | $-\frac{2}{\sqrt{3}}$ | 0 | 0 | $\sqrt{\frac{3}{2}}$ | 0 | $-\frac{14}{3}$ | $-\sqrt{\frac{3}{2}}$ | $-\frac{1}{3\sqrt{2}}$ | $-\frac{5}{3}$ | $\frac{5}{3\sqrt{2}}$ | $-\frac{2\sqrt{2}}{3}$ | $\frac{2\sqrt{2}}{3}$ | $-\frac{2}{3}$ |
| $\Xi_c\phi$ | 0 | 0 | 0 | $-\sqrt{2}$ | 0 | 0 | 0 | $-\sqrt{\frac{3}{2}}$ | 0 | 0 | $2\sqrt{\frac{2}{3}}$ | $-\frac{4}{\sqrt{3}}$ | 0 | $\frac{2}{\sqrt{3}}$ | $-2\sqrt{\frac{2}{3}}$ |
| $\Xi_c'\eta'$ | 0 | 0 | $-2\sqrt{\frac{2}{3}}$ | 0 | 0 | 0 | 0 | $-\frac{1}{3\sqrt{2}}$ | 0 | 0 | 0 | 0 | $-\frac{4}{3}$ | 0 | 0 |
| $\Omega_c K^*$ | $-\frac{7}{\sqrt{3}}$ | $\frac{7}{3}$ | 0 | 0 | $\sqrt{\frac{2}{3}}$ | 0 | $-\frac{\sqrt{2}}{3}$ | $-\frac{5}{3}$ | $2\sqrt{\frac{2}{3}}$ | 0 | $-\frac{14}{3}$ | $-\frac{\sqrt{2}}{3}$ | $-\frac{2\sqrt{2}}{3}$ | $\frac{2\sqrt{2}}{3}$ | $\frac{2}{3}$ |
| $\Xi_c'\phi$ | 0 | 0 | 0 | $\sqrt{\frac{2}{3}}$ | 0 | 0 | 0 | $\frac{5}{3\sqrt{2}}$ | $-\frac{4}{\sqrt{3}}$ | 0 | $-\frac{\sqrt{2}}{3}$ | $-\frac{8}{3}$ | $-\frac{4}{3}$ | $\frac{2}{3}$ | $\frac{2\sqrt{2}}{3}$ |
| $\Xi^* D_s^*$ | 0 | 0 | $-8\sqrt{\frac{2}{3}}$ | 0 | 0 | 0 | 0 | $-\frac{2\sqrt{2}}{3}$ | 0 | $-\frac{4}{3}$ | $-\frac{2\sqrt{2}}{3}$ | $-\frac{4}{3}$ | $-\frac{16}{3}$ | $-\frac{2}{3}$ | $-\frac{2\sqrt{2}}{3}$ |
| $\Omega_c^* K^*$ | $\sqrt{\frac{2}{3}}$ | $-\frac{\sqrt{2}}{3}$ | 0 | 0 | $-\frac{8}{\sqrt{3}}$ | 0 | $\frac{8}{3}$ | $\frac{2\sqrt{2}}{3}$ | $\frac{2}{\sqrt{3}}$ | 0 | $\frac{2\sqrt{2}}{3}$ | $\frac{2}{3}$ | $-\frac{2}{3}$ | $-\frac{16}{3}$ | $-\frac{2\sqrt{2}}{3}$ |
| $\Xi_c^*\phi$ | 0 | 0 | 0 | $-\frac{8}{\sqrt{3}}$ | 0 | 0 | 0 | $-\frac{2}{3}$ | $-2\sqrt{\frac{2}{3}}$ | 0 | $\frac{2}{3}$ | $\frac{2\sqrt{2}}{3}$ | $-\frac{2\sqrt{2}}{3}$ | $-\frac{2\sqrt{2}}{3}$ | $-\frac{10}{3}$ |

Table B.7: $C = 1$, $S = -1$, $I = 1/2$, $J = 1/2$ (continued).

| | $\Xi_c^*\pi$ | $\Sigma_c^*\bar{K}$ | $\Lambda D^*$ | $\Lambda_c\bar{K}^*$ | $\Xi_c^*\eta$ | $\Sigma D^*$ | $\Xi_c\rho$ | $\Sigma^* D$ | $\Xi_c\omega$ | $\Omega_c^* K$ | $\Sigma_c\bar{K}^*$ | $\Xi_c'\rho$ | $\Xi_c'\omega$ |
|---|---|---|---|---|---|---|---|---|---|---|---|---|---|
| $\Xi_c^*\pi$ | $-2$ | $\frac{1}{\sqrt{2}}$ | $-\sqrt{\frac{3}{2}}$ | $-\sqrt{\frac{3}{2}}$ | $0$ | $\frac{1}{\sqrt{6}}$ | $-2$ | $\frac{1}{\sqrt{2}}$ | $0$ | $-\sqrt{3}$ | $\frac{1}{\sqrt{6}}$ | $-\frac{2}{\sqrt{3}}$ | $0$ |
| $\Sigma_c^*\bar{K}$ | $\frac{1}{\sqrt{2}}$ | $-3$ | $0$ | $-\sqrt{3}$ | $-\frac{3}{\sqrt{2}}$ | $-\frac{2}{\sqrt{3}}$ | $-\frac{1}{\sqrt{2}}$ | $1$ | $\sqrt{\frac{3}{2}}$ | $0$ | $-\sqrt{3}$ | $\frac{1}{\sqrt{6}}$ | $-\frac{1}{\sqrt{2}}$ |
| $\Lambda D^*$ | $-\sqrt{\frac{3}{2}}$ | $0$ | $-1$ | $2$ | $-\frac{1}{\sqrt{6}}$ | $-1$ | $\sqrt{\frac{3}{2}}$ | $-\sqrt{3}$ | $\frac{1}{\sqrt{2}}$ | $0$ | $0$ | $\frac{1}{\sqrt{2}}$ | $\frac{1}{\sqrt{6}}$ |
| $\Lambda_c\bar{K}^*$ | $-\sqrt{\frac{3}{2}}$ | $-\sqrt{3}$ | $2$ | $-1$ | $-\sqrt{\frac{3}{2}}$ | $0$ | $\sqrt{\frac{3}{2}}$ | $0$ | $\frac{1}{\sqrt{2}}$ | $0$ | $-1$ | $\frac{1}{\sqrt{2}}$ | $\frac{1}{\sqrt{6}}$ |
| $\Xi_c^*\eta$ | $0$ | $-\frac{3}{\sqrt{2}}$ | $-\frac{1}{\sqrt{6}}$ | $-\sqrt{\frac{3}{2}}$ | $0$ | $-\frac{1}{\sqrt{6}}$ | $0$ | $-\frac{1}{\sqrt{2}}$ | $0$ | $\sqrt{3}$ | $-\sqrt{\frac{3}{2}}$ | $0$ | $0$ |
| $\Sigma D^*$ | $\frac{1}{\sqrt{6}}$ | $-\frac{2}{\sqrt{3}}$ | $-1$ | $0$ | $-\frac{1}{\sqrt{6}}$ | $-1$ | $\sqrt{\frac{3}{2}}$ | $-\sqrt{3}$ | $-\frac{3}{\sqrt{2}}$ | $0$ | $\frac{2}{3}$ | $-\frac{1}{3\sqrt{2}}$ | $\frac{1}{\sqrt{6}}$ |
| $\Xi_c\rho$ | $-2$ | $-\frac{1}{\sqrt{2}}$ | $\sqrt{\frac{3}{2}}$ | $\sqrt{\frac{3}{2}}$ | $0$ | $\sqrt{\frac{3}{2}}$ | $-2$ | $0$ | $0$ | $-\sqrt{3}$ | $\frac{1}{\sqrt{6}}$ | $-\frac{1}{\sqrt{3}}$ | $1$ |
| $\Sigma^* D$ | $\frac{1}{\sqrt{2}}$ | $1$ | $-\sqrt{3}$ | $0$ | $-\frac{1}{\sqrt{2}}$ | $-\sqrt{3}$ | $0$ | $-3$ | $0$ | $0$ | $-\frac{2}{\sqrt{3}}$ | $-\sqrt{\frac{2}{3}}$ | $\sqrt{2}$ |
| $\Xi_c\omega$ | $0$ | $\sqrt{\frac{3}{2}}$ | $\frac{1}{\sqrt{2}}$ | $\frac{1}{\sqrt{2}}$ | $0$ | $-\frac{3}{\sqrt{2}}$ | $0$ | $0$ | $0$ | $1$ | $-\frac{1}{\sqrt{2}}$ | $1$ | $-\frac{1}{\sqrt{3}}$ |
| $\Omega_c^* K$ | $-\sqrt{3}$ | $0$ | $0$ | $0$ | $\sqrt{3}$ | $0$ | $-\sqrt{3}$ | $0$ | $1$ | $-2$ | $0$ | $-1$ | $\frac{1}{\sqrt{3}}$ |
| $\Sigma_c\bar{K}^*$ | $\frac{1}{\sqrt{6}}$ | $-\sqrt{3}$ | $0$ | $-1$ | $-\sqrt{\frac{3}{2}}$ | $\frac{2}{3}$ | $\frac{1}{\sqrt{6}}$ | $-\frac{2}{\sqrt{3}}$ | $-\frac{1}{\sqrt{2}}$ | $0$ | $-1$ | $\frac{5}{3\sqrt{2}}$ | $-\frac{5}{\sqrt{6}}$ |
| $\Xi_c'\rho$ | $-\frac{2}{\sqrt{3}}$ | $\frac{1}{\sqrt{6}}$ | $\frac{1}{\sqrt{2}}$ | $\frac{1}{\sqrt{2}}$ | $0$ | $-\frac{1}{3\sqrt{2}}$ | $-\frac{1}{\sqrt{3}}$ | $-\sqrt{\frac{2}{3}}$ | $1$ | $-1$ | $\frac{5}{3\sqrt{2}}$ | $-\frac{4}{3}$ | $-\frac{2}{\sqrt{3}}$ |
| $\Xi_c'\omega$ | $0$ | $-\frac{1}{\sqrt{2}}$ | $\frac{1}{\sqrt{6}}$ | $\frac{1}{\sqrt{6}}$ | $0$ | $\frac{1}{\sqrt{6}}$ | $1$ | $\sqrt{2}$ | $-\frac{1}{\sqrt{3}}$ | $\frac{1}{\sqrt{3}}$ | $-\frac{5}{\sqrt{6}}$ | $-\frac{2}{\sqrt{3}}$ | $\frac{2}{3}$ |

Table B.8: $C = 1$, $S = -1$, $I = 1/2$, $J = 3/2$.

| | $\Sigma^* D^*$ | $\Sigma_c^* \bar{K}^*$ | $\Xi_c^* \rho$ | $\Xi_c^* \omega$ | $\Xi D_s^*$ | $\Xi_c \phi$ | $\Xi^* D_s$ | $\Omega_c K^*$ | $\Xi_c' \phi$ | $\Xi_c^* \eta'$ | $\Xi^* D_s^*$ | $\Omega_c^* K^*$ | $\Xi_c^* \phi$ |
|---|---|---|---|---|---|---|---|---|---|---|---|---|---|
| $\Xi_c^* \pi$ | $-\sqrt{\frac{5}{6}}$ | $-\sqrt{\frac{5}{6}}$ | $2\sqrt{\frac{5}{3}}$ | 0 | 0 | 0 | 0 | $-1$ | 0 | 0 | 0 | $\sqrt{5}$ | 0 |
| $\Sigma_c^* \bar{K}$ | $-\sqrt{\frac{5}{3}}$ | $\sqrt{15}$ | $-\sqrt{\frac{5}{6}}$ | $\sqrt{\frac{5}{2}}$ | 0 | $\sqrt{3}$ | 0 | 0 | $-1$ | 0 | 0 | 0 | $\sqrt{5}$ |
| $\Lambda D^*$ | $\sqrt{5}$ | 0 | $-\sqrt{\frac{5}{2}}$ | $-\sqrt{\frac{5}{6}}$ | $\sqrt{\frac{2}{3}}$ | 0 | $-\sqrt{2}$ | 0 | 0 | $-\frac{1}{\sqrt{3}}$ | $\sqrt{\frac{10}{3}}$ | 0 | 0 |
| $\Lambda_c \bar{K}^*$ | 0 | $\sqrt{5}$ | $-\sqrt{\frac{5}{2}}$ | $-\sqrt{\frac{5}{6}}$ | 0 | 1 | 0 | 0 | $-\frac{1}{\sqrt{3}}$ | 0 | 0 | 0 | $\sqrt{\frac{5}{3}}$ |
| $\Xi_c^* \eta$ | $\sqrt{\frac{5}{6}}$ | $\sqrt{\frac{15}{2}}$ | 0 | 0 | $-\frac{2}{3}$ | 0 | $\frac{2}{\sqrt{3}}$ | 1 | 0 | 0 | $-\frac{2\sqrt{5}}{3}$ | $-\sqrt{5}$ | 0 |
| $\Sigma D^*$ | $\sqrt{5}$ | $-\frac{2\sqrt{5}}{3}$ | $\frac{\sqrt{\frac{5}{2}}}{3}$ | $-\sqrt{\frac{5}{6}}$ | $\sqrt{\frac{2}{3}}$ | 0 | $-\sqrt{2}$ | 0 | 0 | $-\frac{1}{\sqrt{3}}$ | $\sqrt{\frac{10}{3}}$ | 0 | 0 |
| $\Xi_c \rho$ | 0 | $-\sqrt{\frac{5}{6}}$ | $\sqrt{\frac{5}{3}}$ | $-\sqrt{5}$ | 0 | 0 | 0 | $-1$ | 0 | 0 | 0 | $\sqrt{5}$ | 0 |
| $\Sigma^* D$ | $\sqrt{15}$ | $-\sqrt{\frac{5}{3}}$ | $-\sqrt{\frac{5}{6}}$ | $\sqrt{\frac{5}{2}}$ | $\sqrt{2}$ | 0 | $-\sqrt{6}$ | 0 | 0 | $-1$ | $\sqrt{10}$ | 0 | 0 |
| $\Xi_c \omega$ | 0 | $\sqrt{\frac{5}{2}}$ | $-\sqrt{5}$ | $\sqrt{\frac{5}{3}}$ | 0 | 0 | 0 | $\frac{1}{\sqrt{3}}$ | 0 | 0 | 0 | $-\sqrt{\frac{5}{3}}$ | 0 |
| $\Omega_c^* K$ | 0 | 0 | $\sqrt{5}$ | $-\sqrt{\frac{5}{3}}$ | $\frac{2}{\sqrt{3}}$ | $\sqrt{2}$ | 1 | $-\frac{2}{\sqrt{3}}$ | $\sqrt{\frac{2}{3}}$ | 0 | $-\sqrt{\frac{5}{3}}$ | $2\sqrt{\frac{5}{3}}$ | $-\sqrt{\frac{10}{3}}$ |
| $\Sigma_c \bar{K}^*$ | $-\frac{2\sqrt{5}}{3}$ | $\sqrt{5}$ | $\frac{\sqrt{\frac{5}{2}}}{3}$ | $-\sqrt{\frac{5}{6}}$ | 0 | 1 | 0 | 0 | $-\frac{1}{\sqrt{3}}$ | 0 | 0 | 0 | $\sqrt{\frac{5}{3}}$ |
| $\Xi_c' \rho$ | $-\frac{\sqrt{10}}{3}$ | $\frac{\sqrt{\frac{5}{2}}}{3}$ | $\frac{\sqrt{5}}{3}$ | $-\sqrt{\frac{5}{3}}$ | 0 | 0 | 0 | $-\frac{1}{\sqrt{3}}$ | 0 | 0 | 0 | $\sqrt{\frac{5}{3}}$ | 0 |
| $\Xi_c' \omega$ | $\sqrt{\frac{10}{3}}$ | $-\sqrt{\frac{5}{6}}$ | $-\sqrt{\frac{5}{3}}$ | $\frac{\sqrt{5}}{3}$ | 0 | 0 | 0 | $\frac{1}{3}$ | 0 | 0 | 0 | $-\frac{\sqrt{5}}{3}$ | 0 |

Table B.9: $C = 1$, $S = -1$, $I = 1/2$, $J = 3/2$ (continued).

| | $\Sigma^* D^*$ | $\Sigma_c^* \bar{K}^*$ | $\Xi_c^* \rho$ | $\Xi_c^* \omega$ | $\Xi D_s^*$ | $\Xi_c \phi$ | $\Xi^* D_s$ | $\Omega_c K^*$ | $\Xi_c' \phi$ | $\Xi_c^* \eta'$ | $\Xi^* D_s^*$ | $\Omega_c^* K^*$ | $\Xi_c^* \phi$ |
|---|---|---|---|---|---|---|---|---|---|---|---|---|---|
| $\Sigma^* D^*$ | $-5$ | $\frac{1}{3}$ | $\frac{1}{3\sqrt{2}}$ | $-\frac{1}{\sqrt{6}}$ | $-\sqrt{\frac{10}{3}}$ | $0$ | $\sqrt{10}$ | $0$ | $0$ | $\sqrt{\frac{5}{3}}$ | $-5\sqrt{\frac{2}{3}}$ | $0$ | $0$ |
| $\Sigma_c^* \bar{K}^*$ | $\frac{1}{3}$ | $-5$ | $\frac{1}{3\sqrt{2}}$ | $-\frac{1}{\sqrt{6}}$ | $0$ | $-\sqrt{5}$ | $0$ | $0$ | $\sqrt{\frac{5}{3}}$ | $0$ | $0$ | $0$ | $-\frac{5}{\sqrt{3}}$ |
| $\Xi_c^* \rho$ | $\frac{1}{3\sqrt{2}}$ | $\frac{1}{3\sqrt{2}}$ | $-\frac{8}{3}$ | $\frac{2}{\sqrt{3}}$ | $0$ | $0$ | $0$ | $\sqrt{\frac{5}{3}}$ | $0$ | $0$ | $0$ | $-\frac{5}{\sqrt{3}}$ | $0$ |
| $\Xi_c^* \omega$ | $-\frac{1}{\sqrt{6}}$ | $-\frac{1}{\sqrt{6}}$ | $\frac{2}{\sqrt{3}}$ | $-\frac{2}{3}$ | $0$ | $0$ | $0$ | $-\frac{\sqrt{5}}{3}$ | $0$ | $0$ | $0$ | $\frac{5}{3}$ | $0$ |
| $\Xi D_s^*$ | $-\sqrt{\frac{10}{3}}$ | $0$ | $0$ | $0$ | $-\frac{2}{3}$ | $\sqrt{6}$ | $\frac{2}{\sqrt{3}}$ | $-\frac{2}{3}$ | $\frac{\sqrt{2}}{3}$ | $\frac{\sqrt{2}}{3}$ | $-\frac{2\sqrt{5}}{3}$ | $\frac{2\sqrt{5}}{3}$ | $-\frac{\sqrt{10}}{3}$ |
| $\Xi_c \phi$ | $0$ | $-\sqrt{5}$ | $0$ | $0$ | $\sqrt{6}$ | $0$ | $0$ | $-\sqrt{\frac{2}{3}}$ | $\frac{2}{\sqrt{3}}$ | $0$ | $0$ | $\sqrt{\frac{10}{3}}$ | $-2\sqrt{\frac{5}{3}}$ |
| $\Xi^* D_s$ | $\sqrt{10}$ | $0$ | $0$ | $0$ | $\frac{2}{\sqrt{3}}$ | $0$ | $-2$ | $-\frac{2}{\sqrt{3}}$ | $-2\sqrt{\frac{2}{3}}$ | $-\sqrt{\frac{2}{3}}$ | $2\sqrt{\frac{5}{3}}$ | $-\sqrt{\frac{5}{3}}$ | $-\sqrt{\frac{10}{3}}$ |
| $\Omega_c K^*$ | $0$ | $0$ | $\sqrt{\frac{5}{3}}$ | $-\frac{\sqrt{5}}{3}$ | $-\frac{2}{3}$ | $-\sqrt{\frac{2}{3}}$ | $-\frac{2}{\sqrt{3}}$ | $-\frac{2}{3}$ | $\frac{5\sqrt{2}}{3}$ | $0$ | $-\frac{2\sqrt{5}}{3}$ | $\frac{2\sqrt{5}}{3}$ | $\frac{\sqrt{10}}{3}$ |
| $\Xi_c' \phi$ | $0$ | $\sqrt{\frac{5}{3}}$ | $0$ | $0$ | $\frac{\sqrt{2}}{3}$ | $\frac{2}{\sqrt{3}}$ | $-2\sqrt{\frac{2}{3}}$ | $\frac{5\sqrt{2}}{3}$ | $\frac{4}{3}$ | $0$ | $-\frac{2\sqrt{10}}{3}$ | $\frac{\sqrt{10}}{3}$ | $\frac{2\sqrt{5}}{3}$ |
| $\Xi_c^* \eta'$ | $\sqrt{\frac{5}{3}}$ | $0$ | $0$ | $0$ | $\frac{\sqrt{2}}{3}$ | $0$ | $-\sqrt{\frac{2}{3}}$ | $0$ | $0$ | $0$ | $\frac{\sqrt{10}}{3}$ | $0$ | $0$ |
| $\Xi^* D_s^*$ | $-5\sqrt{\frac{2}{3}}$ | $0$ | $0$ | $0$ | $-\frac{2\sqrt{5}}{3}$ | $0$ | $2\sqrt{\frac{5}{3}}$ | $-\frac{2\sqrt{5}}{3}$ | $-\frac{2\sqrt{10}}{3}$ | $\frac{\sqrt{10}}{3}$ | $-\frac{10}{3}$ | $\frac{1}{3}$ | $\frac{\sqrt{2}}{3}$ |
| $\Omega_c^* K^*$ | $0$ | $0$ | $-\frac{5}{\sqrt{3}}$ | $\frac{5}{3}$ | $\frac{2\sqrt{5}}{3}$ | $\sqrt{\frac{10}{3}}$ | $-\sqrt{\frac{5}{3}}$ | $\frac{2\sqrt{5}}{3}$ | $\frac{\sqrt{10}}{3}$ | $0$ | $\frac{1}{3}$ | $-\frac{10}{3}$ | $\frac{\sqrt{2}}{3}$ |
| $\Xi_c^* \phi$ | $0$ | $-\frac{5}{\sqrt{3}}$ | $0$ | $0$ | $-\frac{\sqrt{10}}{3}$ | $-2\sqrt{\frac{5}{3}}$ | $-\sqrt{\frac{10}{3}}$ | $\frac{\sqrt{10}}{3}$ | $\frac{2\sqrt{5}}{3}$ | $0$ | $\frac{\sqrt{2}}{3}$ | $\frac{\sqrt{2}}{3}$ | $-\frac{4}{3}$ |

Table B.10: $C = 1$, $S = -1$, $I = 1/2$, $J = 3/2$ (continued).

| | $\Xi_c\bar{K}$ | $\Xi_c'\bar{K}$ | $\Xi D$ | $\Omega_c\eta$ | $\Xi D^*$ | $\Xi_c\bar{K}^*$ | $\Xi_c'\bar{K}^*$ | $\Omega_c\omega$ | $\Xi_c^*\bar{K}^*$ | $\Xi^*D^*$ | $\Omega_c^*\omega$ | $\Omega_c\eta'$ | $\Omega_c\phi$ | $\Omega D_s^*$ | $\Omega_c^*\phi$ |
|---|---|---|---|---|---|---|---|---|---|---|---|---|---|---|---|
| $\Xi_c\bar{K}$ | $-1$ | $0$ | $\sqrt{\frac{3}{2}}$ | $0$ | $-\frac{3}{\sqrt{2}}$ | $0$ | $-3$ | $-\sqrt{2}$ | $3\sqrt{2}$ | $0$ | $2$ | $0$ | $-2$ | $0$ | $2\sqrt{2}$ |
| $\Xi_c'\bar{K}$ | $0$ | $-1$ | $\frac{1}{\sqrt{2}}$ | $-\sqrt{6}$ | $\frac{1}{\sqrt{6}}$ | $-3$ | $\frac{2}{\sqrt{3}}$ | $2\sqrt{\frac{2}{3}}$ | $\sqrt{\frac{2}{3}}$ | $\frac{4}{\sqrt{3}}$ | $\frac{2}{\sqrt{3}}$ | $0$ | $\frac{4}{\sqrt{3}}$ | $0$ | $2\sqrt{\frac{2}{3}}$ |
| $\Xi D$ | $\sqrt{\frac{3}{2}}$ | $\frac{1}{\sqrt{2}}$ | $-2$ | $\frac{1}{\sqrt{3}}$ | $-\frac{2}{\sqrt{3}}$ | $-\frac{3}{\sqrt{2}}$ | $\frac{1}{\sqrt{6}}$ | $\frac{1}{\sqrt{3}}$ | $\frac{2}{\sqrt{3}}$ | $4\sqrt{\frac{2}{3}}$ | $2\sqrt{\frac{2}{3}}$ | $\sqrt{\frac{2}{3}}$ | $0$ | $4$ | $0$ |
| $\Omega_c\eta$ | $0$ | $-\sqrt{6}$ | $\frac{1}{\sqrt{3}}$ | $0$ | $\frac{1}{3}$ | $-\sqrt{6}$ | $2\sqrt{2}$ | $0$ | $2$ | $-\frac{2\sqrt{2}}{3}$ | $0$ | $0$ | $0$ | $\frac{4}{\sqrt{3}}$ | $0$ |
| $\Xi D^*$ | $-\frac{3}{\sqrt{2}}$ | $\frac{1}{\sqrt{6}}$ | $-\frac{2}{\sqrt{3}}$ | $\frac{1}{3}$ | $-\frac{2}{3}$ | $-\sqrt{\frac{3}{2}}$ | $\frac{5}{3\sqrt{2}}$ | $\frac{5}{3}$ | $-\frac{2}{3}$ | $\frac{4\sqrt{2}}{3}$ | $-\frac{2\sqrt{2}}{3}$ | $\frac{\sqrt{2}}{3}$ | $0$ | $\frac{4}{\sqrt{3}}$ | $0$ |
| $\Xi_c\bar{K}^*$ | $0$ | $-3$ | $-\frac{3}{\sqrt{2}}$ | $-\sqrt{6}$ | $-\sqrt{\frac{3}{2}}$ | $-1$ | $\frac{2}{\sqrt{3}}$ | $-2\sqrt{\frac{2}{3}}$ | $\sqrt{\frac{2}{3}}$ | $0$ | $-\frac{2}{\sqrt{3}}$ | $0$ | $\frac{4}{\sqrt{3}}$ | $0$ | $2\sqrt{\frac{2}{3}}$ |
| $\Xi_c'\bar{K}^*$ | $-3$ | $\frac{2}{\sqrt{3}}$ | $\frac{1}{\sqrt{6}}$ | $2\sqrt{2}$ | $\frac{5}{3\sqrt{2}}$ | $\frac{2}{\sqrt{3}}$ | $-5$ | $\frac{\sqrt{2}}{3}$ | $\sqrt{2}$ | $-\frac{4}{3}$ | $-\frac{2}{3}$ | $0$ | $-\frac{14}{3}$ | $0$ | $\frac{2\sqrt{2}}{3}$ |
| $\Omega_c\omega$ | $-\sqrt{2}$ | $2\sqrt{\frac{2}{3}}$ | $\frac{1}{\sqrt{3}}$ | $0$ | $\frac{5}{3}$ | $-2\sqrt{\frac{2}{3}}$ | $\frac{\sqrt{2}}{3}$ | $0$ | $-\frac{2}{3}$ | $\frac{2\sqrt{2}}{3}$ | $0$ | $0$ | $0$ | $0$ | $0$ |
| $\Xi_c^*\bar{K}^*$ | $3\sqrt{2}$ | $\sqrt{\frac{2}{3}}$ | $\frac{2}{\sqrt{3}}$ | $2$ | $-\frac{2}{3}$ | $\sqrt{\frac{2}{3}}$ | $\sqrt{2}$ | $-\frac{2}{3}$ | $-6$ | $-\frac{2\sqrt{2}}{3}$ | $\frac{2\sqrt{2}}{3}$ | $0$ | $\frac{2\sqrt{2}}{3}$ | $0$ | $-\frac{16}{3}$ |
| $\Xi^*D^*$ | $0$ | $\frac{4}{\sqrt{3}}$ | $4\sqrt{\frac{2}{3}}$ | $-\frac{2\sqrt{2}}{3}$ | $\frac{4\sqrt{2}}{3}$ | $0$ | $-\frac{4}{3}$ | $\frac{2\sqrt{2}}{3}$ | $-\frac{2\sqrt{2}}{3}$ | $-\frac{16}{3}$ | $\frac{2}{3}$ | $-\frac{4}{3}$ | $0$ | $-8\sqrt{\frac{2}{3}}$ | $0$ |
| $\Omega_c^*\omega$ | $2$ | $\frac{2}{\sqrt{3}}$ | $2\sqrt{\frac{2}{3}}$ | $0$ | $-\frac{2\sqrt{2}}{3}$ | $-\frac{2}{\sqrt{3}}$ | $-\frac{2}{3}$ | $0$ | $\frac{2\sqrt{2}}{3}$ | $\frac{2}{3}$ | $0$ | $0$ | $0$ | $0$ | $0$ |
| $\Omega_c\eta'$ | $0$ | $0$ | $\sqrt{\frac{2}{3}}$ | $0$ | $\frac{\sqrt{2}}{3}$ | $0$ | $0$ | $0$ | $0$ | $-\frac{4}{3}$ | $0$ | $0$ | $0$ | $-2\sqrt{\frac{2}{3}}$ | $0$ |
| $\Omega_c\phi$ | $-2$ | $\frac{4}{\sqrt{3}}$ | $0$ | $0$ | $0$ | $\frac{4}{\sqrt{3}}$ | $-\frac{14}{3}$ | $0$ | $\frac{2\sqrt{2}}{3}$ | $0$ | $0$ | $0$ | $-\frac{16}{3}$ | $-2\sqrt{\frac{2}{3}}$ | $\frac{4\sqrt{2}}{3}$ |
| $\Omega D_s^*$ | $0$ | $0$ | $4$ | $\frac{4}{\sqrt{3}}$ | $\frac{4}{\sqrt{3}}$ | $0$ | $0$ | $0$ | $0$ | $-8\sqrt{\frac{2}{3}}$ | $0$ | $-2\sqrt{\frac{2}{3}}$ | $-2\sqrt{\frac{2}{3}}$ | $-8$ | $-\frac{2}{\sqrt{3}}$ |
| $\Omega_c^*\phi$ | $2\sqrt{2}$ | $2\sqrt{\frac{2}{3}}$ | $0$ | $0$ | $0$ | $2\sqrt{\frac{2}{3}}$ | $\frac{2\sqrt{2}}{3}$ | $0$ | $-\frac{16}{3}$ | $0$ | $0$ | $0$ | $\frac{4\sqrt{2}}{3}$ | $-\frac{2}{\sqrt{3}}$ | $-\frac{20}{3}$ |

Table B.11: $C = 1$, $S = -2$, $I = 0$, $J = 1/2$.

| | $\Xi_c^*\bar{K}$ | $\Omega_c^*\eta$ | $\Xi D^*$ | $\Xi_c\bar{K}^*$ | $\Xi^* D$ | $\Xi_c'\bar{K}^*$ | $\Omega_c\omega$ | $\Xi_c^*\bar{K}^*$ | $\Xi^* D^*$ | $\Omega_c^*\omega$ | $\Omega D_s$ | $\Omega_c\phi$ | $\Omega_c^*\eta'$ | $\Omega D_s^*$ | $\Omega_c^*\phi$ |
|---|---|---|---|---|---|---|---|---|---|---|---|---|---|---|---|
| $\Xi_c^*\bar{K}$ | $-1$ | $-\sqrt{6}$ | $-\sqrt{\frac{2}{3}}$ | $-3$ | $\sqrt{2}$ | $-\frac{1}{\sqrt{3}}$ | $-\sqrt{\frac{2}{3}}$ | $\sqrt{\frac{5}{3}}$ | $-\sqrt{\frac{10}{3}}$ | $\sqrt{\frac{10}{3}}$ | $0$ | $-\frac{2}{\sqrt{3}}$ | $0$ | $0$ | $2\sqrt{\frac{5}{3}}$ |
| $\Omega_c^*\eta$ | $-\sqrt{6}$ | $0$ | $-\frac{2}{3}$ | $-\sqrt{6}$ | $-\frac{1}{\sqrt{3}}$ | $-\sqrt{2}$ | $0$ | $\sqrt{10}$ | $\frac{\sqrt{5}}{3}$ | $0$ | $\sqrt{2}$ | $0$ | $0$ | $-\sqrt{\frac{10}{3}}$ | $0$ |
| $\Xi D^*$ | $-\sqrt{\frac{2}{3}}$ | $-\frac{2}{3}$ | $-\frac{8}{3}$ | $\sqrt{6}$ | $-\frac{4}{\sqrt{3}}$ | $\frac{\sqrt{2}}{3}$ | $\frac{2}{3}$ | $-\frac{\sqrt{10}}{3}$ | $\frac{4\sqrt{5}}{3}$ | $-\frac{2\sqrt{5}}{3}$ | $-2\sqrt{2}$ | $0$ | $-\frac{2\sqrt{2}}{3}$ | $2\sqrt{\frac{10}{3}}$ | $0$ |
| $\Xi_c\bar{K}^*$ | $-3$ | $-\sqrt{6}$ | $\sqrt{6}$ | $-1$ | $0$ | $-\frac{1}{\sqrt{3}}$ | $\sqrt{\frac{2}{3}}$ | $\sqrt{\frac{5}{3}}$ | $0$ | $-\sqrt{\frac{10}{3}}$ | $0$ | $-\frac{2}{\sqrt{3}}$ | $0$ | $0$ | $2\sqrt{\frac{5}{3}}$ |
| $\Xi^* D$ | $\sqrt{2}$ | $-\frac{1}{\sqrt{3}}$ | $-\frac{4}{\sqrt{3}}$ | $0$ | $-2$ | $-2\sqrt{\frac{2}{3}}$ | $\frac{2}{\sqrt{3}}$ | $-\sqrt{\frac{10}{3}}$ | $2\sqrt{\frac{5}{3}}$ | $\sqrt{\frac{5}{3}}$ | $-\sqrt{6}$ | $0$ | $-\sqrt{\frac{2}{3}}$ | $\sqrt{10}$ | $0$ |
| $\Xi_c'\bar{K}^*$ | $-\frac{1}{\sqrt{3}}$ | $-\sqrt{2}$ | $\frac{\sqrt{2}}{3}$ | $-\frac{1}{\sqrt{3}}$ | $-2\sqrt{\frac{2}{3}}$ | $1$ | $-\frac{5\sqrt{2}}{3}$ | $\sqrt{5}$ | $-\frac{2\sqrt{10}}{3}$ | $-\frac{\sqrt{10}}{3}$ | $0$ | $-\frac{2}{3}$ | $0$ | $0$ | $\frac{2\sqrt{5}}{3}$ |
| $\Omega_c\omega$ | $-\sqrt{\frac{2}{3}}$ | $0$ | $\frac{2}{3}$ | $\sqrt{\frac{2}{3}}$ | $\frac{2}{\sqrt{3}}$ | $-\frac{5\sqrt{2}}{3}$ | $0$ | $-\frac{\sqrt{10}}{3}$ | $\frac{2\sqrt{5}}{3}$ | $0$ | $0$ | $0$ | $0$ | $0$ | $0$ |
| $\Xi_c^*\bar{K}^*$ | $\sqrt{\frac{5}{3}}$ | $\sqrt{10}$ | $-\frac{\sqrt{10}}{3}$ | $\sqrt{\frac{5}{3}}$ | $-\sqrt{\frac{10}{3}}$ | $\sqrt{5}$ | $-\frac{\sqrt{10}}{3}$ | $-3$ | $\frac{\sqrt{2}}{3}$ | $-\frac{\sqrt{2}}{3}$ | $0$ | $\frac{2\sqrt{5}}{3}$ | $0$ | $0$ | $-\frac{10}{3}$ |
| $\Xi^* D^*$ | $-\sqrt{\frac{10}{3}}$ | $\frac{\sqrt{5}}{3}$ | $\frac{4\sqrt{5}}{3}$ | $0$ | $2\sqrt{\frac{5}{3}}$ | $-\frac{2\sqrt{10}}{3}$ | $\frac{2\sqrt{5}}{3}$ | $\frac{\sqrt{2}}{3}$ | $-\frac{10}{3}$ | $-\frac{1}{3}$ | $\sqrt{10}$ | $0$ | $\frac{\sqrt{10}}{3}$ | $-5\sqrt{\frac{2}{3}}$ | $0$ |
| $\Omega_c^*\omega$ | $\sqrt{\frac{10}{3}}$ | $0$ | $-\frac{2\sqrt{5}}{3}$ | $-\sqrt{\frac{10}{3}}$ | $\sqrt{\frac{5}{3}}$ | $-\frac{\sqrt{10}}{3}$ | $0$ | $-\frac{\sqrt{2}}{3}$ | $-\frac{1}{3}$ | $0$ | $0$ | $0$ | $0$ | $0$ | $0$ |
| $\Omega D_s$ | $0$ | $\sqrt{2}$ | $-2\sqrt{2}$ | $0$ | $-\sqrt{6}$ | $0$ | $0$ | $0$ | $\sqrt{10}$ | $0$ | $-3$ | $-2$ | $-1$ | $\sqrt{15}$ | $-\sqrt{5}$ |
| $\Omega_c\phi$ | $-\frac{2}{\sqrt{3}}$ | $0$ | $0$ | $-\frac{2}{\sqrt{3}}$ | $0$ | $-\frac{2}{3}$ | $0$ | $\frac{2\sqrt{5}}{3}$ | $0$ | $0$ | $-2$ | $\frac{8}{3}$ | $0$ | $-2\sqrt{\frac{5}{3}}$ | $\frac{4\sqrt{5}}{3}$ |
| $\Omega_c^*\eta'$ | $0$ | $0$ | $-\frac{2\sqrt{2}}{3}$ | $0$ | $-\sqrt{\frac{2}{3}}$ | $0$ | $0$ | $0$ | $\frac{\sqrt{10}}{3}$ | $0$ | $-1$ | $0$ | $0$ | $\sqrt{\frac{5}{3}}$ | $0$ |
| $\Omega D_s^*$ | $0$ | $-\sqrt{\frac{10}{3}}$ | $2\sqrt{\frac{10}{3}}$ | $0$ | $\sqrt{10}$ | $0$ | $0$ | $0$ | $-5\sqrt{\frac{2}{3}}$ | $0$ | $\sqrt{15}$ | $-2\sqrt{\frac{5}{3}}$ | $\sqrt{\frac{5}{3}}$ | $-5$ | $\frac{1}{\sqrt{3}}$ |
| $\Omega_c^*\phi$ | $2\sqrt{\frac{5}{3}}$ | $0$ | $0$ | $2\sqrt{\frac{5}{3}}$ | $0$ | $\frac{2\sqrt{5}}{3}$ | $0$ | $-\frac{10}{3}$ | $0$ | $0$ | $-\sqrt{5}$ | $\frac{4\sqrt{5}}{3}$ | $0$ | $\frac{1}{\sqrt{3}}$ | $-\frac{8}{3}$ |

Table B.12: $C = 1$, $S = -2$, $I = 0$, $J = 3/2$.

| | $\Xi_{cc}\pi$ | $\Xi_{cc}\eta$ | $\Lambda_c D$ | $\Omega_{cc}K$ | $\Xi_{cc}\rho$ | $\Lambda_c D^*$ | $\Xi_{cc}\omega$ | $\Sigma_c D$ | $\Xi^*_{cc}\rho$ | $\Xi^*_{cc}\omega$ | $\Xi_c D_s$ | $\Sigma_c D^*$ | $\Xi_{cc}\eta'$ | $\Sigma^*_c D^*$ | $\Xi_{cc}\phi$ | $\Xi'_c D_s$ | $\Xi_c D^*_s$ | $\Omega_{cc}K^*$ | $\Xi^*_{cc}\phi$ | $\Omega^*_{cc}K^*$ | $\Xi'_c D^*_s$ | $\Xi^*_c D^*_s$ |
|---|---|---|---|---|---|---|---|---|---|---|---|---|---|---|---|---|---|---|---|---|---|---|
| $\Xi_{cc}\pi$ | $-2$ | $0$ | $\frac{3}{2}$ | $-\sqrt{\frac{3}{2}}$ | $-\frac{2}{\sqrt{3}}$ | $-\frac{\sqrt{3}}{2}$ | $0$ | $\frac{1}{2}$ | $4\sqrt{\frac{2}{3}}$ | $0$ | $0$ | $-\frac{5}{2\sqrt{3}}$ | $0$ | $\sqrt{\frac{2}{3}}$ | $0$ | $0$ | $0$ | $-\frac{1}{\sqrt{2}}$ | $0$ | $2$ | $0$ | $0$ |
| $\Xi_{cc}\eta$ | $0$ | $0$ | $\frac{1}{2}$ | $\sqrt{\frac{3}{2}}$ | $0$ | $-\frac{1}{2\sqrt{3}}$ | $0$ | $-\frac{1}{2}$ | $0$ | $0$ | $1$ | $\frac{5}{2\sqrt{3}}$ | $0$ | $-\sqrt{\frac{2}{3}}$ | $0$ | $\frac{1}{\sqrt{3}}$ | $-\frac{1}{\sqrt{3}}$ | $\frac{1}{\sqrt{2}}$ | $0$ | $-2$ | $-\frac{5}{3}$ | $\frac{2\sqrt{2}}{3}$ |
| $\Lambda_c D$ | $\frac{3}{2}$ | $\frac{1}{2}$ | $0$ | $0$ | $-\frac{\sqrt{3}}{2}$ | $-\sqrt{3}$ | $-\frac{1}{2}$ | $0$ | $\sqrt{6}$ | $\sqrt{2}$ | $1$ | $-\sqrt{3}$ | $\frac{1}{\sqrt{2}}$ | $\sqrt{6}$ | $0$ | $0$ | $0$ | $0$ | $0$ | $0$ | $-1$ | $\sqrt{2}$ |
| $\Omega_{cc}K$ | $-\sqrt{\frac{3}{2}}$ | $\sqrt{\frac{3}{2}}$ | $0$ | $-1$ | $-\frac{1}{\sqrt{2}}$ | $0$ | $\frac{1}{\sqrt{6}}$ | $0$ | $2$ | $-\frac{2}{\sqrt{3}}$ | $-\sqrt{\frac{3}{2}}$ | $0$ | $0$ | $0$ | $\frac{1}{\sqrt{3}}$ | $\frac{1}{\sqrt{2}}$ | $\frac{1}{\sqrt{2}}$ | $-\frac{1}{\sqrt{3}}$ | $-2\sqrt{\frac{2}{3}}$ | $2\sqrt{\frac{2}{3}}$ | $-\frac{5}{\sqrt{6}}$ | $\frac{2}{\sqrt{3}}$ |
| $\Xi_{cc}\rho$ | $-\frac{2}{\sqrt{3}}$ | $0$ | $-\frac{\sqrt{3}}{2}$ | $-\frac{1}{\sqrt{2}}$ | $-\frac{4}{3}$ | $\frac{1}{2}$ | $-\frac{2}{\sqrt{3}}$ | $-\frac{5}{2\sqrt{3}}$ | $\frac{2\sqrt{2}}{3}$ | $-2\sqrt{\frac{2}{3}}$ | $0$ | $-\frac{7}{6}$ | $0$ | $-\frac{\sqrt{2}}{3}$ | $0$ | $0$ | $0$ | $-\frac{1}{\sqrt{6}}$ | $0$ | $\frac{2}{\sqrt{3}}$ | $0$ | $0$ |
| $\Lambda_c D^*$ | $-\frac{\sqrt{3}}{2}$ | $-\frac{1}{2\sqrt{3}}$ | $-\sqrt{3}$ | $0$ | $\frac{1}{2}$ | $-2$ | $\frac{1}{2\sqrt{3}}$ | $-\sqrt{3}$ | $-\sqrt{2}$ | $-\sqrt{\frac{2}{3}}$ | $0$ | $2$ | $-\frac{1}{\sqrt{6}}$ | $\sqrt{2}$ | $0$ | $-1$ | $1$ | $0$ | $0$ | $0$ | $\frac{2}{\sqrt{3}}$ | $\sqrt{\frac{2}{3}}$ |
| $\Xi_{cc}\omega$ | $0$ | $0$ | $-\frac{1}{2}$ | $\frac{1}{\sqrt{6}}$ | $-\frac{2}{\sqrt{3}}$ | $\frac{1}{2\sqrt{3}}$ | $\frac{2}{3}$ | $\frac{5}{2}$ | $-2\sqrt{\frac{2}{3}}$ | $\frac{2\sqrt{2}}{3}$ | $0$ | $\frac{7}{2\sqrt{3}}$ | $0$ | $\sqrt{\frac{2}{3}}$ | $0$ | $0$ | $0$ | $\frac{1}{3\sqrt{2}}$ | $0$ | $-\frac{2}{3}$ | $0$ | $0$ |
| $\Sigma_c D$ | $\frac{1}{2}$ | $-\frac{1}{2}$ | $0$ | $0$ | $-\frac{5}{2\sqrt{3}}$ | $-\sqrt{3}$ | $\frac{5}{2}$ | $-2$ | $-\sqrt{\frac{2}{3}}$ | $\sqrt{2}$ | $0$ | $\frac{7}{\sqrt{3}}$ | $-\frac{1}{\sqrt{2}}$ | $5\sqrt{\frac{2}{3}}$ | $0$ | $-\sqrt{3}$ | $\sqrt{3}$ | $0$ | $0$ | $0$ | $2$ | $\sqrt{2}$ |
| $\Xi^*_{cc}\rho$ | $4\sqrt{\frac{2}{3}}$ | $0$ | $\sqrt{6}$ | $2$ | $\frac{2\sqrt{2}}{3}$ | $-\sqrt{2}$ | $-2\sqrt{\frac{2}{3}}$ | $-\sqrt{\frac{2}{3}}$ | $-\frac{11}{3}$ | $\frac{5}{\sqrt{3}}$ | $0$ | $\frac{\sqrt{2}}{3}$ | $0$ | $-\frac{2}{3}$ | $0$ | $0$ | $0$ | $\frac{2}{\sqrt{3}}$ | $0$ | $-4\sqrt{\frac{2}{3}}$ | $0$ | $0$ |
| $\Xi^*_{cc}\omega$ | $0$ | $0$ | $\sqrt{2}$ | $-\frac{2}{\sqrt{3}}$ | $-2\sqrt{\frac{2}{3}}$ | $-\sqrt{\frac{2}{3}}$ | $\frac{2\sqrt{2}}{3}$ | $\sqrt{2}$ | $\frac{5}{\sqrt{3}}$ | $-\frac{5}{3}$ | $0$ | $-\sqrt{\frac{2}{3}}$ | $0$ | $\frac{2}{\sqrt{3}}$ | $0$ | $0$ | $0$ | $-\frac{2}{3}$ | $0$ | $\frac{4\sqrt{2}}{3}$ | $0$ | $0$ |
| $\Xi_c D_s$ | $0$ | $1$ | $1$ | $-\sqrt{\frac{3}{2}}$ | $0$ | $0$ | $0$ | $0$ | $0$ | $0$ | $0$ | $\sqrt{3}$ | $-\frac{1}{\sqrt{2}}$ | $-\sqrt{6}$ | $-\frac{1}{\sqrt{2}}$ | $0$ | $-\sqrt{3}$ | $\frac{1}{\sqrt{2}}$ | $2$ | $-2$ | $1$ | $-\sqrt{2}$ |
| $\Sigma_c D^*$ | $-\frac{5}{2\sqrt{3}}$ | $\frac{5}{2\sqrt{3}}$ | $-\sqrt{3}$ | $0$ | $-\frac{7}{6}$ | $2$ | $\frac{7}{2\sqrt{3}}$ | $\frac{7}{\sqrt{3}}$ | $\frac{\sqrt{2}}{3}$ | $-\sqrt{\frac{2}{3}}$ | $\sqrt{3}$ | $-\frac{16}{3}$ | $\frac{5}{\sqrt{6}}$ | $\frac{\sqrt{2}}{3}$ | $0$ | $2$ | $-2$ | $0$ | $0$ | $0$ | $-\frac{7}{\sqrt{3}}$ | $\sqrt{\frac{2}{3}}$ |
| $\Xi_{cc}\eta'$ | $0$ | $0$ | $\frac{1}{\sqrt{2}}$ | $0$ | $0$ | $-\frac{1}{\sqrt{6}}$ | $0$ | $-\frac{1}{\sqrt{2}}$ | $0$ | $0$ | $-\frac{1}{\sqrt{2}}$ | $\frac{5}{\sqrt{6}}$ | $0$ | $-\frac{2}{\sqrt{3}}$ | $0$ | $-\frac{1}{\sqrt{6}}$ | $\frac{1}{\sqrt{6}}$ | $0$ | $0$ | $0$ | $\frac{5}{3\sqrt{2}}$ | $-\frac{2}{3}$ |
| $\Sigma^*_c D^*$ | $\sqrt{\frac{2}{3}}$ | $-\sqrt{\frac{2}{3}}$ | $\sqrt{6}$ | $0$ | $-\frac{\sqrt{2}}{3}$ | $\sqrt{2}$ | $\sqrt{\frac{2}{3}}$ | $5\sqrt{\frac{2}{3}}$ | $-\frac{2}{3}$ | $\frac{2}{\sqrt{3}}$ | $-\sqrt{6}$ | $\frac{\sqrt{2}}{3}$ | $-\frac{2}{\sqrt{3}}$ | $-\frac{26}{3}$ | $0$ | $\sqrt{2}$ | $-\sqrt{2}$ | $0$ | $0$ | $0$ | $\sqrt{\frac{2}{3}}$ | $-\frac{8}{\sqrt{3}}$ |
| $\Xi_{cc}\phi$ | $0$ | $0$ | $0$ | $\frac{1}{\sqrt{3}}$ | $0$ | $0$ | $0$ | $0$ | $0$ | $0$ | $-\frac{1}{\sqrt{2}}$ | $0$ | $0$ | $0$ | $0$ | $-\frac{5}{\sqrt{6}}$ | $\frac{1}{\sqrt{6}}$ | $\frac{5}{3}$ | $0$ | $\frac{2\sqrt{2}}{3}$ | $-\frac{7}{3\sqrt{2}}$ | $-\frac{2}{3}$ |
| $\Xi'_c D_s$ | $0$ | $\frac{1}{\sqrt{3}}$ | $0$ | $\frac{1}{\sqrt{2}}$ | $0$ | $-1$ | $0$ | $-\sqrt{3}$ | $0$ | $0$ | $0$ | $2$ | $-\frac{1}{\sqrt{6}}$ | $\sqrt{2}$ | $-\frac{5}{\sqrt{6}}$ | $0$ | $1$ | $-\frac{5}{\sqrt{6}}$ | $-\frac{2}{\sqrt{3}}$ | $-\frac{2}{\sqrt{3}}$ | $\sqrt{3}$ | $\sqrt{6}$ |
| $\Xi_c D^*_s$ | $0$ | $-\frac{1}{\sqrt{3}}$ | $0$ | $\frac{1}{\sqrt{2}}$ | $0$ | $1$ | $0$ | $\sqrt{3}$ | $0$ | $0$ | $-\sqrt{3}$ | $-2$ | $\frac{1}{\sqrt{6}}$ | $-\sqrt{2}$ | $\frac{1}{\sqrt{6}}$ | $1$ | $-2$ | $-\frac{1}{\sqrt{6}}$ | $-\frac{2}{\sqrt{3}}$ | $\frac{2}{\sqrt{3}}$ | $-\frac{2}{\sqrt{3}}$ | $-\sqrt{\frac{2}{3}}$ |
| $\Omega_{cc}K^*$ | $-\frac{1}{\sqrt{2}}$ | $\frac{1}{\sqrt{2}}$ | $0$ | $-\frac{1}{\sqrt{3}}$ | $-\frac{1}{\sqrt{6}}$ | $0$ | $\frac{1}{3\sqrt{2}}$ | $0$ | $\frac{2}{\sqrt{3}}$ | $-\frac{2}{3}$ | $\frac{1}{\sqrt{2}}$ | $0$ | $0$ | $0$ | $\frac{5}{3}$ | $-\frac{5}{\sqrt{6}}$ | $-\frac{1}{\sqrt{6}}$ | $-\frac{1}{3}$ | $\frac{2\sqrt{2}}{3}$ | $\frac{2\sqrt{2}}{3}$ | $-\frac{7}{3\sqrt{2}}$ | $-\frac{2}{3}$ |
| $\Xi^*_{cc}\phi$ | $0$ | $0$ | $0$ | $-2\sqrt{\frac{2}{3}}$ | $0$ | $0$ | $0$ | $0$ | $0$ | $0$ | $2$ | $0$ | $0$ | $0$ | $0$ | $-\frac{2}{\sqrt{3}}$ | $-\frac{2}{\sqrt{3}}$ | $\frac{2\sqrt{2}}{3}$ | $0$ | $-\frac{2}{3}$ | $\frac{2}{3}$ | $-\frac{2\sqrt{2}}{3}$ |
| $\Omega^*_{cc}K^*$ | $2$ | $-2$ | $0$ | $2\sqrt{\frac{2}{3}}$ | $\frac{2}{\sqrt{3}}$ | $0$ | $-\frac{2}{3}$ | $0$ | $-4\sqrt{\frac{2}{3}}$ | $\frac{4\sqrt{2}}{3}$ | $-2$ | $0$ | $0$ | $0$ | $\frac{2\sqrt{2}}{3}$ | $-\frac{2}{\sqrt{3}}$ | $\frac{2}{\sqrt{3}}$ | $\frac{2\sqrt{2}}{3}$ | $-\frac{2}{3}$ | $-\frac{8}{3}$ | $\frac{2}{3}$ | $-\frac{2\sqrt{2}}{3}$ |
| $\Xi'_c D^*_s$ | $0$ | $-\frac{5}{3}$ | $-1$ | $-\frac{5}{\sqrt{6}}$ | $0$ | $\frac{2}{\sqrt{3}}$ | $0$ | $2$ | $0$ | $0$ | $1$ | $-\frac{7}{\sqrt{3}}$ | $\frac{5}{3\sqrt{2}}$ | $\sqrt{\frac{2}{3}}$ | $-\frac{7}{3\sqrt{2}}$ | $\sqrt{3}$ | $-\frac{2}{\sqrt{3}}$ | $-\frac{7}{3\sqrt{2}}$ | $\frac{2}{3}$ | $\frac{2}{3}$ | $-\frac{2}{3}$ | $-\frac{\sqrt{2}}{3}$ |
| $\Xi^*_c D^*_s$ | $0$ | $\frac{2\sqrt{2}}{3}$ | $\sqrt{2}$ | $\frac{2}{\sqrt{3}}$ | $0$ | $\sqrt{\frac{2}{3}}$ | $0$ | $\sqrt{2}$ | $0$ | $0$ | $-\sqrt{2}$ | $\sqrt{\frac{2}{3}}$ | $-\frac{2}{3}$ | $-\frac{8}{\sqrt{3}}$ | $-\frac{2}{3}$ | $\sqrt{6}$ | $-\sqrt{\frac{2}{3}}$ | $-\frac{2}{3}$ | $-\frac{2\sqrt{2}}{3}$ | $-\frac{2\sqrt{2}}{3}$ | $-\frac{\sqrt{2}}{3}$ | $-\frac{10}{3}$ |

Table B.13: $C = 2$, $S = 0$, $I = 1/2$, $J = 1/2$.

| | $\Xi_{cc}^*\pi$ | $\Xi_{cc}^*\eta$ | $\Omega_{cc}^*K$ | $\Xi_{cc}\rho$ | $\Lambda_cD^*$ | $\Xi_{cc}\omega$ | $\Xi_{cc}^*\rho$ | $\Xi_{cc}^*\omega$ | $\Sigma_c^*D$ | $\Sigma_cD^*$ | $\Sigma_c^*D^*$ | $\Xi_{cc}\phi$ | $\Xi_{cc}^*\eta'$ | $\Xi_cD_s^*$ | $\Omega_{cc}K^*$ | $\Xi_c^*D_s$ | $\Xi_{cc}^*\phi$ | $\Omega_{cc}^*K^*$ | $\Xi_c'D_s^*$ | $\Xi_c^*D_s^*$ |
|---|---|---|---|---|---|---|---|---|---|---|---|---|---|---|---|---|---|---|---|---|
| $\Xi_{cc}^*\pi$ | $-2$ | $0$ | $-\sqrt{\frac{3}{2}}$ | $-\frac{4}{\sqrt{3}}$ | $-\sqrt{3}$ | $0$ | $2\sqrt{\frac{5}{3}}$ | $0$ | $1$ | $\frac{1}{\sqrt{3}}$ | $-\sqrt{\frac{5}{3}}$ | $0$ | $0$ | $0$ | $-\sqrt{2}$ | $0$ | $0$ | $\sqrt{\frac{5}{2}}$ | $0$ | $0$ |
| $\Xi_{cc}^*\eta$ | $0$ | $0$ | $\sqrt{\frac{3}{2}}$ | $0$ | $-\frac{1}{\sqrt{3}}$ | $0$ | $0$ | $0$ | $-1$ | $-\frac{1}{\sqrt{3}}$ | $\sqrt{\frac{5}{3}}$ | $0$ | $0$ | $-\frac{2}{\sqrt{3}}$ | $\sqrt{2}$ | $\frac{2}{\sqrt{3}}$ | $0$ | $-\sqrt{\frac{5}{2}}$ | $\frac{2}{3}$ | $-\frac{2\sqrt{5}}{3}$ |
| $\Omega_{cc}^*K$ | $-\sqrt{\frac{3}{2}}$ | $\sqrt{\frac{3}{2}}$ | $-1$ | $-\sqrt{2}$ | $0$ | $\sqrt{\frac{2}{3}}$ | $\sqrt{\frac{5}{2}}$ | $-\sqrt{\frac{5}{6}}$ | $0$ | $0$ | $0$ | $\frac{2}{\sqrt{3}}$ | $0$ | $\sqrt{2}$ | $-\frac{2}{\sqrt{3}}$ | $\sqrt{2}$ | $-\sqrt{\frac{5}{3}}$ | $\sqrt{\frac{5}{3}}$ | $\sqrt{\frac{2}{3}}$ | $-\sqrt{\frac{10}{3}}$ |
| $\Xi_{cc}\rho$ | $-\frac{4}{\sqrt{3}}$ | $0$ | $-\sqrt{2}$ | $-\frac{7}{3}$ | $2$ | $\frac{1}{\sqrt{3}}$ | $\frac{2\sqrt{5}}{3}$ | $-2\sqrt{\frac{5}{3}}$ | $-\frac{1}{\sqrt{3}}$ | $\frac{4}{3}$ | $-\frac{\sqrt{5}}{3}$ | $0$ | $0$ | $0$ | $-2\sqrt{\frac{2}{3}}$ | $0$ | $0$ | $\sqrt{\frac{10}{3}}$ | $0$ | $0$ |
| $\Lambda_cD^*$ | $-\sqrt{3}$ | $-\frac{1}{\sqrt{3}}$ | $0$ | $2$ | $1$ | $\frac{2}{\sqrt{3}}$ | $-\sqrt{5}$ | $-\sqrt{\frac{5}{3}}$ | $-\sqrt{3}$ | $-1$ | $\sqrt{5}$ | $0$ | $-\sqrt{\frac{2}{3}}$ | $1$ | $0$ | $-1$ | $0$ | $0$ | $-\frac{1}{\sqrt{3}}$ | $\sqrt{\frac{5}{3}}$ |
| $\Xi_{cc}\omega$ | $0$ | $0$ | $\sqrt{\frac{2}{3}}$ | $\frac{1}{\sqrt{3}}$ | $\frac{2}{\sqrt{3}}$ | $-\frac{1}{3}$ | $-2\sqrt{\frac{5}{3}}$ | $\frac{2\sqrt{5}}{3}$ | $1$ | $-\frac{4}{\sqrt{3}}$ | $\sqrt{\frac{5}{3}}$ | $0$ | $0$ | $0$ | $\frac{2\sqrt{2}}{3}$ | $0$ | $0$ | $-\frac{\sqrt{10}}{3}$ | $0$ | $0$ |
| $\Xi_{cc}^*\rho$ | $2\sqrt{\frac{5}{3}}$ | $0$ | $\sqrt{\frac{5}{2}}$ | $\frac{2\sqrt{5}}{3}$ | $-\sqrt{5}$ | $-2\sqrt{\frac{5}{3}}$ | $-\frac{8}{3}$ | $\frac{2}{\sqrt{3}}$ | $-\sqrt{\frac{5}{3}}$ | $\frac{\sqrt{5}}{3}$ | $\frac{1}{3}$ | $0$ | $0$ | $0$ | $\sqrt{\frac{10}{3}}$ | $0$ | $0$ | $-\frac{5}{\sqrt{6}}$ | $0$ | $0$ |
| $\Xi_{cc}^*\omega$ | $0$ | $0$ | $-\sqrt{\frac{5}{6}}$ | $-2\sqrt{\frac{5}{3}}$ | $-\sqrt{\frac{5}{3}}$ | $\frac{2\sqrt{5}}{3}$ | $\frac{2}{\sqrt{3}}$ | $-\frac{2}{3}$ | $\sqrt{5}$ | $-\sqrt{\frac{5}{3}}$ | $-\frac{1}{\sqrt{3}}$ | $0$ | $0$ | $0$ | $-\frac{\sqrt{10}}{3}$ | $0$ | $0$ | $\frac{5}{3\sqrt{2}}$ | $0$ | $0$ |
| $\Sigma_c^*D$ | $1$ | $-1$ | $0$ | $-\frac{1}{\sqrt{3}}$ | $-\sqrt{3}$ | $1$ | $-\sqrt{\frac{5}{3}}$ | $\sqrt{5}$ | $-2$ | $-\frac{5}{\sqrt{3}}$ | $2\sqrt{\frac{5}{3}}$ | $0$ | $-\sqrt{2}$ | $\sqrt{3}$ | $0$ | $-\sqrt{3}$ | $0$ | $0$ | $-1$ | $\sqrt{5}$ |
| $\Sigma_cD^*$ | $\frac{1}{\sqrt{3}}$ | $-\frac{1}{\sqrt{3}}$ | $0$ | $\frac{4}{3}$ | $-1$ | $-\frac{4}{\sqrt{3}}$ | $\frac{\sqrt{5}}{3}$ | $-\sqrt{\frac{5}{3}}$ | $-\frac{5}{\sqrt{3}}$ | $-\frac{1}{3}$ | $\frac{\sqrt{5}}{3}$ | $0$ | $-\sqrt{\frac{2}{3}}$ | $1$ | $0$ | $-1$ | $0$ | $0$ | $-\frac{1}{\sqrt{3}}$ | $\sqrt{\frac{5}{3}}$ |
| $\Sigma_c^*D^*$ | $-\sqrt{\frac{5}{3}}$ | $\sqrt{\frac{5}{3}}$ | $0$ | $-\frac{\sqrt{5}}{3}$ | $\sqrt{5}$ | $\sqrt{\frac{5}{3}}$ | $\frac{1}{3}$ | $-\frac{1}{\sqrt{3}}$ | $2\sqrt{\frac{5}{3}}$ | $\frac{\sqrt{5}}{3}$ | $-\frac{14}{3}$ | $0$ | $\sqrt{\frac{10}{3}}$ | $-\sqrt{5}$ | $0$ | $\sqrt{5}$ | $0$ | $0$ | $\sqrt{\frac{5}{3}}$ | $-\frac{5}{\sqrt{3}}$ |
| $\Xi_{cc}\phi$ | $0$ | $0$ | $\frac{2}{\sqrt{3}}$ | $0$ | $0$ | $0$ | $0$ | $0$ | $0$ | $0$ | $0$ | $0$ | $0$ | $2\sqrt{\frac{2}{3}}$ | $\frac{2}{3}$ | $-\sqrt{\frac{2}{3}}$ | $0$ | $\frac{2\sqrt{5}}{3}$ | $\frac{4\sqrt{2}}{3}$ | $-\frac{\sqrt{10}}{3}$ |
| $\Xi_{cc}^*\eta'$ | $0$ | $0$ | $0$ | $0$ | $-\sqrt{\frac{2}{3}}$ | $0$ | $0$ | $0$ | $-\sqrt{2}$ | $-\sqrt{\frac{2}{3}}$ | $\sqrt{\frac{10}{3}}$ | $0$ | $0$ | $\sqrt{\frac{2}{3}}$ | $0$ | $-\sqrt{\frac{2}{3}}$ | $0$ | $0$ | $-\frac{\sqrt{2}}{3}$ | $\frac{\sqrt{10}}{3}$ |
| $\Xi_cD_s^*$ | $0$ | $-\frac{2}{\sqrt{3}}$ | $\sqrt{2}$ | $0$ | $1$ | $0$ | $0$ | $0$ | $\sqrt{3}$ | $1$ | $-\sqrt{5}$ | $2\sqrt{\frac{2}{3}}$ | $\sqrt{\frac{2}{3}}$ | $1$ | $-2\sqrt{\frac{2}{3}}$ | $1$ | $-\sqrt{\frac{10}{3}}$ | $\sqrt{\frac{10}{3}}$ | $\frac{1}{\sqrt{3}}$ | $-\sqrt{\frac{5}{3}}$ |
| $\Omega_{cc}K^*$ | $-\sqrt{2}$ | $\sqrt{2}$ | $-\frac{2}{\sqrt{3}}$ | $-2\sqrt{\frac{2}{3}}$ | $0$ | $\frac{2\sqrt{2}}{3}$ | $\sqrt{\frac{10}{3}}$ | $-\frac{\sqrt{10}}{3}$ | $0$ | $0$ | $0$ | $\frac{2}{3}$ | $0$ | $-2\sqrt{\frac{2}{3}}$ | $-\frac{4}{3}$ | $-\sqrt{\frac{2}{3}}$ | $\frac{2\sqrt{5}}{3}$ | $\frac{2\sqrt{5}}{3}$ | $\frac{4\sqrt{2}}{3}$ | $-\frac{\sqrt{10}}{3}$ |
| $\Xi_c^*D_s$ | $0$ | $\frac{2}{\sqrt{3}}$ | $\sqrt{2}$ | $0$ | $-1$ | $0$ | $0$ | $0$ | $-\sqrt{3}$ | $-1$ | $\sqrt{5}$ | $-\sqrt{\frac{2}{3}}$ | $-\sqrt{\frac{2}{3}}$ | $1$ | $-\sqrt{\frac{2}{3}}$ | $0$ | $-\sqrt{\frac{10}{3}}$ | $-\sqrt{\frac{10}{3}}$ | $-\sqrt{3}$ | $0$ |
| $\Xi_{cc}^*\phi$ | $0$ | $0$ | $-\sqrt{\frac{5}{3}}$ | $0$ | $0$ | $0$ | $0$ | $0$ | $0$ | $0$ | $0$ | $0$ | $0$ | $-\sqrt{\frac{10}{3}}$ | $\frac{2\sqrt{5}}{3}$ | $-\sqrt{\frac{10}{3}}$ | $0$ | $\frac{1}{3}$ | $\frac{\sqrt{10}}{3}$ | $\frac{\sqrt{2}}{3}$ |
| $\Omega_{cc}^*K^*$ | $\sqrt{\frac{5}{2}}$ | $-\sqrt{\frac{5}{2}}$ | $\sqrt{\frac{5}{3}}$ | $\sqrt{\frac{10}{3}}$ | $0$ | $-\frac{\sqrt{10}}{3}$ | $-\frac{5}{\sqrt{6}}$ | $\frac{5}{3\sqrt{2}}$ | $0$ | $0$ | $0$ | $\frac{2\sqrt{5}}{3}$ | $0$ | $\sqrt{\frac{10}{3}}$ | $\frac{2\sqrt{5}}{3}$ | $-\sqrt{\frac{10}{3}}$ | $\frac{1}{3}$ | $-\frac{5}{3}$ | $\frac{\sqrt{10}}{3}$ | $\frac{\sqrt{2}}{3}$ |
| $\Xi_c'D_s^*$ | $0$ | $\frac{2}{3}$ | $\sqrt{\frac{2}{3}}$ | $0$ | $-\frac{1}{\sqrt{3}}$ | $0$ | $0$ | $0$ | $-1$ | $-\frac{1}{\sqrt{3}}$ | $\sqrt{\frac{5}{3}}$ | $\frac{4\sqrt{2}}{3}$ | $-\frac{\sqrt{2}}{3}$ | $\frac{1}{\sqrt{3}}$ | $\frac{4\sqrt{2}}{3}$ | $-\sqrt{3}$ | $\frac{\sqrt{10}}{3}$ | $\frac{\sqrt{10}}{3}$ | $\frac{1}{3}$ | $-\frac{\sqrt{5}}{3}$ |
| $\Xi_c^*D_s^*$ | $0$ | $-\frac{2\sqrt{5}}{3}$ | $-\sqrt{\frac{10}{3}}$ | $0$ | $\sqrt{\frac{5}{3}}$ | $0$ | $0$ | $0$ | $\sqrt{5}$ | $\sqrt{\frac{5}{3}}$ | $-\frac{5}{\sqrt{3}}$ | $-\frac{\sqrt{10}}{3}$ | $\frac{\sqrt{10}}{3}$ | $-\sqrt{\frac{5}{3}}$ | $-\frac{\sqrt{10}}{3}$ | $0$ | $\frac{\sqrt{2}}{3}$ | $\frac{\sqrt{2}}{3}$ | $-\frac{\sqrt{5}}{3}$ | $-\frac{4}{3}$ |

Table B.14: $C = 2$, $S = 0$, $I = 1/2$, $J = 3/2$.

| | $\Xi_{cc}\bar{K}$ | $\Omega_{cc}\eta$ | $\Xi_c D$ | $\Xi_{cc}\bar{K}^*$ | $\Xi_c' D$ | $\Xi_c D^*$ | $\Xi_{cc}^*\bar{K}^*$ | $\Omega_{cc}\omega$ | $\Omega_{cc}^*\omega$ | $\Xi_c' D^*$ | $\Xi_c^* D^*$ | $\Omega_c D_s$ | $\Omega_{cc}\eta'$ | $\Omega_{cc}\phi$ | $\Omega_c D_s^*$ | $\Omega_{cc}^*\phi$ | $\Omega_c^* D_s^*$ |
|---|---|---|---|---|---|---|---|---|---|---|---|---|---|---|---|---|---|
| $\Xi_{cc}\bar{K}$ | $-2$ | $-\sqrt{3}$ | $\sqrt{\frac{3}{2}}$ | $-\frac{2}{\sqrt{3}}$ | $\frac{1}{\sqrt{2}}$ | $-\frac{1}{\sqrt{2}}$ | $4\sqrt{\frac{2}{3}}$ | $-\frac{1}{\sqrt{3}}$ | $2\sqrt{\frac{2}{3}}$ | $-\frac{5}{\sqrt{6}}$ | $\frac{2}{\sqrt{3}}$ | $0$ | $0$ | $-\sqrt{\frac{2}{3}}$ | $0$ | $\frac{4}{\sqrt{3}}$ | $0$ |
| $\Omega_{cc}\eta$ | $-\sqrt{3}$ | $0$ | $\frac{1}{\sqrt{2}}$ | $-1$ | $-\frac{1}{\sqrt{6}}$ | $-\frac{1}{\sqrt{6}}$ | $2\sqrt{2}$ | $0$ | $0$ | $\frac{5}{3\sqrt{2}}$ | $-\frac{2}{3}$ | $\sqrt{\frac{2}{3}}$ | $0$ | $0$ | $-\frac{5\sqrt{2}}{3}$ | $0$ | $\frac{4}{3}$ |
| $\Xi_c D$ | $\sqrt{\frac{3}{2}}$ | $\frac{1}{\sqrt{2}}$ | $-1$ | $-\frac{1}{\sqrt{2}}$ | $0$ | $-\sqrt{3}$ | $2$ | $-\frac{1}{\sqrt{2}}$ | $2$ | $-2$ | $2\sqrt{2}$ | $0$ | $1$ | $0$ | $-2$ | $0$ | $2\sqrt{2}$ |
| $\Xi_{cc}\bar{K}^*$ | $-\frac{2}{\sqrt{3}}$ | $-1$ | $-\frac{1}{\sqrt{2}}$ | $-\frac{2}{3}$ | $-\frac{5}{\sqrt{6}}$ | $\frac{1}{\sqrt{6}}$ | $\frac{4\sqrt{2}}{3}$ | $-\frac{5}{3}$ | $-\frac{2\sqrt{2}}{3}$ | $-\frac{7}{3\sqrt{2}}$ | $-\frac{2}{3}$ | $0$ | $0$ | $-\frac{\sqrt{2}}{3}$ | $0$ | $\frac{4}{3}$ | $0$ |
| $\Xi_c' D$ | $\frac{1}{\sqrt{2}}$ | $-\frac{1}{\sqrt{6}}$ | $0$ | $-\frac{5}{\sqrt{6}}$ | $-1$ | $-2$ | $-\frac{2}{\sqrt{3}}$ | $\frac{5}{\sqrt{6}}$ | $\frac{2}{\sqrt{3}}$ | $\frac{5}{\sqrt{3}}$ | $4\sqrt{\frac{2}{3}}$ | $-2$ | $-\frac{1}{\sqrt{3}}$ | $0$ | $\frac{4}{\sqrt{3}}$ | $0$ | $2\sqrt{\frac{2}{3}}$ |
| $\Xi_c D^*$ | $-\frac{1}{\sqrt{2}}$ | $-\frac{1}{\sqrt{6}}$ | $-\sqrt{3}$ | $\frac{1}{\sqrt{6}}$ | $-2$ | $-3$ | $-\frac{2}{\sqrt{3}}$ | $\frac{1}{\sqrt{6}}$ | $-\frac{2}{\sqrt{3}}$ | $\frac{4}{\sqrt{3}}$ | $2\sqrt{\frac{2}{3}}$ | $-2$ | $-\frac{1}{\sqrt{3}}$ | $0$ | $\frac{4}{\sqrt{3}}$ | $0$ | $2\sqrt{\frac{2}{3}}$ |
| $\Xi_{cc}^*\bar{K}^*$ | $4\sqrt{\frac{2}{3}}$ | $2\sqrt{2}$ | $2$ | $\frac{4\sqrt{2}}{3}$ | $-\frac{2}{\sqrt{3}}$ | $-\frac{2}{\sqrt{3}}$ | $-\frac{16}{3}$ | $-\frac{2\sqrt{2}}{3}$ | $\frac{2}{3}$ | $\frac{2}{3}$ | $-\frac{2\sqrt{2}}{3}$ | $0$ | $0$ | $\frac{4}{3}$ | $0$ | $-\frac{8\sqrt{2}}{3}$ | $0$ |
| $\Omega_{cc}\omega$ | $-\frac{1}{\sqrt{3}}$ | $0$ | $-\frac{1}{\sqrt{2}}$ | $-\frac{5}{3}$ | $\frac{5}{\sqrt{6}}$ | $\frac{1}{\sqrt{6}}$ | $-\frac{2\sqrt{2}}{3}$ | $0$ | $0$ | $\frac{7}{3\sqrt{2}}$ | $\frac{2}{3}$ | $0$ | $0$ | $0$ | $0$ | $0$ | $0$ |
| $\Omega_{cc}^*\omega$ | $2\sqrt{\frac{2}{3}}$ | $0$ | $2$ | $-\frac{2\sqrt{2}}{3}$ | $\frac{2}{\sqrt{3}}$ | $-\frac{2}{\sqrt{3}}$ | $\frac{2}{3}$ | $0$ | $0$ | $-\frac{2}{3}$ | $\frac{2\sqrt{2}}{3}$ | $0$ | $0$ | $0$ | $0$ | $0$ | $0$ |
| $\Xi_c' D^*$ | $-\frac{5}{\sqrt{6}}$ | $\frac{5}{3\sqrt{2}}$ | $-2$ | $-\frac{7}{3\sqrt{2}}$ | $\frac{5}{\sqrt{3}}$ | $\frac{4}{\sqrt{3}}$ | $\frac{2}{3}$ | $\frac{7}{3\sqrt{2}}$ | $-\frac{2}{3}$ | $-3$ | $0$ | $\frac{4}{\sqrt{3}}$ | $\frac{5}{3}$ | $0$ | $-\frac{14}{3}$ | $0$ | $\frac{2\sqrt{2}}{3}$ |
| $\Xi_c^* D^*$ | $\frac{2}{\sqrt{3}}$ | $-\frac{2}{3}$ | $2\sqrt{2}$ | $-\frac{2}{3}$ | $4\sqrt{\frac{2}{3}}$ | $2\sqrt{\frac{2}{3}}$ | $-\frac{2\sqrt{2}}{3}$ | $\frac{2}{3}$ | $\frac{2\sqrt{2}}{3}$ | $0$ | $-6$ | $2\sqrt{\frac{2}{3}}$ | $-\frac{2\sqrt{2}}{3}$ | $0$ | $\frac{2\sqrt{2}}{3}$ | $0$ | $-\frac{16}{3}$ |
| $\Omega_c D_s$ | $0$ | $\sqrt{\frac{2}{3}}$ | $0$ | $0$ | $-2$ | $-2$ | $0$ | $0$ | $0$ | $\frac{4}{\sqrt{3}}$ | $2\sqrt{\frac{2}{3}}$ | $-1$ | $-\frac{1}{\sqrt{3}}$ | $-\frac{5}{\sqrt{3}}$ | $\frac{5}{\sqrt{3}}$ | $-2\sqrt{\frac{2}{3}}$ | $4\sqrt{\frac{2}{3}}$ |
| $\Omega_{cc}\eta'$ | $0$ | $0$ | $1$ | $0$ | $-\frac{1}{\sqrt{3}}$ | $-\frac{1}{\sqrt{3}}$ | $0$ | $0$ | $0$ | $\frac{5}{3}$ | $-\frac{2\sqrt{2}}{3}$ | $-\frac{1}{\sqrt{3}}$ | $0$ | $0$ | $\frac{5}{3}$ | $0$ | $-\frac{2\sqrt{2}}{3}$ |
| $\Omega_{cc}\phi$ | $-\sqrt{\frac{2}{3}}$ | $0$ | $0$ | $-\frac{\sqrt{2}}{3}$ | $0$ | $0$ | $\frac{4}{3}$ | $0$ | $0$ | $0$ | $0$ | $-\frac{5}{\sqrt{3}}$ | $0$ | $\frac{4}{3}$ | $-\frac{7}{3}$ | $\frac{4\sqrt{2}}{3}$ | $-\frac{2\sqrt{2}}{3}$ |
| $\Omega_c D_s^*$ | $0$ | $-\frac{5\sqrt{2}}{3}$ | $-2$ | $0$ | $\frac{4}{\sqrt{3}}$ | $\frac{4}{\sqrt{3}}$ | $0$ | $0$ | $0$ | $-\frac{14}{3}$ | $\frac{2\sqrt{2}}{3}$ | $\frac{5}{\sqrt{3}}$ | $\frac{5}{3}$ | $-\frac{7}{3}$ | $-3$ | $\frac{2\sqrt{2}}{3}$ | $0$ |
| $\Omega_{cc}^*\phi$ | $\frac{4}{\sqrt{3}}$ | $0$ | $0$ | $\frac{4}{3}$ | $0$ | $0$ | $-\frac{8\sqrt{2}}{3}$ | $0$ | $0$ | $0$ | $0$ | $-2\sqrt{\frac{2}{3}}$ | $0$ | $\frac{4\sqrt{2}}{3}$ | $\frac{2\sqrt{2}}{3}$ | $-\frac{10}{3}$ | $-\frac{4}{3}$ |
| $\Omega_c^* D_s^*$ | $0$ | $\frac{4}{3}$ | $2\sqrt{2}$ | $0$ | $2\sqrt{\frac{2}{3}}$ | $2\sqrt{\frac{2}{3}}$ | $0$ | $0$ | $0$ | $\frac{2\sqrt{2}}{3}$ | $-\frac{16}{3}$ | $4\sqrt{\frac{2}{3}}$ | $-\frac{2\sqrt{2}}{3}$ | $-\frac{2\sqrt{2}}{3}$ | $0$ | $-\frac{4}{3}$ | $-6$ |

Table B.15: $C = 2$, $S = -1$, $I = 0$, $J = 1/2$.

| | $\Xi_{cc}^*\bar{K}$ | $\Omega_{cc}^*\eta$ | $\Xi_{cc}\bar{K}^*$ | $\Xi_c D^*$ | $\Xi_{cc}^*\bar{K}^*$ | $\Omega_{cc}\omega$ | $\Xi_c^* D$ | $\Omega_{cc}^*\omega$ | $\Xi_c' D^*$ | $\Xi_c^* D^*$ | $\Omega_{cc}\phi$ | $\Omega_c^* D_s$ | $\Omega_{cc}^*\eta'$ | $\Omega_c D_s^*$ | $\Omega_{cc}^*\phi$ | $\Omega_c^* D_s^*$ |
|---|---|---|---|---|---|---|---|---|---|---|---|---|---|---|---|---|
| $\Xi_{cc}^*\bar{K}$ | $-2$ | $-\sqrt{3}$ | $-\frac{4}{\sqrt{3}}$ | $-\sqrt{2}$ | $2\sqrt{\frac{5}{3}}$ | $-\frac{2}{\sqrt{3}}$ | $\sqrt{2}$ | $\sqrt{\frac{5}{3}}$ | $\sqrt{\frac{2}{3}}$ | $-\sqrt{\frac{10}{3}}$ | $-2\sqrt{\frac{2}{3}}$ | 0 | 0 | 0 | $\sqrt{\frac{10}{3}}$ | 0 |
| $\Omega_{cc}^*\eta$ | $-\sqrt{3}$ | 0 | $-2$ | $-\sqrt{\frac{2}{3}}$ | $\sqrt{5}$ | 0 | $-\sqrt{\frac{2}{3}}$ | 0 | $-\frac{\sqrt{2}}{3}$ | $\frac{\sqrt{10}}{3}$ | 0 | $2\sqrt{\frac{2}{3}}$ | 0 | $\frac{2\sqrt{2}}{3}$ | 0 | $-\frac{2\sqrt{10}}{3}$ |
| $\Xi_{cc}\bar{K}^*$ | $-\frac{4}{\sqrt{3}}$ | $-2$ | $-\frac{8}{3}$ | $2\sqrt{\frac{2}{3}}$ | $\frac{4\sqrt{5}}{3}$ | $-\frac{2}{3}$ | $-\sqrt{\frac{2}{3}}$ | $-\frac{2\sqrt{5}}{3}$ | $\frac{4\sqrt{2}}{3}$ | $-\frac{\sqrt{10}}{3}$ | $-\frac{4\sqrt{2}}{3}$ | 0 | 0 | 0 | $\frac{2\sqrt{10}}{3}$ | 0 |
| $\Xi_c D^*$ | $-\sqrt{2}$ | $-\sqrt{\frac{2}{3}}$ | $2\sqrt{\frac{2}{3}}$ | 0 | $-\sqrt{\frac{10}{3}}$ | $2\sqrt{\frac{2}{3}}$ | $-2$ | $-\sqrt{\frac{10}{3}}$ | $-\frac{2}{\sqrt{3}}$ | $2\sqrt{\frac{5}{3}}$ | 0 | $-2$ | $-\frac{2}{\sqrt{3}}$ | $-\frac{2}{\sqrt{3}}$ | 0 | $2\sqrt{\frac{5}{3}}$ |
| $\Xi_{cc}^*\bar{K}^*$ | $2\sqrt{\frac{5}{3}}$ | $\sqrt{5}$ | $\frac{4\sqrt{5}}{3}$ | $-\sqrt{\frac{10}{3}}$ | $-\frac{10}{3}$ | $-\frac{2\sqrt{5}}{3}$ | $-\sqrt{\frac{10}{3}}$ | $-\frac{1}{3}$ | $\frac{\sqrt{10}}{3}$ | $\frac{\sqrt{2}}{3}$ | $\frac{2\sqrt{10}}{3}$ | 0 | 0 | 0 | $-\frac{5\sqrt{2}}{3}$ | 0 |
| $\Omega_{cc}\omega$ | $-\frac{2}{\sqrt{3}}$ | 0 | $-\frac{2}{3}$ | $2\sqrt{\frac{2}{3}}$ | $-\frac{2\sqrt{5}}{3}$ | 0 | $\sqrt{\frac{2}{3}}$ | 0 | $-\frac{4\sqrt{2}}{3}$ | $\frac{\sqrt{10}}{3}$ | 0 | 0 | 0 | 0 | 0 | 0 |
| $\Xi_c^* D$ | $\sqrt{2}$ | $-\sqrt{\frac{2}{3}}$ | $-\sqrt{\frac{2}{3}}$ | $-2$ | $-\sqrt{\frac{10}{3}}$ | $\sqrt{\frac{2}{3}}$ | $-1$ | $\sqrt{\frac{10}{3}}$ | $-\frac{4}{\sqrt{3}}$ | $\sqrt{\frac{5}{3}}$ | 0 | $-2$ | $-\frac{2}{\sqrt{3}}$ | $-\frac{2}{\sqrt{3}}$ | 0 | $2\sqrt{\frac{5}{3}}$ |
| $\Omega_{cc}^*\omega$ | $\sqrt{\frac{5}{3}}$ | 0 | $-\frac{2\sqrt{5}}{3}$ | $-\sqrt{\frac{10}{3}}$ | $-\frac{1}{3}$ | 0 | $\sqrt{\frac{10}{3}}$ | 0 | $-\frac{\sqrt{10}}{3}$ | $-\frac{\sqrt{2}}{3}$ | 0 | 0 | 0 | 0 | 0 | 0 |
| $\Xi_c' D^*$ | $\sqrt{\frac{2}{3}}$ | $-\frac{\sqrt{2}}{3}$ | $\frac{4\sqrt{2}}{3}$ | $-\frac{2}{\sqrt{3}}$ | $\frac{\sqrt{10}}{3}$ | $-\frac{4\sqrt{2}}{3}$ | $-\frac{4}{\sqrt{3}}$ | $-\frac{\sqrt{10}}{3}$ | 0 | 0 | 0 | $-\frac{2}{\sqrt{3}}$ | $-\frac{2}{3}$ | $-\frac{2}{3}$ | 0 | $\frac{2\sqrt{5}}{3}$ |
| $\Xi_c^* D^*$ | $-\sqrt{\frac{10}{3}}$ | $\frac{\sqrt{10}}{3}$ | $-\frac{\sqrt{10}}{3}$ | $2\sqrt{\frac{5}{3}}$ | $\frac{\sqrt{2}}{3}$ | $\frac{\sqrt{10}}{3}$ | $\sqrt{\frac{5}{3}}$ | $-\frac{\sqrt{2}}{3}$ | 0 | $-3$ | 0 | $2\sqrt{\frac{5}{3}}$ | $\frac{2\sqrt{5}}{3}$ | $\frac{2\sqrt{5}}{3}$ | 0 | $-\frac{10}{3}$ |
| $\Omega_{cc}\phi$ | $-2\sqrt{\frac{2}{3}}$ | 0 | $-\frac{4\sqrt{2}}{3}$ | 0 | $\frac{2\sqrt{10}}{3}$ | 0 | 0 | 0 | 0 | 0 | $-\frac{2}{3}$ | $-\frac{2}{\sqrt{3}}$ | 0 | $\frac{8}{3}$ | $\frac{4\sqrt{5}}{3}$ | $-\frac{2\sqrt{5}}{3}$ |
| $\Omega_c^* D_s$ | 0 | $2\sqrt{\frac{2}{3}}$ | 0 | $-2$ | 0 | 0 | $-2$ | 0 | $-\frac{2}{\sqrt{3}}$ | $2\sqrt{\frac{5}{3}}$ | $-\frac{2}{\sqrt{3}}$ | $-1$ | $-\frac{2}{\sqrt{3}}$ | $-\frac{4}{\sqrt{3}}$ | $-2\sqrt{\frac{5}{3}}$ | $\sqrt{\frac{5}{3}}$ |
| $\Omega_{cc}^*\eta'$ | 0 | 0 | 0 | $-\frac{2}{\sqrt{3}}$ | 0 | 0 | $-\frac{2}{\sqrt{3}}$ | 0 | $-\frac{2}{3}$ | $\frac{2\sqrt{5}}{3}$ | 0 | $-\frac{2}{\sqrt{3}}$ | 0 | $-\frac{2}{3}$ | 0 | $\frac{2\sqrt{5}}{3}$ |
| $\Omega_c D_s^*$ | 0 | $\frac{2\sqrt{2}}{3}$ | 0 | $-\frac{2}{\sqrt{3}}$ | 0 | 0 | $-\frac{2}{\sqrt{3}}$ | 0 | $-\frac{2}{3}$ | $\frac{2\sqrt{5}}{3}$ | $\frac{8}{3}$ | $-\frac{4}{\sqrt{3}}$ | $-\frac{2}{3}$ | 0 | $\frac{2\sqrt{5}}{3}$ | 0 |
| $\Omega_{cc}^*\phi$ | $\sqrt{\frac{10}{3}}$ | 0 | $\frac{2\sqrt{10}}{3}$ | 0 | $-\frac{5\sqrt{2}}{3}$ | 0 | 0 | 0 | 0 | 0 | $\frac{4\sqrt{5}}{3}$ | $-2\sqrt{\frac{5}{3}}$ | 0 | $\frac{2\sqrt{5}}{3}$ | $-\frac{4}{3}$ | $\frac{2}{3}$ |
| $\Omega_c^* D_s^*$ | 0 | $-\frac{2\sqrt{10}}{3}$ | 0 | $2\sqrt{\frac{5}{3}}$ | 0 | 0 | $2\sqrt{\frac{5}{3}}$ | 0 | $\frac{2\sqrt{5}}{3}$ | $-\frac{10}{3}$ | $-\frac{2\sqrt{5}}{3}$ | $\sqrt{\frac{5}{3}}$ | $\frac{2\sqrt{5}}{3}$ | 0 | $\frac{2}{3}$ | $-3$ |

Table B.16: $C = 2$, $S = -1$, $I = 0$, $J = 3/2$.

| | $\Xi_{cc}D$ | $\Xi_{cc}D^*$ | $\Omega_{ccc}\omega$ | $\Xi^*_{cc}D^*$ | $\Omega_{cc}D_s$ | $\Omega_{ccc}\phi$ | $\Omega_{cc}D^*_s$ | $\Omega^*_{cc}D^*_s$ |
|---|---|---|---|---|---|---|---|---|
| $\Xi_{cc}D$ | $0$ | $-2\sqrt{3}$ | $2\sqrt{2}$ | $2\sqrt{6}$ | $-\sqrt{2}$ | $0$ | $-\sqrt{\frac{2}{3}}$ | $\frac{4}{\sqrt{3}}$ |
| $\Xi_{cc}D^*$ | $-2\sqrt{3}$ | $-\frac{4}{3}$ | $-2\sqrt{\frac{2}{3}}$ | $\frac{2\sqrt{2}}{3}$ | $-\sqrt{\frac{2}{3}}$ | $0$ | $-\frac{\sqrt{2}}{3}$ | $\frac{4}{3}$ |
| $\Omega_{ccc}\omega$ | $2\sqrt{2}$ | $-2\sqrt{\frac{2}{3}}$ | $0$ | $\frac{2}{\sqrt{3}}$ | $0$ | $0$ | $0$ | $0$ |
| $\Xi^*_{cc}D^*$ | $2\sqrt{6}$ | $\frac{2\sqrt{2}}{3}$ | $\frac{2}{\sqrt{3}}$ | $-\frac{20}{3}$ | $\frac{4}{\sqrt{3}}$ | $0$ | $\frac{4}{3}$ | $-\frac{8\sqrt{2}}{3}$ |
| $\Omega_{cc}D_s$ | $-\sqrt{2}$ | $-\sqrt{\frac{2}{3}}$ | $0$ | $\frac{4}{\sqrt{3}}$ | $1$ | $-2\sqrt{2}$ | $-\frac{5}{\sqrt{3}}$ | $4\sqrt{\frac{2}{3}}$ |
| $\Omega_{ccc}\phi$ | $0$ | $0$ | $0$ | $0$ | $-2\sqrt{2}$ | $0$ | $2\sqrt{\frac{2}{3}}$ | $-\frac{2}{\sqrt{3}}$ |
| $\Omega_{cc}D^*_s$ | $-\sqrt{\frac{2}{3}}$ | $-\frac{\sqrt{2}}{3}$ | $0$ | $\frac{4}{3}$ | $-\frac{5}{\sqrt{3}}$ | $2\sqrt{\frac{2}{3}}$ | $-1$ | $0$ |
| $\Omega^*_{cc}D^*_s$ | $\frac{4}{\sqrt{3}}$ | $\frac{4}{3}$ | $0$ | $-\frac{8\sqrt{2}}{3}$ | $4\sqrt{\frac{2}{3}}$ | $-\frac{2}{\sqrt{3}}$ | $0$ | $-4$ |

Table B.17: $C = 3$, $S = 0$, $I = 0$, $J = 1/2$.

| | $\Omega_{ccc}\eta$ | $\Xi^*_{cc}D$ | $\Xi_{cc}D^*$ | $\Omega_{ccc}\omega$ | $\Xi^*_{cc}D^*$ | $\Omega_{ccc}\eta'$ | $\Omega^*_{cc}D_s$ | $\Omega_{ccc}\phi$ | $\Omega_{cc}D^*_s$ | $\Omega^*_{cc}D^*_s$ |
|---|---|---|---|---|---|---|---|---|---|---|
| $\Omega_{ccc}\eta$ | $0$ | $-1$ | $-\frac{2}{\sqrt{3}}$ | $0$ | $\sqrt{\frac{5}{3}}$ | $0$ | $\sqrt{2}$ | $0$ | $2\sqrt{\frac{2}{3}}$ | $-\sqrt{\frac{10}{3}}$ |
| $\Xi^*_{cc}D$ | $-1$ | $0$ | $-2\sqrt{3}$ | $\sqrt{5}$ | $0$ | $-\sqrt{2}$ | $-\sqrt{2}$ | $0$ | $-2\sqrt{\frac{2}{3}}$ | $\sqrt{\frac{10}{3}}$ |
| $\Xi_{cc}D^*$ | $-\frac{2}{\sqrt{3}}$ | $-2\sqrt{3}$ | $\frac{2}{3}$ | $-2\sqrt{\frac{5}{3}}$ | $\frac{2\sqrt{5}}{3}$ | $-2\sqrt{\frac{2}{3}}$ | $-2\sqrt{\frac{2}{3}}$ | $0$ | $-\frac{4\sqrt{2}}{3}$ | $\frac{2\sqrt{10}}{3}$ |
| $\Omega_{ccc}\omega$ | $0$ | $\sqrt{5}$ | $-2\sqrt{\frac{5}{3}}$ | $0$ | $-\frac{1}{\sqrt{3}}$ | $0$ | $0$ | $0$ | $0$ | $0$ |
| $\Xi^*_{cc}D^*$ | $\sqrt{\frac{5}{3}}$ | $0$ | $\frac{2\sqrt{5}}{3}$ | $-\frac{1}{\sqrt{3}}$ | $-\frac{8}{3}$ | $\sqrt{\frac{10}{3}}$ | $\sqrt{\frac{10}{3}}$ | $0$ | $\frac{2\sqrt{10}}{3}$ | $-\frac{5\sqrt{2}}{3}$ |
| $\Omega_{ccc}\eta'$ | $0$ | $-\sqrt{2}$ | $-2\sqrt{\frac{2}{3}}$ | $0$ | $\sqrt{\frac{10}{3}}$ | $0$ | $-1$ | $0$ | $-\frac{2}{\sqrt{3}}$ | $\sqrt{\frac{5}{3}}$ |
| $\Omega^*_{cc}D_s$ | $\sqrt{2}$ | $-\sqrt{2}$ | $-2\sqrt{\frac{2}{3}}$ | $0$ | $\sqrt{\frac{10}{3}}$ | $-1$ | $1$ | $-\sqrt{5}$ | $-\frac{4}{\sqrt{3}}$ | $-\sqrt{\frac{5}{3}}$ |
| $\Omega_{ccc}\phi$ | $0$ | $0$ | $0$ | $0$ | $0$ | $0$ | $-\sqrt{5}$ | $0$ | $2\sqrt{\frac{5}{3}}$ | $\frac{1}{\sqrt{3}}$ |
| $\Omega_{cc}D^*_s$ | $2\sqrt{\frac{2}{3}}$ | $-2\sqrt{\frac{2}{3}}$ | $-\frac{4\sqrt{2}}{3}$ | $0$ | $\frac{2\sqrt{10}}{3}$ | $-\frac{2}{\sqrt{3}}$ | $-\frac{4}{\sqrt{3}}$ | $2\sqrt{\frac{5}{3}}$ | $2$ | $0$ |
| $\Omega^*_{cc}D^*_s$ | $-\sqrt{\frac{10}{3}}$ | $\sqrt{\frac{10}{3}}$ | $\frac{2\sqrt{10}}{3}$ | $0$ | $-\frac{5\sqrt{2}}{3}$ | $\sqrt{\frac{5}{3}}$ | $-\sqrt{\frac{5}{3}}$ | $\frac{1}{\sqrt{3}}$ | $0$ | $-1$ |

Table B.18: $C = 3$, $S = 0$, $I = 0$, $J = 3/2$.

# Appendix C

# $D$-matrices for hidden-charm sectors

In this appendix we show the $D$-matrices in the hidden-charm sector with total charm $C = 0$ and strangeness $S = 0$, and isospin $I = 1/2$ and $3/2$. There are three possible values of spin for each case of isospin: $J = 1/2,\ 3/2,\ 5/2$.

| | $N\eta_c$ | $NJ/\psi$ | $\Lambda_c\bar{D}$ | $\Lambda_c\bar{D}^*$ | $\Sigma_c\bar{D}$ | $\Sigma_c\bar{D}^*$ | $\Sigma_c^*\bar{D}^*$ |
|---|---|---|---|---|---|---|---|
| $N\eta_c$ | $0$ | $0$ | $\sqrt{\frac{3}{2}}$ | $-\frac{3}{\sqrt{2}}$ | $\sqrt{\frac{3}{2}}$ | $\frac{1}{\sqrt{2}}$ | $2$ |
| $NJ/\psi$ | $0$ | $0$ | $-\frac{3}{\sqrt{2}}$ | $-\sqrt{\frac{3}{2}}$ | $\frac{1}{\sqrt{2}}$ | $\frac{5}{\sqrt{6}}$ | $-\frac{2}{\sqrt{3}}$ |
| $\Lambda_c\bar{D}$ | $\sqrt{\frac{3}{2}}$ | $-\frac{3}{\sqrt{2}}$ | $1$ | $0$ | $0$ | $-\sqrt{3}$ | $\sqrt{6}$ |
| $\Lambda_c\bar{D}^*$ | $-\frac{3}{\sqrt{2}}$ | $-\sqrt{\frac{3}{2}}$ | $0$ | $1$ | $-\sqrt{3}$ | $-2$ | $-\sqrt{2}$ |
| $\Sigma_c\bar{D}$ | $\sqrt{\frac{3}{2}}$ | $\frac{1}{\sqrt{2}}$ | $0$ | $-\sqrt{3}$ | $-1$ | $\frac{2}{\sqrt{3}}$ | $\sqrt{\frac{2}{3}}$ |
| $\Sigma_c\bar{D}^*$ | $\frac{1}{\sqrt{2}}$ | $\frac{5}{\sqrt{6}}$ | $-\sqrt{3}$ | $-2$ | $\frac{2}{\sqrt{3}}$ | $\frac{1}{3}$ | $-\frac{\sqrt{2}}{3}$ |
| $\Sigma_c^*\bar{D}^*$ | $2$ | $-\frac{2}{\sqrt{3}}$ | $\sqrt{6}$ | $-\sqrt{2}$ | $\sqrt{\frac{2}{3}}$ | $-\frac{\sqrt{2}}{3}$ | $\frac{2}{3}$ |

Table C.1: $C = 0$, $S = 0$, $I = 1/2$, $J = 1/2$.

| | $NJ/\psi$ | $\Lambda_c\bar{D}^*$ | $\Sigma_c^*\bar{D}$ | $\Sigma_c\bar{D}^*$ | $\Sigma_c^*\bar{D}^*$ |
|---|---|---|---|---|---|
| $NJ/\psi$ | $0$ | $\sqrt{6}$ | $-\sqrt{2}$ | $\sqrt{\frac{2}{3}}$ | $-\sqrt{\frac{10}{3}}$ |
| $\Lambda_c\bar{D}^*$ | $\sqrt{6}$ | $1$ | $-\sqrt{3}$ | $1$ | $-\sqrt{5}$ |
| $\Sigma_c^*\bar{D}$ | $-\sqrt{2}$ | $-\sqrt{3}$ | $-1$ | $-\frac{1}{\sqrt{3}}$ | $\sqrt{\frac{5}{3}}$ |
| $\Sigma_c\bar{D}^*$ | $\sqrt{\frac{2}{3}}$ | $1$ | $-\frac{1}{\sqrt{3}}$ | $-\frac{5}{3}$ | $-\frac{\sqrt{5}}{3}$ |
| $\Sigma_c^*\bar{D}^*$ | $-\sqrt{\frac{10}{3}}$ | $-\sqrt{5}$ | $\sqrt{\frac{5}{3}}$ | $-\frac{\sqrt{5}}{3}$ | $-\frac{1}{3}$ |

Table C.2: $C = 0$, $S = 0$, $I = 1/2$, $J = 3/2$.

| | $\Sigma_c^*\bar{D}^*$ |
|---|---|
| $\Sigma_c^*\bar{D}^*$ | $-2$ |

Table C.3: $C = 0$, $S = 0$, $I = 1/2$, $J = 5/2$.

| | $\Delta J/\psi$ | $\Sigma_c^*\bar{D}^*$ |
|---|---|---|
| $\Delta J/\psi$ | 0 | $2\sqrt{3}$ |
| $\Sigma_c^*\bar{D}^*$ | $2\sqrt{3}$ | 4 |
| hline | | |

Table C.4: $C = 0$, $S = 0$, $I = 3/2$, $J = 5/2$.

| | $\Delta J/\psi$ | $\Sigma_c\bar{D}$ | $\Sigma_c\bar{D}^*$ | $\Sigma_c^*\bar{D}^*$ |
|---|---|---|---|---|
| $\Delta J/\psi$ | 0 | $2\sqrt{2}$ | $-2\sqrt{\frac{2}{3}}$ | $-\frac{2}{\sqrt{3}}$ |
| $\Sigma_c\bar{D}$ | $2\sqrt{2}$ | 2 | $-\frac{4}{\sqrt{3}}$ | $-2\sqrt{\frac{2}{3}}$ |
| $\Sigma_c\bar{D}^*$ | $-2\sqrt{\frac{2}{3}}$ | $-\frac{4}{\sqrt{3}}$ | $-\frac{2}{3}$ | $\frac{2\sqrt{2}}{3}$ |
| $\Sigma_c^*\bar{D}^*$ | $-\frac{2}{\sqrt{3}}$ | $-2\sqrt{\frac{2}{3}}$ | $\frac{2\sqrt{2}}{3}$ | $-\frac{4}{3}$ |

Table C.5: $C = 0$, $S = 0$, $I = 3/2$, $J = 1/2$.

| | $\Delta\eta_c$ | $\Delta J/\psi$ | $\Sigma_c^*\bar{D}$ | $\Sigma_c\bar{D}^*$ | $\Sigma_c^*\bar{D}^*$ |
|---|---|---|---|---|---|
| $\Delta\eta_c$ | 0 | 0 | $\sqrt{3}$ | $-2$ | $-\sqrt{5}$ |
| $\Delta J/\psi$ | 0 | 0 | $-\sqrt{5}$ | $-2\sqrt{\frac{5}{3}}$ | $\frac{1}{\sqrt{3}}$ |
| $\Sigma_c^*\bar{D}$ | $\sqrt{3}$ | $-\sqrt{5}$ | 2 | $\frac{2}{\sqrt{3}}$ | $-2\sqrt{\frac{5}{3}}$ |
| $\Sigma_c\bar{D}^*$ | $-2$ | $-2\sqrt{\frac{5}{3}}$ | $\frac{2}{\sqrt{3}}$ | $\frac{10}{3}$ | $\frac{2\sqrt{5}}{3}$ |
| $\Sigma_c^*\bar{D}^*$ | $-\sqrt{5}$ | $\frac{1}{\sqrt{3}}$ | $-2\sqrt{\frac{5}{3}}$ | $\frac{2\sqrt{5}}{3}$ | $\frac{2}{3}$ |

Table C.6: $C = 0$, $S = 0$, $I = 3/2$, $J = 3/2$.

# Nederlandse Samenvatting

Al eeuwen probeert de mensheid te begrijpen hoe ons universum is opgebouwd. Wat zijn de objecten die we om ons heen zien, en wat zijn de wetten van de natuur die de structuur van deze objecten bepalen? Tegenwoordig geeft de natuurkunde antwoorden op deze vragen. Er is al veel bekend over de structuur van de materie, maar er zijn nog vele niet-beantwoorde vragen, niet-verklaarde fenomenen en ontdekte deeltjes die niet begrepen zijn, of omgekeerd, deeltjes die worden voorspeld, maar nog niet zijn ontdekt. Laten we beginnen met hoe we tegenwoordig materie beschrijven.

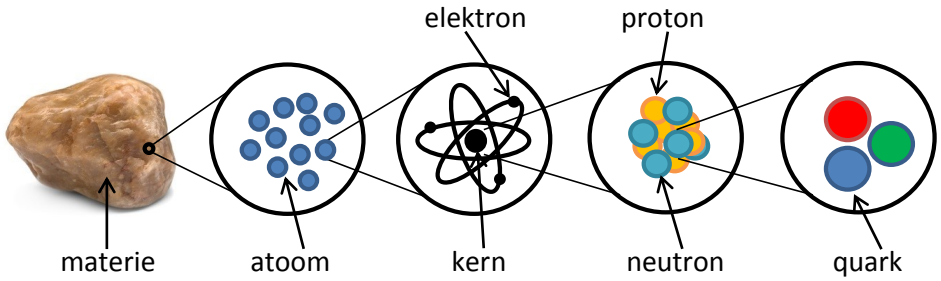


Figure C.1: De bouwstenen van materie.

De zichtbare materie in het universum is opgebouwd uit atomen; elk atoom bestaat uit een kern van protonen en neutronen, omgeven door een wolk van elektronen. Het proton en neutron zijn voorbeelden van deeltjes die baryonen genoemd worden. Baryonen, samen met mesonen, vormen een groep van deeltjes die hadronen genoemd worden. Het wordt verondersteld dat veel van de bekende mesonen uit een quark-antiquarkpaar bestaan ($q\bar{q}$, $q$ is een quark, $\bar{q}$ is een antiquark), en dat veel baryonen uit drie quarks bestaan ($qqq$). De quarks in hadronen worden aan elkaar "gelijmd" door uitwisseling van gluonen, een dergelijke interactie wordt de sterke kernkracht genoemd. De theorie die de sterke interactie beschrijft is de kwantumchromodynamica, in het Engels Quantum Chromodynamics of QCD (uit het Grieks $\chi\rho\omega\mu\alpha$, dat kleur betekent, een kwantumgetal dat de structuur van de sterke wisselwerking definieert). De sterke kernkracht is één van de vier bekende interacties in de natuur. De andere drie zijn de zwaartekracht, de elektromagnetische interactie en zwakke kernkracht. Om de interacties van quarks in hadronen te beschrijven worden de laatste drie interacties vaak verwaarloosd omdat zij veel zwakker zijn dan de sterke kernkracht op de schaal van subatomaire deeltjes.

Maar laten we terugkeren naar quarks. Vrije quarks zijn nooit waargenomen, vanwege de manier waarop ze op elkaar inwerken. Wanneer men probeert een quark van een hadron te scheiden, door de afstand tussen de quark en de rest van het systeem te vergroten, dan wordt de sterkte van de samenbindende kracht tussen de quarks steeds groter en wordt het onmogelijk om de quarks in het hadron te scheiden. Dit verschijnsel heet opsluiting of "confinement". Anderzijds, wanneer de afstand tussen quarks zeer klein is, gedragen ze zich als vrije deeltjes. De interactiesterkte tussen quarks neigt dan naar nul en dit wordt de asymptotische vrijheid genoemd. Bij hoge energie, in het regime van de asymptotische vrijheid, kan de zogenaamde storingsrekening worden toegepast. Het idee is om de interactie te ontwikkelen in termen van een kleine parameter, waarna men de termen van de expansie die de grootste bijdrages leveren behoudt en de kleinste verwaarloost. Bij lage energieën, wanneer confinement een cruciale rol speelt, blijkt de situatie lastiger om te behandelen. Storingsrekening techniken kunnen hier niet worden toegepast. Het theoretische alternatief voor dit regime is rooster-QCD, een methode waarin de ruimte wordt opgebouwd uit een rooster van punten, met quarkvelden gedefinieerd op roosterpunten, en gluonen die worden gedefinieerd op de lijnen die deze plaatsen verbinden. Deze methode is zeer succesvol in het beschrijven van de bestaande hadronen met de laagste massa's, maar vergt veel tijd en computerkracht. Gelukkig is er een andere werkwijze die kan worden toegepast voor het oplossen van de problemen van elementaire deeltjes bij lage energieën. Dit zijn effectieve veldentheorieën. De belangrijkste ideeën hier zijn dat ten eerste alleen relevante deeltjes worden beschouwd, en, ten tweede, rekening wordt gehouden met de symmetrieën van QCD. Laten we de eerste uitspraak uitleggen. Zoals hierboven vermeld zijn quarks als gevolg van de confinement gebonden in hadronen. Daarom is het bij lage energieën voldoende om slechts de interactie tussen hadronen te beschouwen, en is het niet nodig om specifiek te kijken naar het gedrag van de afzonderlijke quarks. Natuurkundigen zeggen dat in een dergelijke situatie de hadronen de relevante vrijheidsgraden zijn.

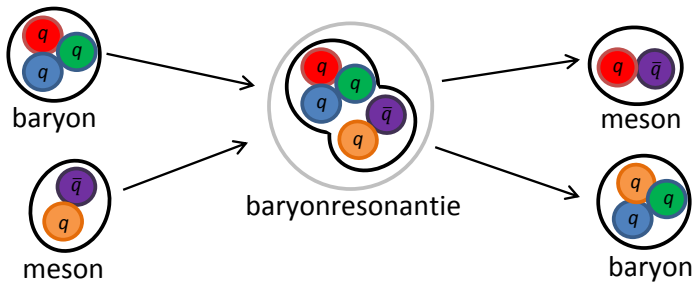


Figure C.2: Weergave van een baryonresonantie die ontstaat uit een baryon en een meson, en het opeenvolgende verval.

Dit nemen we ook aan in dit proefschrift. Wij beschouwen hadronen als onze relevante vrijheidsgraden en we kijken naar de interacties tussen baryonen en mesonen. Wanneer de interactie aantrekkend is, is er de mogelijkheid dat een deeltje ontstaat. Dit heet een baryonresonantie. Deeltjes die op deze manier ontstaan worden ook wel moleculaire toestanden genoemd. Deze deeltjes zijn meestal onstabiel en vervallen direct na hun

ontstaan.

Het tweede idee achter het gebruik van effectieve veldentheorie is om rekening te houden met de symmetrieën van QCD. De interactie van elementaire deeltjes is onderhevig aan de symmetrieën in de natuur. Sommige symmetrien zijn niet exact, maar geven een goede beschrijving van de natuur. Een voorbeeld van een dergelijke benaderende symmetrie is chirale symmetrie. Chirale symmetrie betekent invariantie (onafhankelijkheid) van het systeem onder de chirale transformaties, spiegeltransformaties (bijv. de linker- en de rechterhand transformeren in elkaar onder een chirale transformatie). Voor elementaire deeltjes betekent de chirale symmetrie dat quarks massaloos zijn. Chirale storingstheorie is een model op basis van deze symmetrie en geeft goede resultaten, in overeenstemming met de experimenten. Dit lijkt verrassend, omdat quarks wel degelijk massa hebben. Er zijn zes typen quarks, ook wel smaken genoemd. In het Engels worden ze aangeduid als up ($u$), down ($d$), strange ($s$), charm ($c$), bottom of beauty ($b$) en top of true ($t$). De eerste drie zijn licht, en kunnen dus worden behandeld als massaloze deeltjes.[1] De andere quarks, vanaf de charm-quark, zijn veel zwaarder. Deze quarks worden beschreven met de zwarequarksymmetrie. Er is de zwarequarksmaaksymmetrie en de zwarequarkspinsymmetrie, beide zijn exact in de limiet van oneindig zware quarks. De zwarequarksmaaksymmetrie stelt dat oneindig zware quarks van verschillende smaken zich op dezelfde manier gedragen. De zwarequarkspinsymmetrie (verder ZQSS) stelt dat de spin van de zware quark niet van belang is voor de interactie. De spin in dit geval is niet een beestje maar een andere parameter (kwantumgetal) van de elementaire deeltjes. In analogie met de klassieke mechanica kan de spin worden opgevat als een getal dat de rotatie van het deeltje beschrijft.

In dit proefschrift bestuderen we baryonresonanties die vier smaken bevatten. Dit betekent dat ze vier soorten quarks bevatten: drie lichte smaken ($u$, $d$, $s$), en een zware smaak ($c$ or $b$). We houden rekening met de ZQSS en het model dat we gebruiken neemt de chirale symmetrie voor lichte quarks in acht. Daarnaast maken we gebruik van andere benaderende symmetrieën van QCD, namelijk de smaaksymmetrie en de spin-smaaksymmetrie. De smaaksymmetrie voor drie lichtste quarks heet SU(3) en betekent dat de interactie niet afhankelijk van smaak is. Deze SU(3) symmetrie komt goed overeen met het gemeten baryonspectrum. De SU(3) symmetrie stelt dat er een octet is van baryonen (acht deeltjes) met spin 1/2 en ook een decuplet van baryonen (tien deeltjes) met spin 3/2. Al deze deeltjes kunnen geïdentificeerd worden met experimenteel bekende baryonen. Een andere symmetrie van QCD is de isospinsymmetrie, in feite de smaaksymmetrie voor $u$ en $d$ quarks. Deze symmetrie werd geïnspireerd door de gelijkenis tussen de massa's van het proton ($uud$) en het neutron ($udd$), respectievelijk $m_p = 938.3\,\mathrm{MeV}/c^2$ en $m_n = 939.6\,\mathrm{MeV}/c^2$. De spin-smaaksymmetrie combineert de smaaksymmetrie en de spinsymmetrie – invariantie van het systeem van de rotaties van de spins van de quarks. Het combineert dus het bovengenoemde octet van spin-1/2 en het decuplet van spin-3/2 baryonen.

Het is een gebruikelijke manier in de theoretische natuurkunde om een model eerst symmetrisch te maken, en vervolgens deze symmetrie te breken. Op deze manier kan het aantal onbekende parameters van de interactie worden verminderd. In dit proefschrift

[1] De massa's van lichte quarks zijn aanzienlijk lichter dan de massa's van nucleonen. Nucleonen krijgen hun massa's dankzij de grote bindingsenergie tussen quarks.

gebruiken we een model dat de SU(6) spin-smaaksymmetrie bevat, een combinatie van de SU(3) smaaksymmetrie en de spinsymmetrie, en dat ook de beperkingen die uit de ZQSS komen omvat. Daarna breken we de symmetrie tot de isospinsymmetrie. Dit doen we door het veranderen van de massa's van de hadronen en andere fysische waarden van het systeem. Op die manier bestudeerden we het resultaat van baryon-mesoninteracties, moleculaire baryonresonanties, en ook vonden we hoe de ontdekte toestanden zijn verbonden door verschillende symmetrieën. Bijvoorbeeld, dat baryonresonanties die door de ZQSS zijn verbonden ongeveer gelijke massa's hebben.

Met alle bovenstaande gegevens hebben we een aantal verschillende baryonresonanties met zware quarks bestudeerd. We onderzochten baryonresonanties met charmgetal $C = 1$, wat betekent dat ze één charm-quark bevatten (en de rest van drie quarks zijn licht, en ook een lichte antiquark dat afkomstig is van een meson). Dus, de quarkinhoud van dergelijke baryonresonanties is $lll c\bar{l}$, waar $l$ een lichte smaak aanduidt. Sommige gevonden baryonresonanties kunnen onmiddellijk geïdentificeerd worden met de experimenteel bekende toestanden. Baryonresonanties met charmgetal $C = 2$ ($llcc\bar{l}$) en met charmgetal $C = 3$ ($lccc\bar{l}$) werden ook bestudeerd. Deze resonanties zijn nog niet in de experimenten gezien, en vragen dus om meer experimentele data. Verder analyseerden we baryonresonanties met verborgen charm. Dit betekent dat deze deeltjes mogelijk meerdere charm-quarks bevatten en een charm-antiquark. In het bijzonder hebben we de toestanden bestudeerd die één charm-quark bevatten, $lll c\bar{c}$, zodat het totale charmgetal nul is. Dergelijke toestanden zijn echter nog niet gezocht in de experimenten hoewel ze worden ook voorspeld door andere theoretische modellen. Ten slotte hebben we ook baryonresonanties met een bottom-quark onderzocht, $lll b\bar{l}$. Dergelijk onderzoek werd geïnspireerd door de bevindingen bij de Large Hadron Collider (LHC), "grote hadronenbotser", bij de Europese Organisatie voor Nucleair Onderzoek (CERN). Daar werden twee zware deeltjes met bottomgetal gevonden, met ongeveer gelijke massa's van $5912\,\mathrm{MeV}/c^2$ en $5920\,\mathrm{MeV}/c^2$. We hebben deze deeltjes in ons model gereproduceerd en konden hun gelijke massa's verklaren door de ZQSS. Ook voorspelden we additionele bottombaryonresonanties.

Het is duidelijk dat de vergelijking van de resultaten van theoretische berekeningen met de experimentele resultaten zeer belangrijk is. Niet alleen om te kunnen testen of het theoretische model correct is, maar ook om waardes te vinden voor parameters in de theorie. Voor de deeltjes die worden bestudeerd in dit proefschrift is het geplande PANDA (Engels: anti-Proton ANnihilation at DArmstadt) experiment bij FAIR (Engels: Facility for Antiproton and Ion Research) in Duitsland veelbelovend.

# Acknowledgments

I would like to thank everyone without whom the completion of this thesis would not have happened, and without whom the last four years would have been different.

First of all, I would like to express my gratitude to my supervisor Laura Tolos. Dear Laura, thank you very much for being my advisor in the last four years. For me it is difficult to imagine a better thesis advisor than you are. You always answered my questions, also when it cost you some troubles. I realize that you are very good in management of working time, meaning pushing when it is needed, and giving some time for learning new things, sending to schools and conferences for meeting people, and even giving advice about how to make valuable connections. At the end of my first year you have moved to Barcelona to work at ICE, CSIC-IEEC, and I must admit that sometimes it was difficult to work in this situation. But the reason was not difficulty in communication, that went surprisingly without any troubles, but rather psychological, it turned out that it is very important to have discussions about work to stay motivated. Nevertheless, I believe that we have reached the desired result (of course with a feeling that there could have been done more, but I guess that it is a normal perception of finishing PhD students). I would also like to mention that sometimes I was not only happy, but also surprised with your style of hardworking, for example when receiving an email with an answer to my question a few minutes after it was sent, around 1:30 AM. Finally, I had a lot of fun having you as my supervisor, I really enjoyed all the tapas we had together, experiencing other aspects of Spanish culture, meeting you at conferences in different places, going to Barcelona regularly, and seeing you acting in a theater.

Next, I would like to thank my promotor Rob Timmermans. Dear Rob, thank you very much for supervising my PhD research. It is really a pity that I did not manage to do the project that we have planned, being involved in other projects instead. You helped me many times with answering my questions regarding different theoretical issues. Also thanks a lot for signing all the documents that I needed, and always supporting my working visits to Spain and the conferences I wanted to attend.

I would like to thank the members of the reading committee, Daniel Boer, Angels Ramos, and Daisuke Jido, for spending time for reading my manuscript, approving it, and sending valuable comments.

I would like to express my gratitude to my collaborators Carmen Garcia-Recio, Lorenzo Luis Salcedo, and Juan Nieves. Dear Carmen and Lorenzo Luis, thank you very much for your help, for answering an enormous amount of my questions. I really enjoyed my visits to Granada and many nice discussions that we had there. Dear Carmen, a separate thank for suggesting nice places to stay in Granada, "Carmen de la Victoria" has overcome all my expectations. Dear Lorenzo Luis, I believe that I have asked you the biggest part

of the questions. Thank you very much for answering them in a very detailed way. It was really fun when answering the question was transformed into a long discussion. I also enjoyed a lot your subtle humor, and I still think that we should have sent the first version of the reply to a referee of the "Bottom" paper that you had written.

Dear Juan, I really appreciate your help, especially with the Riemann sheets. I have enjoyed a few visits to Valencia at the beginning of my PhD. Also thank you for finding time to join us in Granada and answering my emails in the circumstances of your busy researcher life.

I would like to express my gratitude to my paranymphs Olga Bondarenko and Wouter Dekens. Many thanks for both of you, it is really nice to have your support. Dear Olga, thanks for being my good friend, my paranymph, and my colleague. It is fun to share an office with you, since it means having nice conversations (by the way the combination of a theorist and an experimentalist in one office seems to be very educational for both parties), respecting each others right to sometimes sleep during the day, or to have a meal in the office. It is really hard to remember all nice moments with you, because there were too many, but you know what I want to thank you for. I would like to thank Oksana and Myroslav for many valuable advices and a lot of support. Oksana, you know that I adore your culinary delights, thank you for sharing them with me.

I would also like to thank the rest of my friends and colleagues for having nice time and for their support. Thanks to Keri and Joost for helping to correct my Dutch summary (Joost, bitterballen will be there at the reception). Thanks to Olmo for helping me with all details regarding the preparation for a thesis defense. Many thanks to Olga, Segey, Keri, Corine, Jacob, Joost, Wouter, Sreekanth, Stefano, Sophie, Marcel, Zahra, Nafise, Josbert, Soumya, Ayan, Olmo, Alexandra, Oksana, Myroslav, Geert, Leon, Roxana, Olivier, Tom, Auke, Mayerlin, Daren, David, Andrii, Hossein, Johan, Alex, Renato, Ali, Qader, Manisha, Ganesh, Jordy, Krein, Vanni, Simona, Victor, Sybren, Wilco. I would also like to express thanks to my Lithuanian friends Ruta, Rita, and Tadas for having a great time together. I would like to express my gratitude to the participants of the FAIR meetings for interesting presentations, and the members of the KVI Movie Club for the nice time.

Many thanks to Hilde and Amarins for a lot of help with documents, and the financial department for their work. Thanks to Alfred for the necessary supplies, and thanks to Ralf for help with the PC. Many thanks to Marjan for organizing the FANTOM schools.

I would like to express my gratitude to Max Sluiman and the students of ZA-ZEN school of Japanese martial arts for the nice time during the trainings and exciting sparrings. I really enjoyed the budo camp and all the nice activities that we had. Dear Max, thanks a lot for offering the dojo as a place to celebrate my birthday party, and thanks to you and Carel for making ginger and tangerine beer. Max, also thanks for the nice dinners, your cooking skills are amazing. Further, thanks to Faust for the warm fur. Thanks to Jan and Nynke for being great friends, sparring partners, and very nice and reliable ukes.

Finally, I would like to thank my family, my beloved parents Valentyna and Roman, and my sister Tanya for the constant support and encouragement.

# Bibliography


[1] A. Pich, *Effective field theory: Course*, FTUV-98-46, IFIC-98-47 (Course given at Les Houches Summer School in Theoretical Physics), Jun 1998, 106 pp.

[2] H. Georgi, *Effective field theory*, Ann. Rev. Nucl. Part. Sci. **43**, 209 (1993).

[3] C. P. Burgess, *Introduction to effective field theory*, Ann. Rev. Nucl. Part. Sci. **57**, 329 (2007).

[4] J. Beringer et al., *Particle Data Group* (PDG), *Review of particle physics*, Phys. Rev. D **86**, 010001 (2012).

[5] F. Olness, R. Scalise, *Regularization, renormalization, and dimensional analysis: dimensional regularization meets Freshman E&M*, American Journal of Physics **79**, 306 (2011).

[6] S. Weinberg, *Phenomenological Lagrangians*, Physica **96 A**, 327 (1979).

[7] S. Scherer and M. R. Schindler, *A Chiral perturbation theory primer*, arXiv:hep-ph/0505265 (2005).

[8] A. Pich, *Chiral perturbation theory*, Rept. Prog. Phys. **58**, 563 (1995).

[9] G. Ecker, *Chiral perturbation theory*, Prog. Part. Nucl. Phys. **35**, 1 (1995).

[10] S. Scherer, *Introduction to chiral perturbation theory*, Adv. Nucl. Phys. **27**, 277 (2003).

[11] J. A. Oller, E. Oset, and A. Ramos, *Chiral unitary approach to meson-meson and meson-baryon interactions and nuclear applications*, Prog. Part. Nucl. Phys. **45**, 157 (2000).

[12] N. Isgur and M. B. Wise, *Weak decays of heavy mesons in the static quark approximation*, Phys. Lett. B **232**, 113 (1989).

[13] M. Neubert, *Heavy-quark symmetry*, Phys. Rept. **245**, 259 (1994).

[14] A. V. Manohar and M. B. Wise, *Heavy quark physics*, Cambridge Monographs on Particle Physics, Nuclear Physics and Cosmology, vol. **10** (2000).

[15] V. E. Barnes *et al.*, *Observation of a hyperon with strangeness minus three*, Phys. Rev. Lett. **12**, 204 (1964).

[16] M. Gell-Mann, *Symmetries of baryons and mesons*, Phys. Rev. **125**, 1067 (1962).

[17] M. Gell-Mann, *A schematic model of baryons and mesons*, Phys. Lett. **8**, 214 (1964).

[18] N. Brambilla *et al.*, *Heavy Quarkonium Physics*, CERN Yellow Report, CERN-2005-005, Geneva: CERN, 2005.

[19] A. De Rujula, H. Georgi, and S. L. Glashow, *Hadron masses in a gauge theory*, Phys. Rev. D **12**, 147 (1975).

[20] S. Capstick and N. Isgur, *Baryons in a relativized quark model with chromodynamics*, Phys. Rev. D **34**, 2809 (1986).

[21] U. Loring, K. Kretzschmar, B. Ch. Metsch, and H. R. Petry, *Relativistic quark models of baryons with instantaneous forces*, Eur. Phys. J. A **10**, 309 (2001).

[22] U. Loring, B. Ch. Metsch, and H. R. Petry, *The light-baryon spectrum in a relativistic quark model with instanton-induced quark forces*, Eur. Phys. J. A **10**, 395 (2001).

[23] K. Johnson, *The M.I.T. bag model*, Acta Physica Polonica B **6**, 865 (1975).

[24] M. Karliner, and M. P. Mattis, *$\pi N$, $KN$, and $\bar{K}N$ scattering: Skyrme model versus experiment*, Phys. Rev. D **34**, 1991 (1986).

[25] H. Weigel, *Chiral Soliton Models for Baryons*, Lect. Notes Phys. **743**, 1 (2008).

[26] M. A. Shifman, A. I. Vainshtein, and V. I. Zakharov *QCD and resonance physics. Theoretical foundations*, Nucl. Phys. B **147**, 385 (1979).

[27] L. J. Reinders, H. Rubinstein, and S. Yazaki, *Hadron properties from QCD sum rules*, Phys. Rep. **127**, 1 (1985).

[28] C. Gattringer and C. B. Lang, *Quantum Chromodynamics on the Lattice (an introductory presentation)*, Lect. Notes Phys. **788** (2010).

[29] H.-W. Lin, *Review of Baryon Spectroscopy in Lattice QCD*, Chin. J. Phys. **49**, 827 (2011).

[30] O. Krehl, C. Hanhart, S. Krewald, and J. Speth, *What is the structure of the Roper resonance?*, Phys. Rev. C **62**, 025207 (2000).

[31] I. G. Aznauryan *et al.* [CLAS Collaboration], *Electroexcitation of the Roper resonance for $1.7 < Q^2 < 4.5\mathrm{GeV}^2$ in $ep \to en\pi^+$*, Phys. Rev. C **78**, 045209 (2008).

[32] I. G. Aznauryan *et al.*, *Electroexcitation of nucleon resonances from CLAS data on single pion electroproduction*, Phys. Rev. C **80**, 055203 (2009).

[33] H. P. Morsch, and P. Zupranski, *Structure of the $P_{11}(1440$ MeV$)$ resonance from $\alpha - p$ and $\pi - N$ scattering*, Phys. Rev. C **61**, 024002 (1999).

[34] A. V. Sarantsev *et al.* [CB-ELSA and A2-TAPS Collaborations], *New results on the Roper resonance and the $P_{11}$ partial wave*, Phys. Lett. B **659**, 94 (2008).

[35] N. Kaiser, P. B. Siegel, and W. Weise, *Chiral dynamics and the low-energy kaon-nucleon interaction*, Nucl. Phys. A **594**, 325 (1995).

[36] R. H. Dalitz and S. F. Tuan, *Possible resonant state in pion-hyperon scattering*, Phys. Rev. Lett. **2**, 425 (1959).

[37] R. H. Dalitz and S. F. Tuan, *The phenomenological representation of $K$-nucleon scattering and reaction amplitudes*, Ann. Phys. (N.Y.) **10**, 307 (1960).

[38] D. Jido, J. A. Oller, E. Oset, A. Ramos, and U. G. Meissner, *Chiral dynamics of the two $\Lambda(1405)$ states*, Nucl. Phys. A **725**, 181 (2003).

[39] C. Gignoux, B. Silvestre-Brac, and J. M. Richard, *Possibility of stable multiquark baryons*, Phys Lett. B **193**, 323 (1987).

[40] H. J. Lipkin, *New possibilities for exotic hadrons  anticharmed strange baryons*, Phys Lett. B **195**, 484 (1987).

[41] D. Ashery, *Search for the pentaquark and H dibaryon*, Hyperfine Interact. **103**, 253 (1996).

[42] E. M. Aitala *et al.* [Fermilab E791 Collaboration], *Search for the pentaquark via the $P^0_{c\bar{s}} \to \phi\pi p$ decay*, Phys. Rev. Lett. **81**, 44 (1998).

[43] T. Nakano *et al.*, *Evidence for a narrow $S = +1$ baryon resonance in photoproduction from the neutron*, Phys. Rev. Lett. **91**, 012002 (2003).

[44] K. Hicks, *An experimental review of the $\Theta^+$ pentaquark*, Journal of Physics: Conference Series **9**, 183 (2005).

[45] N. Kaiser, P. B. Siegel, and W. Weise, *Chiral dynamics and the $S_{11}(1535)$ nucleon resonance*, Phys. Lett. B **362**, 23 (1995).

[46] N. Kaiser, T. Waas, and W. Weise, *SU(3) chiral dynamics with coupled channels Eta and kaon photoproduction*, Nucl. Phy. A **612**, 297 (1997).

[47] E. Oset and A. Ramos, *Non-perturbative chiral approach to s-wave $\bar{K}N$ interactions*, Nucl. Phys. A **635**, 99 (1998).

[48] B. Krippa, *Chiral dynamics of the low energy kaon-baryon interactions*, Phys. Rev. C **58**, 1333 (1998).

[49] B. Krippa and J. T. Londergan, *Chiral dynamics of low-energy kaon-baryon interactions with explicit resonance*, Phys. Rev. C **58**, 1634 (1998).

[50] J. C. Nacher, A. Parreno, E. Oset, A. Ramos, A. Hosaka, and M. Oka, *Chiral unitary approach to the $\pi N^* N^*$, $\eta N^* N^*$ couplings for the $N^*(1535)$ resonance*, Nucl. Phys. A **678**, 187 (2000).

[51] U. G. Meissner and J. A. Oller, *Chiral unitary meson-baryon dynamics in the presence of resonances: Elastic pion-nucleon scattering*, Nucl. Phys. A **673**, 311 (2000).

[52] J. A. Oller and U. G. Meissner, *Chiral dynamics in the presence of bound states: kaon-nucleon interactions revisited*, Phys. Lett. B **500**, 263 (2001).

[53] J. Nieves and E. Ruiz Arriola, $S_{11} - N(1535)$ *and* $-N(1650)$ *resonances in meson-baryon unitarized coupled channel chiral perturbation theory*, Phys. Rev. D **64**, 116008 (2001).

[54] T. Inoue, E. Oset and M. J. Vicente Vacas, *Chiral unitary approach to S-wave meson baryon scattering in the strangeness* $S = 0$ *sector*, Phys. Rev. C **65**, 035204 (2002).

[55] M. F. M. Lutz and E. E. Kolomeitsev, *Relativistic chiral SU(3) symmetry, large-*$N_c$ *sum rules and meson-baryon scattering*, Nucl. Phys. A **700**, 193 (2002).

[56] C. Garcia-Recio, J. Nieves, E. Ruiz Arriola, and M. J. Vicente Vacas, $S = -1$ *meson baryon unitarized coupled channel chiral perturbation theory and the* $S_{01}$ *resonances* $\Lambda(1405)$ *and* $\Lambda(1670)$ , Phys. Rev. D **67**, 076009 (2003).

[57] E. Oset, A. Ramos, and C. Bennhold, *Low lying* $S = 1$ *excited baryons and chiral symmetry*, Phys. Lett. B **527**, 99 (2002).

[58] A. Ramos, E. Oset, and C. Bennhold, *Spin, parity, and nature of the* $\Xi(1620)$ *resonance*, Phys. Rev. Lett. **89**, 252001 (2002).

[59] C. Garcia-Recio, M. F. M. Lutz, and J. Nieves, *Quark mass dependence of s-wave baryon resonances*, Phys. Lett. B **582**, 49 (2004).

[60] J. A. Oller, J. Prades, and M. Verbeni, *Surprises in threshold antikaon-nucleon physics*, Phys. Rev. Lett. **95**, 172502 (2005).

[61] B. Borasoy, R. Nissler, and W. Weise, *Chiral dynamics of kaon-nucleon interactions, revisited*, Eur. Phys. J. A **25**, 79 (2005) [Erratum-ibid. **37**, 326 (1965)].

[62] B. Borasoy, U. G. Meissner, and R. Nissler, $K^-p$ *scattering length from scattering experiments*, Phys. Rev. C **74**, 055201 (2006).

[63] J. A. Oller, *On the strangeness -1 S-wave meson-baryon scattering*, Eur. Phys. J. A **28**, 63 (2006).

[64] T. Hyodo, D. Jido, and A. Hosaka, *Origin of the resonances in the chiral unitary approach*, Phys. Rev. C **78**, 025203 (2008).

[65] D. Jido, A. Hosaka, J. C. Nacher, E. Oset, and A. Ramos, *Magnetic moments of the* $\Lambda(1405)$ *and* $\Lambda(1670)$ *resonances*, Phys. Rev. C **66**, 025203 (2002).

[66] T. Hyodo, S. I. Nam, D. Jido, and A. Hosaka, *Flavor SU(3) breaking effects in the chiral unitary model for meson-baryon scatterings*, Phys. Rev. C **68**, 018201 (2003).

[67] S. I. Nam, H. C. Kim, T. Hyodo, D. Jido, and A. Hosaka, *Regularization dependence of the $S = 0$ and the $S = -1$ meson-baryon system in the chiral unitary model*, J. Korean Phys. Soc. **45**, 1466 (2004).

[68] D. W. Thomas, A. Engler, H. E. Fisk, and R. W. Kraemer, *Strange particle production from p interactions at 1.69* GeV/$c$, Nucl. Phys. B **56**, 15 (1973).

[69] S. Prakhov *et al.* [The Crystal Ball Collaboration], *$K^- p \to \pi^0\pi^0\Sigma^0$ at $p_{K^-} = 504 - 750$ MeV/$c$ and comparison with other $\pi^0\pi^0$*, Phys. Rev. C **70**, 034605 (2004).

[70] E. E. Kolomeitsev and M. F. M. Lutz, *On baryon resonances and chiral symmetry*, Phys. Lett. B **585**, 243 (2004).

[71] S. Sarkar, E. Oset, and M. J. Vicente Vacas, *Baryonic resonances from baryon decuplet-meson octet interaction*, Nucl. Phys. A **750**, 294 (2005).

[72] S. Sarkar, E. Oset, and M. J. Vicente Vacas, *Chiral coupled channel dynamics of the $\Lambda(1520)$ and the $K^- p \to \pi^0\pi^0\Lambda$ reaction*, Phys. Rev. C **72**, 015206 (2005).

[73] L. Roca, S. Sarkar, V. K. Magas, and E. Oset, *Unitary coupled channel analysis of the $\Lambda(1520)$ resonance*, Phys. Rev. C **73**, 045208 (2006).

[74] T. Hyodo, S. Sarkar, A. Hosaka, and E. Oset, *Coupling of $\bar{K}^* N$ to the $\Lambda(1520)$*, Phys. Rev. C **73**, 035209 (2006); Phys. Rev. C **75**, 029901(E) (2007).

[75] M. Doring, E. Oset, and S. Sarkar, *Radiative decay of the $\Lambda^*(1520)$*, Phys. Rev. C **74**, 065204 (2006).

[76] M. Doring, E. Oset, and D. Strottman, *Chiral dynamics in the $\eta p \to \pi^0\eta p$ and $\eta p \to \pi^0 K^0\Sigma^+$ reactions*, Phys. Rev. C **73**, 045209 (2006).

[77] M. Doring, E. Oset, and D. Strottman, *Clues to the nature of the $\Delta^*(1700)$ resonance from pion- and photon-induced reactions*, Phys. Lett. B **639**, 59 (2006).

[78] C. Garcia-Recio, J. Nieves, and L. L. Salcedo, SU(6) *extension of the Weinberg-Tomozawa meson-baryon Lagrangian*, Phys. Rev. D **74**, 034025 (2006).

[79] C. Garcia-Recio, J. Nieves, and L. L. Salcedo, *Resonances and the Weinberg-Tomozawa 56-baryon-35-meson interaction*, Eur. Phys. J. A **31**, 499 (2007).

[80] C. Garcia-Recio, J. Nieves, and L. L. Salcedo, *Meson-baryon s-wave resonances with strangeness -3*, Eur. Phys. J. A **31**, 540 (2007).

[81] H. Toki, C. Garcia-Recio, and J. Nieves, *Photon induced $\Lambda(1520)$ production and the role of the $K^*$ exchange*, Phys. Rev. D **77**, 034001 (2008).

[82] L. Roca, E. Oset, and J. Singh, *Low lying axial-vector mesons as dynamically generated resonances*, Phys. Rev. D **72**, 014002 (2005).

[83] M. F. M. Lutz and E. E. Kolomeitsev, *On meson resonances and chiral symmetry*, Nucl. Phys. A **730**, 392 (2004).

[84] J. J. Aubert *et al.*, *Experimental observation of a heavy particle $J$*, Phys. Rev. Lett. **33**, 1404 (1974).

[85] J.-E. Augustin *et al.*, *Discovery of a narrow resonance in $e^+e^-$ annihilation*, Phys. Rev. Lett. **33**, 1406 (1974).

[86] G. Goldhaber *et al.*, *Observation in $e^+e^-$ annihilation of a narrow state at 1865MeV/$c^2$ decaying to $K\pi$ and $K\pi\pi\pi$*, Phys. Rev. Lett. **37**, 255 (1976).

[87] M. K. Gaillard and B. W. Lee, *Search for charm*, Rev. Mod. Phys. **47**, 277 (1975).

[88] E. G. Cazzoli, A. M. Cnops, P. L. Connolly, R. I. Louttit, M. J. Murtagh, R. B. Palmer, N. P. Samios, T. T. Tso, and H. H. Williams, *Evidence for $\Delta S = -\Delta Q$ currents or charmed-baryon production by neutrinos*, Phys. Rev. Lett. **34**, 1125 (1975).

[89] B. Aubert *et al.* [BABAR Collaboration], *Observation of a narrow meson decaying to $D_s^+\pi^0$ at a mass of 2.32* GeV/$c^2$, Phys. Rev. Lett. **90**, 242001 (2003).

[90] R. A. Briere *et al.* [CLEO Collaboration], *Observation of $\psi(3770) \to \gamma\chi_{c0}$*, Phys. Rev. D **74**, 031106 (2006).

[91] P. Krokovny *et al.* [Belle Collaboration], *Observation of the $D_{sJ}(2317)$ and $D_{sJ}(2457)$ in $B$ decays*, Phys. Rev. Lett. **91**, 262002 (2003).

[92] K. Abe *et al.* [Belle Collaboration], *Measurements of the $D_{sJ}$ resonance properties*, Phys. Rev. Lett. **92**, 012002 (2004).

[93] S. K. Choi *et al.* [Belle Collaboration], *Observation of a new narrow charmoniumlike state in exclusive $B^\pm \to K^\pm\pi^+\pi^- J/\psi$ decays*, Phys. Rev. Lett. **91**, 262001 (2003).

[94] D. E. Acosta *et al.* [CDF II Collaboration], *Observation of the narrow state $X(3872) \to J/\psi\pi^+\pi^-$ in $\bar{p}p$ collisions at $\sqrt{s} = 1.96$ TeV*, Phys. Rev. Lett. **93**, 072001 (2004).

[95] V. M. Abazov *et al.* [D0 Collaboration], *Observation and properties of the $X(3872)$ decaying to $J/\psi\pi^+\pi^-$ in $p\bar{p}$ collisions at $\sqrt{s} = 1.96$ TeV*, Phys. Rev. Lett. **93**, 162002 (2004).

[96] B. Aubert *et al.* [BABAR Collaboration], *Study of the $B^- \to J/\psi K^-\pi^+\pi^-$ decay and measurement of the $B^- \to X(3872)K^-$ branching fraction*, Phys. Rev. D **71**, 071103 (2005).

[97] K. Abe *et al.* [Belle Collaboration], *Observation of a charmoniumlike state produced in association with a $J/\psi$ in $e^+e^-$ annihilation at $\sqrt{s} \approx 10.6$ GeV*, Phys. Rev. Lett. **98**, 082001 (2007).

[98] P. Pakhlov *et al.* [Belle Collaboration], *Production of new charmoniumlike states in $e^+e^- \to J/\psi D^{(*)}\bar{D}^{(*)}$ at $\sqrt{s} \approx 10.6$ GeV* , Phys. Rev. Lett. **100**, 202001 (2008).

[99] K. Abe *et al.* [Belle Collaboration], *Observation of a near-threshold $\omega J/\psi$ mass enhancement in exclusive $B \to K\omega J/\psi$ decays*, Phys. Rev. Lett. **94**, 182002 (2005).

[100] B. Aubert *et al.* [BaBar Collaboration], *Observation of $Y(3940) \to J/\psi\omega$ in $B \to J/\psi\omega K$ at BABAR*, Phys. Rev. Lett. **101**, 082001 (2008).

[101] S. Uehara *et al.* [Belle Collaboration], *Observation of a $\chi'_{c2}$ candidate in $\gamma\gamma \to D\bar{D}$ production at Belle*, Phys. Rev. Lett. **96**, 082003 (2006).

[102] H. Albrecht *et al.* [ARGUS Collaboration, *Evidence for $Lambda_c(2593)^+$ production*, Phys. Lett. B **402**, 207 (1997).

[103] P. L. Frabetti *et al.* [E687 Collaboration], *Study of higher mass charm baryons decaying to $\Lambda_c^+$*, Phys. Lett. B **365**, 461 (1996).

[104] B. Aubert *et al.* [BABAR Collaboration], *Observation of a charmed baryon decaying to $D^0 p$ at a mass near 2.94 GeV/$c^2$*, Phys. Rev. Lett. **98**, 012001 (2007).

[105] R. Mizuk *et al.* [Belle Collaboration], *Experimental constraints on the spin and parity of the $\Lambda_c(2880)^+$*, Phys. Rev. Lett. **98**, 262001 (2007).

[106] M. Artuso *et al.* [CLEO Collaboration], *Observation of new states decaying into $\Lambda_c^+\pi^-\pi^+$*, Phys. Rev. Lett. **86**, 4479 (2001).

[107] P. L. Frabetti *et al.* [E687 Collaboration], *Observation of an excited state of the $\Lambda_c^+$ baryon*, Phys. Rev. Lett. **72**, 961 (1994).

[108] H. Albrecht *et al.* [ARGUS Collaboration], *Observation of a new charmed baryon*, Phys. Lett. B **317**, 227 (1993).

[109] K. W. Edwards *et al.* [CLEO Collaboration], *Observation of excited baryon states decaying to $\Lambda_c^+\pi^+\pi^-$*, Phys. Rev. Lett. **74**, 3331 (1995).

[110] M. Artuso *et al.* [CLEO Collaboration], *Measurement of the decay constant $f_{D_s^+}$ using $D_s^+ \to l^+ v$*, Phys. Rev. Lett. **99**, 071802 (2007).

[111] R. Ammar *et al.* [CLEO Collaboration], *First observation of the $\Sigma_c^{*+}$ baryon and a new measurement of the $\Sigma_c^{*+}$ mass*, Phys. Rev. Lett. **86**, 1167 (2001).

[112] G. Brandenburg *et al.* [CLEO Collaboration], *Observation of two excited charmed baryons decaying into $\Lambda_c^+\pi^\pm$*, Phys. Rev. Lett. **78**, 2304 (1997).

[113] V. V. Ammosov, I. L. Vasilev, A. A. Ivanilov, P. V. Ivanov, V. I. Konyushko, V. M. Korablev, V. A. Korotkov, V. V. Makeev *et al.*, *Observation of the production of charmed $\Sigma_c^{*++}$ baryons in neutrino interactions at the SKAT bubble chamber*, JETP Lett. **58**, 247 (1993).

[114] B. Aubert *et al.* [BABAR Collaboration], *Measurements of $\mathrm{B}(\bar{B}^0 \to \Lambda_c^+\bar{p})$ and $\mathrm{B}(B^- \to \Lambda_c^+\bar{p}\pi^-)$ and studies of $\Lambda_c^+\pi^-$ resonances*, Phys. Rev. D **78**, 112003 (2008).

[115] R. Mizuk *et al.* [Belle Collaboration], *Observation of an isotriplet of excited charmed baryons decaying to* $\Lambda_c^+\pi$, Phys. Rev. Lett. **94**, 122002 (2005).

[116] T. Lesiak *et al.* [Belle Collaboration], *Measurement of masses of the* $\Xi_c(2645)$ *and* $\Xi_c(2815)$ *baryons and observation of* $\Xi_c(2980) \to \Xi_c(2645)\pi$, Phys. Lett. B **665**, 9 (2008).

[117] P. L. Frabetti *et al.* [The E687 Collaboration], *Observation of a narrow state decaying into* $\Xi_c^0\pi^+$, Phys. Lett. B **426**, 403 (1998).

[118] L. Gibbons *et al.* [CLEO Collaboration], *Observation of an excited charmed baryon decaying into* $\Xi_c^0\pi^+$, Phys. Rev. Lett. **77**, 810 (1996).

[119] P. Avery *et al.* [CLEO Collaboration], *Observation of a narrow state decaying into* $\Xi_c^+\pi^-$, Phys. Rev. Lett. **75**, 4364 (1995).

[120] S. E. Csorna *et al.* [CLEO Collaboration], *Evidence of new states decaying into* $\Xi_c^*\pi$, Phys. Rev. Lett. **86**, 4243 (2001).

[121] J. P. Alexander *et al.* [CLEO Collaboration], *Evidence of new states decaying into* $\Xi_c^*\pi$, Phys. Rev. Lett. **83**, 3390 (1999).

[122] B. Aubert *et al.* [BABAR Collaboration], *Study of excited charm-strange baryons with evidence for new baryons* $\Xi_c(3055)^+$ *and* $\Xi_c(3123)^+$, Phys. Rev. D **77**, 012002 (2008).

[123] R. Chistov *et al.* [BELLE Collaboration], *Observation of new states decaying into* $\Lambda_c^+K^-\pi^+$ *and* $\Lambda_c^+K_S^0\pi^-$, Phys. Rev. Lett. **97**, 162001 (2006).

[124] C. P. Jessop *et al.* [CLEO Collaboration], *Observation of two narrow states decaying into* $\Xi_c^+\gamma$ *and* $\Xi_c^0\gamma$, Phys. Rev. Lett. **82**, 492 (1999).

[125] B. Aubert *et al.* [BaBar Collaboration], *Observation of an excited charm baryon* $\Omega_c^*$ *decaying to* $\Omega_c^0\gamma$, Phys. Rev. Lett. **97**, 232001 (2006).

[126] R. Aaij *et al.* [LHCb Collaboration], *Observation of excited* $\Lambda_b^0$ *baryons*, Phys. Rev. Lett. **109**, 172003 (2012).

[127] B. Schmidt, *Selection of LHCb physics results*, EPJ Web Conf. **49**, 03002 (2013).

[128] R. Aaij *et al.* [LHCb Collaboration], *Differential branching fraction and angular analysis of the decay* $B_s^0 \to \phi\mu^+\mu^-$, JHEP **1307**, 084 (2013).

[129] R. Aaij *et al.* [LHCb Collaboration], *Observation of* $B_s^0 \to \chi_{c1}\phi$ *decay and study of* $B^0 \to \chi_{c1,2}K^{*0}$ *decays*, Nucl.Phys. B **874**, 663 (2013).

[130] T. Blake [for the LHCb Collaboration], *Rare B decays at LHCb*, EPJ Web Conf. **49**, 15001 (2013).

[131] J. Aichelin et al., *The CBM Physics Book*, Lect. Notes in Phys. **814**, 1 (2011), eds. B. Friman, C. Hohne, J. Knoll, S. Leupold, J. Randrup, R. Rapp, and P. Senger (Springer).

[132] *Physics Performance Report for PANDA: Strong Interaction Studies with Antiprotons*, PANDA Collaboration, arXiv:0903.3905 [http://www.gsi.de/PANDA].

[133] *Physics at BES-III*, BES-III Collaboration, IHEP Physics Report BES-III, 2008 [http://bes.ihep.ac.cn/bes3/phy˙book/index.html].

[134] *Large Hadron Collider Beauty Experiment* [http://lhcb-public.web.cern.ch/lhcb-public/].

[135] *Jefferson Lab,* 12 GeV *Collaboration* [https://www.jlab.org/12GeV/unique.html].

[136] Y. Huang, J. He, H.-F. Zhang, and X.-R. Chen, *Discovery potential of hidden charm baryon resonances via photoproduction*, arXiv:1305.4434 [nucl-th].

[137] L. Tolos, J. Schaffner-Bielich, and A. Mishra, *Properties of D-mesons in nuclear matter within a self-consistent coupled-channel approach*, Phys. Rev. C **70**, 025203 (2004).

[138] L. Tolos, J. Schaffner-Bielich, and H. Stoecker, *D-mesons: In-medium effects at FAIR*, Phys. Lett. B **635**, 85 (2006).

[139] M. F. M. Lutz and E. E. Kolomeitsev, *On charm baryon resonances and chiral symmetry*, Nucl. Phys. A **730**, 110 (2004).

[140] M. F. M. Lutz and E. E. Kolomeitsev, *Baryon resonances from chiral coupled-channel dynamics*, Nucl. Phys. A **755**, 29 (2005).

[141] J. Hofmann and M. F. M. Lutz, *Coupled-channel study of crypto-exotic baryons with charm*, Nucl. Phys. A **763**, 90 (2005).

[142] J. Hofmann and M. F. M. Lutz, *D-wave baryon resonances with charm from coupled-channel dynamics*, Nucl. Phys. A **776**, 17 (2006).

[143] M. F. M. Lutz and C. L. Korpa, *Open-charm systems in cold nuclear matter*, Phys. Lett. B **633**, 43 (2006).

[144] T. Mizutani and A. Ramos, *D mesons in nuclear matter: A DN coupled-channel equations approach*, Phys. Rev. C **74**, 065201 (2006).

[145] L. Tolos, A. Ramos, and T. Mizutani, *Open charm in nuclear matter at finite temperature*, Phys. Rev. C **77**, 015207 (2008).

[146] C. E. Jimenez-Tejero, A. Ramos, and I. Vidana, *Dynamically generated open-charm baryons beyond the zero range approximation*, Phys. Rev. C **80**, 055206 (2009).

[147] J. Haidenbauer, G. Krein, U. G. Meissner, and A. Sibirtsev, *$\bar{D}N$ interaction from meson-exchange and quark-gluon dynamics*, Eur. Phys. J. A **33**, 107 (2007).

[148] J. Haidenbauer, G. Krein, U. G. Meissner, and A. Sibirtsev, *Charmed meson rescattering in the reaction $\bar{p}d \to \bar{D}DN$*, Eur. Phys. J. A **37**, 55 (2008).

[149] J. Haidenbauer, G. Krein, U. G. Meissner, and L. Tolos, *$DN$ interaction from meson exchange*, Eur. Phys. J. A **47**, 18 (2011).

[150] J. -J. Wu, R. Molina, E. Oset, and B. S. Zou, *Prediction of narrow $N^*$ and $\Lambda^*$ resonances with hidden charm above 4 GeV*, Phys. Rev. Lett. **105**, 232001 (2010).

[151] J. -J. Wu, R. Molina, E. Oset, and B. S. Zou, *Dynamically generated $N^*$ and $\Lambda^*$ resonances in the hidden charm sector around 4.3 GeV*, Phys. Rev. C **84**, 015202 (2011).

[152] J. -J. Wu, T. -S. H. Lee, and B. S. Zou, *Nucleon Resonances with hidden charm in coupled-channels models*, Phys. Rev. C **85**, 044002 (2012).

[153] E. Oset, A. Ramos, E. J. Garzon, R. Molina, L. Tolos, C. W. Xiao, J. J. Wu, and B. S. Zou, *Interaction of vector mesons with baryons and nuclei*, International Journal of Modern Physics E, Vol. **21**, 1230011 (2012).

[154] E. Oset and A. Ramos, *Non-perturbative chiral approach to s-wave $\bar{K}N$ interaction*, Nuclear Physics A **635**, 99 (1998).

[155] J. J. de Swart, *The Octet Model and its Clebsch-Gordan Coefficients*, Rev. Mod. Phys. **35**, 916 (1963).

[156] G. E. Baird, L. C. Biedenharn, *On the representation of the semisimple Lie groups. 3. The explicit conjugation operator for SU(n)*, J. Math. Phys. **5**, 1723 (1964).

[157] C. Garcia-Recio and L. L. Salcedo, SU(6)$\supset$SU(3)$\otimes$SU(2) *and* SU(8)$\supset$SU(4)$\otimes$SU(2) *Clebsch-Gordan coefficients*, J. Math. Phys. **52**, 043503 (2011).

[158] J. D. Bjorken and S. D. Drell, *Relativistic quantum fields*, McGraw-Hill, New York, 1965.

[159] S. Weinberg, *Pion scattering lengths*, Phys. Rev. Lett. **17**, 616 (1966).

[160] Y. Tomozawa, *Axial-vector coupling constant renormalization and the meson-baryon scattering lengths*, Nuovo Cim. **46A**, 707 (1966).

[161] F. Gursey and L. A. Radicati, *Spin and unitary spin independence of strong interactions*, Phys. Rev. Lett. **13**, 173 (1964).

[162] A. Pais, *Implications of spin-unitary spin independence*, Phys. Rev. Lett. **13**, 175 (1964).

[163] B. Sakita, *Supermultiplets of elementary particles*, Phys. Rev. **136**, B1756 (1964).

[164] S. Coleman and J. Mandula, *All possible symmetries of the S matrix*, Phys. Rev. **159**, 1251 (1967).

[165] R. F. Lebed, *Determination of SU(6) Clebsch-Gordan coefficients and baryon mass and electromagnetic moment relations*, Phys. Rev. D **51**, 5039 (1995).

[166] R. Dashen, E. Jenkins, and A. V. Manohar, $1/N_c$ *expansion for baryons*, Phys. Rev. D **49**, 4713 (1994).

[167] J. L. Goity and C. L. Schat, *Negative parity 70-plet baryon masses in the* $1/N_c$ *expansion*, Phys. Rev. D **66**, 114014 (2002).

[168] D. G. Caldi and H. Pagels, *A solution to the* $\rho$-$\pi$ *puzzle: Spontaneously broken symmetries of the quark model*, Phys. Rev. D **14**, 809 (1976).

[169] S. Ishida and P. Roman, *Static SU(6) and Fundamental Substitution*, Phys. Rev. **172**, 5 (1968).

[170] D. G. Caldi and H. Pagels, *Spontaneous symmetry breaking and vector-meson dominance*, Phys. Rev. D **15**, 2668 (1977).

[171] D. Gamermann, C. Garcia-Recio, J. Nieves, and L. L. Salcedo, *Odd-parity light baryon resonances*, Phys. Rev. D **84**, 056017 (2011).

[172] C. Garcia-Recio, J. Nieves, and L. L. Salcedo, *Large* $N_c$ *Weinberg-Tomozawa interaction and negative parity s-wave baryon resonances*, Phys. Rev. D **74**, 036004 (2006).

[173] C. Garcia-Recio, J. Nieves, and L. L. Salcedo, *Large-*$N_c$ *Weinberg-Tomozawa interaction and spin-flavor symmetry*, Eur. Phys. J. A **31**, 491 (2007).

[174] J. C. Carter, J. J. Coyne, and S. Meshkov, *SU(6) Clebsch-Gordan Coefficients for the Product* $35 \times 56$, Phys. Rev. Lett. **14**, 523 (1965).

[175] C. Garcia-Recio, V. K. Magas, T. Mizutani, J. Nieves, A. Ramos, L. L. Salcedo, and L. Tolos, *s-wave charmed baryon resonances from a coupled-channel approach with heavy quark symmetry*, Phys. Rev. D **79**, 054004 (2009).

[176] D. Gamermann, C. Garcia-Recio, J. Nieves, L. L. Salcedo, and L. Tolos, *Exotic dynamically generated baryons with negative charm quantum number*, Phys. Rev. D **81**, 094016 (2010).

[177] O. Romanets, L. Tolos, C. Garcia-Recio, J. Nieves, L. L. Salcedo, and R. G. E. Timmermans, *Charmed and strange baryon resonances with heavy-quark spin symmetry*, Phys. Rev. D **85**, 114032 (2012).

[178] T. Hyodo, D. Jido, and L. Roca, *Structure of the* $\Lambda(1405)$ *baryon resonance from its large* $N_c$ *behavior*, Phys. Rev. D **77**, 056010 (2008).

[179] E. E. Salpeter and H. A. Bethe, *A relativistic equation for bound-state problems*, Phys. Rev. **84** 1232 (1951).

[180] B. A. Lippmann and J. Schwinger, *Variational principles for scattering processes. I*, Phys. Rev. **79** 469 (1950).

[181] J. A. Oller and E. Oset, *Chiral Symmetry amplitudes in the S-wave isoscalar and isovector channels and the $\sigma$ $f_0(980)$, $a_0(980)$ scalar mesons*, Nucl. Phys. A **620**, 438 (1997).

[182] S. Sarkar, B.-X. Sun, E. Oset, and M. J. Vicente Vacas, *Dynamically generated resonances from the vector octet-baryon decuplet interaction*, Eur. Phys. J. A **44**, 431 (2010).

[183] E. Oset and A. Ramos, *Dynamically generated resonances from the vector octet-baryon octet interaction*, Eur. Phys. J. A **44**, 445 (2010).

[184] M. Doring, C. Hanhart, F. Huang, S. Krewald, U.-G. Meissner, and D. Ronchen, *The reaction $\pi^+ p \to K^+\Sigma^+$ in a unitary coupled-channels model*, Nucl.Phys. A **851**, 58 (2011).

[185] C. Albertus, E. Hernandez, and J. Nieves, *Hyperfine mixing in $b \to c$ semileptonic decay of doubly heavy baryons*, Phys. Lett. B **683**, 21 (2010).

[186] J. M. Flynn, E. Hernandez, and J. Nieves, *Triply heavy baryons and heavy quark spin symmetry*, Phys. Rev. D **85**, 014012 (2012).

[187] J. J. Dudek, R. G. Edwards, and D. G. Richards, *Radiative transitions in charmonium from lattice QCD*, Phys. Rev. D **73**, 074507 (2006).

[188] C. Garcia-Recio, J. Nieves, O. Romanets, L. L. Salcedo, and L. Tolos, *Hidden charm $N$ and $\Delta$ resonances with heavy-quark symmetry*, Phys. Rev. D **87**, 074034 (2013).

[189] A. E. Blechman, A. F. Falk, D. Pirjol, and J. M. Yelton, *Threshold effects in excited charmed baryon decays*, Phys. Rev. D **67**, 074033 (2003).

[190] A. F. Falk, *Hadrons of arbitrary spin in the heavy-quark effective theory*, Nucl. Phys. B **378**, 79 (1992).

[191] S. G. Yuan, K. W. Wei, J. He, H. S. Xu, and B. S. Zou, *Study of $qqqc\bar{c}$ five quark system with three kinds of quark-quark hyperfine interaction*, Eur. Phys. J. A **48**, 61 (2012).

[192] C. Garcia-Recio, J. Nieves, O. Romanets, L. L. Salcedo, and L. Tolos, *Odd parity bottom-flavored baryon resonances*, Phys. Rev. D **87**, 034032 (2013).

[193] Combination of the world average [4] and the LHCb measurement [207] employed in [126] for analyzing the $\Lambda_b^0\pi^+\pi^-$ spectrum.

[194] Average of [208] (lattice), [209] (quark model), [210] (QCD sum rules), and [211] ($1/N_c$ expansion).

[195] S. Chatrchyan *et al.* [CMS Collaboration], *Observation of a new $\Xi_b$ baryon*, Phys. Rev. Lett. **108**, 252002 (2012).

[196] LHCb Collaboration, *Measurement of the masses of the $\Xi_b^-$ and $\Omega_b^-$*, CERN Report No.LHCb-CONF-2011-060, CERN-LHCb-CONF-2011-060, http://cdsweb.cern.ch/record/1395530/files/LHCb-CONF-2011-060.pdf.

[197] A. Ali Khan, T. Bhattacharya, S. Collins, C. T. H. Davies, R. Gupta, C. Morningstar, J. Shigemitsu and J. H. Sloan, *Heavy-light mesons and baryons with b quarks*, Phys. Rev. D **62**, 054505 (2000).

[198] H. Na, C. J. Monahan, C. T. H. Davies, R. Horgan, G. P. Lepage, and J. Shigemitsu, *B and $B_s$ meson decay constants from Lattice QCD*, Phys. Rev. D **86**, 034506 (2012).

[199] C. McNeile, C. T. H. Davies, E. Follana, K. Hornbostel, and G. P. Lepage, *High-precision $f_{B_s}$ and heavy quark effective theory from relativistic lattice QCD*, Phys. Rev. D **85**, 031503 (2012).

[200] A. Poluektov (LHCb Collaboration), private communication.

[201] H. Garcilazo, J. Vijande, and A. Valcarce, *Faddeev study of heavy-baryon spectroscopy*, J. Phys. G **34**, 961 (2007).

[202] D. Ebert, R. N. Faustov, and V. O. Galkin, *Masses of excited heavy baryons in the relativistic quarkdiquark picture*, Phys. Lett. B **659**, 612 (2008).

[203] M. Karliner, B. Keren-Zur, H. J. Lipkin, and J. L. Rosner, *The quark model and b baryons*, Annals Phys. **324**, 2 (2009).

[204] W. Roberts and M. Pervin, *Heavy baryons in a quark model*, Int. J. Mod. Phys. A **23**, 2817 (2008).

[205] P. G. Ortega, D. R. Entem, and F. Fernandez, *Quark model description of the $\Lambda_c(2940)^+$ as a molecular $D^*N$ state and the possible existence of the $\Lambda_b(6248)$* , Phys. Lett. B **718**, 1381 (2013).

[206] E. Klempt and J. -M. Richard, *Baryon spectroscopy*, Rev. Mod. Phys. **82**, 1095 (2010).

[207] R. Aaij *et al.* [LHCb Collaboration], *Measurement of b-hadron masses*, Phys. Lett. B **708**, 241 (2012).

[208] K. C. Bowler *et al.* [UKQCD Collaboration], *Heavy baryon spectroscopy from the lattice*, Phys. Rev. D **54**, 3619 (1996).

[209] C. Albertus, J. E. Amaro, E. Hernandez, and J. Nieves, *Charmed and bottom baryons: a variational approach based on heavy quark symmetry*, Nucl. Phys. A **740**, 333 (2004).

[210] Z. -G. Wang, *Reanalysis of the heavy baryon states* $\Omega_b$, $\Omega_c$, $\Xi_b'$, $Xi_c'$, $\Sigma_b$, *and* $\Sigma_c$ *with QCD sum rules*, Phys. Lett. B **685**, 59 (2010).

[211] E. E. Jenkins, *Model-independent bottom baryon mass predictions in the* $1/N_c$ *expansion*, Phys. Rev. D **77**, 034012 (2008).